BINDING SERVICES
Tel +44 (0)29 2087 4949
Fax +44 (0)29 20371921
e-mail bindery@cardiff.ac.uk

Corneal Development and the Role of Keratan Sulphate

Thesis submitted to Cardiff University, University of Wales for the degree of

Doctor of Philosophy
in the discipline of Biophysics

Melody Liles (BSc)

The Structural Biophysics Group,
School of Optometry and Vision Sciences,
Cardiff University
2006

UMI Number: U584887

All rights reserved

INFORMATION TO ALL USERS
The quality of this reproduction is dependent upon the quality of the copy submitted.

In the unlikely event that the author did not send a complete manuscript
and there are missing pages, these will be noted. Also, if material had to be removed,
a note will indicate the deletion.

UMI U584887
Published by ProQuest LLC 2013. Copyright in the Dissertation held by the Author.
Microform Edition © ProQuest LLC.
All rights reserved. This work is protected against
unauthorized copying under Title 17, United States Code.

ProQuest LLC
789 East Eisenhower Parkway
P.O. Box 1346
Ann Arbor, MI 48106-1346

DECLARATION

This work has not previously been accepted in substance for any degree and is not concurrently submitted in candidature for any degree.

Signed ...Melody Liles..... (candidate) Date ..26/1/2007

STATEMENT 1

This thesis is being submitted in partial fulfillment of the requirements for the degree of PhD.

Signed ..Melody Liles..... (candidate) Date ..26/1/2007

STATEMENT 2

This thesis is the result of my own independent work/investigation, except where otherwise stated. Other sources are acknowledged by explicit references.

Signed ..Melody Liles..... (candidate) Date ..26/1/2007

STATEMENT 3

I hereby give consent for my thesis, if acceptable, to be available for photocopying and for inter-library loan, and for the title and summary to be made available to outside organisations.

Signed..Melody Liles..... (candidate) Date...26/1/2007...

Summary

In the week before hatch, the embryonic chick cornea thins and becomes transparent (Coulombre and Coulombre, 1958; Hay and Revel, 1969; Connon *et al.*, 2003). Proteoglycans (PGs), have long been envisaged as potential modulators of corneal structure during the latter stages of development; previous quantification of corneal glycosaminoglycans has indicated no change in the amount, molecular size, or degree of sulphation between developmental days 10 and 14 (Hart, 1976). After this time, keratan sulphate (KS) becomes more highly sulphated. This study aims to investigate changes in highly and lesser sulphated KS levels with collagen order and spacing in the developing chick cornea during the week before hatch around day 21 of development.

Microscopy studies were used to follow the emergence of highly and lesser/undersulphated KS at both the light and electron level. Immunostaining of corneas from select developmental timepoints showed accumulation in an anterior-posterior fashion, becoming homogeneous shortly before hatch. Immunolocalisation of KSPGs show association with collagen fibrils at the cell surface, with a corresponding increase in labelling as fibrils become more aligned. Collagen fibrils show uniform spacing in bundles as fibrils are extruded, with highly sulphated KS already associated with collagen at the cell surface.

X-ray diffraction was used to deduce mean centre to centre collagen fibril spacing and local order at specific timepoints in a large sample group of developing chick corneas. These same corneas were then analysed for highly and lesser sulphated KS content, collagen content and wet weight. A separate cohort of corneas were analysed for collagen fibril spacing and keratanase sensitive KS content. KS was found to increase as collagen fibrils condense and collagen deposition increases, significantly so when highly sulphated.

In summary, as the secondary chick cornea develops and becomes transparent, the compaction of stromal collagen fibrils is accompanied by an increase in tissue levels of sulphated KS. Remodelling of the fibrillar arrangement may be related to a switch to highly sulphated KS production, with a role for KS in the structural "fine tuning" of the fibrillar array.

Acknowledgements

Above all others, I would like to thank my benevolent supervisor Dr. Andrew J. Quantock, who has been an unending source of inspiration and encouragement during this Herculean journey. I would also like to offer my sincere gratitude to co-supervisor Professor Keith M. Meek, whose expertise and patience has paved the way across my various shortcomings, and Professor Bruce Caterson who has extended every generosity in his laboratory, and effervesced with brilliance at each encounter. I am also extremely grateful to Professor Shigeru Kinoshita at Kyoto Prefectural University of Medicine, who generously hosted my JSPS Fellowship.

For their limitless kind instruction, advice and support, I would like to thank Dr. Rob D. Young (chapter 3), Dr. Craig Boote (chapter 4), Dr. Briedgeen Kerr and Dr. Clare Hughes (chapters 4 and 5), and Dr. Sally Hayes (chapter 4), who have shown stoic equanimity over the past three years despite my errant pestering.

For both timely academic and personal support, I would like to thank Dr. Che J. Connon and Dr. Philip Lewis, who have never faltered in their comprehensive knowledge, even under fire. I would also like to thank Professor Vic Duance for his wise counsel and tolerance in desperate times.

Many thanks also to Dr. Emma Blain, Elizabeth Sowter and Antony Harris, who have been exceedingly generous in both time and reagents, and Dr. Gunter Grossman for his kind help during data collection at Daresbury SRS.

Finally, I would like to thank my family, friends, and felines for their unwavering, unconditional love and support, in what could have easily become an extended "*annus horribilis*".

CONTENTS

		Page
	Chapter One: Introduction	
1.1	General introduction	1
1.2	The ocular surface	2
1.3	The cornea: structure and function	3
1.3.1	Corneal layers	4
1.4	Corneal collagen	6
1.5	Collagen biosynthesis	8
1.6	Different classes of collagens in the cornea	12
1.7	Fibril forming collagens in the developing avian cornea	13
	Type I	*13*
	Type II	*14*
	Type III	*14*
	Type V	*14*
1.8	Collagen fibrillogenesis	15
1.9	FACIT	18
1.10	Other collagens	19
1.11	Collagen packing	20
1.12	Proteoglycans, PGs	22
1.12.1	Glycosaminoglycans, GAGs	24
1.12.2	Keratan sulphate, KS	25
1.12.3	Keratan sulphate biosynthesis	27
1.13	The corneal proteglycans	27
1.13.1	CS/DS proteoglycan: Decorin	28
1.13.2	Lumican	30
1.13.3	Keratocan	32
1.13.4	Mimecan	33
1.14	Proteoglycans and the collagen matrix	34
1.15	The importance of proteoglycans	35
1.16	Chick corneal development	36
1.16.1	Development of the primary stroma	37
1.16.2	Development of the secondary stroma	39
1.16.3	Collagen structure during development	41
1.16.4	Glycosaminoglycans during development	42
1.16.5	The mature stroma	43
1.16.6	Potentially significant events	43
1.17	Corneal transparency	44
1.18	Aims and objectives	46

Chapter Two: General methods

2.1	Introduction to chapter	47
2.2.1	Sample collection	48
2.2.2	Sample storage	48
2.3	Small angle x-ray scattering	48
2.3.1	A brief background	49
2.3.2	Small angle x-ray scattering data collection	50
2.3.3	Analysis of small angle x-ray scattering patterns	51
2.3.4	Local order	56
2.4	Biochemical analyses	57
2.4.1	Antibodies and ELISA	57
2.4.2	Isotypes	*58*
	IgG	*58*
	IgM	58
	Monoclonal Antibodies	59
2.5	Keratan sulphate antibodies used in this study	59
2.5.1	KSPG extraction	61
	Papain digest	*62*
	Cyanogen Bromide, CnBr digest	*62*
2.5.2	Keratanase digest of CnBr digested samples	63
2.5.3	Enzyme - linked immunosorbant assay, ELISA	64
2.5.4	Keratan sulphate quantification	66
2.6	Hydroxyproline assay	67
2.7	Immunofluorescence microscopy	68
2.7.1	Sample preparation	69
2.7.2	Immunofluorescence	70
2.8	Electron microscopy	70
2.8.1	Low temperature embedding	71
	Rationale	*72*
2.8.2	Sectioning	73
2.8.3	Immunostaining	74

Chapter Three: Localisation of Keratan Sulphate

3.1	Introduction to chapter	76
3.2	Light level immunofluorescence	77
3.2.1	Introduction	77
3.2.2	Methods	78
3.2.3	Results	79

3.2.4	Discussion	86
3.2.5	Further work	87
3.3	Low temperature embedded TEM	88
3.3.1	Introduction	88
3.3.2	Methods	89
3.3.3	Results	90
3.3.4	Discussion	98
3.3.5	Further work	99
3.4	Summary	99

Chapter Four: Collagen Spacing and the Sulphation of Keratan Sulphate

4.1	Introduction to chapter	101
4.2	Introduction	102
4.3	Materials and methods	103
4.3.1	Specimens	103
4.3.2	Data collection and processing for Bragg spacing	103
4.3.4	Local order	104
4.3.5	Isolation of KS chains	104
4.3.6	Competitive ELISA analysis	105
4.3.7	Hydroxyproline assay	106
4.4	Results	106
4.4.1	Collagen fibril spacing and organisation	106
4.4.2	Keratan sulphate quantification	110
4.4.3	Hydroxyproline assay	115
4.5	Discussion	120
4.6	Further work	122
4.7	Summary	123

Chapter Five: Collagen spacing and the Influence of Keratan Sulphate

5.1	Introduction to chapter	124
5.2	Introduction	125
5.3	Methods	126
5.3.1	Specimens	126
5.3.2	Data collection and processing	126
5.3.3	Generation of the KS "stub" neoepitope	126
5.3.4	Competitive ELISA analysis	127
5.4	Results	127
5.4.1	Collagen spacing	128
5.4.2	KS neoepitope quantification	130

5.5 Discussion 133
5.6 Further work 134
5.7 Summary 135

Chapter Six: Concluding discussion

6.1 Introduction to chapter 136
6.2 Concluding Remarks 136

Appendix One

A1.1 Introduction to chapter 143
A1.2 Biochemistry recipes 143
A1.3 Microscopy recipes 145
A1.4 Serial dilutions 146
A1.5 Optimisation 151
A1.5.1 Proteoglycan/GAG extraction method analysis 151
Methods *151*
Results *152*
Inference *157*
A1.5.2 Storage study: Silicon oil 157
Methods 157
Results *157*
Inference *158*
A1.6 ELISA coating and primary antibody dilutions 159
Methods *159*
Results *161*
Inference *163*
A1.7 Inhibition optimisation ELISA 163
Methods *163*
Results *164*
Inference *165*
A1.8 Hydroxyproline assay 165
A1.9 Standard curve calculations 166

Appendix Two

A2.1 Introduction to chapter 169
A2.2 Statistics 169
A2.2.1 The P-value 170
A2.3 The Normal distribution 170
A2.4 Testing for Normality 171

A2.5	Data screening	171
A2.6	The T-test	172
A2.7	One-way analysis of variance (ANOVA)	172
A2.8	Chapter Four: Collagen spacing and the Sulphation of Keratan Sulphate	173
A2.8.1	Results	173
A2.9	Statistics	177
A2.9.1	Bragg Spacing	178
A2.9.2	1B4 labelled KS	179
A2.9.3	5D4 labelled KS	180
A2.9.4	Hydroxyproline content	182
A2.10	Chapter Five: Collagen spacing and the Influence of Keratan Sulphate	183
A2.10.1	Results	183
A2.11	Statistics	188
A2.11.1	Bragg Spacing	189
A2.11.2	Height to width ratio	190
A2.11.3	BKS-1 labelled KS	190

References 192

List of figures

Chapter One: Introduction

1.1	The mammalian (A) and avian eye (B) in cross section	2
1.2	Cross section of the human cornea	4
1.3	Stepwise biosynthesis of type I collagen	9
1.4	The collagen molecule triple helix	12
1.5	Summary diagram of the human corneal collagens	15
1.6	Axial structure of D-periodic collagen fibrils	16
1.7	Lamellar organisation in the cornea	21
1.8	Proteoglycan structure	22
1.9	Summary of keratan sulphate structure	26
1.10.	Small proteodermatan sulphates isolated in bovine sclera	28
1.11	Two-dimensional theoretical model of keratan sulphate subsitution sites	31
1.12	Events leading to the formation of the primary stroma	37
1.13	Development of the primary stroma between stages 19 and 22	38
1.14	Development of the Brille between stages 23 and 35	38
1.15	Camera lucida drawings showing the formation of the primary stroma	39
1.16	Invasion of the primary stroma by mesenchymal cells	39
1.17	Chick corneal stromal changes from developmental day 6.5 to hatch	41

Chapter Two: General Methods

2.1	Schematic diagram showing the principles of x-ray scattering	49
2.2	Small angle scattering pattern, D18 chick cornea	50
2.3	Small angle x-ray scattering pattern and intensity profile	52
2.4	Linear background generation	53
2.5	Background scatter subtraction	54
2.6	Scattering angle calculation	55
2.7	Calculating peak height and width at half height	56
2.8	Antibody structure and binding	57
2.9	Tissue processing post small angle scattering experiments	61
2.10	Keratanase action and antigenicity	63
2.11	Phosphatase action produces a colour shift	65
2.12	Example of standard curve calculations from optical density	66-67

Chapter Three: Localisation of Keratan Sulphate

3.1	Fluorescence microscopy of the developing chick cornea using 2D3	80-81
	Day 12	*80*

	Day 14	*80*
	Day 16	*81*
	Day 18	*81*
3.2	Fluorescence microscopy of the developing chick cornea using 2D3	83-84
	Day 12	*83*
	Day 14	*83*
	Day 16	*84*
	Day 18	*84*
3.3	Negative control images	85
3.4	Transmission electron micrographs from the developing chick cornea	93-96
	A, Day 10, 5D4	*93*
	B, Day 12, 1B4	*93*
	C, Day 12, 5D4	*93*
	D, Day 14, 1B4	*94*
	E, Day 14, 5D4	*94*
	F, Day 15, 1B4	*94*
	G, Day 15, 5D4	*94*
	H, Day 16, 1B4	*95*
	I, Day 16, 5D4	*95*
	J, Day 16, 1B4	*95*
	K, Day 18, 5D4	*95*
	L, 3 days post hatch, 1B4	*96*
	M, 3 days post hatch, 5D4	*96*
3.5	Negative control image for TEM immunolabelling using 1B4 and 5D4	97
3.6	TEM image from day 15 of development	97

Chapter Four: Collagen spacing and the Sulphation of Keratan Sulphate

4.1	Low angle x-ray scatter patterns from day 12 and 18 chick corneas	107
4.2	Mean interfibrillar Bragg spacing from days 12-18 of development	108
4.3	Mean height/width at half height ratio from days 12-18 of incubation	110
4.4	Mean 1B4 KS labelling per mg cornea	111
4.5	Mean 5D4 labelled KS per mg cornea	112
4.6	Comparing mean Bragg spacing, 1B4 and 5D4 KS labelling per mg cornea	113
4.7	Bragg spacing in relation to tetrasulphated hexasaccharides on KS chains	114
4.8	Bragg spacing in relation to pentasulphated hexasaccharides on KS chains	114
4.9	Hydroxyproline content between days 12 to 18	115
4.10	The ratio of sulphated KS content to hydroxyproline content	116
4.11	The relationship between Bragg spacing, 1B4 KS, 5D4 KS and hydroxyproline	117
4.12	The relationship between Bragg spacing and KS in relation to hydroxyproline	119

Chapter Five: Collagen Spacing and the Influence of Keratan Sulphate

5.1	Mean collagen spacing in the week leading up to hatch	128
5.2	Mean height to width at half height ratio from days 12 to 18	129
5.3	KS content measured using BKS-1 from days 12 to 18	130
5.4	The relationship between BKS-1 labelled KS content and Bragg spacing	131
5.5	Keratanase sensitive KS content per mg cornea	132
5.6	The relationship between BKS-1 KS per mg cornea and Bragg spacing	132

Appendix 1

A1.1	Triplicate primary antibody dilutions	160
A1.2	Secondary antibody dilutions	161
A1.3	Competing antibody concentrations	164
A1.4	Standard curve dilutions	164
A1.5	Standard curve generated from table A1.5.	167

Appendix 2

A2.1	Standard deviation	169
A2.2	Standard error	170
A2.3	The Shapiro-Wilk's test	171

List of tables

Chapter One: Introduction

1.1	Vertebrate collagen groups	7
1.2	FACITs	19
1.3	Other corneal collagens	20
1.4	The corneal SLRPs	23

Chapter Two: General Methods

2.1	Specificities of anti-KS antibodies used in this study	60

Appendix One

A1.1	Individual GAG extraction results	154-156
A1.2	Silicon oil study results	158
A1.3	Results of coating ELISAs and primary antibody dilutions	162
A1.4	Optimisation results	165
A1.5	Example of standards from hydroxyproline assay	167
A1.6	Hydroxyproline assay calculations	168

Appendix Two

A2.1	Mean results for small angle x-ray scattering, height to width at half height ratio, highly and lesser sulphated KS ELISA assay, and collagen content	174
A2.2	Results for KS quantification in terms of corneal wet weight	175
A2.3	Combined individual results showing collagen spacing, highly and lesser sulphated KS and hydroxyproline content	176-177
A2.4	Bragg spacing statistics calculations	179
A2.5	1B4 lesser sulphated KS ELISA statistics calculations	180
A2.6	5D4 highly sulphated KS ELISA statistics calculations	181
A2.7	Hydroxyproline assay statistics calculations	183
A2.8	Mean results for small angle x-ray scattering, height to width at half height ratio, BKS-1 ELISA assay, wet weight for ELISA corneas, and local order for ELISA corneas	183-184
A2.9	Individual results for Bragg spacing of 81 corneas, and BKS-1 corneas	185-188
A2.10	Statistical tables for Bragg spacing	189
A2.11	Mean peak height to width at half height ratio	190
A2.12	Statistical tables for BKS-1 labelled KS ELISA	191

List of abbreviations

Ab	Antibody
ANOVA	Analysis of Variance
Asn	Asparagine
Asp	Aspartate
ELISA	Enzyme Linked Immunosorbant Assay
BSA	Bovine Serum Albumin
cDNA	Complementary DNA
CHST6	carbohydrate (N-acetylglucosamine 6-O) sulfotransferase 6
CS	Chondroitin Sulphate
CNBr	Cyanogen Bromide
DEA	Diethanolamine
DMMB	Dimethylmethylene blue
DNA	DeoxyriboNucleic Acid
DS	Dermatan Sulphate
ER	Endoplasmic Reticulum
EtOH	Ethanol
GAG	Glycosaminoglycan
Gal	Galactose
Glc	Glucose
GlcNAc	N-acetylglucosamine
Gly	Glycine
H	Hydrogen
Keratanase I	Keratanase
KS	Keratan Sulphate
KSPG	Keratan Sulphate Proteoglycan
Leu	Leucine
LRR	Leucine Rich Repeat
MAb	Monoclonal Antibody
Man	Mannose
Met	Methionine
mRNA	Messenger RNA
PG	Proteoglycan

PBS	Phosphate Buffered Saline
PI	Propidium Iodide
RNA	RiboNuceleic Acid
SE	Standard Error
Ser	Serine
σ	Standard Deviation
SLRP	Small Leucine-Rich Proteoglycan
SRS	Synchotron Radiation Source
TEM	Transmission electron microscope
Thr	Threonine
TSA	Tris Sodium Azide
Tyr	Tyrosine
UV	Ultra Violet

Scaling

10-3	Milli, m
10-6	Micro, μ
10-9	Nano, n

CHAPTER ONE: Introduction

In this chapter a brief description of ocular anatomy will be presented, particularly focussed on corneal structure. Collagen structure and function will then be outlined, and the importance of proteoglycan interactions discussed. Key aspects of corneal development and transparency will be presented, and finally, a number of aims and objectives will be identified.

1.1 General Introduction

The avian sensory world is primarily visual, enlisting capabilities comparable to those of another visually dependent vertebrate, the diurnal primates. In The Origin of the Species (1859), Darwin exalted eyes as "organs of extreme perfection". There are many basic similarities in the visual pathways of birds and mammals, rooted both in distant ancestral phylogenetic relationships and the operation of convergent evolution. Historical evidence suggests that the avian visual system emerged from the basic reptilian plan (Chatterjee, 1997), primarily in support of flight.

The shape of the eye is almost spherical for mammals, whereas the avian eye is most often flattened, although also globose in diurnal species, or tubular in predatory birds. Birds have comparatively large eyes to their body size, which allows larger retinal images and increased depth of focus. The adult human eye has a diameter of almost 25 mm; compared to the 11.86 mm equatorial (nasotemporal and dorsoventral) diameter and 8.70 mm axial length (from the cornea to the inner surface of the retina) of a hen eye 14 days after hatch (Gottlieb *et al.*, 1987).

Despite mammalian similarities, a few reptilian characteristics remain within avian optics. One more important vestige is the presence of scleral ossicles that support the ocular globe, and a pecten structure found near the retina, which may play a role in enhancing perception of movement. The embryonic chick is a widely used lower vertebrate model for studying the controlled sequence of events culminating in the formation of such an acute visual system.

1.2 The Ocular Surface

The healthy ocular surface is composed of highly specialised conjunctival and corneal epithelia, which are formed by two phenotypically distinct cell types (Wei *et al.*, 1996). The cornea is the transparent, anterior portion of the outer shell of the eye, and together with the limbus and sclera forms a tough protective envelope which encloses the ocular tissues. Uniquely, the cornea is mechanically tough, but visually transparent, a characteristic vital for the efficient transmission and refraction of light.

Both the cornea and sclera fundamentally comprise of similar, densely woven collagen fibrils that confer rigidity, protection of delicate inner layers and resistance to penetration. The opaque sclera, with larger collagen fibrils of varying diameters, mechanically guards vulnerable ocular tissues, providing structural integrity, encircled by the limbus, a transition zone between cornea and sclera.

The cornea is the principal refractive element of the human eye, responsible for more than two-thirds of dioptric power equal to 42.4 Dioptres; the crystalline lens provides the remainder (Davson, 1990). In the hatched chick, corneal accommodation of up to 10 Dioptres may be induced by electrical stimulation (Troilo *et al.*, 1987), and accounts for 40% of focussing power. Light strikes the smooth, convex surface of the cornea and is refracted onto the retina. Despite similarities in composition, the cornea and sclera are strikingly different in that the cornea is transparent whilst the sclera is opaque.

The general structures of the mammalian eye and avian eye are shown below in figure 1.1.

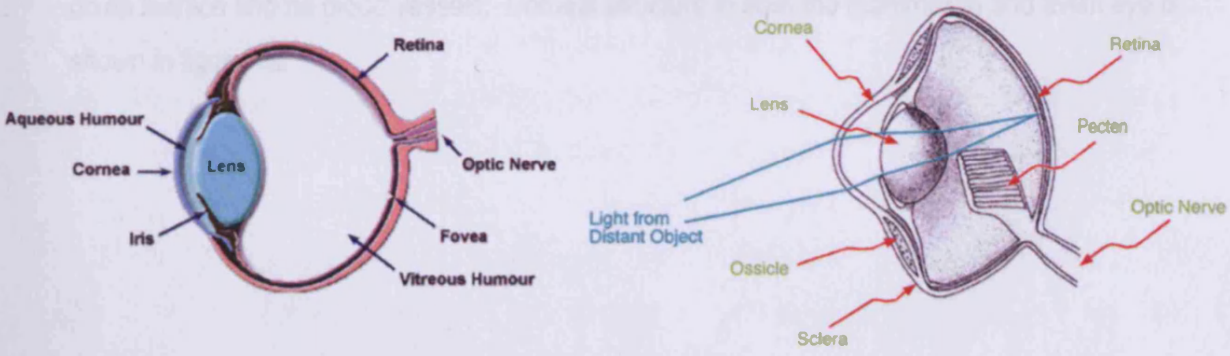

Figures 1.1 A) and (B). Mammalian eye (A) and avian eye (B) in cross-section.

Adapted from: (A) www.photo.net/photo/ edscott/vis00010.htm and (B) Rowe M P (2000). Inferring the retinal anatomy and visual capacities of extinct vertebrates. *Palaeontologia Electronica* 3: 1.

In the avian eye, small bones called scleral ossicles are arranged in the sclera around the cornea, supporting the eye and providing an attachment site for the ciliary muscles (Rowe, 2000). Lens tension is controlled by muscles of the ciliary body, attached by thin zonular fibres to the lens capsule. These fibres in turn influence lens shape, dioptric power, and focal point.

Eye movement is controlled by six extraocular muscles inserted into the sclera. Avian focussing employs either one or both corneal and lenticular accommodations (Glasser and Howland, 1996). Unlike mammals, chicks also utilise corneal accommodation, using the anterior ciliary muscle to pull backwards on the inner lamella of the cornea (Troilo *et al.*, 1987).

1.3 The Cornea: Structure and function

The cornea is primarily composed of closely packed type I (and V in a hybrid form) collagen fibrils. Parallel stacked collagen lamellae in the stromal region (Maurice, 1957) confer corneal transparency, and disruption of this regular array limits visual acuity. Thus, curvature and clarity are critical for good vision.

The embryonic chick is a commonly used model for the human cornea, as they share fundamental similarities in their basic structure. Essentially a collagenous connective tissue, the cornea is composed of five layers (Hay and Revel, 1969): epithelium, Bowmans layer, stroma, Descemet's membrane and endothelium, and is avascular in the normal physiological state. The metabolic requirements of corneal tissue are supplied anteriorly and posteriorly by the tear film, and aqueous humor respectively. The cornea has tightly packed nerve endings on its surface and no blood vessels. Corneal structure in both the mammalian and avian eye is shown in figure 1.2.

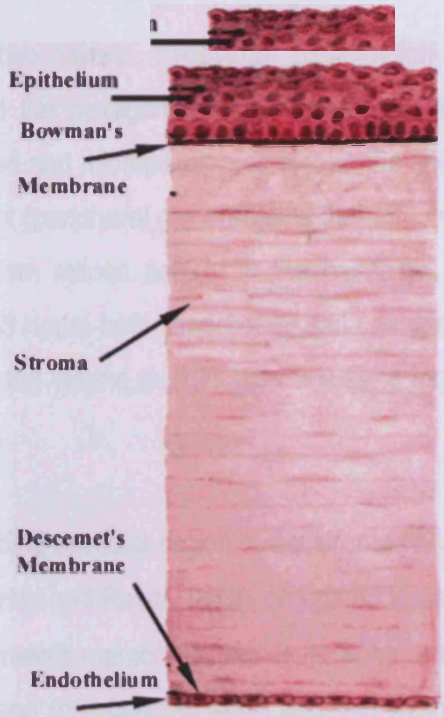

Figure 1.2. Cross section of the human cornea.

Taken from: education.vetmed.vt.edu/. ../EYE/CRNSCLRA.HTM

Chick corneal thickness evolves throughout embryogenesis, and continues to grow even after hatch, from 160 μm thick at hatch to 250 μm in the young hen (Hay and Revel, 1969). Chick development is discussed further in section 1.16.

1.3.1 Corneal Layers

The corneal epithelium is a major refractive surface, forming a barrier to fluid loss and pathogen invasion. These qualities require epithelial cells to tightly adhere to the underlying matrix, as well as to one another. The corneal epithelium must also retain a rapid, highly efficient, and well developed wound healing capability (Lanza, 2000). The epithelium represents 10% of corneal thickness and can be stratified into distinct layers; superficial cells are flattened, nucleated, non-keratinized squamous cells. Underlying these superficial cells are two or three layers of polygonal, wing-shaped cells, and an inner layer of cuboid basal cells (Pfister, 1973). The basal epithelial cells rest upon a thin basal lamina, which anchors the epithelium to Bowman's layer via a basement membrane complex; an attachment complex of anchoring fibrils (type VII collagen) and plaques (type VI collagen), which interact with the lamina densa and collagen fibrils of Bowman's layer (Pfister, 1973).

Superficial cells lie in two layers. Previous examination under the scanning electron microscope has revealed flat hexagonal cells attached by straight cell boundaries (Pfister, 1973). Numerous microvilli and microplicae project from the apical surface to enhance tear film adhesion to the glycocalyx (peripheral glycoproteins that attach themselves to the membrane). New cells are derived from mitotic activity in the basal cell layer, which displace existing epithelial cells every 24-48 hours both superficially and centripetally. The epithelium responds quickly to injury; cells on the wound margin slide across to maintain integrity, followed by cell replication (Pfister, 1973).

Bowman's layer is a modified acellular region of the stroma beneath the epithelium, constituting 4-5 μm in the adult hen (Hay and Revel, 1969), compared to around 10-12μm in adult humans. Often referred to as Bowman's membrane, this layer is not a true membrane at all, but a thin structure of compacted and disorganized short and thin hybrid type I and V collagen fibrils. Although these components are also found in the stroma, in Bowman's layer these fibrils are smaller in diameter and less uniform.

The corneal stroma is a dense connective tissue of remarkable regularity. It constitutes 90% of corneal thickness (Davson, 1990) and consists predominantly of approximately 2μm thick, flattened collagenous lamellae orientated parallel to the corneal surface (Komai and Ushiki, 1991) and continuous with the sclera at the limbus. Between the lamellae lie flattened, modified fibroblasts, or keratocytes. Keratocytes are stellate in shape with thin cytoplasmic extensions containing few distinctive organelles. As my work is concerned solely with stromal ultrastructure, this will be discussed in more detail at a later stage.

Descemet's membrane forms the modified basement membrane of the corneal endothelium, from which it can become detached. It occupies only 1% of total corneal thickness of adult chick corneas, around 2.5 μm (Hay and Revel, 1969) - this thickness is composed of two parts, one third the anterior banded zone; containing wide spaced collagen VIII strands, and two thirds posterior non-banded zone - granular and amorphous, attached to the stroma by a narrow interfacial matrix (Jakus, 1956). Descemet's is rich in glycoproteins and some collagens, types V and VI are implicated in maintaining stromal adherence (Pfister, 1973).

The endothelium is a simple squamous cell layer on the posterior surface of the cornea, critical in maintaining the correct hydration. The endothelium is a single layer of mostly flat hexagonal cells forming a mosaic pattern, 2-3 μm thick in the young hen or 0.8-1.2% of corneal thickness (Hay and Revel, 1969). These regularly arranged cells have a long life but low regenerative capacity, lost cells are quickly replaced by spreading of adjacent cells. With age, the endothelial cell population density decreases, and the variability in cell shape and size increases to maintain membrane integrity. The biological activity of the endothelium is very important; this layer governs fluid and solute transport across the posterior surface of the cornea and actively maintains optimum conditions for corneal transparency, and to this end, endothelial cells contain many mitochondria. If the endothelial pump fails, too much water leaks into the stroma and the precise arrangement of collagen fibrils is disturbed, leading to a loss in transparency (Stiemke *et al.* 1992). In fact, the cornea contains the most water of all connective tissues, human corneal hydration is about 78% (Maurice, 1970). Corneal proteins contribute to 20% of tissue mass. This dry mass is primarily collagens, but also glycoproteins and other soluble proteins. Critically, collagen provides the strength to resist intraocular pressure and maintain optimal curvature for light refraction.

1.4 Corneal Collagen

The collagen superfamily constitutes a quarter of total mammalian protein content (Marshall *et al.*, 1993) and has been extended to 27 members in vertebrates (Pace *et al.*, 2003). This family is defined according to characteristics, which are summarised in table 1.1.

Group	Collagen type
Fibril forming collagens	I, II, III, V, XI, XXIII, XXIV, XXVII
Fibril associated collagens (facit-s)	IX, XII, XIV, XVI, XIX, XX, XXI, XXII,
Non-fibrillar collagens	
Short chain collagens	VIII, X
Basement membrane collagen	IV
Anchoring fibrils	VII
Microfibrillar	VI
Collagens with transmembrane domains	XIII, XVII, XXIII, XXV
Other collagens	XV, XVI, XIX, XVIII
Non collagenous molecules with collagen-type triple helices	C1q of complement A special form of acetylcholinesterase Scavenger receptor of macrophages

Table 1.1. Vertebrate collagen groups, *adapted from*: (Robert *et al.*, 2001) and (Pace *et al.*, 2003)

Collagens are characteristic components of the extracellular matrix, involved in various structural, developmental and physiological functions, and in a wide range of connective tissues such as cornea, bone, cartilage, skin and blood vessels. The different types are closely related and always characterised by three subunit polypeptide α-chains, and a distinctive triple-helical conformation in at least one of the domains. Each of the known 40 distinct collagen α-chains is unique and relies on specific amino-acid sequences, coded by different genes. The triple-helical domain occupies more than 95 % of a fibril-forming collagen molecule.

Collagens commonly self-assemble into fibrils (Kadler *et al.*, 1987), however some collagen molecules associate in a non-fibrillar fashion, specific to biological function (Marshall *et al.*, 1993). These non-fibril forming collagens contain only short segments of triple helix domains, with the rest of the molecule incorporating non-triple helical structural motifs, often composed of non-collagenous proteins, which can form bridges to bind other proteins, or complex protein aggregates such as basement membranes. Accordingly, there are clear chemical and ultrastructural differences associated with collagen type; so that the function, and localisation (both temporal and tissue) of each collagen is very specific.

1.5 Collagen biosynthesis

The pathway of collagen biosynthesis is an intricate combination of temporal and spatial biochemical events. For ease of reading, the following section refers to collagen type I, which is most relevant to this thesis, and has been extensively studied and considered to be a prototypical collagen. There is some variation, but pathways are likely to be generic with specialised collagens undertaking additional steps for more complex biosynthesis; for example the processed form of fibrillar type V collagen retains a large N-terminal domain, and is believed to play an important role in fibril diameter control (Birk, 2001). Recent studies suggest that triple-helical regions have structures and properties specific for each type. The characteristic features of the various collagens result from differences in charge distribution along the triple helix, content of glycosylated hydroxylysine and bulky hydrophobic residues, as well as imperfections in the Gly – X - Y repeat, which is a prerequisite for the triple-helical conformation (Hayashi and Mizuno, 1999).

Most collagen genes encode procollagen, an immature form of the collagen molecule with increased molecular weight. Collagen mRNA translation products are directed on the rough endoplasmic reticulum (ER) within stromal keratocytes, where the three α-chains are synthesised and combined into procollagen (Mathews and van Holde, 1995).

The post-translational processing of fibrillar collagens can be regarded in two stages. Intracellular modifications combined with polypeptide synthesis form the triple helical procollagen molecule (Prockop and Kivirikko, 1995; Kadler 1995). Extracellular processing renders the collagen molecule from its precursor, and incorporates collagen molecules into stable, crosslinked fibres or other supramolecular aggregates. Post-translational modifications are a critical determinant to collagen structure, and therefore function. Triple helix stability arises from hydrogen bonding involving hydroxyproline residues, which are produced via the enzymatic hydroxylation of proline (Hay, 1991). Crosslinks which serve to stabilise within and between collagen molecules are formed from the hydroxylation of lysine residues.

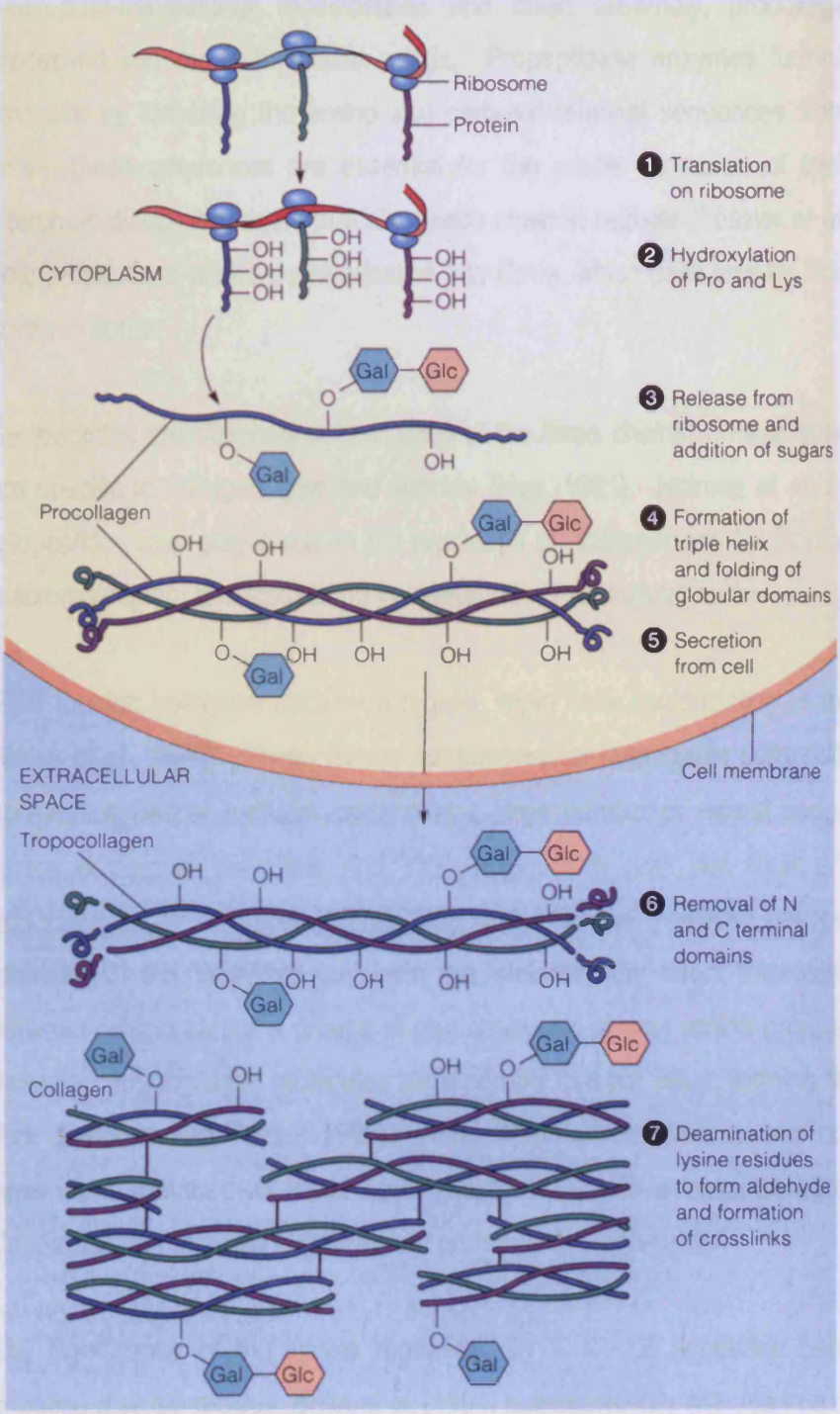

Figures 1.3(A) left and (B) right Stepwise biosynthesis of type I collagen.

(A) Biosynthesis and assembly of collagen, steps 1-4 occur in cytoplasm, 6 and 7 in the extracellular region of collagen-synthesising cells. Gal = galactose, Glc = glucose.

(B) Electron micrograph: Production of collagen molecules and assembly into fibrils, (2) Post translation modification and procollagen assembly in the ER. (3) Transportation of procollagen molecules through the Golgi complex and secretion into the extracellular space. (4) Production of collagen molecules and assembly into fibrils. (Magnification x44000)

Taken from: (A) Mathews and van Holde, 1995, and (B) Comper, 1996

After post-translational modifications and chain assembly, procollagen is secreted and processed into the extracellular matrix. Propeptidase enzymes further modify procollagen structure by removing the amino and carboxyl terminal sequences from both ends of each chain, these sequences are essential for the proper formation of triple chains: they form interchain disulphide bonds that align each chain in register (Fessler *et al.*, 1975). Excision of both propeptides allows polymerisation into fibres, which pack side by side into parallel fibrils – collagen fibrils.

Telopeptides are attached at both ends of the three chains. These short non helical regions are specific to collagen type and species (Hay, 1991). Holmes *et al.* (1998) suggested that telopeptides may play a role in the regulation of fibrillogenesis by binding extracellular matrix macromolecules, and also acting to stabilise the extracellular matrix.

Fibril forming collagens assume a regular, triple helix conformation in the extracellular space (Wess *et al.*, 1998). These fibrous supramolecular aggregates comprise of three left-handed polypeptide helical α-chains containing a large number of repeat sequences, Gly – X – Y, where commonly X=Proline and Y=Hydroxyproline (van der Rest *et al.*, 1990). These tropocollagen triple helices (300nm long and 1.5nm in diameter) rely on the regular primary structure of the tripeptide unit, and are stabilised by direct interpeptide hydrogen bonds between proline carbonyl groups of one chain and glycine amino groups of another. Several thousand tropocollagen molecules align parallel to each other, forming the individual collagen fibre (Branden and Tooze, 1998). Within flattened lamellae, normal corneal collagen fibres have been assumed to adopt liquid like packing, with a quasi-hexagonal array (Wess and Cairns, 2005), mediated in part by key proteoglycan molecules.

The significance of the simple repeating Gly – X – Y sequence becomes apparent after mutating a single residue; Bella *et al.* (1994) substituted Gly with Ala in a collagen-like synthetic peptide, resulting in crystal rather than fibril formation. Gly is essential for triple-helix formation; it occurs every third residue along the helix, at a distance of 8.6 nm from one to the next (Ottani *et al.*, 2002). Gly packs tightly at the tropocollagen core, thus, a small molecular size facilitates collagen triple-helix monomer structure. Collagen primary structure is tissue and type specific.

Collagen molecules in 36nm diameter fibrils are organised into 4nm diameter microfibrils, packed with a centre to centre spacing of approximately 4.1nm (Holmes, *et al.* 2001). These

microfibrils are tilted by ~15° to the fibril axis in a right handed helix (Holmes *et al.,* 2001), and assume a quasi-hexagonal lattice (Orgel *et al.,* 2001). Interfibrillar and intermolecular cross-links confer stability adding tensile strength. Orgel *et al.,* (2006) recently suggested that collagen structure is similar to a rope network, where each element of the array transmits force across the entire array via lysine-hydroxy-lysine mediated crosslinks. Each microfibril is thought to contain two to three intermicrofibrillar crosslinkages (Piez and Trus, 1981; Nakamura, 1987), and also one intramicrofibrillar linkage. Microfibrils are thought to maintain structural stability through a right-handed supertwist, which may allow collagenous structures to absorb torsion effects without disruption of the superhelix (Orgel *et al.*, 2006).

Collagens may be homo- or heterotypic, i.e. collagens assembled from three identical α-chains. Conversely, two identical chains and one different chain may make up the collagen, in the case of type I, or ($\alpha1(I)_2\alpha2(I)$). The specific triple helical structure was finally characterised by Ramachandran and Kartha in 1954, early interpretations of fibre diffraction studies established that each of the three polypeptide chains is folded into an extended left handed helix, which in turn coil around a central axis to form a right handed superhelix (Ramachandran and Kartha, 1955). This characteristic coiled-coil structure is stabilised by inter- and intramolecular cross-links, hydrogen bonding between the three chains, and electrostatic interactions between the helices (Hay, 1991).

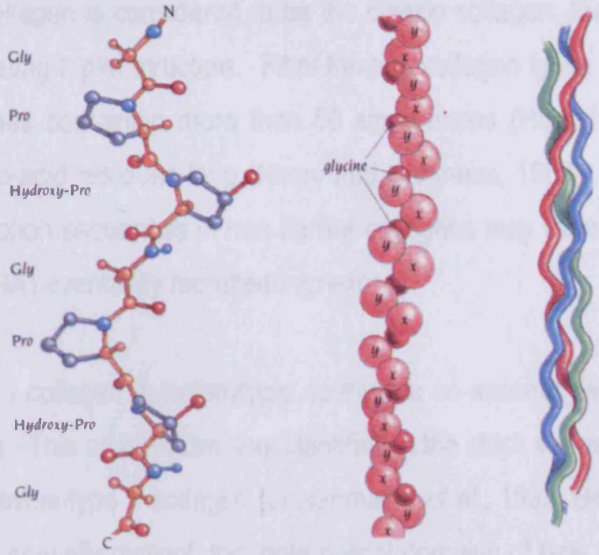

Figure 1.4 (A), (B) and (C): The collagen molecule triple helix. (A) Ball and stick model of two turns of one polypeptide chain. (B) A model of one collagen chain in which each amino acid is represented by a sphere. (C) A small part of the collagen superhelix in which the three chains have a different colour. *Taken from:* Branden and Tooze (1998) pp 284.

A prominent feature of collagen fibrils in the mature stroma is the presence of macromolecules on the fibril surface, current research implies they are proteoglycans (Holmes *et al.*, 2001), believed to regulate collagen interfibrillar spacing and diameter.

1.6 Different classes of collagens in cornea

Traditionally, collagen is attributed to an architectural role; the detailed structure of collagen fibrils underpin the mechanical properties and organisation of the cornea. Corneal function is dependent on the regular spacing of collagen fibrils – interfibrillar distance, which is in turn regulated by glycosaminoglycans (GAGs) and proteoglycan bridges amid collagen fibrils. Stromal collagen fibres are principally heterotypic type I and V mixtures (Newsome *et al.*, 1986), although some type III, VI and XII are interspersed between GAGs, predominantly keratan and chondroitin sulphates. GAG interaction will be discussed later.

Depending on molecular characteristics such as size, structure or supramolecular organisation, collagens are classified into families. Collagen molecules within each family have a similar genomic structure, having commonly evolved from a primordial parent gene by several duplications (Buttice *et al.*, 1990). Currently, collagen classification is based on exon structure – the regions of DNA within a gene retained within the final mRNA molecule.

Type I fibril forming collagen is considered to be the classic collagen, that is characterised by an uninterrupted repeating triplet structure. Fibril forming collagen types I, II, III, V and XI are encoded by large genes containing more than 50 small exons (Hay, 1991), forming chains more than 1000 amino-acid residues long (Nimni and Harkness, 1987). Buttice *et al.* (1990) postulated that interruption sequences in non-fibrillar collagens may have evolved from introns (non-protein coding DNA) eventually recruited into exons.

In corneal tissue type I collagen is heterotypic, forming a co-assembly with type V within the same fibril (Birk, 2001). This architecture was identified in the chick stroma by disrupting hybrid collagen I/V fibrils to reveal type V collagen (Linsenmayer *et al.*, 1983, Birk *et al.*, 1988). Each collagen type remains spatially distinct; the triple-helical domains of type I molecules are found within and at the surface of the fibril, whereas triple helices of type V are only located within the fibril. The large NH_2 terminal tyrosine-rich domain of type V extends outwards through the gap zone to the fibril surface, proposed to abrogate addition of other collagen molecules to the fibril surface (Linsenmayer *et al.*, 1993).

1.7 Fibril forming collagens in the developing avian cornea

As the main focus of this thesis relies on the structure of fibril forming collagens, the main stromal collagen types I, II, III and V found in the developing chick cornea are summarised below:

Type I

Type I is a fibril forming collagen normally synthesised by stromal keratocytes (Ruggiero *et al.*, 1996) in the (corneal) extracellular matrix. Type I is the most abundant collagen type in many connective tissues, with the strongest fibrillar structure conferring tensile strength. In the avian cornea, it is present as a heterotypic structure with type II collagen in the primary stroma, and with type V collagen in the secondary stroma (Birk *et al.*, 1988; Hendrix *et al.*, 1982).

Type II

Transient type II expression is reported in several tissues during embryonic development (Cheah *et al.*, 1991), although it is mostly found in cartilage (Miller and Matukas, 1969). Type II collagen is detectable in the avian primary stroma, where it forms heterotypic structures with

type I and is covalently linked to type IX (Fitch *et al.*, 1994). After mesenchymal cell invasion, levels decrease to become undetectable when the stroma condenses (Cai *et al.*, 1994).

Type III

Type III is a fibril forming collagen synthesised by the keratocytes (Nakaysu *et al.*, 1986), and associated with the stromal lamellae and epithelial substratum. Type III collagen is necessary for function, adhesion and tissue properties, although an age related decrease is not detrimental to transparency (Schmut, 1977)

Type V

Type V is an abundant fibril forming collagen synthesised by stromal keratocytes (Ruggiero *et al.*, 1996), originally thought to be synthesised *in situ*, at the stromal-epithelial and stromal-endothelial interface (Newsome *et al.*, 1982). A regulatory role in the avian secondary stroma is proposed, as part of heterotypic collagen fibrils with type I collagen (Birk *et al.*, 1988; Linsenmayer *et al.*, 1983). Type V is thought to have various functions, such as anchoring basement membranes to their underlying stromal matrix or control of collagen fibril diameter within the stroma (Birk *et al.*, 1990). Birk's *in vitro* fibrillogenesis study (1990) illustrated the importance of this relationship, average heterotypic fibril diameter decreases as type V collagen levels fall in a mixture of type I and V collagens. Collagen fibril diameter is also corrupted in a naturally occurring mutation increasing type V collagen in humans (Wenstrup *et al.*, 1996), and mutations in type V collagens genes were found to cause floppy eyelids, corneal thinning, decreased collagen deposition, increased fibril diameter and decreased fibril density in the mouse (Birk *et al.*, 2006).

Collagen expression is specific throughout corneal layers, as summarised in figure 1.5.

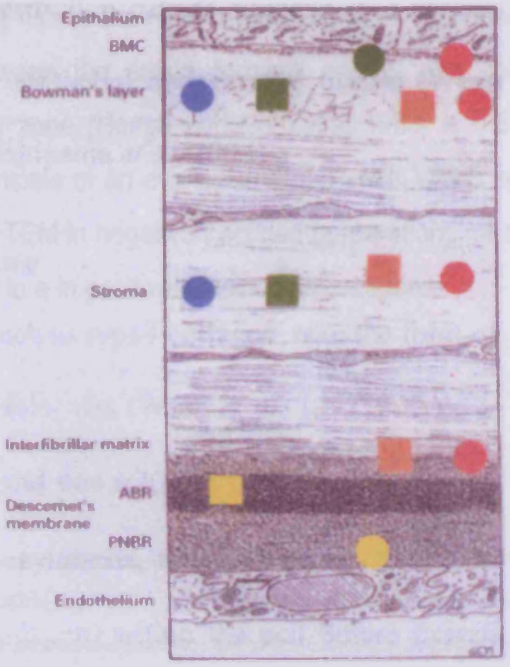

Figure 1.5. Summary diagram of the human corneal collagens. Collagens I (blue circle), III (green square), V (orange square) and VI (red circle) are evenly distributed through Bowmans layer and the corneal stroma. Types V (orange square) and VI (red circle) are also present in the interfacial matrix. Type IV collagen (yellow circle) is present in Descemets membrane. Both types VI (red circle) and VII (green circle) are present in the basement membrane complex (BMC) immediately underneath the epithelium. Type VIII collagen (yellow square) is present in the anterior banded region (ABR) of Descemets membrane. PNBR is the posterior non-banded region. *Taken from:* Marshall *et al* (1993).

1.8 Collagen Fibrillogenesis

Collagen fibrillogenesis describes collagen molecule assembly and packing into fibrils. Collagen molecules within fibrils in tendons and bones are staggered longitudinally by a 67nm axial translation called the D-periodicity (Hodge and Petruska, 1963). Tissue specific axial periodicity is seen in cornea and skin, which is closer to 65 nm (Marchini *et al.*, 1986). These different banding patterns arise from the angular arrangement within collagen fibrils; in C-type fibrils found in the cornea, collagen molecules run around the fibril axis at an angle of ~15° (Holmes *et al.*, 2001), whereas in highly tensile structures T-type fibrils run straighter at an angle of ~5° (Ottani *et al.*, 2001).

The quasihexagonal packing of collagen molecules is continuous and uninterrupted because neighbouring N- and C- terminal-containing molecular segments are contained within neighboring microfibrils, rather than being internally directed within the microfibril (Orgel *et al.*, 2006). Adjacent monomers overlay each other by 234.2 ± 0.5 amino-acid residue overlaps

(Meek *et al.*, 1979), giving rise to the 67-nm wide D-period, the basic repeat structure of the fibril. The distance between the amino terminal end of one collagen molecule and its successor, called the gap zone (Hodge and Petruska, 1963) is 0.6D (Meek and Quantock, 2001). Each D-period consists of an overlap and gap zone, which appear as alternating light and dark bands under the TEM in negatively stained preparations, or as a pattern of fine cross-fibril bands ranging from a to e in positively stained preparations.

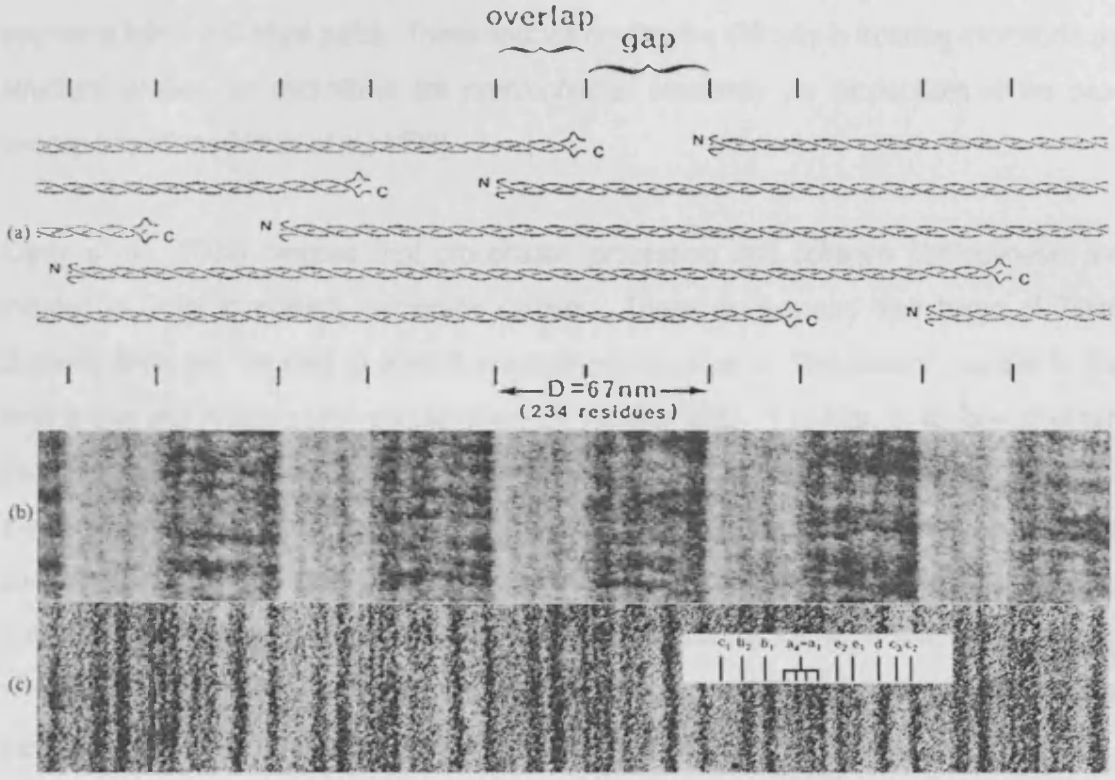

Figures 1.6A, B and C. Axial structure of *D*-periodic collagen fibrils. (A) Schematic representation of the axial packing arrangement of triple-helical collagen molecules in a fibril, as derived from analysis of the positive (C) and negative (B) staining patterns. (B) Collagen fibril negatively stained with sodium phosphotungstic acid (1%, pH 7). The fibril is from a gel of fibrils reconstituted from acetic-acid-soluble calf-skin collagen. The repeating broad dark and light zones are produced by preferential stain penetration into regions of lowest packing (the gap regions). (c) Similar fibril positively stained with phosphotungstic acid (1%, pH 3.4) and then uranyl acetate (1%, pH 4.2). The darkly staining transverse bands are the result of uptake of electron-dense heavy-metal ions from the staining solutions on to charged residue side groups of collagen. *Taken from:* Kadler *et al.*, (1996)

Proposed three-dimensional organisation of collagen molecules has evolved with scientific method. The first five-stranded microfibrillar model proposed by Smith (1968) described collagen molecules laterally packed perpendicular to the fibril axis, and then developed by Piez

and Trus on the basis of sequence regularities and X-ray diffraction data (1978, 1981). Intermediate structures termed microfibrils also followed Smith's original theory (Miller and Parry, 1973), then later models interjected an hexagonal quasi-crystalline supramolecular arrangement, called sheet structures (Hulmes and Miller, 1979).

A more recent model developed by Wess *et al.* (1998) suggests that type I collagen fibrils are composed of five left-handed stranded microfibrils; although there is a difference between the overlap zones with tight quasi-hexagonal packing, and disordered gap zones where molecular segments follow individual paths. These findings confirm the difficulty in isolating microfibrils as structural entities, as microfibrils are interconnected covalently via telopeptides at the gap-overlap transitions (Wess *et al.*, 1998).

Canty *et al.* (2004) propose that procollagen processing and collagen fibrillogenesis are initiated in Golgi to plasma membrane carriers. These carriers and their cargo of 28nm diameter fibrils are targeted to plasma membrane protrusions or "fibripositors", parallel to the tendon axis and projected into parallel channels between cells. The base of fibripositor lumen (buried several microns within the cell) is a nucleation site of collagen fibrillogenesis, the tip of the fibripositor is the site of fibril deposition to the matrix. Fibripositors are absent at murine postnatal stages when fibrils increase in diameter by accretion of extracellular collagen, thereby maintaining parallelism of the tendon. Kadler's group in Manchester imply that the parallelism of tendon is determined by the late secretory pathway and interaction of adjacent plasma membranes to form extracellular channels (Canty *et al.*, 2004).

Three-dimensional organisation studies in adult bovine corneal fibrillar collagen molecules nominate each collagen fibril as consisting of ~4nm diameter right-handed microfibrils, all tilted by an angle of ~15° to the fibril axis, irrespective of radial position within that fibril (Holmes *et al.* 2001). The lateral packing of these microfibrils varies according to position along the D-period; an ordered hexagonal arrangement was found at the C- and N- telopeptides and within gap zones, where extracellular macromolecules would tend to bind fibrillar sites, although molecular packing was more disordered in other regions along the D-period. A recently published study by Orgel *et al.* (2006) investigated microfibrillar structure of type I collagen, to find that neighbouring collagen strands are arranged to form a supertwisted (discontinuous) right-handed microfibril that interdigitates with other neighbouring microfibrils. This interplay

creates the crystallographic superlattice, formed from quasihexagonally packed collagen molecules.

1.9 FACIT

Fibril associated collagens with interrupted triple helices, FACITs, share a common multiple triple helical domain interrupted by non-triple helical domain motif. Recently discovered FACITs bolster the current family number to seven; namely collagens IX, XII, XIV, XVI, XIX, XX and XXI (Fitzergerald *et al.*, 2001; Koch *et al.*, 2001; Gordon *et al.*, 1989). FACIT structure is integral to function - several domains are strategically organised, hence some domains lie along fibrillar surfaces while others extend outwards from fibrils to interact with adjacent fibrils and matrix components. These ranging domains allow interaction with fibril-forming collagens and other matrix components, however, the precise supramolecular arrangement has yet to be established. The reader is referred to papers of interest concerning the avian stroma given in table 1.2.

FACIT	Notes	Paper
Type IX	• Immunochemically detected on surface of fibrillar type II structures • Implicated in stabilising primary corneal matrix • Noticeably absent at time of stromal swelling • Two isoforms detected in primary stroma	Fitch *et al.*, 1998; Fitch *et al.*, 1988 Cai *et al.*, 1994 Fitch *et al.*, 1998 Fitch *et al.*, 1995
Type XII	• Distribution pattern suggests involvement in cell-matrix interactions in epithelial and stromal tissues • Strengthening association with fibrils containing types I and II • Long and short forms expressed in several tissues during embryogenesis; localised in the primary and secondary stroma at variable temporal and spatial locations • Implied in fibril organisation • Long, but not short form carry GAGs • Long form in bovine and human and bovine stroma, also human epithelial basement membrane and Bowmans layer	Wessel *et al* 1997 Akimoto *et al.*, 2002 Kato *et al.* 2000 Wessel *et al.* 1997
Type XIV	• Sister structure to type XII • Interacts with adjacent cells and ECM components • Strengthens architecture with types I and II • mRNA can be differentially spliced, forming "long" or "short" form polypeptide • Thought to regulate fibrillogenesis in the developing chick	 Chiquet *et al.*, 1998; Gordon *et al.*, 1987 Young *et al.*, 2002
Type XX	• Weak expression; minor quantities found in embryonic chick connective tissues • More prevalent in corneal epithelium, thought to be expressed in a similar way to type XII	Koch *et al.*, 2001

Table 1.2. FACITs

1.10 Other collagens

Descriptions of other non-fibril forming collagens found in the chick cornea are provided in table 1.3.

Collagen	Notes	Paper
Type IV	• Network forming structural component of basement membranes, non fibril forming • Ubiquitous insulators, found between Descemets and stroma in developing chick • Promotes adhesion of Descemets, stroma and endothelium • Present in two forms; stromal strings and plaques of basement-like material	Linsenmayer *et al.*, 1998 Fitch *et al.*, 1991 Fitch *et al.*, 1991
Type VI	• Synthesised by keratocytes, component of mature secondary corneal stroma • Appears at the time of fibroblast invasion • Common association with type I suggesting bridging properties, filamentous	Linsenmayer *et al* 1986 Bonaldo *et al* 1990
Type XVII	• First identified in avian cornea • Thought to be involved in hemidesmosomal attachment in avian cornea	Marchant *et al.*, 1991, Linsenmayer *et al.*, 1998; Gordon *et al.*, 1997
Type VII	• Major component of anchoring fibrils • Present at epithelial stromal interface	Burgeson *et al.*, 1990, Linsenmayer, 1996,
Type VIII	• Belongs to class of small collagens half the size of fibrillar collagens • Found in Descemets, consisting of small molecules forming hexagonal network	Yamaguchi *et al.*, 1991, Linsenmayer *et al.*, 1998
Type XXIII	• First identified as BP180 • Related to collagens VIII and XV • Thought to be involved in production/assembly of Descemets, and enhance stability of interfacial matrix • mRNA present in endothelium and epithelium, but only trace in stroma. • Author postulates therefore not involved in transparency	Koch *et al.*, 2006

Table 1.3. Other corneal collagens.

1.11 Collagen Packing

Collagenous lamellae form a highly organised orthogonal tier, in which adjacent lamellae are orientated at approximate right angles, with the exception of the anterior third in which the lamellae display a more slanted orientation. The highly ordered fibrillar structure of collagen, and avascular nature of the tissue confers basic transparency.

Flattened collagenous lamellae extend from limbus to limbus, crossing the apex of the corneal dome. Collagen lamellae in the anterior third of the human stroma are thin; 0.2-1.2μm thick and 0.5-30μm wide, running obliquely to the corneal surface (Komai and Ushuki, 1991). These

bands sometimes split into 2-3 sub layers which become interwoven, conferring cohesive and tensile strength. Conversely, collagen lamellae in the posterior stroma tend to be arranged parallel to the surface and are thicker; 1.0-2.3μm thick and 100-250μm wide, perhaps a causative factor in the absence of interlacing. There is no comparable in-depth study of the chick cornea as yet, although Connon *et al.* (2003) has carried out an electron microscopy study to examine collagen compaction in the final stages of development, which will be discussed later in chapter 3.

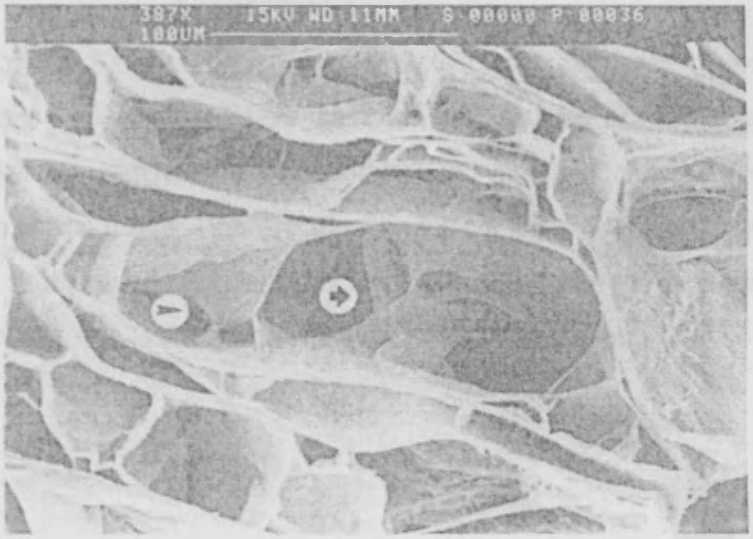

Figure 1.7. Lamellar organisation in the cornea; interlamellar spaces give a polymorphic honeycomb appearance - lamellae appear as cross-sectioned sheets. A large interweaving zone (arrow) can be seen in the central interlamellar opening, in which several types of interlacing are found close together. To the left of this zone a lamella crosses upwards through a larger one (arrow head). *Taken from:* Radner and Mallinger, (2002) Cornea 21: 6, pp598-601.

The lamellae have no limiting membrane and are connected by several methods:

i. disulphide cross links (between collagen fibrils)

ii. fibrils woven into adjacent lamellae

iii. lamellae split into 2-3 sub layers which later interlace

Collagen arrangement is not uniform. Lamellae in the anterior portion of the cornea run in random directions, often oblique to the surface and are irregularly interwoven. Lamellar bundles in the central section of the cornea cross irregularly and form interlaced networks. In contrast, lamellae in the posterior region are piled up parallel to the corneal surface. These layers run across their neighbours at varying angles, often dividing into smaller components

that later merge with adjoining layers. An interesting future study would be to investigate collagen at the periphery of the chick cornea using SEM.

1.12 Proteoglycans

The extracellular matrix of the corneal stroma is principally composed of collagen fibrils stacked in orderly lamellae, a feature fundamental to corneal transparency. The small leucine-rich proteoglycans, SLRPs are a well documented factor governing collagen fibril spacing and diameter within the ECM (Chakravati *et al.*, 1998, Quantock *et al.*, 2001, Carlson *et al.*, 2003).

PGs are hybrid molecules consisting of a protein core covalently bound to one or more polysaccharide GAG chains. There are two major classes of stromal proteoglycans, one possessing keratan sulphate (KS) side chains, and the other chondroitin/dermatan (CS/DS) sulphate side chains (Iozzo, 1999). Proteoglycans can be distinguished from glycoproteins by core protein structure; sugar chains are longer, less variable and non-branching; and more acidic in character, due to sulphation and a strong negative charge.

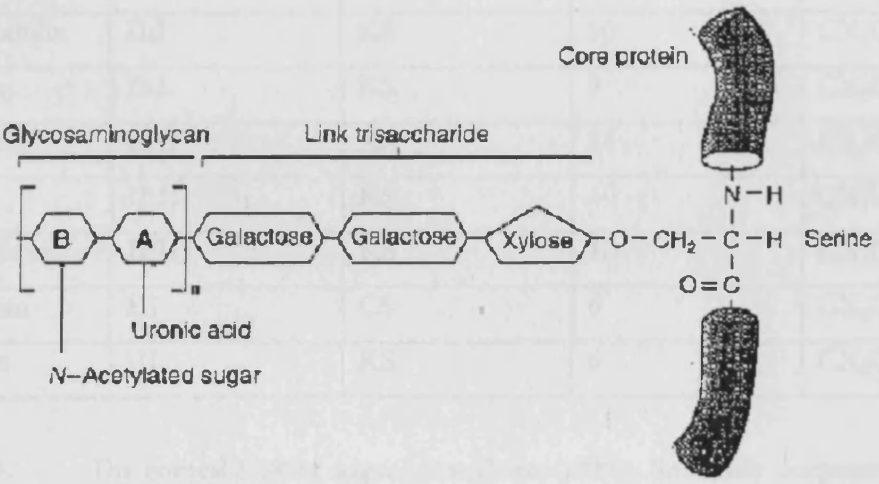

Figure 1.8. Proteoglycan structure. GAG chains extend assuming a bottle-brush conformation. Each PG molecule has a protein core and GAG side chains of keratan sulphate and chondroitin sulphate linked to a hyaluronic acid backbone and link protein (not shown) which increases the bonding strength. *Adapted from* : www.dentistry.leeds.ac.uk

Proteoglycans are largely ubiquitous, found within intracellular vesicles, on the surface of the cells and in the extracellular matrix. These long unbranched glycans are the most abundant heteropolysaccharides in the body; SLRPs form a twelve-member superfamily, synthesised

either as glycoproteins or as CS/DS or KS containing proteoglycans (Iozzo, 1999). The first members of this family to be cloned were decorin and biglycan (Fisher *et al.*, 1989; Krusius and Ruoslahti, 1986), instigating a wealth of discoveries including fibromodulin (Oldberg *et al.*, 1989), epiphycan or proteoglycan-Lb (Shinomura and Kimata, 1992), lumican (Blochberger *et al.*, 1992), keratocan (Corpuz *et al.*, 1996); mimecan or osteoglycin (Funderburgh *et al.*, 1997; Madisen *et al.*, 1990); PRELP (Bengtsson *et al.*, 1995) and osteoadherin (Wendel *et al.*, 1998). New members have recently been added to this expanding group; namely iris specific oculoglycan (Friedman *et al*, 2000), opticin (Reardon *et al*, 2000) and asporin (although not a proteoglycan) (Henry *et al*, 2001; Lorenzo *et al*, 2001).

Three classes of SLRPs have been identified based upon evolutionary protein conservation, the presence of a cysteine-rich cluster in the N-terminal region and their genomic organisation. Structural classifications of corneal SLRPs are shown in table 1.4.

Proteoglycan	Class	GAG chain(s)	Number of LRRs	N-terminal sequence
Decorin	I	CS	10	CX_3CXCX_6C
Biglycan	I	CS	10	CX_3CXCX_6C
Fibromodulin	II:I	KS	10	CX_3CXCX_9C
Lumican	II:I	KS	9	CX_3CXCX_9C
Keratocan	II:II	KS	11	CX_3CXCX_9C
PRELP	II:II	KS	10	CX_3CXCX_9C
Osteoadherin	II:III	KS	10	CX_3CXCX_9C
Epiphycan	III	CS	6	CX_2CXCX_6C
Mimecan	III	KS	6	CX_2CXCX_6C

Table 1.4. The corneal SLRPs, *adapted from:* (Iozzo 1999). Subfamily designation is shown for class II, X represents any amino acid in the N-terminal sequence.

The molecular size of the PG core protein varies from 36 to 40 kDa, with some amino acid sequence homology (Blochberger *et al.*, 1992). The core proteins have 9-12 Leu-rich motif repeats in the C-terminal end, which probably confers their collagen-binding properties. Conversely, the N-terminal end shows high variability in both amino acid sequence and glycosylation (Neame *et al.*, 1989). The N- and C-terminal domains are suggested to be involved in the protein-protein, cell-cell and cell-matrix interactions (Inatani, 2002). Although

SLRPs share more than 70% similar leucine-rich motifs repeats (LRR) in the central domain of their protein core, there is no amino-acid sequence common to all protein cores.

Current literature suggests that the three-dimensional structure of proteoglycans very similar to an intracellular protein called the ribonuclease inhibitor (Weber *et al.*, 1996). The leucine-rich motifs create a horseshoe shaped coil of parallel alternating α-helices and β-sheets, stabilised by interchain H-bonds, which interact with collagen molecules through their concave surface - the space inside the horseshoe is able to accommodate a single triple helix of collagen (Weber *et al.*, 1996).

The proteoglycan protein core is made on membrane bound ribosomes in the keratocytes. GAGs are then attached to the protein core via specific tetrasaccharide sequences, and the proteoglycans secreted into the extracellular matrix, as explained in section 1.12.3. The biological functions of proteoglycans are primarily derived from the GAG and protein component of the molecule, as outlined in section 1.12.1 below.

1.12.1 Glycosaminoglycans, GAGS

GAGs are sulphated carbohydrate polymers composed of 40-100 repeating disaccharide units held together by molecular bonds (Scott 1992), routinely based on uronic acid (or galactose) and hexosamines. KS is either N-linked to Asn residues (in cornea), or O-linked to Ser or Thr (in skeletal tissues) (Funderburgh *et al.*, 2000). An additional linkage Man-O-Ser is also indicated, present in brain tissue (Krusius and Rouslahti, 1986).

GAGs assume extended structures in aqueous solutions because of their strong hydrophilic nature. This is a result of extensive sulphation, which is further exaggerated when GAGs are covalently linked to core proteins, which will be further discussed later. The two major GAGs of the corneal stroma are KS and CS, responsible for unique proteoglycan function. One of the two sugars in the repeating disaccharide unit is always an amino sugar (where an acetyl group $COCH_3$ is attached to N of the amino group), an N-acetylhexosamine, either N-acetylglucosamine or N-acetyl galactosamine. The different GAGs may be distinguished by various sugar residues and their linkage, as well as the possible location and number of sulphation sites.

Sulphation of GAGs in CS chains is usually regular, one sulphate per disaccharide throughout the chain. Conversely in corneal heparan sulphate chains, sulphation is irregular, resulting in intensely and sparsely sulphated regions on a single GAG chain. In addition to GAGs, proteoglycans normally have other carbohydrate units including O-linked and N-linked oligosaccharides, as found in other glycosylated proteins.

Carboxyl (COO^-) groups are usually bound to C-6 of the uronic acid sugar, and sulphate ester ($CH_2OSO_3^-$) groups found O-linked to various sugar residues, hexosamine and/or uronic acid sites of a particular GAG. Therefore, under physiological conditions, GAGs exhibit a varying sulphation level and a high negative charge, allowing electrostatic interaction and PG association with other macromolecules. Polyanionic GAG sulphation is considered critical to the maintenance of the collagen matrix; electrostatic forces exert a repulsive force on neighbouring fibrils, thus contributing to interfibrillar spacing (Scott 1992). GAGs also hold a large number of water molecules in their molecular domain and occupy enormous hydrodynamic space in solution, essentially forming an aqueous gel to bear compressive forces (Kreis and Vale, 1993).

1.12.2 Keratan Sulphate, KS

Keratan sulphate is the principal stromal GAG, making up 50% of total GAG content in mature chick cornea (Anseth, 1961). First identified by Suzuki in 1939, KS is present as one of three isoforms in mammalian tissues, defined by their linkage to the PG core protein. Linkage of corneal KS to the protein core involves a complex-type biantennary oligosaccharide N-linked to asparagine (Choi and Meyer, 1975) in the core protein as shown in figure 1.9.

A. Corneal KSI

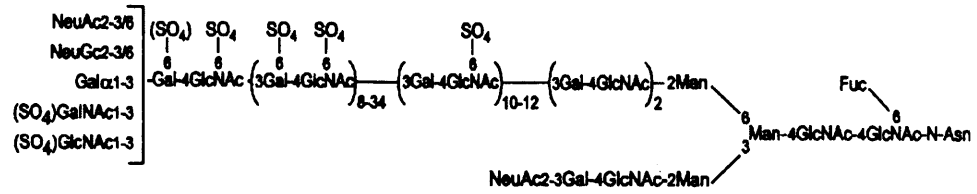

B. Articular Cartilage KSII

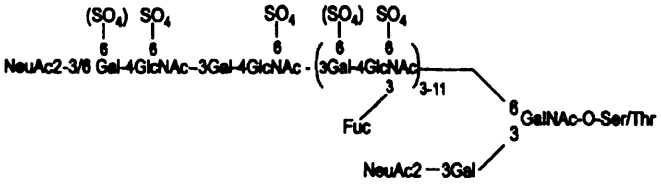

Figure 1.9. Summary of Keratan Sulphate structure. Numbers to the lower right of the large parenthesis show approximate number of N-acetyllactosamine monomers in each domain. Numbers separated by a forward slash present optional attachment locations. Sulphates in parentheses indicates partial or incomplete sulphation of monomers at this site. *Adapted from:* Funderburgh (2000)

Originally, KSI and KSII were designated according to differences between cornea and cartilage. In time however, this system has evolved and class designations are now applied with respect to linkage structure. Corneal KS is the prototype for KSI, and the most extensively characterised. KSI is found in small proteoglycans such as lumican, and expressed in quantities 10-times those found in cartilage (Funderburgh *et al.*, 1987). KSII is found in large proteoglycans of skeletal tissues attached through an oligosaccharide structure O-linked to hydroxyl groups of serine or threonine residues of the core protein (Choi and Meyer, 1975).

The commonly accepted model for KSI structure (shown in figure 1.9), developed by Oeben *et al.*, (1987) found that in porcine corneal KS, the C-3 branch of the linkage oligosaccharide ends with a single lactosamine capped by sialic acid. However, subsequent work (Nilsson *et al.*, 1983, Tai *et al.*, 1996), and particularly that of Jim Funderburgh (1991) suggests that both mono- and bi-antennary extensions of the linkage region exist for KS type I.

KSI contains short repeats of N-acetyglucosamine (GlcNAc) and galactose (Gal), usually sulphated at every sixth position (C6) of the acetylglucosamine unit, but also sometimes on the sixth position of the galactose (Hounsell *et al.*, 1986). Funderburgh (2000) has implied that N-sulphation of N-glucosamine (GlcN) may also exist in corneal KS. The reducing-end

disaccharides are exceptional, as they are never sulphated. In fact the degree of KS sulphation also varies between species (Scott and Haigh, 1988; Young *et al.*, 2005).

1.12.3 Keratan sulphate biosynthesis

Glycosyltransferase enzymes elongate the KS polymer by alternately adding Gal and GlcNAc residues (Funderburgh *et al.*, 2000). Galactose-transferase activity increases in parallel with KS biosynthesis during embryonic chick development, and is maintained at an unusually high level in adult cells (Cai *et al.*, 1996). Although the ß-1, 4-galactosyl transferase 1 enzyme appears to be involved in corneal KS synthesis, this specific enzyme has not been linked to KS biosynthesis in other tissues. No N-acetylglucosamine transferase enzyme has yet been linked to KS biosynthesis (Zhou *et al.*, 1999; Sasaki *et al.*, 1997).

KS sulphation is carried out by at least two sulphotransferase enzymes; (Fukuta *et al.*, 1997; Habuchi *et al.*, 1996; Ruter and Kresse, 1984) the first, abundant in cornea, adds sulphates to galactose elements of only KS. The second enzyme adds sulphate groups not only to Gal moieties, but also GlcNAc residues of CS, although the latter mechanism remains unclear in humans. A carbohydrate sulphotransferase gene, CHST6, was found to encode the corneal N-acetylglucosamine-6-sulphotransferase enzyme, mutations of which are linked to macular dystrophies types I and II (Akama *et al.*, 2000). Recent analyses suggest that both sulphation and KS elongation occur simultaneously (Uchimura *et al.*, 1998; Degroote *et al.*, 1997).

1.13 The corneal proteoglycans

Proteoglycans interact with cells and may contribute to their adhesion, proliferation and migration (Davies *et al.*, 1999; Funderburgh *et al.*, 1997; Fullwood *et al.*, 1996). As previously mentioned, there are two types of corneal proteoglycans, those expressing CS/DS GAGs, and those containing KS side chains. Corneal KS is a highly sulphated, linear polymer of N-acetyllactosamine, linked to asparagine residues in the KSPG core proteins, and is the basis of these immunochemical studies. Of the KS proteoglycans, lumican, keratocan and mimecan are unusually abundant in corneal tissue, and decorin of the CS/DS fraction.

Corneal proteoglycans are thought to interact with specific bands of collagen (a-e), via their protein core. Meek *et al.* (1986) identified proteoglycan binding sites at positions a, c, d and e in bovine corneal stromal collagen fibrils. Scott (1991) also distinguished that different GAGs are present at the four binding sites: the a and c bands bind KSPGs, whilst d and e bands bind CS or DSPGs. Earlier rabbit studies by Scott also pointed to a single binding site per proteoglycan (Scott and Haigh, 1988).

Proteoglycans potentially interact with several fibrillar collagens of the extracellular matrix. The relationship between proteoglycans and collagen remains hazy, but a fundamental role in corneal ultrastructure is apparent from *in vivo* studies using knockout mice. Only three different protein cores bear KS GAGs in the corneal stroma; the resulting proteoglycans being lumican (Blochberger *et al.*, 1992), keratocan (Corpuz *et al.*, 1996), and mimecan (Funderburgh *et al.*, 1997). Decorin is the primary stromal PG of the CS/DS fraction.

1.13.1 CS/DS proteoglycan : Decorin

Decorin is proposed to be a bidentate ligand attached to two parallel neighbouring collagen molecules within collagen fibrils (see figure 1.10) helping to stabilise fibrils and orientate fibrillogenesis (Scott, 1996), and is also suggested to participate in collagen fibril thickness regulation (Vogel *et al.*, 1984). Under the electron microscope, decorin fulfills its namesake to "decorate" collagen fibrils at the 'd' and 'e' bands (Scott, 1980; Scott and Orford, 1981). Decorin was initially discovered in cartilage and bone (Rosenberg *et al.*, 1985; Fisher *et al.*, 1989), and later identified in a wide range of connective tissues; including cornea, sclera, skin, and tendon.

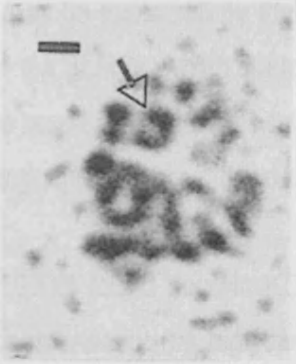

Figure 1.10. Small proteodermatan sulphates isolated in bovine sclera and prepared for rotary shadowing and electron microscopy; horseshoe arrowed, scale bar = 4.5nm. *Adapted from:* Ward *et al.* (1987)

The decorin core protein has one GAG chain substitution on an N-terminal Ser-Gly site (Krusius and Ruoslahti, 1986). The core protein itself contains 10 leucine rich repeats, which contain additional sites for glycosylation (N-linked glycosylation sites) (Krusius and Ruoslahti, 1986). The GAG chain backbone is composed of repeating disaccharide units of GlcNAc and glucuronic acid, although the latter is often converted into iduronic acid through epimerization at C5. Chains are modified by sulphation as they are elongated, resulting in CS and DS respectively. Decorin can also exist without GAG substitutions (Fleischmajer *et al.*, 1991, Sampaio *et al.*, 1988) or with two GAG substitutions (Pringle and Dodd, 1990).

Interestingly, Midura *et al.* (1989) has shown that the decorin in the developing chick cornea also contains 1 to 3 N-linked oligosaccharides, and one O-linked oligosaccharide. Adult hen cornea contains two isoforms of decorin, one with CS/DS side chains, and one hybrid isoform with both CS/DS and KS chains (Blochberger *et al.*, 1992).

Despite the prevalence of decorin in cornea, there are no known human diseases associated with mutations in the decorin gene, however defects in glucose metabolism such as N-acetyl-galactosamine 4-sulphatase deficiency causes decorin to accumulate which has a catastrophic effect on corneal clarity. Danielson *et al.* (1997) reported decorin null mice to show pronounced alterations in skin collagen, with a haphazardly packed fibrillar network resulting in reduced tensile strength and an abnormally fragile skin phenotype. The presence of small proteoglycans occupying the d band of collagen fibrils decorin KO animals suggests that other members of the SLRP gene family may bind the same sites. However, neither biglycan nor lumican were upregulated at the mRNA level, which the author postulates disproves obligatory compensation for the lack of decorin by these two SLRPs. The author goes on to suggest that the absence of overt abnormalities may be explained by the larger requirement for KS and the presence of at least five members of the SLRPs, which could more tightly control fibril diameter requirements for transparency. This result is intriguing, as although corneas appeared normal on a superficial level, no ultrastructural studies were carried out in this case.

A more recent study by Birk *et al.* (2006) found decorin KO mice to have increased biglycan mRNA expression, but no similar compensation by biglycan KO mice. Loss of both decorin and biglycan caused severe fibril disruption in both structure and organisation in the murine cornea, with larger more irregular abnormal fibrils in the posterior stroma. These findings led

the author to conclude that decorin is key to fibril assembly, with loss effects masked by biglycan in the KO model. As these PGs share the same binding site, only with different affinities, double KO mice show a phenotype, as there can be no compensation. Specific disruption of CS/DS PG synthesis by β-D-xyloside in the developing avian cornea causes no alterations in fibril diameter but induces disruption of lamellar organisation and fibril packing (Hahn and Birk,1992).

1.13.2 Lumican

Originally isolated and sequenced from the chick cornea, lumican is a KS proteoglycan that shares 50% genetic homology with fibromodulin (Grover *et al* 2000), and is so named for its role in corneal transparency. Expression is highest but not exclusive to the cornea - lumican is also found in muscle, cartilaginous tissues (Samaanen *et al.,* 2001), kidney (Schaefer *et al*, 2000), and lung (Ying *et al*, 1997). Corneal lumican is normally expressed by stromal keratocytes, however during the early phase of corneal wound healing it is transiently expressed by the corneal epithelium (Saika *et al* 2000).

The lumican core protein consists of a 338 amino acid residue sequence (37 kDa). Corneal lumican has highly sulphated KS chains, suggesting an important role in the acquisition and maintenance of corneal transparency. Lumican is found in other tissues as a poorly sulphated or non-sulphated glycoprotein. There are 2-3 KS attachment sites (Funderburgh *et al.,* 1997) shown in figure 1.11, and a single Tyr site adjacent to the acidic residues Glu/Asp, which may be a signal for post-translation addition of further KS chains (Carlson *et al* 2003).

Bovine corneal lumican carries only one KS chain (Funderburgh *et al.*, 1991), although the amino acid sequence of mature chick corneal lumican documents five potential KS attachment sites: 4 N-linked glycosylation sites in the leucine region and the fifth located outside that region (Blochberger *et al.*, 1992). A more recent study by Dunlevy *et al.* (1998) supported by the work of Midura *et al.* (1989), which suggested only three of those oligosaccharides are substituted with KS chains in the mature chick cornea.

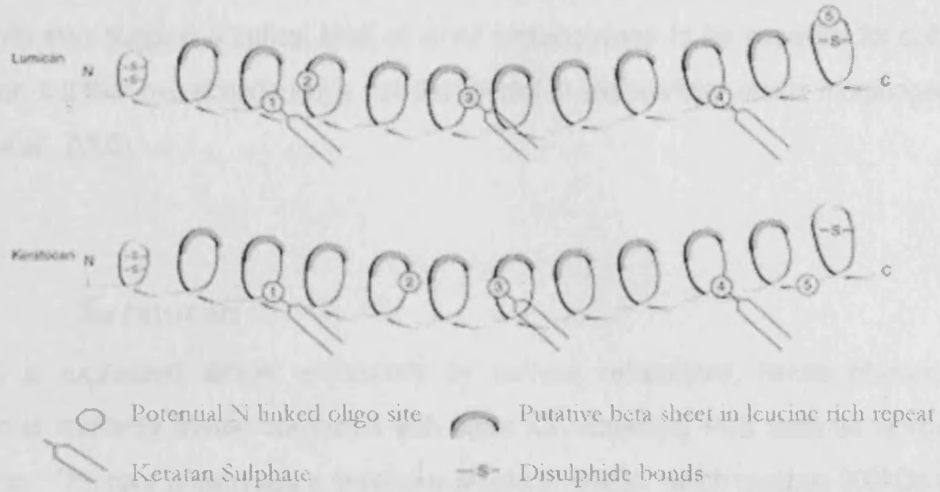

Figure 1.11. Two-dimensional theoretical model of keratan sulphate substitution sites on lumican and keratocan. *Taken from*: Dunlevy *et al.*, 1998

The precise spacing and thickness of corneal collagen fibrils is critical to transparency, therefore function. The exact role of lumican is yet unclear, although an analogous structure with fibromodulin, coupled with *in vitro* fibrillogenesis experiments (Rada *et al.*, 1993) suggests participation in maintenance of the collagen network. In support of this, lumican-null mice have opaque corneas with occasional abnormally thick collagen fibrils formed by fibril fusion (Chakravati *et al.*, 2000).

Developmental studies have determined that the emergence of KS in the cornea correlates with transparency, and such a role for KSPGs has recently been verified by results from lumican knockout mice that displayed bilateral corneal opacity. Collagen structure in the posterior stroma was also found to be altered in the lumican deficient mouse with both increased fibril diameter and abnormal lateral growth (Chakravati *et al.*, 2000). Interestingly, the initial production of the sulphated form of lumican is concomitant with the onset of corneal transparency in the developing chick cornea (Cornuet *et al.*, 1994).

Studies into lumican overexpression in corneas of wild type mice have indicated some degree of interplay between the KSPGs. These mice showed no alteration in collagen organisation or transparency but had increased keratocan expression at both protein and mRNA levels. Corneas of lumican-null mice showed decreased keratocan expression (Carlson *et al.*, 2005). These observations demonstrate that lumican may play a novel regulatory role in keratocan

expression at the transcriptional level. Such results help provide an explanation for the differences in severity of corneal manifestation found in lumican and keratocan knockout mice. Their results also suggest a critical level of small proteoglycans to be essential for collagen organisation but that overabundance is not detrimental to extracellular matrix morphogenesis (Carlson *et al.*, 2005).

1.13.3 Keratocan

Keratocan is expressed almost exclusively by corneal keratocytes, hence physiological distribution is markedly limited compared with other KS containing PGs such as lumican or fibromodulin. The core protein has a molecular weight of 38kDa, which reaches 200kDa when bound with up to three high molecular weight long sulphate chains (Corpuz *et al.*, 1996). Keratocan is abundant in the cornea and sclera, and is also found to a lesser degree in non-corneal tissues (skin, ligament and cartilage), primarily as a non-sulphated glycoprotein.

Dunlevy *et al.* (1998) proposed that lumican and keratocan may have a very similar 3-dimensional arrangement. This structure is also similar to that of porcine ribonuclease inhibitor, a protein composed of Leu-rich motifs which are coiled in a spiral with the Leu-rich regions stacked in a parallel β-sheet array. It appears that the location of the first 10 Leu-rich repeats of lumican and keratocan are located in the central part of the spiraled coil which bend into a horseshoe-like structure, whereas the putative β-sheet is found at the top surface of the coiled domain. Three of the KS attachment sites are thought to extend outward on the convex surface of the horseshoe. The inner Leu-rich domain of the horseshoe has been implicated in protein-protein interactions such as collagen binding, whereas the outer surface with protruding GAG side suggested to occupy space between collagen molecules.

Along with lumican and mimecan, keratocan makes up the major KSPG content in the cornea. Although specific mechanisms remain undefined, it is generally believed that keratocan, like lumican, may also take part in regulating both corneal transparency and collagen fibrillogenesis due to a strategic cluster of Tyr-sulphate residues.

1.13.4 Mimecan

Osteoglycin was intially isolated from bovine bone, and later isolated and cloned in the bovine cornea as a minor KSPG , now renamed mimecan. This 25kDa corneal PG is a product of the gene producing osteoglycin (Funderburgh *et al.,* 1997), and is expressed during chick corneal development. It is, however, undetectable in adult hen corneas, maybe because its level is low (Dunlevy *et al.*, 2000). Interestingly, mimecan carries KS GAGs in human, bovine and developing chick cornea, but not in the murine cornea (Funderburgh *et al.*, 1997). In bovine cornea, mimecan has only one KS side chain (Funderburgh *et al.*, 1991).

Northern blotting has revealed three distinct size classes of mimecan mRNA that vary in abundance depending on the tissue source, the smallest 2.4 kb form is predominant in corneal and scleral tissue. Such heterogeneity can arise as a result of alternate splicing of RNA or by alternate usage of polyadenylation sites.

Chick mimecan contains a 60 amino acid sequence that does not share identity with the (presumed) mammalian homolog. The 177 base pair DNA coding for this unique sequence shows 47% identity to an 189 base pair sequence between exons 4 and 5 of the bovine osteoglycin/mimecan gene (Funderburgh *et al.,* 1997). This indicates that the avian cDNA represents an alternatively spliced form of mimecan containing a unique N-terminal sequence.

Alignment of the mimecan amino acid sequence with established corneal KSPGs lumican and keratocan does not show high sequence identity. However, comparison of structural domains among all three proteins, indicates molecular feature conservation. Each protein contains one or more Tyr residues adjacent to acidic amino acids in the N-terminal region; consensus sites for Tyr sulphation (Funderburgh *et al.* 1997).

As for lumican and keratocan, the mimecan protein is present in many tissues as a non-sulphated glycoprotein, although corneal mimecan, lumican and keratocan are expressed to a greater extent than their systemic counterparts. This is an example of a phenomenon known as gene sharing. For example, lens genes for common intracellular proteins are massively overexpressed to produce the crystalline proteins that confer basic transparency. Studies of the transketolase enzyme in the corneal epithelium suggests a similar mechanism is also important to corneal integrity. An analogous process is also apparent in the keratocytes,

however, tissue-specific glycosylation of lumican, keratocan, mimecan and decorin in the stroma converts them from non-sulphated matrix glycoproteins to a unique class of proteoglycans.

1.14 Proteoglycans and the collagen matrix

The most current model of PG – collagen interaction suggests that the protein core lies along the length of the collagen fibril, to which it is non-covalently attached, and that highly charged hydrophilic GAG chains protrude outwards from the fibril to regulate collagen spacing. Scott (1991) proposed that GAGs of neighbouring collagen fibrils interact with each other to form a duplex, which serve to maintain collagen fibril separation; in support of this, Rada *et al.* (1993) reported that PGs bind to collagen fibrils with their GAG chains extending into the interfibrillar space.

Lumican is believed critical to normal collagen architecture. Lumican-null mice have opaque corneas with increased collagen fibril diameter and abnormal fibril architecture in the posterior stroma containing mature collagens, whilst newly synthesized fibrils in the anterior stroma remain normal (Chakravarti *et al.*, 2000). In fact, KS content decreases in the whole eye of lumican deficient mice, which furthers the role of KS in transparency.

Keratocan-null mice are reported to have normal corneal transparency, however subtle abnormalities in collagen fibril organisation such as increased fibril diameter, thinned stroma, and a smaller angle over the anterior cornea and iris, are reported (Liu *et al.*, 2003). Similarly, human mutations in the keratocan gene cause corneal flattening and a consequent decrease in visual acuity (Pellegata *et al.*, 2000). There is no change in the superficial corneal clarity or thickness in mimecan-deficient mice (Tasheva *et al.*, 2002), however corneal tissue is ultrastructurally altered.

Gene-targeted mutations in decorin lead to significant collagen organisation abnormalities in skin and tendon, however there is no obvious corneal phenotype in the whole animal study (Danielson *et al.*, 1997). *In vitro* experiments in support of KSPGs governing collagen fibril architecture show that lumican and decorin core proteins delay fibril formation and prevent diameter growth (Rada *et al.*, 1993; Vogel *et al.*, 1984), although this finding has been

contradicted by Li *et al.* (1992) who reported that decorin does not regulate collagen fibril diameter. An alternative role for decorin in collagen architecture has been suggested by Kadler's group (1996), who propose that decorin is secreted along procollagen molecules within vesicles, thus preventing lateral association of procollagen molecules to aid fibril formation.

To date, only lumican-null mice exhibit a clinical corneal phenotype (Chakravarti *et al.*, 2000). Murine deficiencies in mimecan, decorin and keratocan retain normal corneal transparency; however it is prudent to remember that transparency is difficult to measure in the mouse cornea. Points of interest are:

- KS levels are unchanged in decorin-null mice
- mimecan is a KSPG in bovine and human cornea, but not in murine cornea
- there is a decrease in KSPG content in keratocan-null mice cornea
- keratocan-null mice have normal corneal transparency
- lumican and keratocan could bind to different sites of the collagen fibril

1.15 The importance of proteoglycans

Stromal thinning is seen in lumican- and keratocan-null mice (Chakravati *et al.*, 2000 and Liu *et al.*, 2003). This loss is thought to be a result of dehydration in the absence of KSPGs; KS has a higher water binding capacity than CS or DS (Bettelheim and Plessy, 1975) which is evident in the bovine cornea -- the posterior stroma in bovine cornea shows a parallel increase in KS and hydration (Castoro *et al.*, 1988) in low oxygen conditions, thought necessary for KS synthesis (Scott and Haigh, 1988).

Disruption of KS synthesis exerts a catastrophic effect on corneal clarity. Type I Macular Dystrophy (MCD I) corneas produce an immature form of KS with a smaller protein core (Nakazawa *et al.* 1984) resulting in progressive clouding from reduced interfibrillar spacing and corneal thickness (Quantock *et al.*, 1990). Although MCD I phenotype is linked to heritable defects in KS synthesis, more C-6-S (Klintworth *et al.* 1976) is found, and oversulphated CSPGs are reported (Nakazawa *et al.* 1984; Meek *et al.*, 1989). Hyaluronan, absent in normal cornea, is also expressed (Plaas *et al.* 2001).

Corneal scars also show altered GAG sulphation patterns (Funderburgh *et al.*, 1988; Hassell *et al.*, 1983; Cintron *et al.*, 1990), which implies a relationship in structurally disorganised, opaque tissue. Large highly sulphated CS/DG PGs appear, and are activated to divide, adopting a fibroblastic phenotype and KSPG synthesis is reduced (Funderburgh, 2000). Corneal scars also synthesise hyaluronate (Hassell *et al.*, 1983). Reduction of KS in both Alzheimer's disease afflicted brain and cornea appears in association with inflammation, suggesting a role for proinflammatory cytokines in the downregulation of KS biosynthesis (Lindahl *et al.*, 1996).

1.16 Chick corneal development

In lower vertebrates such as the chicken, the formation of the corneal stroma is the result of a precisely controlled developmental sequence. The beauty of the developing chick cornea for these investigations is that it is a reproducible model system in which the cornea is becoming naturally transparent over a defined timescale, and develops early, reaching a large size relative to the embryo.

Central to the understanding of chick corneal morphogenesis lie the molecular mechanisms that drive the structural reorganisation of fibrillar collagen, and persuasive arguments have been advanced in favour of a functional role for KSPGs (see section 1.15) as potential regulators of matrix architecture and tissue transparency.

It is well established that corneal transparency is facilitated by the regular arrangement of uniformly sized collagen fibrils in the stroma, a change in structural organisation may compromise the optical properties of the cornea. Proteoglycan expression fluctuates during corneal development, which coincides with physiological changes resulting in transparency (Hay and Revel, 1969). The development of the avian cornea principally involves the synthesis of a primary stroma, consisting of striated collagen types I and II (hybrid fibrils), and III (Hendrix *et al.*, 1982); as a foundation for the subsequent secondary (mature) stroma.

1.16.1 Development of the primary stroma

Before developmental day 3 the optic vesicle induces lens placode development by forming a cup-shaped structure around which the lens placode develops from the overlying ectoderm, shown below in figure 1.12.

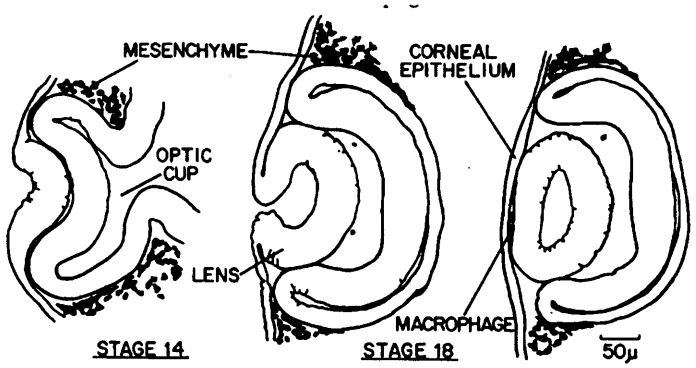

Figure 1.12 Events leading to the formation of the primary stroma, Hamilton Hamburger stages 14-18 (50 hours-3 days of incubation). *Taken from:* Hay and Revel (1969)

At 3 days of incubation, the lens vesicle has detached from the overlying ectoderm – now the corneal epithelium which is two cells thick, and the beginnings of the extracellular matrix are laid down between the corneal epithelium and the basal surface of the anterior lens epithelium. This fibrous and acellular primary stroma is synthesised by the corneal epithelium (Hay and Revel, 1969), and increases in thickness three times in a 12 hour period during developmental day three, and reaches 12μm thick by day 5, as shown in figure 1.13. The primary stroma reaches 10μm thick by the beginning of developmental day 5, and 60μm by day 5½ of development. At this time, the stroma appears wavy, with largely striated fibrils of uniform diameter moving towards and away from the endothelium. These heterotypic collagen fibril structures consist of at least two fibrillar collagens, in that types I and II are deposited in an orthogonal fashion (Trelstad and Coulombre, 1971).

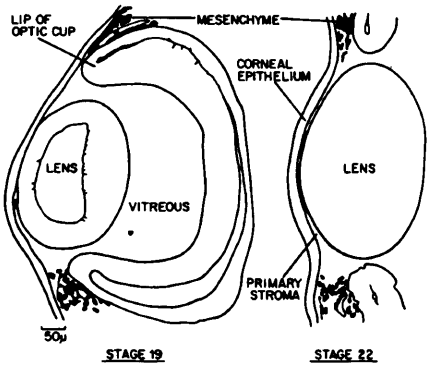

Figure 1.13. Development of the primary stroma between stages 19 and 22, 3 to 3½ days of incubation. *Taken from:* Hay and Revel (1969)

The corneal endothelium arises from the vascular mesenchyme near the lip of the optic cup, which migrates between the primary stroma and lens on day 4 to form the *Brille*. The Brille consists of epithelium, stroma and endothelium, and constitutes a functional cornea for larval amphibians (Hay and Revel, 1969), see figure 1.14.

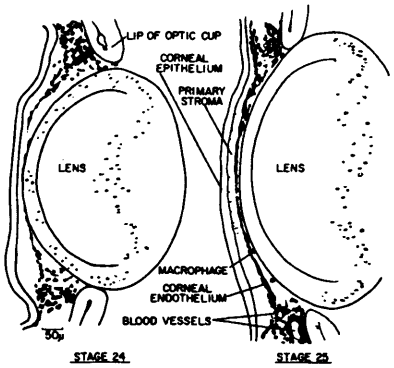

Figure 1.14. Development of the Brille between stages 23 and 25, 4 to 5 days of incubation. *Taken from:* Hay and Revel (1969)

Vertebrates undergo synthesis of secondary stromal tissue on day 5; the acellular primary stroma is invaded by secondary mesenchymal cells followed by rapid migration and proliferation. By developmental day 7 these mesechymal cells differentiate into fibroblasts and produce collagen. Corneal development is dominated by these newly acquired fibroblasts as numerous collagen fibrils are added to the stroma; in fact the mesenchmal cells are thought to utilise the collagenous lamellae of the primary stroma in secondary stromal formation.

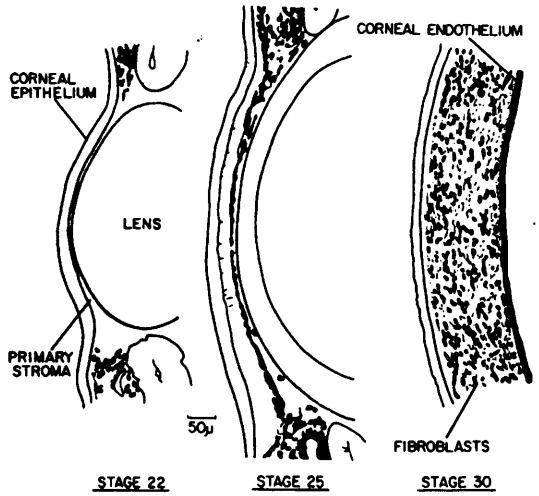

Figure 1.15. Camera lucida drawings showing the formation of the primary stroma and subsequent developmental events. The endothelium begins to migrate along the posterior surface of the stroma at the end of stage 22 (3½-4 days), and is almost complete by stage 25 (4½-5 days). After stromal swelling and fibroblast invasion at stage 30 numerous fibroblasts are present. *Taken from:* Hay and Revel (1969)

1.16.2 Development of the secondary stroma

Immediately after the Brille stage on day 5 of development, the primary corneal stroma is invaded by the secondary mesenchymal cells (Linsenmayer *et al.*, 1998) via the posterior stroma, which rapidly migrate and proliferate - see figure 1.16.

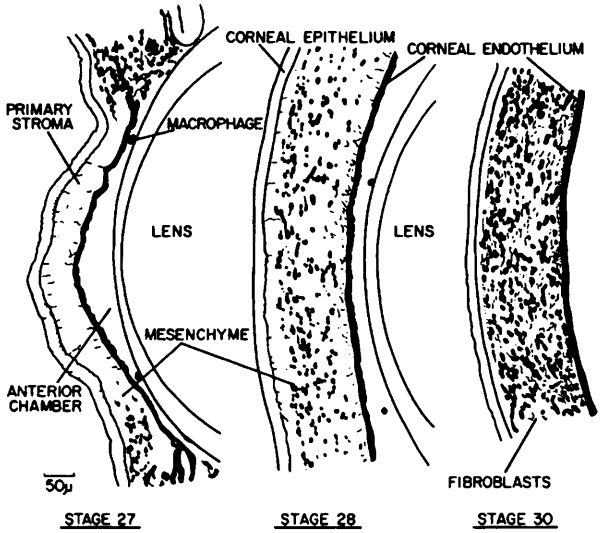

Figure 1.16. Invasion of the primary corneal stroma by mesenchymal cells (which become fibroblasts) at stages 27, 28 and 30; days 5, 5½ and 7 of development. *Taken from:* Hay and Revel (1969)

By developmental day 7, mesenchymal cells have differentiated into fibroblasts and produce collagen and other non-collagenous stromal components (Linsenmayer, 1998). These newly differentiated fibroblasts add numerous collagen fibrils to the stroma, which are deposited onto the scaffold of collagenous lamellae produced by the primary stroma (Trelstad and Coulombre, 1971). The mesenchymal cells penetrate between the lamellae of the primary stroma up to the epithelium, which forms Bowmans layer around 14 days of incubation. Descemets layer is formed from the endothelium when stromal swelling is at a maximum between days 8½ and 9 of incubation. Corneal curvature also becomes apparent at this time (Coulombre and Coulombre, 1958), and is dependent on intraocular pressure, the corneal-scleral junction, and stromal composition (Coulombre, 1965).

Two distinct stromal regions become apparent from day 5 of incubation. The first is the posterior cellular area, which becomes the secondary stroma under the activity of mesenchymal cells, and the second, anterior acellular area more recently deposited by the epithelium of the primary stroma. By developmental day 6, the entire corneal stroma is about 110μm thick; the posterior 100μm region is transformed into the secondary stroma, and the anterior 10μm not yet invaded by mesenchymal cells. Total thickness increases to 140μm twelve hours later. The cornea attains a maximum thickness of between 190μm (Trelstad and Coulombre, 1971) and 220μm (Hay and Revel, 1969) on developmental day 9.

From day 9 of development, the cornea begins to dehydrate and progressively thin; by day 12 of development it is less than 200μm thick and only 150μm by developmental day 14 (Hay and Revel, 1969). The secondary stroma undergoes compaction to about 50% of its thickness. During stromal compaction there is a marked increase in PG synthesis (Nakazawa *et al.*, 1995). Corneal thickness is 160μm at hatch, and continues to grow reaching 250μm in the young hen. Stromal fluctations are summarised in figure 1.17.

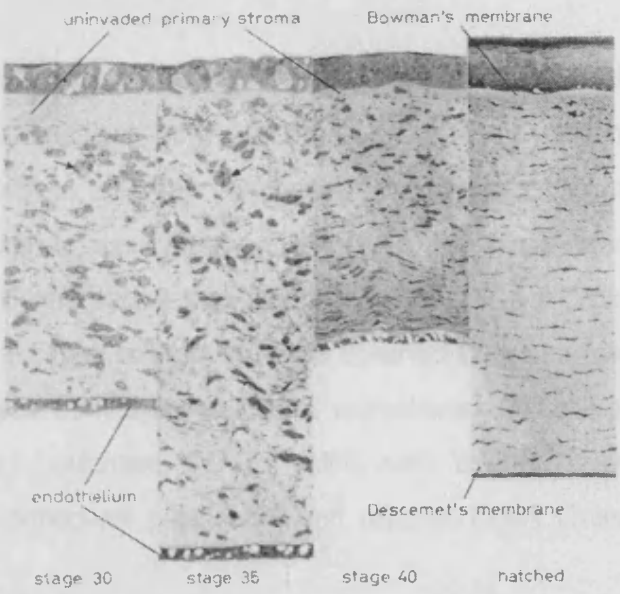

Figure 1.17. Chick corneal stromal changes from developmental day 6 ½ to hatch. Where; stage 30 - day 7, stage 35 - day 9 and stage 40 - day 14. Taken from: Hay and Revel (1969)

1.16.3 Collagen structure during development

The secondary stroma is principally composed of heterotypic types I and V collagen fibrils, beaded filaments of type VI collagen, and proteoglycans. Synthesis of the secondary stroma leads to corneal swelling and a maximal thickness of 220μm at day 9; thickening is a consequence of two factors, secretion of heterotypic type I/V collagen fibrils, and more noticeably, oedema. Dehydration and corneal compaction follow, and as mentioned by day 12 thickness is reduced to 200μm, and only 150μm by day 14.

Prior to day 14 of embryonic chick development, the cornea is soft and easily detached from the sclera. The advent of collagen fibril order brings about corneal strength and resistance to manipulation (Coulombre and Coulombre, 1958). Tensile strength is due in part to the interlacing of collagen lamellae in the posterior stroma (Maurice and Monroe, 1990; Radner and Mallinger, 2002).

In embryonic chicks the primary stroma is composed of orthogonal layers of one or two heterotypic fibrils, in a pattern similar to the adult stromal collagenous arrangement (Trelstad and Coulombre, 1971). Experimentally altering this specific pattern also reverses the collagen fibril orientation, implying that the primary stroma acts as a template for collagenous arrangement in the secondary stroma (Coulombre and Coulombre, 1975).

From day 6 of development, collagen lamellae are displaced clockwise from the outer to the inner layers in both left and right corneas and equal to 2.5 - 5° per micron of corneal thickness (Trelstad and Coulombre, 1971). Interestingly, collagen compaction during stromal condensation is thought to occur initially in this undeviated posterior area (Hay and Revel, 1969), where the orthogonal stroma shows no rotation (Trelstad and Coulombre, 1971). Unlike other higher vertebrate tissue, collagen fibrils are observed in discrete layers 2-4 microns thick in mature avian corneas, each layer made up of approximately 25 fibrils parallel to the anterior surface (Trelstad and Coulombre, 1971). Within each layer, collagen fibrils are aligned, arranged in a quasi-orthogonal pattern between adjacent layers (Trelstad and Coulombre, 1971).

The secondary stroma is almost complete by day 14 of incubation, collagen fibril layers are all well formed and oriented, although more GAGs and collagen are added later in development (Trelstad and Coulombre, 1971; Hay and Revel, 1969; Anseth, 1961). Only 24 hours later, previous micorscopy studies have suggested that the cornea is mature and collagen organisation is little different to corneas at 18 days of development at the electron level (Hirsch *et al.*, 1999). Increasingly obvious collagen bands showing high thermal stability have been detected from developmental day 12 (Linsenmayer *et al.*, 1986), implicated in stabilising corneal shape or adjusting curvature as the scleral ossicles appear to form a ring over the same time frame.

1.16.4 Glycosaminoglycans during development

Despite the suspected importance of KS and CS/DS to stromal structure, the major GAG synthesised before developmental day 9 is an unsulphated hyaluronate (Toole and Trelstad, 1971), presumably synthesised by the endothelium or epithelium in the primary stroma, and keratocytes in the secondary stroma (Conrad, 1970). KSPGs are thought to influence development, with lumican, keratocan and mimecan present in the ratio of 6:3:2 throughout development (Funderburgh *et al.*, 1991).

Lumican mRNA declines slightly after day 15 of development, which is mirrored by similar decreases in keratocan and mimecan mRNA levels (Dunlevy *et al.*, 2000), although a relatively

high level remains throughout development. Keratocan mRNA is detected in similar quantities to lumican at day 9, but follows the same trend at a much lower level as the cornea becomes transparent. Mimecan mRNA expression is even less, tailing off as development progresses (Dunlevy *et al.*, 2000). The mRNA levels of β-1, 4-galactosyltransferases responsible for glycosylation in lumican also increase almost three-fold from developmental day 8 to 13 (Cai *et al.*, 1996).

1.16.5 The mature stroma

The mature avian stroma predominantly consists of type I collagen, combined into heterotypic fibrils with type V. Type V collagen typically makes up 5-20% of the collagen content, unusually high compared to other similar tissues (Linsenmayer, 1988). Type VI is also abundant, running between collagen layers or fibrils (Linsenmayer *et al.*, 1986), possibly interacting via decorin, KS- or DSPGs (Takahashi *et al.*, 1993).

Lumican, keratocan and mimecan are all found in the adult hen cornea (Dunlevy *et al.*, 2000); lumican mRNA levels are 38 times higher than mimecan, and five times greater than keratocan (Dunlevy *et al.*, 2000). Decorin is also present after hatch, but as CS/DS or hybrid CS/DS and KS carrying isoforms, which suggests that the decorin gene undergoes posttranslational modification during maturation (Blochberger *et al.*, 1992).

1.16.6 Potentially significant events

After developmental day 12, collagen fibrils condense, becoming more closely packed (Quantock *et al.*, 1998), despite the deposition of an increased amount of collagen. Collagen synthesis is thought to continue until after hatch (Hay and Revel, 1969), believed to be intralamellar following day 14 of development (Coulombre and Coulombre, 1958).

Dunlevy *et al.* (2000) suggests two important stages in avian corneal development, the first at the same time as dehydration and initial compaction between days 9 and 12, and the second between days 15 to 18, leading to transparency. Based on tissue hydration measurements, Siegler and Quantock (2002) report a two stage compaction of the secondary avian cornea, first between days 13 and 14, and the second between days 16 and 17 of development,

independent of the lactosaminoglycan to GAG switch in KS proteoglycan production (Cornuet *et al*, 1994) from days 12 – 15.

Before day 14 of incubation only 40% incident light is transmitted through the poorly defined cornea (Coulombre and Coulombre, 1958), rising by day 15 onwards. Loose networks of apparently unordered collagen fibrils are well documented through quick-freeze, deep-etch electron microscopy from developmental days 8 – 13 (Hirsch *et al*, 1999), along with roughly parallel collagen fibrils arranged into perpendicular bundles. By day 15, these ordered regions dominate corneal morphology (Connon *et al.*, 2003).

Transparency of the embryonic chick cornea develops only as the PG form of lumican begins to accumulate (Cornuet *et al.*, 1994). The functional role of the murine lumican N-terminal domain during fibrillogenesis recently has been investigated (Carlson *et al.*, 2003) after suggestion of collagen binding properties (Rada *et al.*, 1993), warranting further investigation in the avian model.

1.17 Corneal Transparency

Corneal transparency is based upon the minimal scattering of light to maintain clarity (Benedek, 1971). Uniform refractive index theory assumes close similarity between the refractive indices of collagen fibrils and matrix components, resulting in minimal light scattering – hence transparency (Smith, 1969). This theory has since been contradicted by Leonard and Meek (1997), whose species study revealed a higher refractive index for collagen fibrils than the surrounding matrix.

The most widely accepted theory of corneal transparency is based on the regular arrangement of collagen fibrils (Caspersson and Engstrom, 1949) causing individual scattered waves to destructively interfere in all directions *except* the forward direction. Lattice theory proposes that as collagen fibril spacing is an order of magnitude less than the wavelength of visible light, individual scattered waves interfere destructively in all directions except that of the incident beam. Scattered light is projected in a forward direction and tissue appears transparent (Maurice, 1957).

"Perfect" lattice array is not a pre-requisite of corneal transparency, however the structure of collagen fibrils within individual lamellae and fibril diameters must be known (Worthington and Inouye, 1985). Various investigators have concluded collagen fibril diameter to be 25 nm (Birk *et al.*, 1986; Trelstad and Coulombre, 1971; Hay and Revel, 1969), however as the preparation stages of electron microscopy involve considerable shrinkage (Fullwood and Meek, 1994), these values are likely to be an underestimate of true collagen fibril diameter values *in vivo*.

X-ray diffraction studies with no prior fixation have yielded an average collagen fibril diameter value of 35.4nm across a range of birds (Meek and Leonard, 1993). Using quick freeze, deep etch electron microscope, Hirsch *et al.* (1999) reported that despite an increase in lamellar organisation throughout development, mean collagen fibril diameter always lies between 30.3 and 31.2 nm. Unfortunately this study contains wide variation within each developmental day. Nevertheless, current literature implies that collagen fibril diameter is independent of spatial organisation and collagen packing. This correlation suggests collagen fibril deposition at a mature diameter (Birk *et al.*, 1986).

Electron micrographs indicate that collagen fibrils in the developing chick cornea are organised into groups separated by large spaces devoid of collagen until day 14 of development (Hay and Revel, 1969; Connon *et al.*, 2003). Theory predicts that stromal opacity will ensue if these collagen-free "lakes" approach or exceed half the wavelength of visible light (Benedek, 1971). After day 14, despite lamellar disarray, collagen fibril groups become more organised (Hay and Revel, 1969). Tissue hydration has a critical bearing on tissue transparency, unidirectional stromal swelling causes collagen disarray (Goodfellow *et al.*, 1978), which can result in "lake" formation. Endothelial cells maintain interfibrillar spacing to counteract the hydrophillic effect of polyanionic PGs (Hassell *et al*, 1983), which also contribute to this elegant mechanism.

KSPGs play an integral role in collagen order and corneal transparency. KS levels are high in the highly organised mid cornea, but conspicuously low in the opaque sclera (Borcherding *et al.*, 1975). KSPGs are scarce in corneal scars with large interfibrillar spaces, although a return to normal spacing and tissue transparency complement a rise in concentration (Hassell *et al*, 1983). Repulsive forces generated by PGs are crucial to the maintenance of uniform spacing between neighbouring fibrils (Elliott and Hodson, 1998). This idea has been advanced to include a model where the ratio of GAGs to collagen molecules remains fixed in all species (Meek and Leonard, 1993). Another theory of consistency proposes a fixed charge density as

the source of collagen order, (Elliott *et al.*, 1980; Hodson *et al.*, 1992) dependent on permanent negative charges in collagen fibrils and transient mobile ion binding to the fibrils.

Studies of heritable metabolic diseases demonstrate the catastrophic effect of KSPG dysfunction. Macular dystrophy corneas do not synthesize mature KS proteoglycan (Hassell *et al.*, 1980). Analyses of keratoconus samples have determined that although the amount of keratan sulphate is decreased, the KS core protein content remains unaltered (Sawaguchi *et al.*, 1991). Perhaps the true scale of KSPGs involvement in corneal transparency can only be appreciated by their absence. Transgenic and knock-out studies in mice implicate the physiological consequences of gene deactivation, thus allowing the role of that gene product to be determined.

1.18 Aims and objectives

My aim is to explore the developmental dynamics of the embryonic chick cornea at critical developmental stages as it becomes transparent, and correlate changes in fibrillar collagen packing and orientation with specifically timed developmental events, such as changes in sulphated proteoglycan composition. Matrix collagen reorganisation and proteoglycan alterations are long known to be of importance for corneal functions such as biomechanical stability and transparency. The work in this thesis is seen as a potentially significant step towards a deeper understanding of the role of KS and KS sulphation steps in significant developmental events in the embryonic chick model.

CHAPTER TWO: General Methods

2.1 Introduction to Chapter

This chapter discusses the methods used to characterise collagen fibril spacing and keratan sulphate expression in the developing chick cornea. The methods discussed in this chapter are only those relevant to the entire thesis, and specificities for individual experiments are provided in their appropriate chapters.

All X-ray diffraction work was carried out at the Council for the Central Laboratory of the Research Councils, CCLRC, Synchrotron Radiation Source, SRS, Daresbury Laboratory, Cheshire, UK. Due to the logistics of beam use, samples were stored prior to data collection. A preliminary study (see Appendix 1) determined that tightly wrapping specimens in cling film, freezing at -20°C and storage at -80°C (to minimise dehydration and associated structural changes) was the most suitable method for reproducible results. Previous studies of collagen interfibrillar spacing have utilised freeze-thawed corneas. Although fibril diameter is reduced in frozen tissue (Fullwood and Meek, 1994), normal structural parameters are restored upon thawing.

For ease of understanding, the methodology has been stratified into separate studies; namely X-ray analysis, ELISA, hydroxyproline assay and microscopy to gain both structural and biochemical data. These methods are presented in their most logical order, however they appear in a sequential fashion in each chapter.

2.2.1 Sample collection

Fertilised Lohmann Brown chicken eggs were obtained from a commercial hatchery (Hy-line UK, Warwickshire, UK). At this facility eggs are set into the incubator at 14:00 daily, the majority hatch 21 days and 12hrs later. Fertile chicken eggs were collected daily from days 12 to 18 of incubation, as confirmed by using Hamilton-Hamburger staging (Hamburger and Hamilton 1951; Hamburger 1992). Natural variation means a large sample size is desirable, some chicks inevitably hatch before/after the expected time. The use of animals in this work was carried out in accordance with European Commission Directive 86/609/EEC.

2.2.2 Sample storage

As mentioned, due to the scheduling of beam time, samples inevitably required storage before X-ray studies. Corneas were excised from decapitated embryonic chicks obtained from eggs collected at Hy-Line UK approximately two hours earlier, quickly weighed on an analytical balance, wrapped tightly in cling film to minimise dehydration, and placed into dry ice. Frozen corneas were transferred to -80°C storage until needed. Freezing and thawing have been shown to have little effect on the scattering patterns of corneas (Fratzl and Daxer, 1993; Fullwood and Meek, 1994).

2.3 Small angle X-ray scattering

The high intensity beam at the SRS generates X-ray diffraction patterns in seconds or minutes, allowing structural, quantitative data to be gathered from a close to natural tissue state, without the need for lengthy preparation associated with electron microscopy.

X-ray diffraction patterns from cornea are obtained by passing a monochromatic X-ray beam through the specimen. X-rays passing straight through the specimen are blocked by a lead backstop positioned behind the sample, some rays are absorbed by the specimen itself, and the remaining rays scattered by the constituents of the sample, forming a pattern on a detector placed behind the sample.

2.3.1 A Brief Background

Collagen fibrils, if regularly arranged, give rise to small-angle meridional and equatorial diffraction patterns, when exposed to a focussed X-ray beam. This effect gives rise to diffraction maxima on the detector plate, as shown in figure 2.1 below.

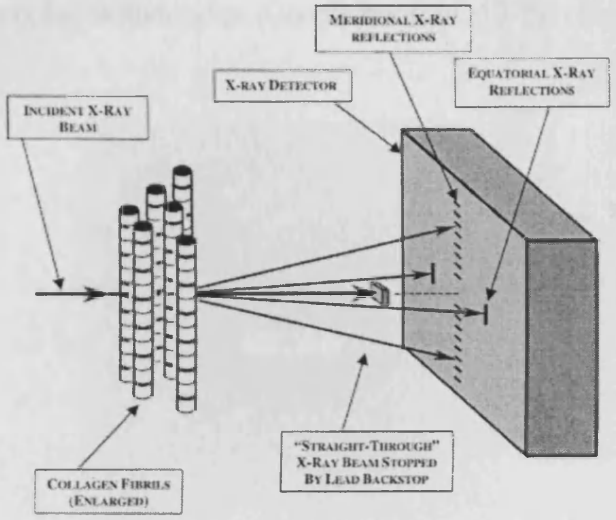

Figure 2.1. Schematic diagram showing how an array of cylindrical fibrils held vertically in an X-ray beam gives rise to meridional reflections in a direction parallel to the fibril axes and equatorial reflections in a direction perpendicular to the fibril axes.
Taken from: Meek and Quantock (2001).

The X-ray diffraction pattern consists of two components, the meridional and equatorial reflections, which can be seen parallel and perpendicular to the fibril axis respectively. Small angle meridional reflections arise from the axial order of collagen molecules or D-period, whereas equatorial reflections are a result of lateral order and collagen fibril packing within lamellae. Collagen fibrils run alongside each other within the same lamella, but if there is no preferential alignment of these lamellae, the effect is to spread fibril alignment so that there is no preferred fibrillar orientation. This isotropic alignment of the fibrils causes both equatorial and meridional scatter patterns to show a circular ring of intensity, as scatter is spread over 360°, forming a set of concentric rings. Although the two patterns are superimposed, they can be distinguished from each other by their position in the pattern, and equatorial patterns are broader than meridional reflections.

A long camera is used to measure small angle scattering, also referred to as small angle X-ray scattering. The resulting X-ray pattern shows rings of diffraction maxima and minima, produced from differing lamellae orientation. Equatorial small angle patterns comprise of two parts, the first being the interference function caused by scattering from an array of cylinder centres, in this case collagen fibrils, and is therefore dependent on the position of the collagen centre. The second component is the diffraction pattern from a single cylinder, which is dependent on the collagen fibril radius (Goodfellow *et al.*, 1978).

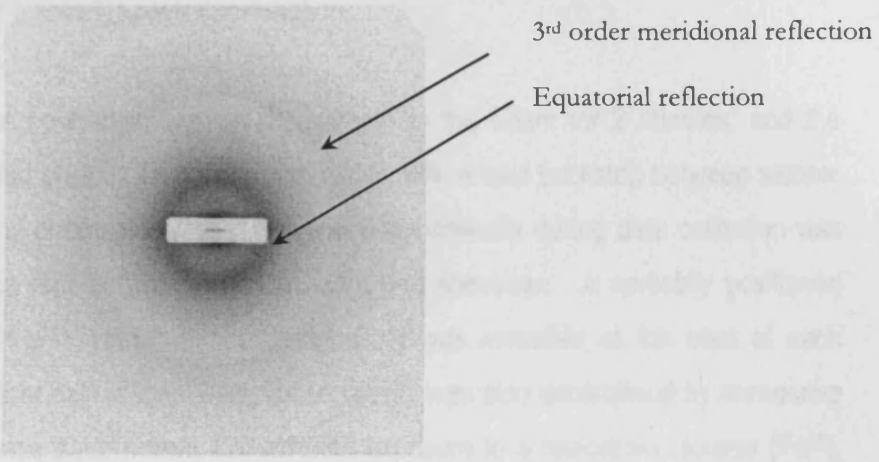

Figure 2.2. Small-angle scattering pattern, D18 chick cornea.

Quantitative data is calibrated using an X-ray diffraction pattern from rat tail tendon, the known axial periodicity of 67nm means sample interfibrillar spacing may be calculated (Goodfellow *et al.*, 1978, Sayers *et al.*, 1982, Worthington and Inouye, 1985).

2.3.2 Small angle X-ray scattering data collection

Prior to data collection, the position which the beam passes through the specimen holder was found by exposing a piece of green x-ray sensitive paper mounted on graph paper that was cut to the size and shape of the sample holder. An exposure of approximately 10 seconds was sufficient to create a red mark demonstrating where the x-ray beam strikes.

Small angle x-ray scattering patterns were obtained using an evacuated camera of in excess of 8.25m and a focussed monochromatic beam (λ=0.154nm) of dimensions 1mm x 1mm at SRS station 2.1. The beam was focussed along the optical axis of the cornea.

Samples were allowed to thaw as they were positioned between two sealed Mylar (Dupont-Teijin, UK) specimen holder sheets. A single layer of cling film was left to cover the epithelial and endothelial face, to help maintain hydration and minimise structural disturbance through handling. Any contribution of the cling-film to the diffraction pattern was subtracted from background scatter during analysis. Silicon grease was then wiped around the specimen holder edges to reduce any further dehydration during exposure. By placing the transparent sample holder over the previously marked graph paper, (with the beam position marked by a red dot), each cornea was carefully positioned to ensure that the beam passed centrally through the sample in the anterior-posterior direction.

The shutters were then opened to expose the sample to the beam for 2 minutes, and the resulting pattern recorded on a 512 x 512 pixel detector, with a lead backstop between sample and detector to stop any undeviated rays. Average x-ray intensity during data collection was recorded by an ion chamber between incident beam and specimen. A vertically positioned piece of rat tail tendon with known 67nm D-periodicity was recorded at the start of each experiment, to enable later calibration. Detector sensitivity was also ascertained by measuring a single detector response pattern from 420 minutes exposure to a radioactive source (Fe^{55}), which recorded any spatial variation for each data set. Once recorded, the patterns were sent electronically to Cardiff for analysis.

Following beam exposure corneas, still tightly wrapped in cling-film were stored in dry ice, until return to Cardiff.

2.3.3 Analysis of small-angle x-ray scattering patterns

The image patterns were analysed using Unix based software (Fit2d, produced by Dr. A. Hammersley, ESRF, Grenoble, France), and a statistics and graphics package (Microsoft Excel, Statsoft Statistica and SPSS 11) was used to obtain values for the Bragg interfibrillar spacing.

Each pattern was normalised using a reading from the ion chamber located between the incident x-ray beam and the specimen, to correct for beam decay. The detector response pattern was then divided point-for-point from each normalised image to account for any spatial

changes in detector sensitivity. Next, a vertical transect was taken through the centre of the pattern (see figure 2.3A) and integrated horizontally, to produce an intensity profile of the first order equatorial x-ray pattern. The signal to noise ratio was increased by doubling up the symmetrical pattern to produce an average intensity profile of the two halves, as shown in figure 2.3B. The intensity distribution is described as a function of radial distance from the centre of the pattern (R). Crucially, the scattering angle and R, are inversely related to the size of the object causing the scattering. This parameter, Q is the reciprocal space coordinate.

(A)

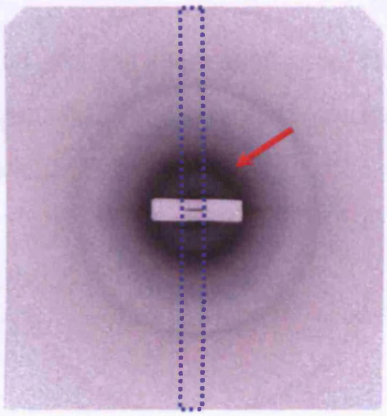

(B)

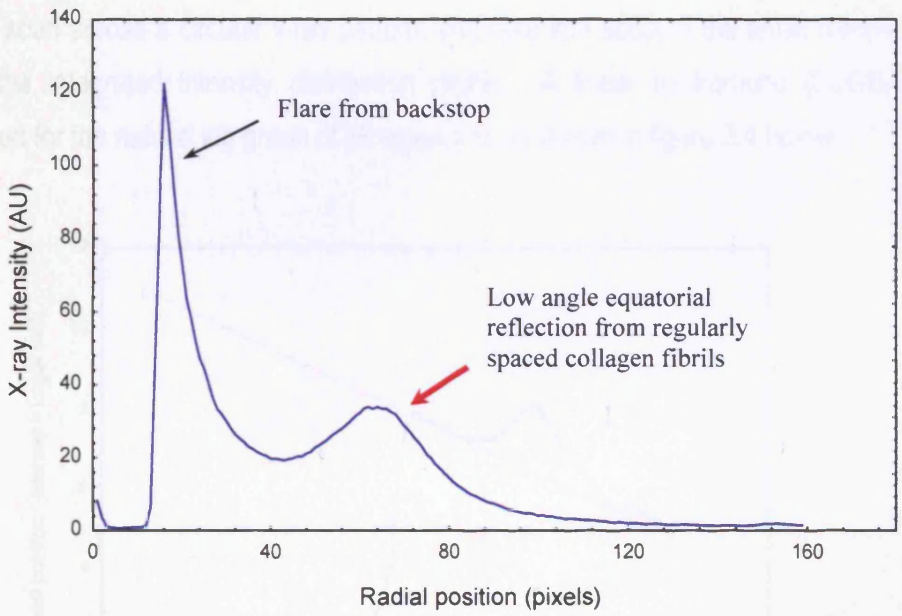

Figures 2.3A and B. Small angle x-ray scatter pattern from the centre of a day 18 chick cornea (A). The marked vertical transect was taken to form an intensity profile of the pattern, and then folded around the centre point to give an average intensity profile for the two halves (B). The first order equatorial used for collagen interfibrillar spacing calculations is shown by an arrow in figures (A) and (B) respectively.

The intensity distribution is calculated using equation 1 below.

Equation 1: $I(Q)=F^2(Q)E(Q)+B(Q)$

Where,

$I(Q)$ = the integrated intensity distribution

F^2 = the fibril transform

$E(Q)$ = fibril interference function

B = background scatter from other components

The interference function E(Q) contains information about the mean centre to centre collagen fibril spacing. This was calculated by rearranging equation 1 into equation 2, and then following the stepwise sequence outlined below.

Equation 2. $$E(Q)=\frac{I(Q)-B(Q)}{F^2(Q)}$$

Step 1: *Remove background scatter, B caused by other components*

Scatter intensity, I is multiplied by its radial position, R to obtain IR - corrected to accommodate a linear scan across a circular x-ray pattern, and take into account the small sampling size to create the integrated intensity distribution profile. A linear background (LOGBACK) was generated for the natural log graph of IR against R, as shown in figure 3.4 below.

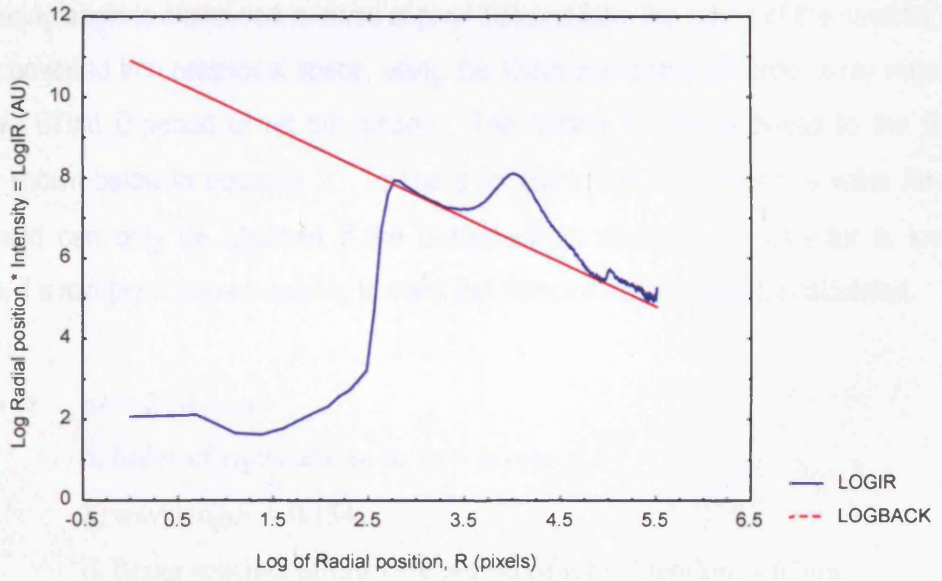

Figure 2.4. Linear background generation, shown in red.

The linear background was then anti-logged, (ANTILOGB) and subtracted from the image profile graph of R against IR to produce a new background subtracted intensity profile, IR-ALB. This removes diffuse x-ray scatter, leaving only peaks associated with low-angle x-ray reflections of the cornea, shown in green on figure 2.5 below.

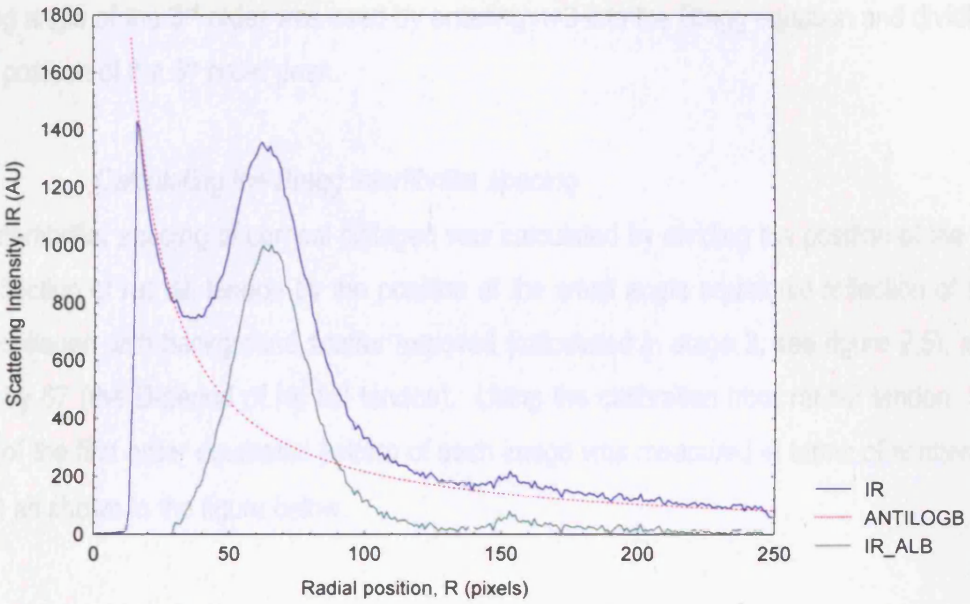

Figure 2.5. Back ground scatter (ANTILOGB) is removed from the profile of scattering intensity against radial position (IR) to leave only corneal small angle reflections (IR-ALB).

Step 2: *Calibration with rat tail tendon*

The scattering angle is expressed in terms of pixel distance from the centre of the detector, and must be converted into reciprocal space, using the sharp meridional 5th order x-ray reflection and known 67nm D-period of rat tail tendon. The reason for this is linked to the Bragg equation, shown below in equation 2. To find d for chick corneal collagen, a value for θ is needed, and can only be obtained if the distance from specimen to detector is known. Therefore, if a sample of known spacing is used, the detector distance can be calculated.

Equation 2: $n\lambda = 2 \cdot d \cdot \sin\theta$

Where; n, order of equatorial peak, in this case = 5

λ, wavelength = 0.154

d, Bragg spacing, in this case period of rat tail tendon = 67nm

θ = half the angle between incident x-ray beam and reflection

Firstly, the scattering angle 2θ of rat tail tendon was calculated by entering the values n=5, λ=0.154 and d=67 into the Bragg Equation, as shown in Equation 2. A calibration was formed for subsequent images by dividing the scattering angle of the rat tail tendon by the position of the most prominent peak, in the case the 5th order. When the 5th order was not achieved, the scattering angle of the 3rd order was used by entering n=3 into the Bragg equation and dividing it by the position of the 3rd order peak.

Step 3: *Calculating the Bragg interfibrillar spacing*

Bragg interfibrillar spacing of corneal collagen was calculated by dividing the position of the 5th order reflection of rat tail tendon by the position of the small angle equatorial reflection of the corneal collagen with background scatter removed (calculated in stage 2, see figure 2.5), and dividing by 67 (the D-period of rat tail tendon). Using the calibration from rat-tail tendon, the position of the first order equatorial pattern of each image was measured in terms of scattering angle 2θ as shown in the figure below.

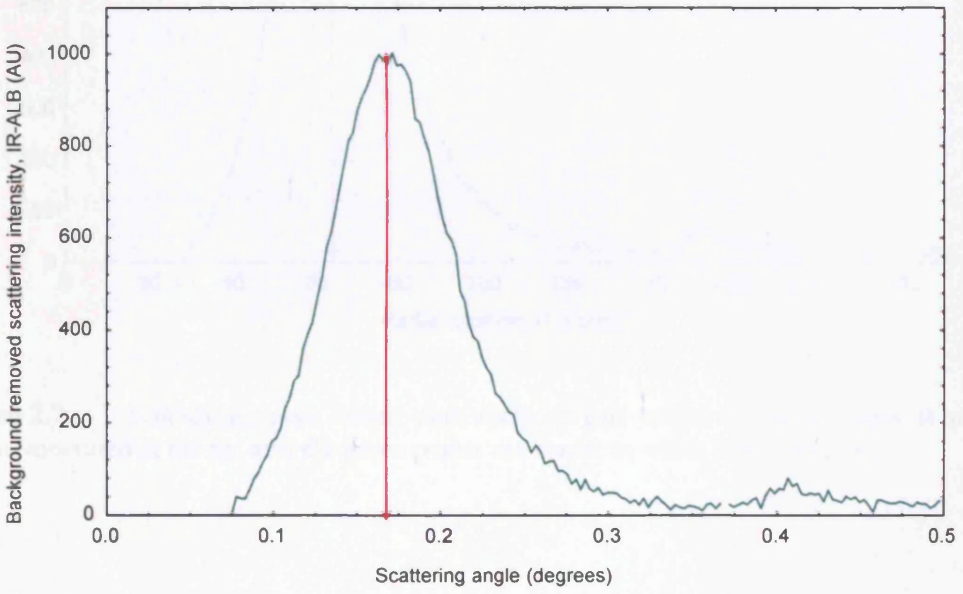

Figure 2.6. Scattering angle calculation.

The scattering angle of the collagen was then halved to produce the Bragg angle θ. The centre-to-centre collagen fibril Bragg spacing for each sample was calculated by entering the

Bragg angle of collagen into Equation 2. Bragg spacing can be converted to actual spacing using a multiplication factor of 1.12, based on the assumption that the cornea has liquid like packing (Worthington and Inouye, 1985).

2.3.4 Local order

The degree of order within the collagen lattice can be approximated using another calculation taken from figure 2.6; the more ordered the lattice, the sharper the x-ray scatter peak. By measuring the ratio of peak height to peak width at half height (shown below in figure 2.7), the peak sharpness, and thus level of collagen order may be appreciated.

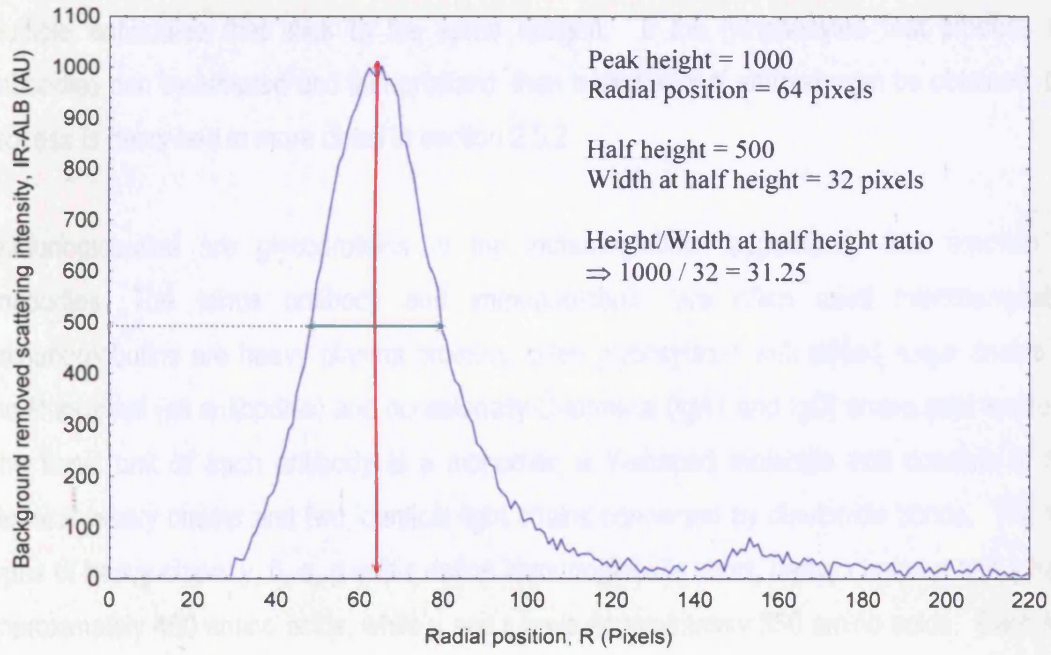

Figure 2.7. Calculating peak height and width at half height. The red lines show peak height, measured at the tip, and the green points the reader to width at half height.

2.4 Biochemical analyses

For ease of reading, reagents are listed in appendix 1. The generic methods are described below, which were individually optimised for each experiment, results are shown in appendix 2. Further details are available within each relevant experimental chapter.

2.4.1 Antibodies and ELISA

A defining characteristic of antibodies is their ability to exclusively bind a particular antigen, and this is utilised in a range of biochemical methods, such as enzyme-linked immunosorbant assays, or ELISA. Purified antibodies are produced by injecting the antigen into a small mammal, such as a mouse, although to obtain large quantity of antibodies goats, sheep, or horses may be used. Blood isolated from these animals contains polyclonal antibodies - multiple antibodies that stick to the same antigen. If the lymphocytes that produce the antibodies can be isolated and immortalized, then a monoclonal antibody can be obtained, this process is described in more detail in section 2.5.2.

Immunoglobulins are glycoproteins in the immunoglobulin superfamily that function as antibodies. The terms antibody and immunoglobulin are often used interchangeably. Immunoglobulins are heavy plasma proteins, often glycosylated with added sugar chains on the N-terminal (all antibodies) and occasionally O-terminal (IgA1 and IgD) amino acid residues. The basic unit of each antibody is a monomer, a Y-shaped molecule that consists of two identical heavy chains and two identical light chains connected by disulphide bonds. The five types of heavy chain: γ, δ, α, μ and ε define immunoglobulin class, heavy chains α and γ have approximately 450 amino acids, while μ and ε have approximately 550 amino acids. Each fork of the Y is an Fab fragment, composed of one constant and one variable domain of each heavy and the light chain, which together shape the antigen binding site at the amino terminal end of the monomer. The two variable domains bind their specific antigens.

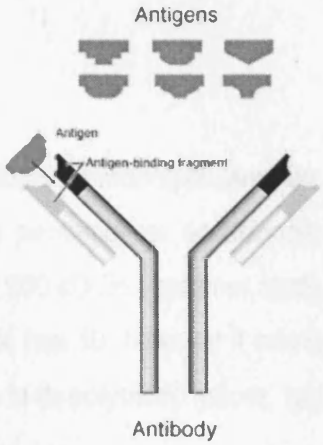

Figure 2.8. Antibody structure and binding. Taken from: http://www.genome.gov/Pages/Hyperion/DIR/VIP/Glossary/Illustration/antibody.cfm?key=antibody

2.4.2 Isotypes

According to differences in their heavy chain constant domains, immunoglobulins are grouped into five classes, or isotypes: IgG, IgA, IgM, IgD, and IgE. The constant binding domain receptors determine interaction with other immune cells *in vivo*. Antibodies produced by a single B lymphocyte can differ in their heavy chain, and different classes of antibodies may be expressed at the same time. However, these antibodies are identical in their specificity for antigen, conferred by the variable region. To achieve the large number of specificities needed to protect the body against different foreign antigens, millions of B lymphoyctes are needed. To produce such a diversity of antigen binding sites from a separate gene for each possible antigen, the immune system would require many more genes than exist in a genome. Instead, as Susumu Tonegawa showed in 1976, portions of the genome in B lymphocytes can recombine to form any variation seen in the antibodies. The discovery of genetic principle for generation of antibody diversity won the Nobel Prize in Physiology or Medicine in 1987.

Of the antibodies used in this work, the KS binding antibodies 5-D-4, 1-B-4, and 2-D-3 are IgG's, and BKS-1 is an IgM:

IgG

IgG is a monomeric immunoglobulin, consisting of two heavy chains γ and two light chains, each molecule has two antigen binding sites. This is the most abundant immunoglobulin and is the only isotype able to pass through the placenta.

IgM

IgM forms polymers where multiple immunoglobulins are covalently linked together with disulphide bonds, normally as a pentamer or occasionally as a hexamer. It has a large molecular mass of approximately 900 kD (in pentamer form). Each monomer has two antigen binding sites, meaning that an IgM has 10, however it cannot bind 10 antigens simultaneously because of steric hindrance. Due to its polymeric nature, IgM possesses high avidity.

Monoclonal Antibodies

Injecting a foreign antigen (in this case KS) into a vertebrate system such as mouse initialises an immune response. B-cells turn into plasma cells and produce antibodies that bind the antigen. B-cells removed from the spleen of a mouse challenged with the KS antigen will produce monoclonal anti-KS antibodies, sensitive to a specific KS epitope. These B-cells are immortalised through fusion with non-antibody producing myeloma tumour cells (which grow indefinitely in culture), and the resulting hybridoma cells retain cancer-like properties; having the ability to multiply rapidly and indefinitely, so producing a large amount of antibodies. The hybridomas are then optimised to find the most effective marker to the original antigen. Monoclonal antibodies can be produced in cell culture or in animals, hybridoma cells injected into mice produce tumours containing an antibody-rich fluid called ascites.

2.5 Keratan Sulphate antibodies used in this study

Of the monoclonal antibodies used in these experiments, 5-D-4 was raised against KS on the core proteins of human articular cartilage proteoglycans (Caterson *et al.*, 1985), recognising the antigenic determinant of linear pentasulphated hexassacharides (Mehmet *et al.*, 1986) as the smallest structure. Chemical desulphation of KS reduces antigenicity (Zanetti *et al.* 1985), and no response is seen with any other GAG, such as dermatan sulphate (Tang *et al.,* 1986).

Another monoclonal antibody (mAb) to originate from the Caterson laboratory, 1-B-4, shows similar reactivity as 5-D-4, although affinity is also shown for a tetrasulphated hexassacharide analogue (Mehmet *et al.*, 1986). MAb 2D3 recognises under-sulphated forms of KS (Caterson *et al.*, 1989) and although the exact epitope has not yet been fully characterised, the antibody

has been well utilised for studies of KS undersulphation (Kavanagh *et al.*, 2002; Caterson *et al.*, 1989). All of these antibodies have been used previously in chicks (Sorrell and Caterson, 1989; Coleman *et al.*, 1998) and require no prior enzymatic treatment.

Monoclonal antibody BKS-1 specifically recognises the keratanase generated neoepitope (N-acetyl-glucosamine-6-sulphate (GlcNAc-6-S)) at the non-reducing terminal of both corneal and skeletal KS GAG chains, produced using keratanase I. BKS-1 has been shown as an effective and specific marker for KS in the human cornea, limbus and sclera (Ahktar *et al.*, 2005)

The relevant role of each antibody in this thesis is justified by their specificities, as shown in table 2.1; for example 5-D-4 recognises all sulphated structures within one KS chain, whereas BKS-1 recognises a single neoepitope on KS after keratanase digestion. It would be very interesting to have conducted each antibody assay on every single digest, but unfortunately due to repetition and digestion requirements the two x-ray data sets had to be split into Papain or Cyanogen Bromide digests.

Antibody	Description	Epitope	Treatment
5D4	Mouse monoclonal IgG	Linear penta-sulphated sequences of N-acetyl lactosamine disaccharides of KSPGs with both GalNAc and Gal sulphated	None - reacts with native epitope
1B4	Mouse monoclonal IgG	Linear hepta-sulphated sequences of N-acetyl lactosamine disaccharides of KSPGs	None - reacts with native epitope
2D3	Mouse monoclonal IgG	Under-sulphated KS GAGs	None - reacts with native epitope
BKS-1	Mouse monoclonal IgM	Keratanase (I) generated 6-sulphated N-acetyl glucosamine stub at non-reducing terminal on KS chains	Requires keratanase treatment to reveal neoepitope

Table 2.1. Specificities of anti-KS antibodies used in this study.

2.5.1 KSPG extraction

Corneas returned from station 2.1 (frozen at -80°C) were separated into two studies, as shown in figure 2.9:

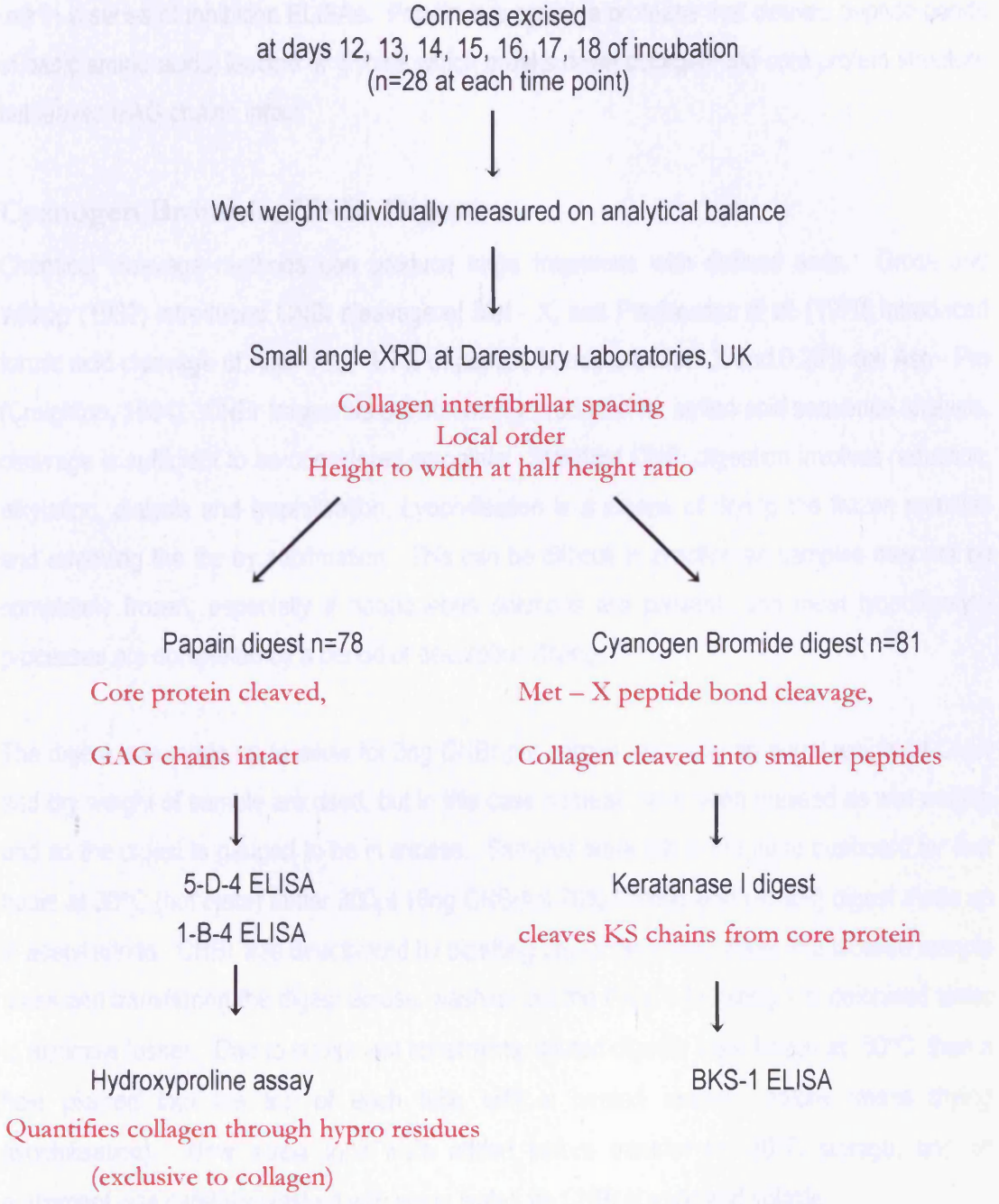

Figure 2.9. Tissue processing post small angle scattering experiments.

Papain Digest

After x-ray analysis, frozen single corneas were transferred to 2ml screw top tubes and digested for 15 hours with 1mg/ml papain (Sigma, P4762) digestion buffer (1ml) at 60°C. Extracts were denatured by boiling for 15 minutes at 100°C and then frozen at -30°C before use in a series of inhibition ELISAs. Papain is a cysteine protease that cleaves peptide bonds of basic amino acids, leucine or glycine which breaks down collagen and core protein structure but leaves GAG chains intact.

Cyanogen Bromide, CNBr Digest

Chemical cleavage methods can produce large fragments with defined ends. Gross and Witkop (1962) introduced CNBr cleavage of Met - X, and Piszkiewicz *et al.* (1970) introduced formic acid cleavage of Asp - Pro. 1.7% of peptide bonds are Met - X and 0.25% are Asp - Pro (Creighton, 1984). CNBr fragments are commonly produced for amino acid sequence analysis, cleavage is sufficient to be considered complete. Standard CNBr digestion involves reduction, alkylation, dialysis and lyophilisation. Lyophilisation is a means of drying the frozen samples and removing the ice by sublimation. This can be difficult in practice as samples may not be completely frozen, especially if nonaqueous solutions are present, and most lyophilisation processes are completed by a period of desorption drying.

The digest was made up to allow for 3ng CNBr per cornea; normally an equal weight of CNBr and dry weight of sample are used, but in this case corneas have been massed as wet weight, and so the digest is gauged to be in excess. Samples were left in the fume cupboard for four hours at 30°C (hot plate) under 300µl 10ng CNBr/ml 70% Formic acid (AnalR) digest made up in acetyl nitride. CNBr was deactivated by pipetting 2ml of deionised water into labelled sample tubes and transferring the digest across, washing out the initial tube using 1ml deionised water to minimise losses. Due to equipment constraints, diluted digests were frozen at -80°C, then a hole pierced into the top of each tube with a heated skewer, before freeze drying (lyophilisation). New screw tops were added before transfer to -80°C storage, and all equipment was carefully washed with warm water, as CNBr is toxic and volatile.

2.5.2 Keratanase digest of CNBr digested samples

Because BKS-1 recognises a neoepitope stub near the core protein, KS chains must be removed to allow antibody binding. Dried CNBr digested corneas were reconstituted in a total volume of 500µl, of this 470µl 1X Tris Ac for Keratanase buffer and 20µl 0.001units/µl stock Keratanase (*Pseudomonas Sp.*, Sigma-Aldrich) to concentrate GAGs and promote keratanase I enzyme action. 10µl (0.01units) chondroitinase was added to remove hindrance from CS chains. Keratanase cleaves β-galactosidic bonds next to unsulphated galactosyl residues to produce disaccharides, and at an unsulphated galactose flanked by sulphated N-acteylglucosamines. Keratanase cleavage results in a large number of oligosaccharides.

(A)

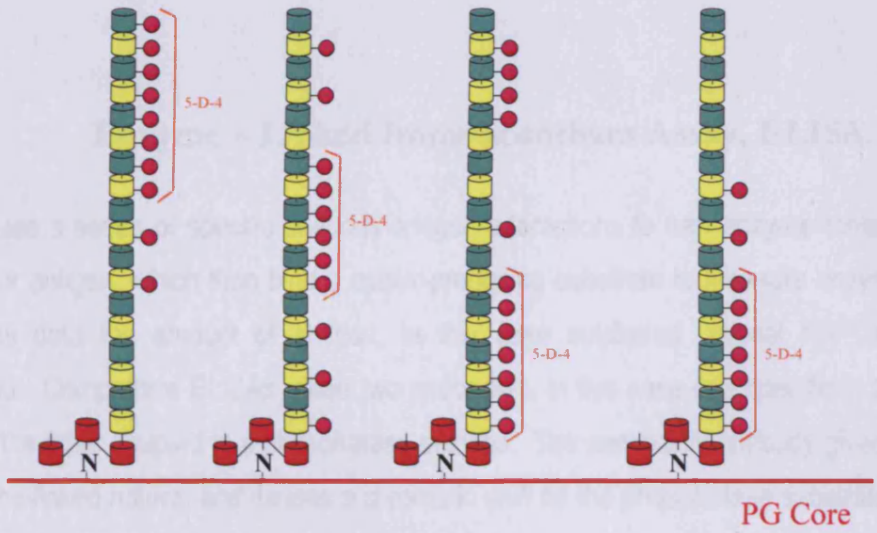

(B)

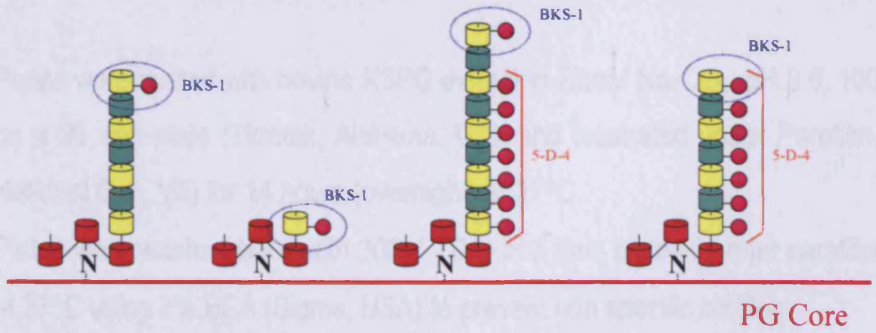

Figures 2.10A, and B. Keratanase action and antigenicity. Red cylinders: mannose, pink circles: sulphates, yellow cylinders: N-acetylglucosamine (GluNAc), green cylinders: galactose (Gal). Figure (A) shows KS structure and reactivity with monoclonal antibody 5-D-4, and (B) shows KS structure after keratanase I digestion and consequent reactivity with BKS-1. *Adapted from*: Kerr, B (Poster)

Normally, keratanase is used at 0.001units/10μl GAG, but as GAGs are an unknown quantity in these corneas, 0.02units were selected for each cornea to ensure an excess without undue wastage. Ideally, a greater volume of keratanase could have been used, but the sheer scaling factor of these experiments (90 corneas) provides an economic balancing factor.

Samples were first reconstituted in 470μl buffer for 1 hour on a rocker at 37°C, and then 20μl 0.001units/μl keratanase I and 10μl 0.001units/μl chondroitinase added before gentle mixing and incubation on a rocker at 37°C overnight. Chondroitinase is also active in the Tris Ac buffer. As the enzymes will be removed from further assays during washing, it is not necessary to denature. Keratanase digests were transferred to 1ml screw top tubes and frozen at -30°C ready for further use.

2.5.3 Enzyme – Linked Immunosorbant Assay, ELISA

ELISAs use a series of specific antibody-antigen interactions to trap enzyme molecules as a marker for antigen, which then bind a colour-producing substrate to measure enzyme activity. From this data the amount of antigen, in this case sulphated corneal KSPGs, may be calculated. Competitive ELISAs utilise two antibodies, in this case one specific to the antigen KS, and the other coupled to a phosphatase enzyme. The secondary antibody gives the assay its enzyme-linked nature, and causes a chromatic shift as the phosphotase substrate produces a signal. In this case, all of the ELISAs used follow the same protocol; the general outline is listed below, and specific details can be found within each experimental chapter.

1. Plates were coated with bovine KSPG extract in 20mM Na_2CO_3, pH 9.6, 100μl per well on a 96 well plate (Titretek, Alabama, US), and incubated under Parafilm (American National Can, WI) for 14 hours (overnight) at 37°C.
2. Plates were washed twice with 300μl TSA, and then blocked under parafilm for 1 hour at 37°C using 1% BSA (Sigma, USA) to prevent non specific binding.
3. Known concentrations of bovine competing antigen were used to generate standard curve serial dilutions. Developing chick corneal digests were serially diluted and incubated with an equal volume of KSmAb, before adding them to the ELISA plate.

Serially diluted primary antibody (KS specific) is made up at half final dilution, and then incubated in the presence of its antigen (creating final dilution) in both the known standards and chick unknown samples for 1 hour at 37°C. Serial dilutions are shown in Appendix 1.

4. Plates were washed 4 times using 300µl TSA, and bound antibody/antigen complexes added to the antigen coated wells, 100µl per well. Chick corneal antigen competes with plate-bound bovine antigen for primary antibody binding, so that higher tissue levels of chick KS result in less antibody binding to the plate bound antigen. Unused wells were then blocked using 100µl 1%BSA. Plates were incubated at 37°C under parafilm for 1 hour.
5. Plates were washed 6 times with 300µl TSA to remove unbound antibody competing with plate bound antigen. In competitive ELISA, the higher the original antigen concentration, the less antibody binding to plate bound bovine antigen, and weaker the eventual signal. A goat anti-mouse (H+L) alkaline phosphatase conjugated secondary antibody (Promega, USA, S372B, 19253403) specific to the murine primary antibody was added, 2µg in 10ml 1% BSA, 100µl/well. This secondary antimouse antibody is coupled to a phosphatase enzyme, which is used to create a colour signal representing KSMAb binding to the ELISA plate – the inverse of competing antigen concentration. Plates were covered in parafilm and incubated for 1 hour at 37°C.
6. The plate is washed 6 times with 300µl TSA to remove unbound antibody, and phosphatase (colour producing) substrate (Promega, Madison, WI) added, 2 tablets in 10ml DEA buffer; 100µl/well. Plates were covered in parafilm and incubated for 1 hour at 37°C. Adding phosphatase substrate causes the following metachromatic shift on reaction, which is used to measure the amount of keratan sulphate in the sample with a spectrophotometer.

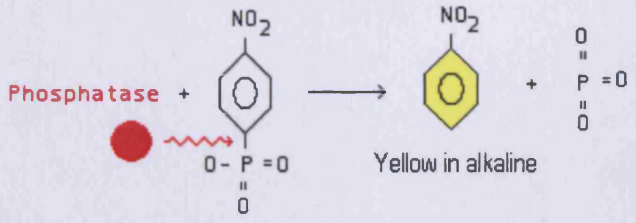

Figure 2.11. Phosphatase action produces a colour shift.

7. Plates were then read at 405nm using labsystems multiscan MS plate reader. From this readout, KS is quantified against a standard curve of known competing antigen aggrecan concentrations from each ELISA plate.

2.5.4 Keratan sulphate quantification

A standard curve was generated from the optical absorbance of known bovine KSPG extracts for each plate, and the chick corneal extract dilutions read from the curve as shown in figure 2.12.

(A)

ng/ml Antigen	Mean Optical Absorbance	% of 0ng/ml Competing Antigen
9000	0.146	11.1
3000	0.322	24.5
1000	0.6865	52.2
333.3'	1.0115	76.9
111.1'	1.211	89.09
37.04	1.241	92.1
12.34	1.172	94.3
0	1.3155	100
D17-13L	0.628	47.7

Figure 2.12A. Example of standard curve calculations from optical density (A), bovine dilutions are shown in black, and nominal chick sample in red. KS content of chick corneal extracts was deduced using a standard curve (Figure 2.12B, overleaf).

(B)

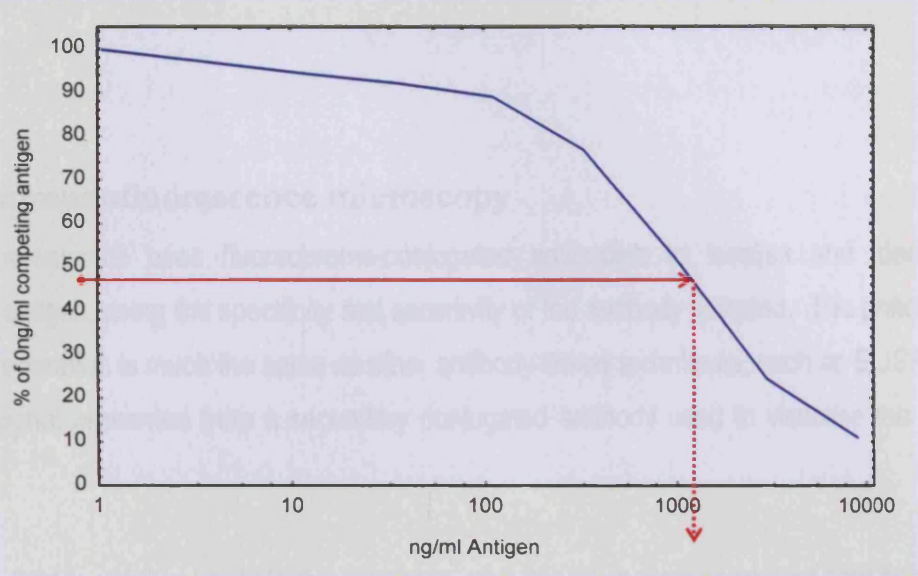

Figure 2.12B. Example of standard curve calculations from optical density (shown in Figure 2.12A). KS content of chick corneal extracts was deduced by reading across from % absorbance compared to 0ng/ml antigen on the standard curve (B), as shown by the red arrows.

The amount of KS was then calculated from the dilution factor and units expressed in ng relative to corneal wet weight and also collagen/hydroxyproline content.

2.6 Hydroxyproline assay

Hydroxyproline stabilises the collagen triple helix by forming hydrogen bonds, and is commonly used to quantify collagen as a marker exclusively to collagenous sequences. Hydroxyproline is commonly found in the third position, but not always, and non-hydroxyproline regions may correspond to enzymatic cleavage sites. Corneal extracts were hydrolysed into single amino acids using equal volumes of 11.7N conc HCl to supernatant at 110°C overnight, and then freeze dried to remove any acid. Dried hydrolysates were then reconstituted in distilled water and centrifuged to remove particulate material. Hydroxyproline residues were assayed in 30µl triplicate against known standard dilutions (shown in Appendix 1) of 0µg/ml, 2µg/ml, 4µg/ml, 6µg/ml, 8µg/ml, and 10µg/ml, with 70µl diluent and 50µl oxidant, and 125µl colour reagent, and read at 540nm after 10-20mins incubation at 70°C. Hydroxyproline content in the unkown chick corneal digests was calculated using a standard curve on each 96 well plate, and the collagen content deduced by calculation. Because hydroxyproline constitutes 14% of collagen

type I, the amount of collagen can be extrapolated by multiplying the hydroxyproline content by 7.

2.7 Immunofluorescence microscopy

Immunofluorescence uses fluorochrome-conjugated antibodies to localise and identify a particular antigen, using the specificity and sensitivity of the antibody selected. The principle of sample preparation is much the same as other antibody-linked techniques, such as ELISA, with the final signal presented from a secondary conjugated antibody used to visualise the target protein.

Excitation light is used to irradiate the specimen, and the much weaker emitted light filtered to form the image. Filtering ensures that only light with the desired wavelength (that of the fluorescing material) is collected. Excitation radiation collides with atoms in the fluorophore, and electrons are excited to a higher energy level, light is emitted as they relax to a lower level. To visualise this process, emitted light is separated from the much brighter excitation light in a second filter. Because the emitted light is of lower energy (longer wavelength), the fluorescing areas can be observed under the microscope and shine out against a dark background with high contrast.

Fluorochromes absorb (invisible) UV radiation and emit a longer wavelength light visible to the human eye; for example, fluorescein isothiocynate (FITC) fluoresces green under blue light, and has an excitation wavelength of 494nm and emission wavelength of 520nm. This fluorochrome is primarily conjugated to antibodies. Once the fluorochrome is attached to the sample, the objective lens of the microscope must perform two roles (Howard,1994). Excitation light is focussed onto the sample, and the resulting fluorescence captured. In this case, the confocal system is supplied with four lasers; allowing excitation of a broad range of fluorochromes within the UV, visible and far red ranges of the electromagnetic spectrum. A significant problem with immunofluorescence is photobleaching, the destruction of the photochemical fluor by high-intensity light.

2.7.1 Sample preparation

Embryonic chicken corneas from developmental days 12 to 18 were orientated in a large droplet of Tissue Tek (Miles, Ind., USA), which was then snap-frozen in liquid nitrogen cooled isopentane on labelled cork disks until the Tissue Tek was solid, and then stored at −80°C until sectioning. Rapid freezing at liquid nitrogen temperatures means that water freezes in a vitreous, non-crystalline manner, which limits structural damage. Sectioning was carried out on a Leica CM 3050S cryostat (Leica, Vienna, Austria) at 7 µm thick, and sections transferred onto sialanised slides (Dako Cytomation, S3003), and then stored at −30°C until use.

As previously mentioned, the use of antibodies in microscopy necessitates a similar preparation protocol to other immunohistochemical techniques – a series of blocking, labelling (primary antibody), washing, and visualisation (secondary antibody) steps must be taken. Selected slides were allowed to thaw from -30ºC under ambient air flow. 0.01M PBS solution was made up: 60ml 0.5M PB solution, 25.5g NaCl into 3l deionised water, and then sections rehydrated for 10 minutes underneath a 1ml droplet in a humidifying box. Slides were flicked dry and sections circled using a super PAP pen (Daido Sangyo Co. Ltd, Tokyo), and any non specific binding blocked using a 1:20 dilution normal goat serum (Dako; X0907), 200µl per section. Slides were then left to incubate for 30 mins in a humidifying box at room temperature.

Serial dilutions of primary antibodies were made up to include negative controls. To check for non specific binding of primary antibody, the KS monoclonal antibody was replaced with naïve mouse immunoglobulin (Dako; X0931) at 1:100 dilution. To rule out non specific binding of the secondary goat anti-mouse antibody, the primary KS antibody was omitted and replaced with antibody diluent (0.01M PBS). Sections were covered with antibody/control droplets and left to incubate for 2 hrs in a humidifying box at room temperature.

Sections were washed using three changes of 0.01m PBS of 5mins to remove unbound primary antibody, and then a secondary, fluorescent anti-mouse antibody (Alexa 488, fluoresces green, with excitation wavelength 488nm) was added (200µl per section) after serial dilutions to a working dilution of 1:1000. *Alexa must be filtered through a syringe (Terumo SS-025z, Corning Incorporated 431215), so is made up in excess for the correct final volume. This secondary antibody is light sensitive so all stages were protected from direct light using either foil (in preparation), or a darkened humidifying box (during incubation). A large droplet of

secondary antibody was pipetted onto each section, and sections incubated for 2 hrs at room temperature in a darkened, covered humidifying box.

Unbound secondary antibody was removed using three washes of 0.01m PBS of 5mins each. Then slides were carefully blotted dry (around sections), mounted using Vectashield mountant (Vector Labs; H-1200) containing Propidium Iodide (fluoresces red, with excitation/emission 535/617nm wavelength) at 5µl per section, and sealed under a 24 x 60mm glass coverslip using clear nail varnish. Recipes are shown in Appendix 1.

2.7.2 Immunofluorescence

A Leica TCS SP2 (Leica, Vienna, Austria) microscope was used to observe the corneal sections at x25 magnification to achieve mid stromal, full thickness images from epithelium to endothelium. Images taken using an Olympus AX470 camera (Olympus, UK) were transferred to Adobe Photoshop (Adobe Systems Incorporated, US) and combined to present an image of propidium iodide and antibody fluorescence.

2.8 Electron microscopy

The transmission electron microscope (TEM) operates using the same basic principles as the light microscope. A beam of electrons is focussed onto the specimen creating an enlarged image on a fluorescent screen, layer of photographic film, or CCD camera. The first practical transmission electron microscope was built by Albert Prebus and James Hillier at the University of Toronto in 1938 using concepts developed earlier by Max Knoll and Ernst Ruska (Bozzola and Russell, 1991).

The maximum resolution of an image is determined by the wavelength of the photons used to probe the sample. Visible light has wavelengths of 400–700nm, larger than many objects of interest. UV could be used to increase resolution, but absorption problems must be overcome. Electrons have both wave and particle properties (established by Louis-Victor de Broglie), and can therefore behave like a beam of radiation. Wavelength is dependent on electron energy, and adjustment of accelerating fields creates wavelengths less than that of light which can

interact with a sample due to their electrical charge. The electrons are focussed onto the sample enabling a high resolution image with improved depth of vision (Bozzola and Russell, 1991). Compounds of heavy metals such as lead or uranium can be used to selectively deposit heavy atoms in the sample and enhance structural detail, the dense electron clouds of the heavy atoms interacting strongly with the electron beam. For further information into the detailed workings of the electron microscope, the reader is directed to Bozzola and Russell (1991).

Electron microscopy has played a major role in studies of collagen type distribution using immunolabelling. However, collagen epitopes for specific antibodies appear intolerant to many routine methods, particularly chemical fixation with aldehydes (Young *et al.,* 2000). Consequently, previous investigations of collagen interactions may have resulted in immunoelectron microscopy of chemically disrupted fibrils. For example, as discussed in chapter 1, type V collagen epitopes were hidden within major interstitial collagen type I fibrils and fibril disruption was necessary to localise the minor collagen (Birk *et al.,* 1988). To overcome the difficulties associated with chemical fixation and to avoid PG extraction and/or precipitation now linked with conventional aqueous fixation and dehydration (Hunziker, 1993), low temperature embedding resins can be used in conjunction with either the progressive lowering of temperature technique or with freeze-substitution.

2.8.1 Low temperature embedding

Before embedding corneas for use in electron microscopy, a compromise had to be made between the preservation of corneal tissue, and antigenicity protection. In this study, two corneas were taken from each developmental day between days 8 and 18 of incubation and each put into a separate vial of weak fix; either 1% glutaraldehyde or "205" for 1 hour to test antigen survival post fixation. As tissue is diffuse and easily torn in the earlier stages of development (less than 12 days), entire heads were dropped into fix after decapitation, and then the cornea carefully dissected away under a Nikon SM21000 light microscope, and the corneas placed into fresh solution to make up to 1hr fixation. All recipes are shown in Appendix 1.

Glutaraldehyde is a high-crosslinking dialdehyde fix which preserves protein structure, but can consequently mask protein epitopes, such as KS, and cause shrinkage at higher concentrations. Lipids are not fixed, and normally secondary fixation by osmium tetroxide is necessary. Because this study is embedding corneas into lowicryl, polymerisation is carried out using UV light, which cannot penetrate the black stain of OsO_4 . making it unsuitable but luckily not indispensable, as fixation is sufficiently complete for these studies. 205 is a milder paraformaldehyde fix (a mono-aldehyde) commonly used for more difficult antigen preservation in immunoelectron microscopy. These different fixes were chosen to optimise antigen preservation. After brief fixation, samples were placed into sodium borohydride in Sorenson Phosphate buffer for 4 hours (stored at 4°C) to block any free aldehyde groups and prevent a false positive antibody result. Corneas were then washed in Sorenson Phosphate buffer and stored at 4°C in fresh buffer before dehydration at low temperatures for embedding into resin.

Fixed corneas were placed into increasing concentrations of ethanol (a cryoprotectant, miscible with lowicryl during substitution), to replace water as the temperature was gradually lowered to -25°C. Substitution was carried out at low temperatures to prevent the denaturation of proteins and lipoproteins involved in conventional embedding. Ethanol was used for sample dehydration prior to freezing to prevent the formation of internal ice crystals and distortion of stromal ultrastructure. After dehydration, specimens may be stained *en bloc* by uranyl acetate to increase contrast and visualise collagen, and then infiltrated by lowicryl resin, however, section staining was used in this study (see 2.8.3). *En bloc* staining at this stage could mask antigenicity by crosslinking epitopes, and also inhibit polymerisation by UV by colouring the tissue. The lowicryl resin was polymerised in an exothermic reaction at low temperatures using long wavelength (360nm) UV light, and the blocks gradually brought up to room temperature. All low temperature embedding in this work was carried out using a Reichert Automated Freeze-Substitution, AFS (Leica, Vienna, Austria).

Rationale

Low temperature embedding was chosen for this study because the adverse effects of organic solvents and resins on biological tissue are reduced. Carlemalm *et al.* (1982) demonstrated that molecular order was better preserved through low temperature embedding compared to experiments conducted at higher temperatures. Low-temperature embedding in Lowicryl resin

also improves ultrastructural preservation (Weibull *et al.* 1980), and could also overcome temperature sensitivity of some antigenic sites to high concentrations of fixatives.

Lowicryl K4M is a polar highly cross-linked acrylate and methacrylate embedding medium formulated to provide low viscosity to around -35°C. The hydrophilic properties of K4M confer two main advantages; during dehydration and infiltration samples may be partially hydrated due to resin water-tolerance (up to 5% by weight), and antigenicity is preserved with significantly lower background labelling (Roth, 1982). Acrylates and methacrylates are common monomers in polymer plastics, as they polymerise easily due to vinyl groups; two carbon atoms double bonded to each other, directly attached to the carbonyl carbon.

2.8.2 Sectioning

Polymerised hygroscopic blocks were further hardened in a dessicator overnight to remove any atmospheric moisture that could weaken bonding. Glass knives were created on an EMKMR2 (Leica, Vienna, Austria), and sections taken using a Leica UC6 microtome.

The glass knife was carefully postioned to avoid any serrated areas (from stress fracture), and tilted to 6° for cutting. The block was trimmed down in rocking mode, and when the trimming was finished, deionised water was dripped into the channel underneath the knife, keeping the meniscus low to prevent hydrophilic lowicryl from degenerating by absorbing water. Sections were carefully removed with a single hair, making sure there was no sticking to the coil. These initial sections were used to check for tissue under a Leica Galen III light microscope (Leica, Vienna, Austria) by placing onto a bonded slide in a drop of water and dried on hot plate, and then stained with toluidine blue. Glass knives were effectively relegated by the advent of diamond knives, but are still commonly used to trim down blocks in preparation for ultrathin sectioning with a diamond knife.

Once desirable sections were confirmed, a Diatome 45° high boat diamond knife was used to cut ~90nm sections at a speed of 1mm/s (only around cutting window), and feed of 100nm advance. The cutting window was set by manually moving the knife from the block (start) to the desired end point (finish), and then programmed to advance to section. Section thickness

is an important aspect of image clarity; if sections are too thin, there is too little contrast for clear pictures, normally silver to grey sections are used from resin blocks (90 to >60nm thick).

Sections were put onto circular support film by scooping them out of the knife boat with a 300 mesh nickel grid (300 bars per inch) held by forceps, and pushing around 6 sections into position on each grid using a single hair. Grids were air dried in the dark to prevent any further cross-linking of the lowicryl resin and obscuring of epitopes. Water was removed from the boat well with a syringe, and the knife cleaned by cutting a foam block to remove any section or resin. Sectioning with the diamond knife was carried out with the generous help of Dr. Rob Young.

2.8.3 Immunostaining

Immuno-electron microscopy is used to localise molecules at an ultrastructural level through labelling with specific antibodies. Antibodies are visualised by electron-opaque markers (colloidal gold particles) attached to them via a secondary antibody (indirect labelling). The effect is to produce an electron-dense label at the site of the antigen-antibody reaction.

All incubation stages were carried out in a dark humidifying box on a strip of Parafilm M (American National Can, WI) using a large droplet of the liquid in question. Grids were rehydrated in PBS for 5 minutes prior to staining, to relax any shrinkage. Enzymatic treatment can be used at this stage to remove any hindrance which could interfere with primary antibody binding, however the KS antibodies selected for this work (5D4 and 1B4) are known to be sufficiently robust to negate the need for enzymatic processing (Young *et al.*, *in press*). This also maintains the integrity of available epitopes, as there is a danger that KS chains could be affected by CS/DS removal and antigenicity reduced. Non specific binding was blocked using PBS/1%BSA for 30 minutes, and then primary antibody added at 1:100 dilution in the same PBS/1%BSA vector and incubated for 2 hours at room temperature.

Sections were washed in PBS/1%BSA (5 washes of 3 minutes) and then incubated for 1 hour with a secondary goat antimouse 10nm gold conjugated antibody, GAM Au_{10} (British Biocell International, UK) to allow primary antibody visualisation. In low magnification work larger gold particles (15-30nm) are more easily seen, however in high magnification studies smaller

particles (5-10nm) are preferred as in principle they yield a higher labelling intensity because of reduced steric hindrance to antigen detection. In addition, increased charge repulsion between larger gold particles reduces the number of labelled antibodies able to access the target antigen. Small gold particles may be subsequently silver enhanced on the section to produce larger particles with this high labelling intensity, although in this case no further enhancement was needed.

The secondary antibody was removed by washing in PBS (5 times for 3 mins) without 1%BSA to remove any superfluous protein, and then incubated with 1% glutaraldehyde in PBS for 5 minutes to crosslink (and preserve) primary/secondary antibody conjugation, preventing dissociation during uranyl acetate staining. Sections were then incubated in PBS for 3 minutes and finally washed with distilled water (5 times for 3 mins) to remove PBS and prevent crystallisation during drying.

Positive uranyl acetate staining was used to increase contrast and collagen definition by placing each dried grid section side down onto a droplet of yellow saturated aqueous uranyl acetate (2-4%), before covering and incubating for 30 minutes at room temperature. Uranyl ions react strongly with phosphate and amino groups, creating electron dense dark areas under the electron microscope. Excess uranyl acetate was washed away by dipping (20 times) into four successive dilutions of ethanol: 100% EtOH, 90% EtOH, 50% EtOH, 25% EtOH. Finally, grids were washed twice in filtered distilled water, and placed onto velin paper until dry.

After uranyl acetate staining, grids were lowered section side down onto a 30μl drop of aqueous Reynolds lead citrate for 7 minutes to further enhance contrast with the electron dense lead ion, followed by washing (20 dips) in three successive containers of fresh filtered distilled water. Extra stages of washing can sometimes include 0.01N NaOH and CO_2 free water (Bozzola and Russell, 1991) to prevent insoluble lead carbonate formation (precipitation), but this is commonly omitted as washing is sufficient to prevent granular contamination. Again, grids were carefully transferred section side up (using forceps) onto velin paper to dry. To ensure that drying was complete, grids were placed onto a circular rubber grid holder (section-side-up) and placed in a desiccator for at least 24 hours before examination. Images were taken on an EM208 transmission electron microscope (Philips, Eindhoven, The Netherlands), between 5000x and 25,000x magnification.

CHAPTER THREE: Localisation of Keratan Sulphate

3.1 Introduction to Chapter

Previous studies have documented the emergence of KS during development (Cornuet *et al.*, 1994; Dunlevy *et al.*, 1998), but a stage-by-stage developmental study remains elusive. It is well known that the chick cornea undergoes a series of compositional and morphological changes in the week leading up to hatch, and that KS has been implicated as a modulator in collagen arrangement: which creates the further question - how, or more specifically *where* does sulphated KS accumulate? A natural progression in this field of research seems to be the location and identification of sulphated KS epitopes at the light and electron level, to try and better understand these changes.

This chapter discusses the methods used to try to define spatial and temporal changes in sulphated KS expression during the latter stages of embryonic chick development. For ease of understanding, this chapter is presented in two sections. The first, section 3.2, is devoted to light level fluoresence microscopy, and the second, section 3.3 uses immunogold labelling in conjunction with transmission electron microscopy to locate sulphated KS at much higher resolution and ascertain the association with collagen fibrils. These methods have been used identify and locate KS in the stromal matrix.

An introduction to previous, relevant work will be first presented, and then each separate methodology outlined. The findings of each study will be presented and discussed, and finally possible future avenues for research identified.

3.2 Light level immunofluoresence

In this section, studies to characterise the emergence of KS using fluorescence microscopy will be covered.

3.2.1 Introduction

As should be clear from chapter 1, PGs are a functionally important molecule in the cornea. Some PGs have been shown to bind directly to fibrillar collagens – mediated by the protein core, namely decorin, fibromodulin and lumican (Rada *et al.*, 1993; Svensson *et al.*, 1995 and 2000). The GAG chains of corneal PGs are believed to function in the maintenance of interfibrillar spacing and normal tissue hydration (Iozzo, 1999), with KS GAGs appearing to play an important role in the acquisition and maintenance of corneal transparency. This is noticeable by the absence, or altered glycosylation state, of KSPGs in opaque corneal scars of adult rabbits (Hassell *et al.*, 1983; Funderburgh *et al.*, 1988; Cintron *et al.*, 1990). Also, KS core proteins are abundant in newborn mice corneas by postnatal day 10, whereas sulphated KSPGs are only detected after eye opening, suggesting a contribution to corneal transparency (Ying *et al.*, 1997). Knockout mice lacking the KSPG lumican develop bilateral corneal haze, display skin laxity and delayed corneal epithelial wound healing; a phenotype consistent with collagen network dysfunction (Chakravati *et al.*, 1998; Saika *et al.*, 2000). Sulphated KS is thought to be of functional importance in human vision too; this sulphated PG is missing in the most common forms of macular corneal dystrophy, (Hassell *et al.*, 1980) as corneal opacification occurs.

It is believed that corneal KS helps to maintain a specific collagen fibril conformation (Borcherding *et al.*, 1975). This arrangement of fibrils, in turn, is indicated as a significant contributory factor to the cornea's light transmission properties (Maurice, 1957). Previous investigators have reported conflicting evidence, with the accumulation of KS reported as posterior-to-anterior in the developing chick (Funderburgh *et al.*, 1986), and homogenous throughout (Takahashi *et al.*, 1999). The current studies hope to document the appearance of KS through the last week of embryonic chick corneal development.

3.2.2 Methods

The use of animals in this experiment was carried out in accordance with European Commission Directive 86/609/EEC. Fertile chicken eggs were collected from a commercial hatchery (Hy-line UK, Warwickshire, UK) at 24 hour intervals from days 12 to 18 of incubation, as confirmed by using Hamilton-Hamburger staging (Hamburger and Hamilton 1951; Hamburger 1992). Twelve corneas were excised at each time-point and immediately processed for immunohistochemistry.

Corneas were embedded in Tissue Tek (Miles, Ind., USA), snap-frozen and sectioned (7 µm thick), then stored at −80°C until use. Cryosections were collected on silanised glass slides, which were allowed to thaw under an ambient air flow prior to use. Sections were rehydrated under 1ml 0.01M phosphate-buffered saline (PBS; 60ml 0.5M PB solution, 25.5g NaCl into 3L deionised water), excess moisture removed, and sections isolated with a super PAP pen (Daido Sangyo Co. Ltd, Tokyo).

Non-specific binding was blocked by incubation for 30 min with 1:20 dilution normal goat serum (Dako; X0907), 200µl per section, before washing in 0.01M PBS. Primary antibodies 5D4 and 2D3 were serially diluted to a working dilution of 1:100, 200µl per section. Two negative controls were used; the first replacing KS mAb with naïve mouse immunoglobulin (Dako; X0931) at 1:100 dilution, and the second omitting KS mAb for antibody diluent (0.01M PBS). Primary antibodies were incubated for 2 hours before washing.

Sections were incubated at room temperature for one hour with anti-mouse IgG (1:1000 dilution) conjugated to Alexa Fluor 488 (Molecular Probes, Ore., USA), 200µl per section. *Alexa must be filtered through a syringe (Terumo SS-025z, Corning Incorporated 431215) to remove coagulated protein, so dilutions were made up in excess for correct final volume.

After washing with PBS, sections were mounted in medium containing PI (Vector Labs H-1300, Calif., USA) which fluoresces red at 535nm wavelength - 5µl per section under a 24 x 60mm glass coverslip. The edges were sealed, and sections examined under the fluorescence microscope (Leica, TCS SP2). This work was carried out at Kyoto Prefectural University of Medicine, Japan, on a JSPS sponsored Fellowship.

3.2.3 Results

Light level microscopy of the developing chick cornea reveals an accumulation of KS during the last week of incubation, as shown in figures 3.1 and 3.2 overleaf. Staining independently with the monoclonal antibodies 5D4 and 2D3 revealed highly-, and under-sulphated KS using immunofluoresence. Negative control images were also taken at each developmental day, shown in figure 3.3.

At day 12 of development, undersulphated KS staining (figure 3.1) is more apparent in the anterior region with a narrow subepithelial zone of staining. By day 13 (not shown), labelling appears increased in comparison to the earlier timepoint, with a more cohesive sub-epithelial band of staining. At day 14, fluoresence is again more apparent in the anterior stroma, although at this point corneas sampled were oedematous, making a full thickness image impossible at this stage. It is also clear that the mid stromal region is less strongly labelled than the anterior portion.

By day 15 (not shown) corneal compaction and dehydration mean that sections are thinner, and a full thickness image may be observed, labelling is positive in the subepithelial zone, and undersulphated KS appears to be accumulating throughout the stroma. On day 16 staining is more homogenous, and the epithelium is also noticeably more organised and three to four cell layers thick. At days 17 (not shown) and 18, the final timepoint considered in this study, undersulphated KS as identified by 2D3 immunofluorescence is homogenous throughout the stromal depth. Considered collectively, the 2D3 findings point to a situation in which before day 16 of development, staining seems more prominent in the anterior cornea, most noticeable subepithelially -- before becoming homogenous.

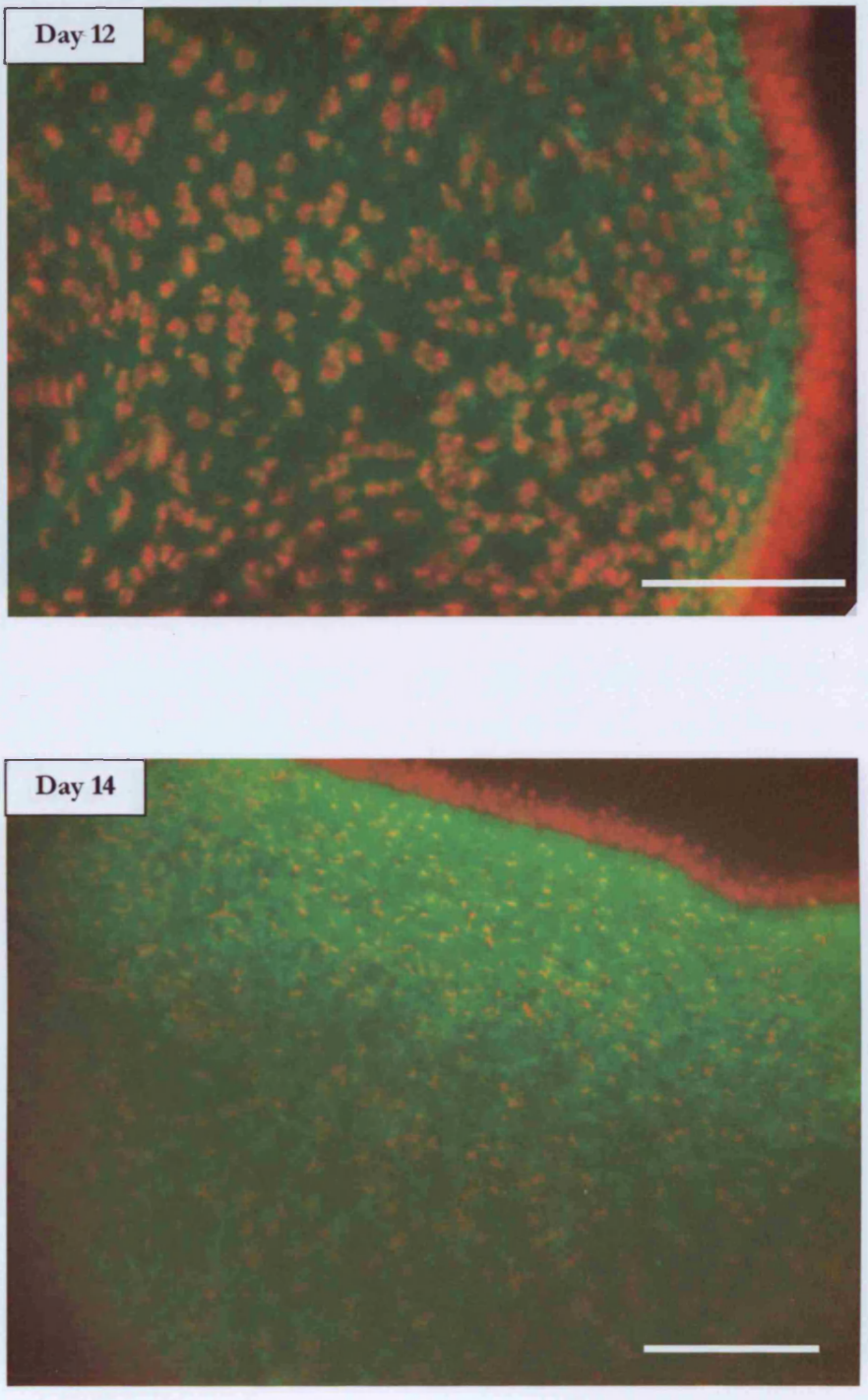

Figure 3.1A. Fluorescence microscopy of the developing chick cornea using undersulphated KS specific antibody 2D3. Day 12 shown at enlarged magnification 29.175x, all other images taken at 25x magnification on a Leica TPS SP2, scale bar = 100μm. 2D3 stained panels have been merged with PI images from the same sample area using Adobe Photoshop.

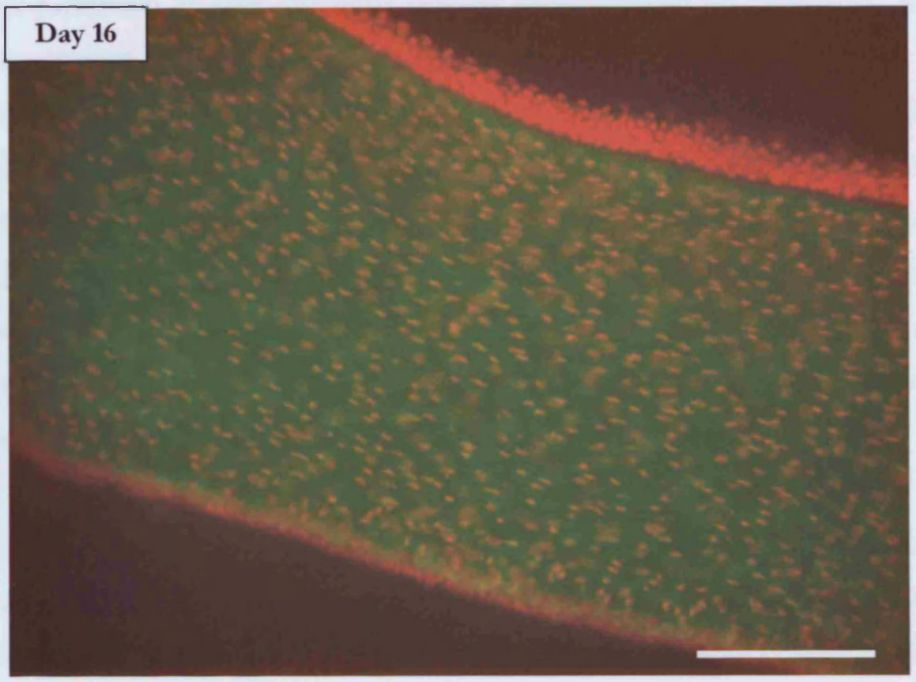

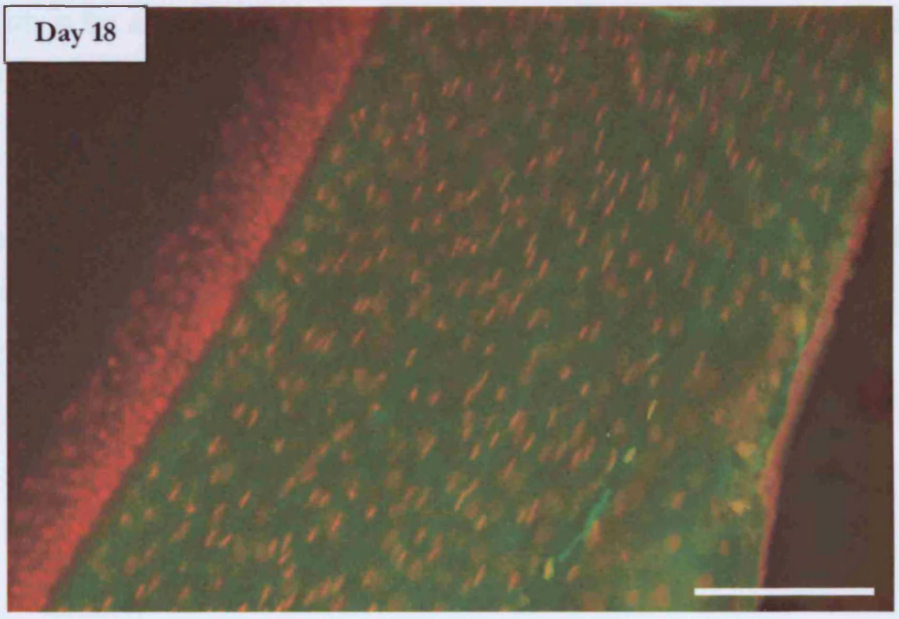

Figure 3.1B. Fluorescence microscopy of the developing chick cornea using undersulphated KS specific antibody 2D3. Both images taken at 25x magnification on a Leica TPS SP2. 2D3 stained panels have been merged with PI images from the same sample area using Adobe Photoshop.

Highly sulphated KS labelled using the monoclonal antibody 5D4 shows a similar spatial and temporal expression as seen previously labelling undersulphated KS using 2D3. At day 12, labelling appears relatively homogenous throughout the stroma, with some antibody fluorescence. At day 13 (not shown) of development, similar to 2D3 labelling, there is an area of heightened intensity seen subepithelially, and by day 14 this area of more intense labelling is still more apparent, despite some glare from excess Alexafluor. Highly sulphated KS labelling is relatively evenly spread, although the endothelium is unfortunately absent in this section, most likely lost as excess moisture was removed during dissection, however the epithelium has increased in thickness to five/six cells deep. At the same time, corneal thickness has increased, as also seen in the undersulphated image (figure 3.1).

At day 15 (not shown), highly sulphated KS labelling was more distinct in the anterior stroma, moreover, a more close inspection would imply that KS is also accumulating throughout the cross section. By day 16, highly sulphated KS labelling appears even across the mid stroma (figure 3.2B). Of the day 17 corneas studied, labelling appears evenly distributed from epithelium to endothelium, with regions of more intensity around the peripheral edges (not shown). This phenomenon is seen throughout the sections, and is most likely due to a greater cell density in the anterior stroma, noted in immuno electron microscopy at low magnifications (2000x).

Finally, by day 18 of development, labelling is more intense across the entire section, and the accumulation of KS appears homogenous throughout the full thickness cross section. The epithelial cell layer has also reached around 7 cells in thickness at the widest point, reflecting the growing maturity of the tissue.

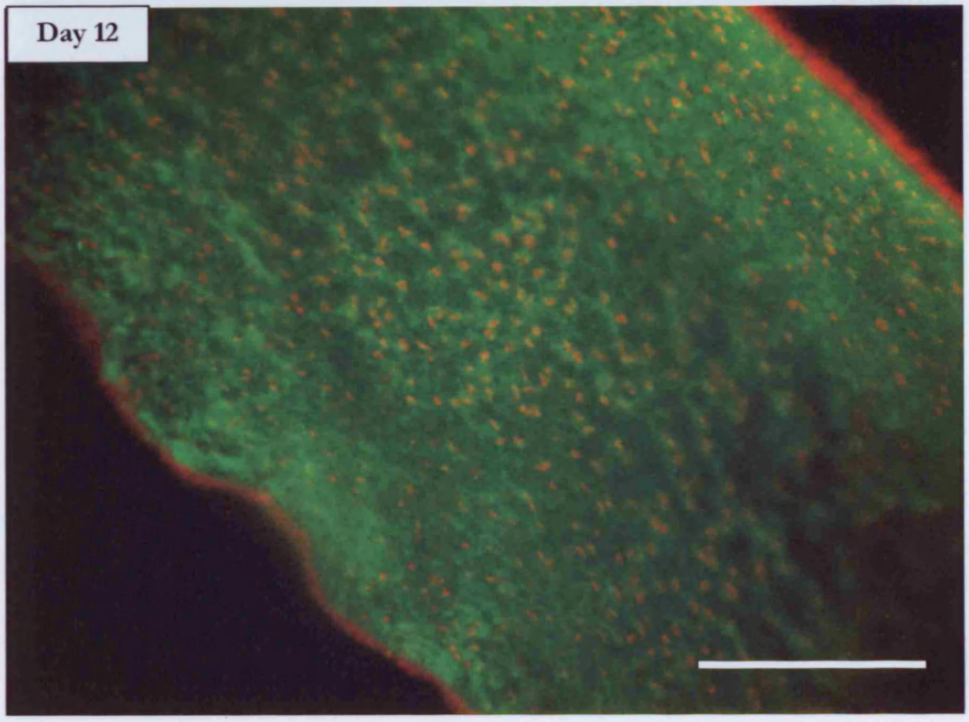

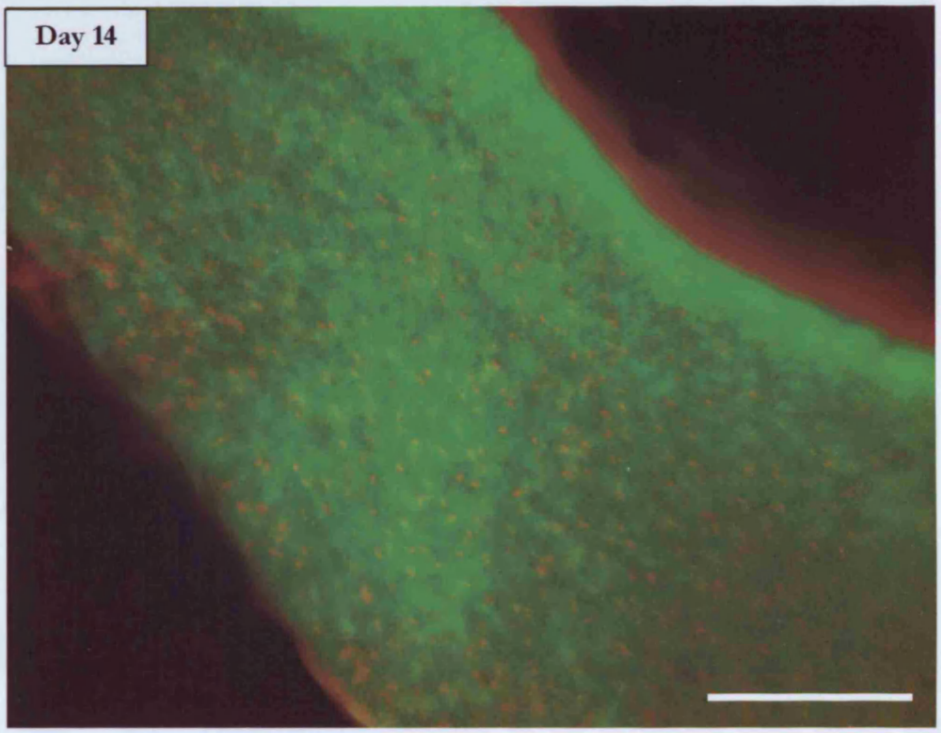

Figure 3.2A. Fluorescence microscopy of the developing chick cornea using the highly sulphated KS specific antibody, 5D4. All taken at 25x magnification on a Leica TPS SP2, scale bar = 100μm. 5D4 stained panels have been merged with PI images from the same sample area using Adobe Photoshop.

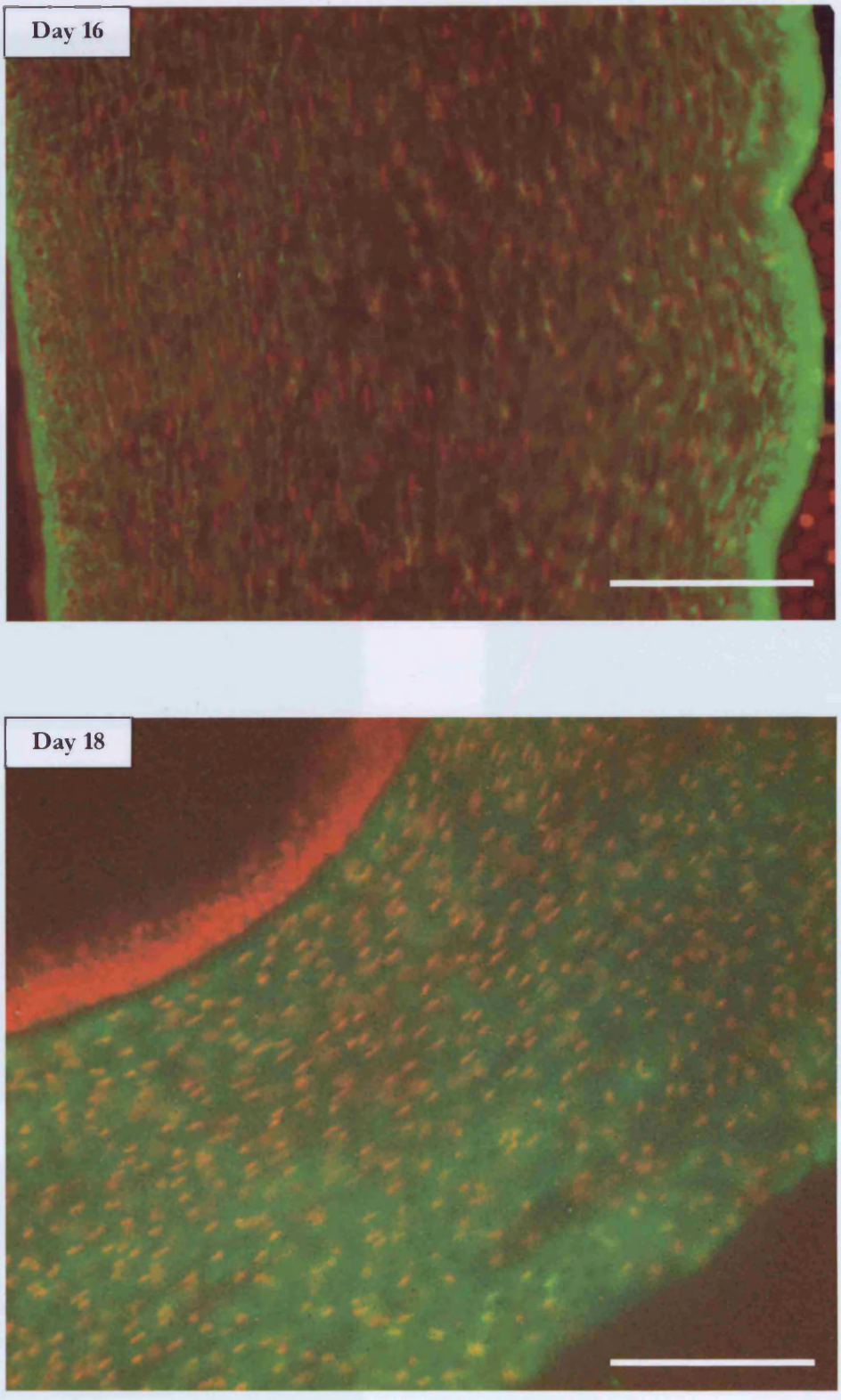

Figure 3.2B. Fluorescence microscopy of the developing chick cornea using the highly sulphated KS specific antibody, 5D4. All taken at 25x magnification on a Leica TPS SP2, scale bar = 100μm. 5D4 stained panels have been merged with PI images from the same sample area using Adobe Photoshop.

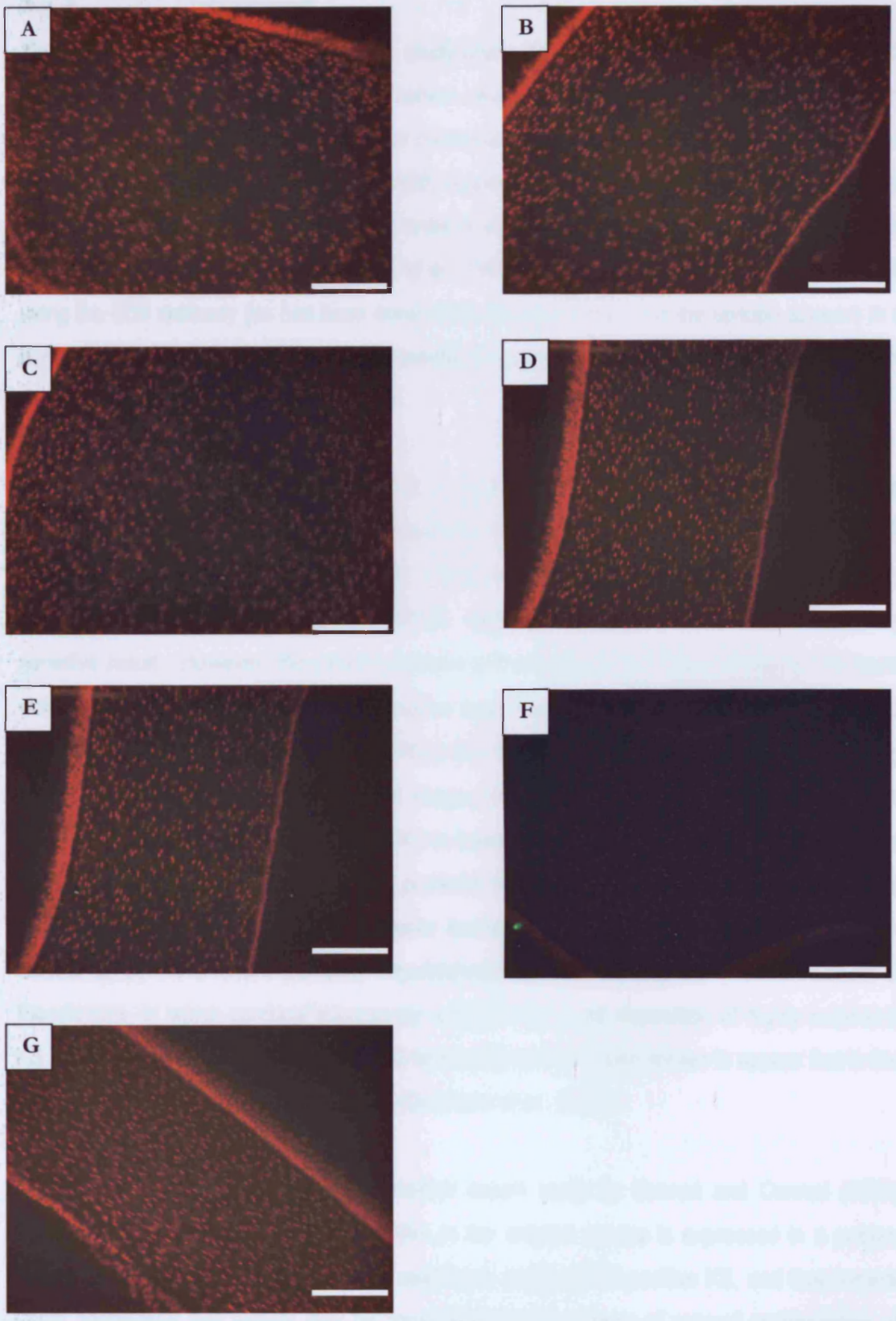

Figure 3.3. Fluorescence microscopy of the developing chick cornea; negative controls - omitting KS specific antibodies 2D3 and 5D4. Panel A = day 12, B = day 13, C = day 14, D = day 15, E = day 16, F = day 17, G = day 18. All taken at 25x magnification on a Leica TPS SP2, scale bar = 100μm.

chains, playing a positive role in defining migration-permissive matrix for some embryonic neural crest cells, corneal and non-corneal nerves, as well as other cell types.

It is also worth considering that the post-translational glycosylation and sulphation of KSPG core proteins require specific glycosyl- and sulfotransferases (Funderburgh, 2000; Funderburgh, 2002), which remain incompletely characterised during development. Although the antibodies used in this study detect highly- and under-sulphated KS, KSPGs expressed in very young embryos may carry no KS chains at all, or truncated KS chains that remain undetected by the antibodies used. Lumican, the principal KSPG thought to bear highly sulphated KS chains is widely expressed as an unsulphated glycoprotein (Funderburgh *et al.*, 1991), and the extent of lumican sulphation is known to change with time in the developing chick cornea (Cornuet *et al.*, 1994). Indeed, there may well be a role for such undersulphated KSPGs during collagen deposition; after all, decorin can regulate collagen fibrillogenesis *in vitro* after removal of its glycosaminoglycan side chain (Vogel *et al.*, 1987).

3.2.5 Further Work

This study has raised some interesting questions. Although reasons for the variance between results from each research group (Funderburgh *et al.*, 1986; Takahashi *et al.*, 1999) can be offered, there seems no definitive explanation for three contrasting data sets. Although the two antibodies used both recognise highly sulphated KS, the precise epitope they are raised against differs (Funderburgh *et al.*, 1986; Funderburgh *et al.*, 1987). This could cause a ripple effect in subsequent labelling. It could be possible that in each study sections were taken from a particular depth; in my work this was mid stroma, but tissue taken from the periphery could show a localised contrast in sulphated KS expression compared to sections from a greater depth; a limitation of microscopy. Confocal microscopy could be used to view adjacent sections through the depth of the tissue to investigate this possibility. Another extension to this study would be to include 1B4 labelling of lesser sulphated KS, as also used in chapter 4.

3.3 Low temperature embedded TEM

The light level immunofluorescence work described in section 3.2 has identified highly and lesser sulphated KS in the developing chick cornea. To achieve better spatial resolution in an attempt to discern KS-collagen associations, investigations were carried out at the electron microscope level. The monoclonal antibody 5D4 is again used to localise highly sulphated KS in a qualitative fashion, and also an antibody to lesser sulphated KS - 1B4, which precedes a quantitative study in chapter 4. A brief introduction to relevant work will be outlined, and a detailed method including experimental specifics described. Pictures from this study will be presented and discussed, and finally, future work outlined.

3.3.1 Introduction

Stromal collagen fibrils are thought to be fundamentally reorganised during the latter stages of chick development. Light transmission begins at developmental day 14, as collagen spacing decreases and sulphated KS content begins to rise (see chapter 4). As light transmission elevates, matrix compaction and major dehydrations occur (Hay and Revel, 1969), likely through the resorption of collagen free "lakes" (Siegler and Quantock, 2002). Hay and Revel (1969) suggested that matrix compaction is driven by a change in water binding capacity, later echoed by Toole and Trelstad (1971) who document the decreasing presence of hyaluronan at the initiation of corneal dehydration. This effect could also be driven by endothelial pump activation.

As outlined in chapter 1, the main KSPGs in chick cornea are lumican, keratocan and mimecan, and it is the sulphation of this KS side chain thought to be critical for corneal transparency. In support of this, previous investigators have reported a lactosaminoglycan to glycosaminoglycan (i.e. an unsulphated to sulphated) switch between days 12 and 15 of development, concomitant with the onset of transparency (Cornuet *et al.*, 1994). The CS/DS PG decorin (see chapter 1, section 1.13.1) is also expressed in the developing cornea, and interestingly, this PG also carries KS side chains in the mature chick (Blochberger *et al.*, 1992).

Connon *et al.* (2003) report that the majority of sulphated PG filaments detected by cuprolinic blue staining (a cationic, electron dense dye, Scott and Haigh (1988)) appear smaller after day 14 of development. Prior to this, large sulphated GAGs were found clustered in collagen free

lakes. Connon also reports a significant decrease in the number of both large and small sulphated GAGs between days 13 and 14 of development. Unlike immuno-electronmicroscopy, cuprolinic blue does not distinguish between KS or CS/DS PGs.

3.3.2 Methods

Fertile chicken eggs at developmental days 10, 12, 14, 15, 16, and 18 were studied. Two corneas were excised at each time-point and immediately processed for immuno-electron microscopy. A more detailed synopsis of transmission electron microscopy can be found in chapter two; section 2.8.

Corneas were fixed in 4% paraformaldehyde for one hour, and placed into sodium borohydride in Sorenson buffer for 4 hours at 4°C to block free aldehyde groups (and prevent a false positive result). They were then washed for 5 minutes in 0.2M Sorenson buffer (used at twice the strength of fix) and stored at 4°C in a fresh change of buffer before dehydration in progressively increasing concentrations of ethanol. During this time, the temperature was lowered to -25°C in a Reichert Automated Freeze-Substitution unit (Leica, Vienna, Austria) to maintain protein stability: 30% EtOh at 4°C for 30 minutes, 55% EtOh at 0°C for 10 minutes, 70% EtOh at -20°C for 10 minutes and 90% EtOh at -25°C for 10 minutes.

In each case, ethanol was used to dehydrate the tissue before lowering the temperature to prevent ice crystal formation, which would distort stromal ultrastructure. Corneas were then immersed in a 1:1 mixture of lowicryl K4M resin and 90% ethanol for one hour, followed by increasing parts of resin to alcohol in a course of gradual infiltration; 2:1 lowicryl resin to 90% ethanol, and finally six changes into lowicryl resin before 12 hour storage at -25°C. Corneas were then transferred into labelled flat embedding moulds (Agar Scientific, UK) covered in sufficient resin to prevent air bubble formation around the sample, before UV polymerisation for 24 hours and a final ascent from low to room temperature, and further polymerisation for an additional 2-3 days. After polymerisation hygroscopic blocks were stored in a dessicator prior to sectioning.

Ultrathin sections were cut from lowicryl blocks on a Reichert Ultramicrotome equipped with a diamond knife, with the help of Dr. Rob Young, and collected onto nickel grids. Sections were

incubated on droplets of primary antibodies diluted 100 times in PBS / 1% BSA. Highly sulphated KS was again studied using 5D4, and lesser sulphated KS using 1B4, another mouse mAb also developed by Professor Bruce Caterson that shows reactivity with a tetrasulphated hexasaccharide analogue. These antibodies have been extensively characterised to exclude cross reactivity with other KS analogues (Mehmet *et al.*, 1986; Zanetti *et al.*, 1985; Tang *et al.*, 1986). For negative control experiments, sections were incubated with PBS/1% BSA without primary antibody.

After 2 hours of incubation and washing with several changes of PBS/1% BSA, sections were transferred to secondary antibodies labelled with colloidal gold particles, or goat anti-mouse IgG (control) as appropriate (Biocell, Cardiff, UK). Secondary antibodies were used at a dilution of 1:20 in PBS / 1% BSA. After immunostaining and washing steps, sections were fixed briefly by floating grids on droplets of 2% glutaraldehyde in PBS, followed by final washes in boiled Millipore-filtered distilled water. The sections were then contrasted in aqueous uranyl acetate and lead citrate for 10 and 7 min, respectively, before examination in a Philips 208 transmission electron microscope at an accelerating voltage of 80 Kv.

3.3.3 Results

Images taken at specific timepoints revealed an increase in KS expression over time during chick corneal morphogenesis, also showing KSPGs associated with collagen fibrils at cell surfaces. KSPG labelling also increased as collagen fibrils become more aligned, labelling more intensely in the superficial stroma at day 12 of development, to become uniform by developmental day 18, as shown in figure 3.4.

At day 12 of development, both 5D4 and 1B4 labelling is distinct, indicating the presence of both highly and lesser sulphated KS at this time. Figure 3.4A shows highly sulphated KS expression at day 10 of development. Unfortunately, it was was not possible to gain pictures from lesser sulphated KS sections. Highly sulphated KS labelling was more intense than the lesser sulphated homologue at every timepoint observed, which is confirmed later in this thesis using ELISA in chapter 4.

In figure 3.4A, we can see evidence of fibrillogenesis at the cell surface and positive labelling on the new collagen for highly sulphated KS in the anterior stroma (shown). There is little or no

labelling in the posterior region, however. Figure 3.4B shows lesser sulphated KS expression at day 12 of development. There are clear, round fibroblasts across the stroma; keratocytes begin to flatten after this point of embryogenesis and become more elongate. Figure 3.4B also shows lesser sulphated KS associated with collagen fibrils distributed throughout the stroma.

By developmental day 14 (figure 3.4D, with insert) KS labelling is clearly collagen fibril associated. Interestingly, both lesser (3.4D) and more highly sulphated KS (3.4E) consort with collagen at the cell surface, implying that KS is not only present by the completion of fibrillogenesis, but that it is already expressed in a fully sulphated form. The presence of KS sites at the cell surface could also be interpreted as evidence for Kadler's "fibripositor" mechanism, a cell surface fibropositor structure proposed to coordinate fibril formation in a partially protected environment, which would allow cellular control of collagen deposition possibly including procollagen processing (Canty and Kadler, 2005). The insert in figure 3.4D shows clusters of lesser sulphated KS forming bridges in between collagen fibrils; even at day 14 of development a clear interplay is apparent.

The distinction between figures 3.4A, B and C becomes even more obvious, when collagen mass is taken into consideration. Before day 14 of development, there are large lakes devoid of collagen fibrils interspersed with bundles of partially organised collagen fibrils running parallel to each other with regular spacing. By developmental day 15, there is clear orthogonality and long fibrillar bundles are spreading to encompass the collagen free areas (figures 3.4F and G) as fibril density increases. Keratocytes also show KS labelling present at the cell surface, and another possible candidate to support Kadler's fibropositor work is indicated in figure 3.4F (arrow). Previous studies have found no change in collagen fibril diameter throughout development (Hirsch *et al.*, 1999; Hay and Revel, 1969), and no obvious change is apparent from the images examined in this study.

Figures 3.4H and I at developmental day 16 show lesser and more highly sulphated KS respectively. Collagen lamellae begin to appear, with markedly more highly sulphated KS labelling in the right hand panel. Figure 3.4I particularly more closely resembles a mature cornea, with cohesive collagen layers beginning to emerge.

By day 18, collagen organisation seems superficially mature; sections are devoid of collagen free lakes, and parallel fibril layers run at angles to each other – regularly spaced and clearly

associated with KS. Figure 3.4J also shows elongate stromal cells. Keratocytes are buried within adjacent collagen layers, with clusters of KS at the cell surface. Lesser sulphated KS signal has increased in the stroma, and labelling is also present on the cell membrane. Electron micrographs from three days post hatch (figures 3.4L and M) show collagen fibrils running in large flattened ribbons across the section in a fluid fashion; there are no collagen free areas in the compacted matrix, and banding patterns can also be seen in figure 3.4M. Interestingly, at this resolution, and as seen in the immunofluorescence results, highly and lesser sulphated KS distribution is similar, appearing regularly spaced across the stroma in small clusters. Negative controls to show primary antibody specificity show unlabelled sections, an example of which is shown in figure 3.5. Figure 3.6 shows highly sulphated KS expression at the glycocalyx in a day 15 chick cornea. Although not directly related to the main thrust of this work, this picture is interesting as there is little collagen association, which could suggest a role in adhesion.

1B4

5D4

This space intentionally left blank

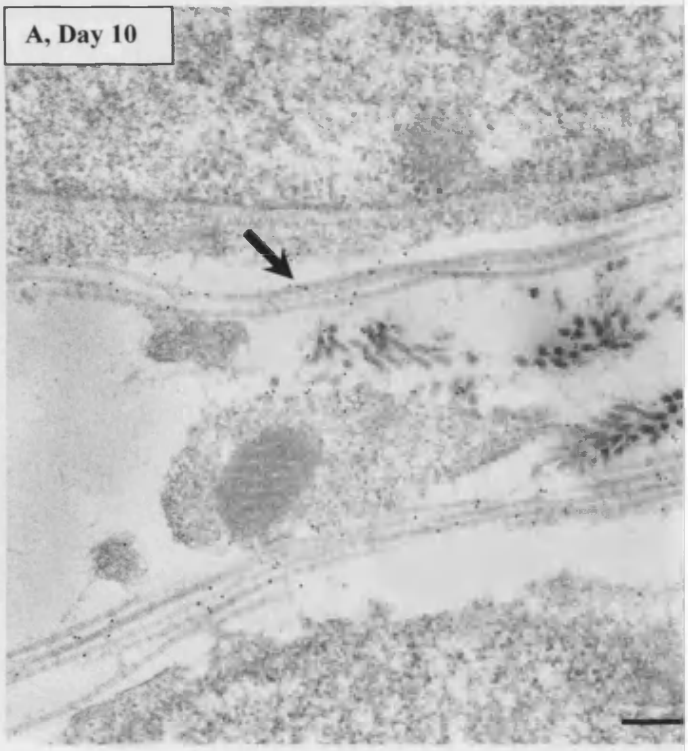

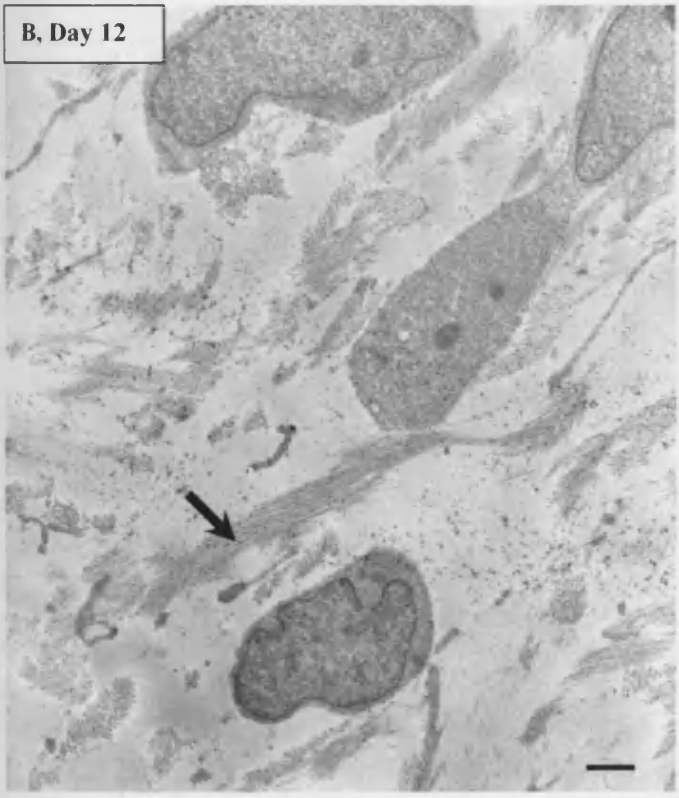

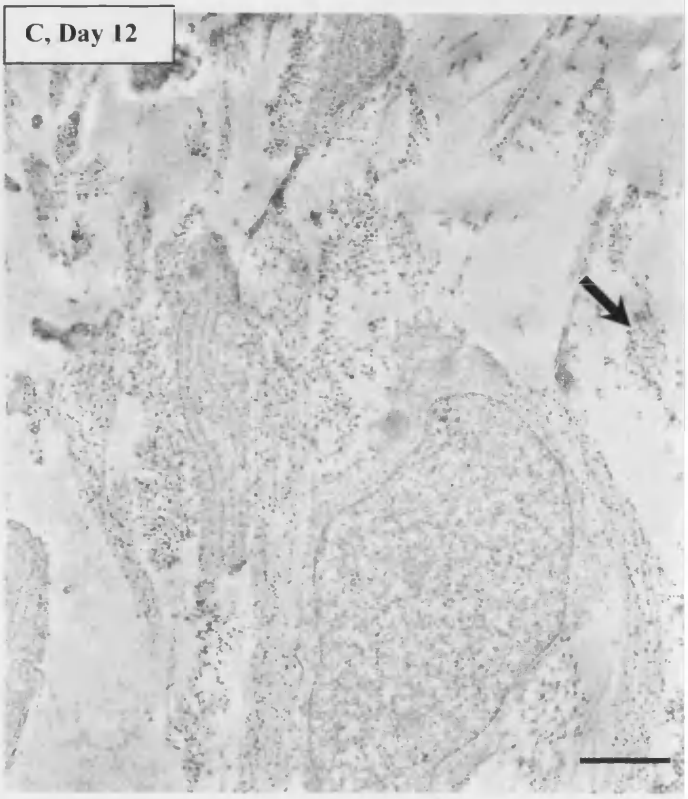

Figure 3.4A, B, and C. Transmission electron micrographs from the developing chick cornea, 4% paraformaldehyde fixation and Lowicryl K4M low temperature embedding. Panels on the left hand side show primary antibody 1B4, right hand panels show primary antibody 5D4. Arrows show examples of labelling.

Scale bars as follows: (A) Day 10 = 300nm, (B) Day 12 = 1μm, (C) Day 12 = 1μm

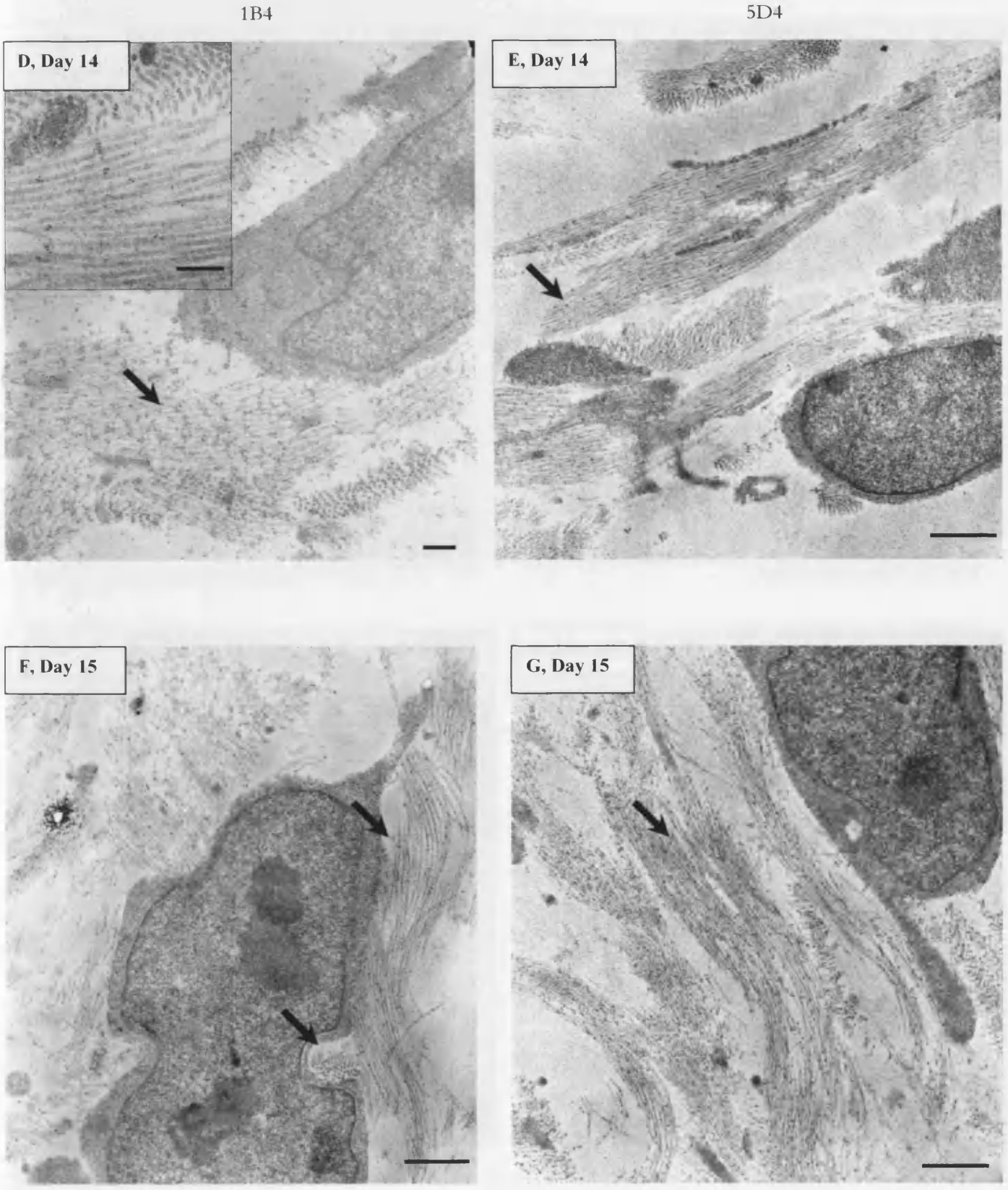

Figure 3.4D, E, F and G. Transmission electron micrographs from the developing chick cornea, 4% paraformaldehyde fixation and Lowicryl K4M low temperature embedding. Panels on the left hand side show primary antibody 1B4, right hand panels show primary antibody 5D4. Arrows show examples of labelling.

Scale bars as follows: (D) Day 14 = 300nm; insert = 300nm (E) Day 14 = 1μm, (F) Day 15 = 1μm, (G) Day 15 = 1μm

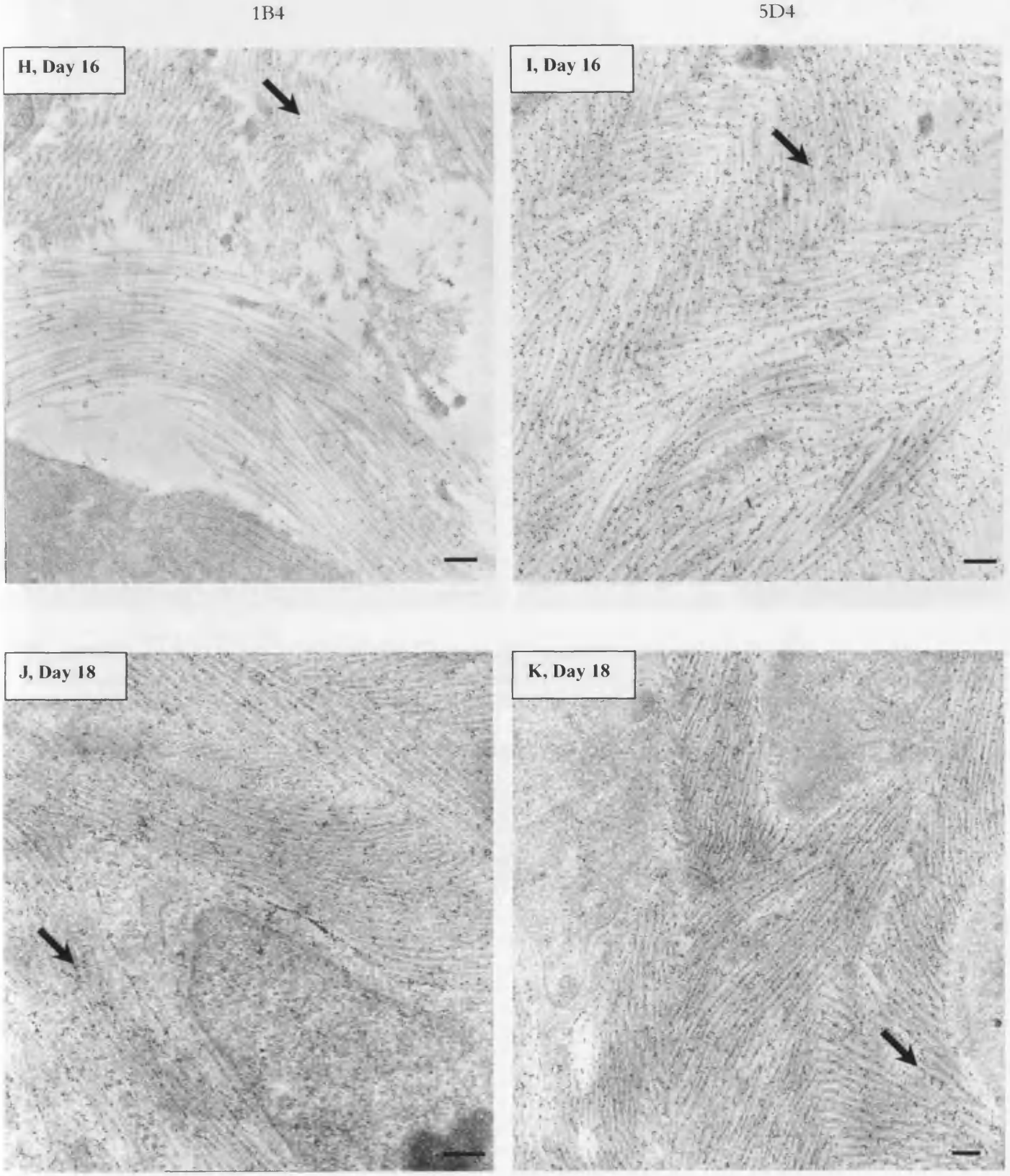

Figure 3.4H, I, J and K. Transmission electron micrographs from the developing chick cornea, 4% paraformaldehyde fixation and Lowicryl K4M low temperature embedding. Panels on the left hand side show primary antibody 1B4, right hand panels show primary antibody 5D4. Arrows show examples of labelling.

Scale bars as follows: (H) Day 16 = 300nm, (I) Day 16 = 300nm, (J) Day 18 = 300nm, (K) Day 18 = 300nm

CARDIFF UNIVERSITY PRIFYSGOL CAERDYDD

1B4 5D4

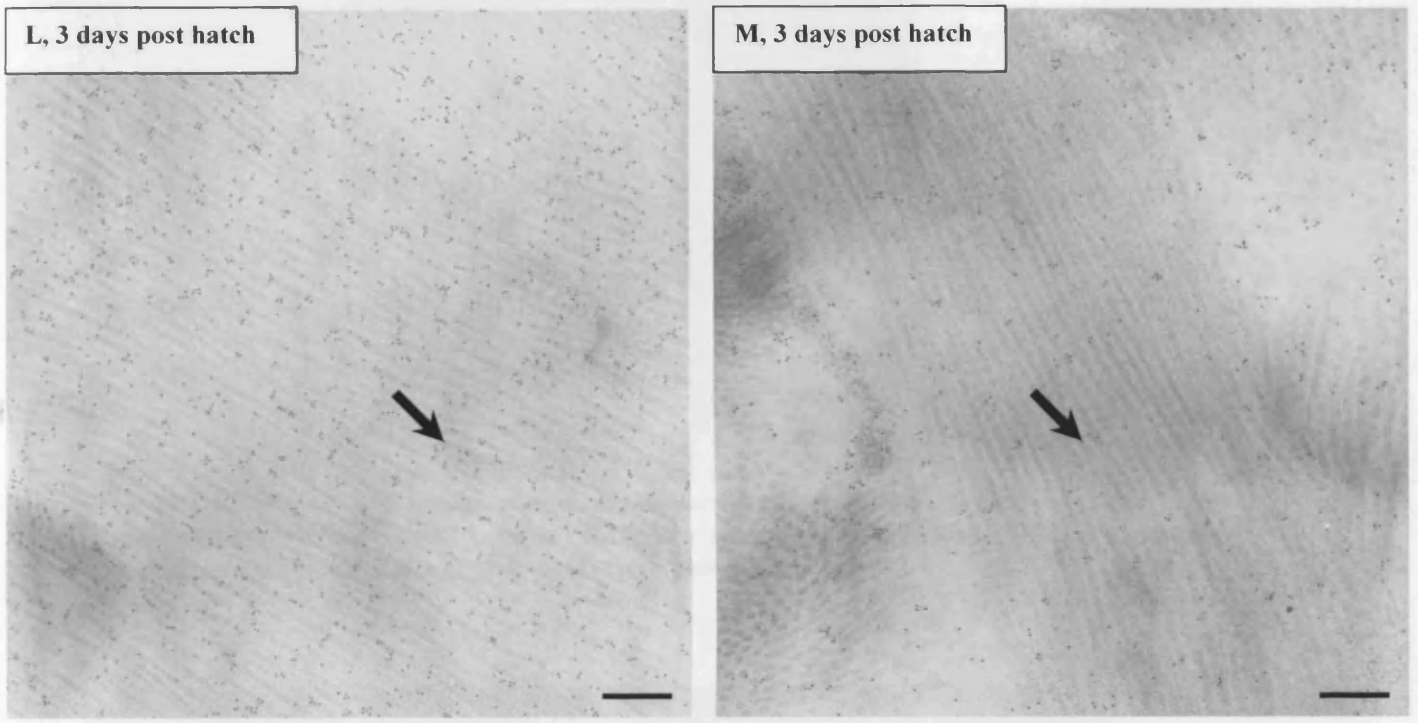

Figure 3.4L and K. Transmission electron micrographs from the developing chick cornea, 4% paraformaldehyde fixation and Lowicryl K4M low temperature embedding. Panels on the left hand side show primary antibody 1B4, right hand panels show primary antibody 5D4. Arrows show examples of labelling.

Scale bars as follows: (L) 3 days post hatch = 300nm, (M) 3 days post hatch = 300nm

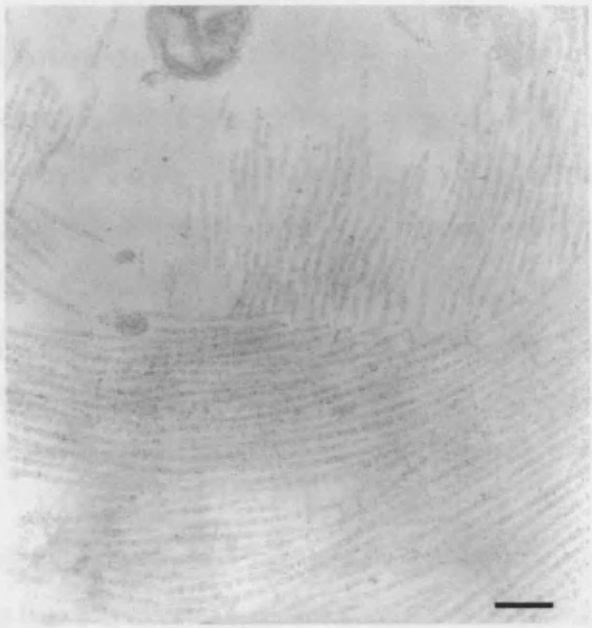

Figure 3.5. Transmission electron micrograph from day 15 of development., 4% paraformaldehyde fixation and Lowicryl K4M low temperature embedding. Negative controls for primary antibodies 5D4 and 1B4. Scale bar = 300nm.

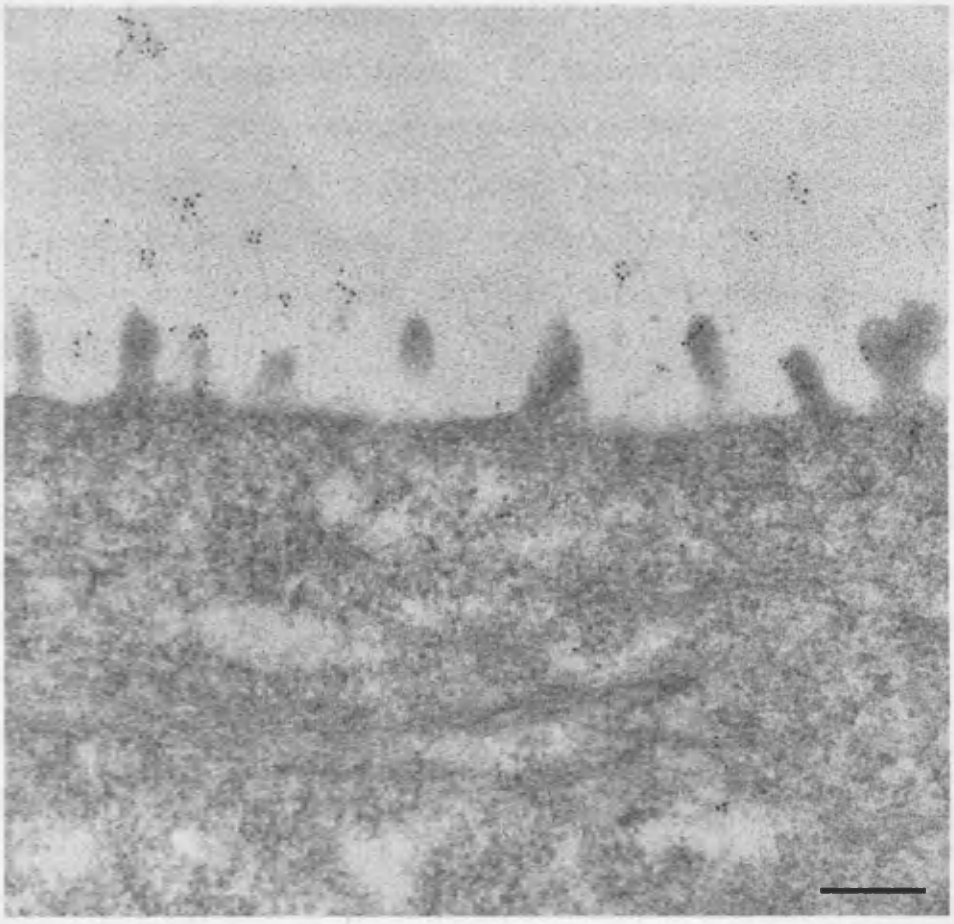

Figure 3.6. Transmission electron micrograph from day 15 of development., 4% paraformaldehyde fixation and Lowicryl K4M low temperature embedding. Scale bar = 300nm.

3.3.4 Discussion

This study was designed to investigate the local emergence of different KS sulphation patterns and collagen association in the developing chick cornea. The technique used for tissue fixation and embedding was a critical parameter in antigen preservation; standard resin techniques often destroy sensitive protein targets, and for this reason measuring both collagen ultrastructure and proteoglycan involvement can be haphazard. Low temperature embedding for electron microscopy is a useful bridge between these objectives, as protein structure can be preserved without masking using gentle fixation, and collagen order is little diminished.

Results from another study by Dr. Rob Young (personal communication) found intracellular KS staining as early as day 8 of development in the posterior stroma, when extracellular collagen fibrils were still 1B4 and 5D4 negative. Interestingly, 5D4 staining was found in the anterior presumptive orthogonal lamellae, but a negative result for 1B4.

Results show that both highly and lesser sulphated KS expression, as identified by 5D4 and 1B4 immunoreactivity, respectively, increases in the week prior to hatch - particularly in the highly sulphated form, and in both cases show a clear association with collagen fibrils. Despite the presence of sulphated KSPGs during collagen fibrillogenesis, bundles of collagen were slightly less well organised before day 16 of development, becoming more cohesive during the latter stages of corneal development. This result concurs with previous findings (Hay and Revel, 1969).

Strategic timepoints were chosen for this study, because a battery of structural and compositional changes are thought to occur around day 14 of development. This critical time is reported to show stromal dehydration (Hay and Revel, 1969; Siegler and Quantock, 2002), matrix compaction (chapter 4), increased KS expression and sulphation (chapter 4; Anseth, 1961; Hart *et al.*, 1976), and the resorption of collagen free lakes, (Siegler and Quantock, 2002). Micrographs from this study show a clear increase in collagen mass with clusters of sulphated KSPGs amoung collagen fibrils at this time.

Connon *et al.*, (2003) noted that sulphated filaments stained after day 14 of development were smaller, coincident with a decrease of larger collagen independent filaments normally found in stromal lakes. This increase in small sulphated filaments could potentially be KS, found to

increase in both highly and lesser sulphated forms between days 14 and 15, and also reported to be present in an unsulphated form prior to days 12 to 15 (Cornuet *et al.*, 1994). A more recent study suggested that KS content increases between developmental days 15 and 18 (Dunlevy *et al.*, 2000). This is confirmed by the results from this study, although it is important to note that in both KS studies described here (chapters 3 and 4), the increase in KS begins before developmental day 15, albeit much more slowly.

Connon's study in 2003 also highlighted that the reported increase in small sulphated filaments is independent of matrix compaction, which would imply that their role in fine tuning the fibrillar array is not a driving force. More likely, activation of the endothelial pump causes tissue dehydration and forces overall collagen condensation and stromal dehydration. Hay and Revel (1969) also suggested that an increase in proteoglycan concentration around day 16 is due to stromal dehydration, although I would suggest that an increase in KSPG synthesis, as seen in chapter 4 and between figures 3.4H, I, J and K could be the culprit.

3.3.5 Further work

A previous microscopy study by Connon *et al.*(2003) quantitatively assessed sulphated filament expression (presumably GAGs) during chick corneal development using a fixed magnification of 30,000x. Collapsed PG filaments were stratified into large (>800nm^2) and small (<800nm^2) categories, which revealed a significant decrease in the total number of GAGs between days 13 and 14 of development. Because the study in this chapter did not examine a complete range of developing corneas in a day by day fashion, it would be interesting to re-examine this sequence with respect to Connon's work, as later ELISA results in chapter 4 imply a continual (if slow) increase in KS expression.

3.4 Summary

- Both highly- and under-sulphated KS accumulates in an anterior to posterior fashion between days 12 and 15 of development, appearing homogenous from day 16 onwards.

- Highly sulphated KS epitopes are expressed early in development, associated with newly formed collagen at the cell surface, with increased labelling as time progresses. Lesser sulphated KS shows a similar expression pattern.

CHAPTER FOUR:
Collagen Organisation and the Sulphation of Keratan Sulphate

4.1 Introduction to Chapter

This chapter follows the progressive analysis of a sample group of developing chick corneas from specific timepoints during the final week of development. A key aim of my thesis is to further current understanding of collagen reorganisation concomitant with KS emergence during the onset of corneal transparency. To this end, this experiment was designed to quantify proteoglycan changes alongside collagen spacing refinements during the final week of corneal morphogenesis prior to hatch.

Firstly, the aims and objectives of this study will be identified, and an introduction to current literature around this investigation presented. Then, the separate methodologies used for this series of experiments will be detailed, and the progression of this sample set from collagen spacing analysis to KS quantification and finally collagen content analysis will be described. Results will be presented in a stepwise fashion to examine the multidisciplinary evaluation of each cornea, and the consequent findings discussed. Lastly, possible further work will be outlined.

Previous studies have used the monoclonal antibody 5D4 to highly sulphated KS (linear pentasulphated hexasaccharides) to investigate chick development (Siegler, 2003), although, in this case, the sample size and range was limited, corneas were digested in pairs (creating a pooled result), and the result was quantified against corneal wet weight – which is largely dependent on hydration at earlier timepoints, rather than collagen content. The purpose of this study was to move current understanding of this sequence forward by isolating single corneas for an optimised, sensitive KS and collagen assay after X-ray analysis of the same tissue. This objective requires a novel method for KS quantification and collagen extraction and detection throughout the final week of chick corneal development.

The undersulphated KS antibody 2D3 used in the previous chapter did not show sufficient reactivity with competing antigens for ELISA, and for this reason the lesser sulphated KS MAb 1B4 was used to complement highly sulphated KS analysis. This chapter is presented in an extended paper format, however a more detailed explanation of method theory can be found in section 2.5.

CHAPTER FOUR:
Collagen Spacing and the Sulphation of Keratan Sulphate

4.2 Introduction

Formation of the corneal stroma in lower vertebrates such as the chicken, is the result of a precisely controlled developmental sequence in which the cornea is becoming naturally transparent over a defined timescale. During the final week of embryonic development, the chick cornea thins and becomes transparent. Proteoglycans (PGs) have been implicated in refinements to chick corneal structure during this time; fluctuations in PG sulphation mirror an increase in collagen content and organisation. The most influential of these changes include matrix compaction (Birk *et al.*, 1986; Siegler and Quantock, 2002), PG alterations (Cornuet *et al.*, 1994; Dunlevy *et al.*, 2000), and changes in collagenous and noncollagenous extracellular matrix components.

Previous chemical quantification of corneal GAGs have suggested no change in the amount, molecular size, or degree of sulphation between developmental days 10 and 14 (Hart, 1976). After this time keratan sulphate (KS) becomes more highly sulphated, with the principal KSPG lumican thought to bear most of these chains (Cornuet *et al*, 1994; Dunlevy *et al.*, 2000). At the same time, early spectrophotometry experiments (Coulombre and Coulombre, 1961) report 40% of incident white light transmission through the chick cornea before and at day 14 of development rising to 95% transmission by day 19, suggesting a relationship between stromal remodelling and transparency.

The early work of Anseth reports substantial changes in the chemical properties of corneal GAGs around developmental day 14 (Anseth, 1961). Subsequent studies indicate that KS is synthesised during developmental days 5 to 7, although normal sulphation patterns only appear from day 14 of incubation (Cai *et al.*, 1996). These changes are concomitant with a lactosaminoglycan to glycosaminoglycan switch in KSPG synthesis at day 14 (Dunlevy *et al.*, 2000; Cornuet *et al.*, 1994).

Shifting PG sulphation during development may be due to temporal alterations in mRNA levels for the different KSPG core proteins, compounded by increases in the sulphation of lumican between days 12 and 15 (Hay and Revel, 1969).

CHAPTER FOUR:
Collagen Spacing and the Sulphation of Keratan Sulphate

Previous small-angle x-ray diffraction studies have indicated fibrillar compaction in a two-stage manner, the most notable drop in collagen fibril spacing occurring between developmental days 16 and 17 (Siegler and Quantock, 2002). KSPG alterations may help drive collagen reorganisation and bring about corneal transparency. The study described in this chapter was designed to ascertain whether or not changes in the levels of highly, and lesser sulphated KS correlate with alterations in collagen fibril spacing.

4.3 Materials and Methods

Because this study is comprised of two main stages; x-ray diffraction and biochemical techniques, methods will be presented in a stepwise fashion. Extensive optimisation of sample storage and biochemical techniques were carried out prior to these experiments, as shown in appendix 2.

4.3.1 Specimens

A total of 78 embryonic corneas were obtained daily from developmental day 12 to day 18 (n=10 to 12 at each timepoint), and corneas dissected around the limbus within 3 to 4 hours of collection. Once excised, corneas wrapped in Cling film™, and frozen in dry ice, and stored at -80°C prior to x-ray analysis. All procedures were carried out in accordance with the ARVO statement for the use of animals in Ophthalmic and Vision Research.

4.3.2 Data Collection and Processing for Bragg spacing

Prior to data collection corneas trapped between single layers of Cling film were securely positioned in a sealed specimen holder between two sheets of Mylar where they were allowed to thaw. Each specimen was individually placed into the path of a highly focussed (1mm x 1mm) monochromatic (λ = 0.154nm) x-ray beam on SRS station 2.1. Corneas were exposed to the x-ray beam for 2 minutes, and the resulting fibre diffraction patterns recorded onto a multiwire, gas

proportional area detector plate positioned 8.25m behind the sample. An evacuated tube separates the sample and detector to reduce air scatter, and unscattered x-rays are blocked by a small lead backstop. All diffraction patterns (512 pixels x 512 pixels) were transferred to the home laboratory for analysis using purpose written Unix-based software (Sun Microsystems, Mountain View, CA), followed by graphics and statistics packages (Unix; Optimas, Bothell, WA, Statistica; Statsoft, Tulsa, OK, Excel; Microsoft, Redmond, WA).

After normalisation, a detector response profile was subtracted from each x-ray scatter pattern, and then a 26 pixel wide vertical scan used to generate an intensity profile of the first-order equatorial x-ray reflection from regularly arranged collagen. This profile was summed about its centre, and a plot of x-ray intensity versus the product of x-ray intensity and radial position generated to correct for the linear scan across a circular x-ray pattern. All Bragg spacing values were calculated after calibration of this system using meridional reflections arising from the known 67nm D-period rat tail tendon. A more detailed account of this process can be found in section 2.3.3.

4.3.4 Local order

The angular width of an interfibrillar reflection can be used to calculate the degree of local order in the collagen array. The sharper the x-ray scatter peak, the smaller the range of collagen fibril spacings sampled, which implies more widespread local order in the collagen array. Local order calculations are shown in section 2.3.4.

4.3.5 Isolation of KS chains

After x-ray analysis, corneas were refrozen before subsequent quantification of highly, and lesser sulphated KS using a sensitive, optimised competitive ELISAs. Background optimisation is shown in Appendix 1. Each cornea was individually digested for 17 hours at 60°C with 1mg/ml papain (Sigma) in a 0.05M sodium acetate buffer, pH 5.6, containing 0.025M ethylenediaminetetraacetic acid (EDTA), 5mM cystine HCl. The enzyme was inactivated at 100°C for 10 minutes and stored at –20°C until use.

4.3.6 Competitive ELISA analysis

The optimised, competitive ELISAs developed here were carried out to quantify selectively pentasulphated hexasaccharides and tetrasulphated hexasaccharides as the smallest linear structures in KS chains, recognised by the monoclonal antibodies 5D4 and 1B4 respectively. 96 well E.I.A. microtitre plates (MP Biomedical) were coated by passive adsorption using a 250ng/ml chondroitinase ABC digested bovine articular cartilage aggrecan (BAC ABC core) antigen in a 20mM sodium carbonate coating buffer, pH 9.6, for 14hours at 37°C. The plates were washed with 300µl Tris saline azide (TSA) and unreacted sites were blocked with the addition of 200µl 1% (w/v) bovine serum albumin (BSA) in TSA to each well for 1 hour at 37°C.

Papain digests from single corneas were serially diluted and allowed to bind with an equal volume of 5D4 (1:8000 dilution in 1%BSA/TSA) for 1 hour at 37°C, and subsequently used to compete against BAC abc core for 1 hour at 37°C using serial dilutions of BAC abc core/5D4 as a standard. Plates were subsequently washed four times with 300µl TSA. An enzyme linked secondary antibody (alkaline phosphatase conjugated goat anti-mouse, 1:5000 dilution in 1%BSA/TSA) was added (200µl / well) for 1 hour at 37°C. Plates were again washed six times with 300µl TSA. Finally an alkaline phosphatase substrate (p-nitrophenyl phosphate, 1mg/ml) was applied in DEA buffer (0.126mM $MgCl_2$, 1M diethanolamine, pH corrected to 9.8) at 100µl/well for 1 hour at 37° C. Colour development was read on a labsystems multiscan MS plate reader at 405nm in order to determine the inhibition of binding of 5D4. Highly sulphated KS was then quantified using a standard curve of known BAC ABC core concentrations from each ELISA plate.

The same stock corneal extracts were then assayed for lesser sulphated KS using the 1-B-4 monoclonal antibody. Optimisation of conditions established that microtitre plates were coated with 125ng/ml BAC ABC core and ELISAs carried out as described using a 1:4000 1B4 dilution. A more detailed account of this process can be found in section 2.5.

4.3.7 Hydroxyproline Assay

Papain digests were hydrolysed using equal volumes of 11.7N conc HCl to supernatant at 110°C overnight, and then freeze dried. Dried hydrolysates were reconstituted in distilled water and centrifuged to remove particulate material. Hydroxyproline residues were assayed in 30μl triplicate against known standards with 70μl diluent and 50μl oxidant, and 125μl colour reagent, and read at 540nm after 10-20mins incubation at 70°C. Hydroxyproline content in the "unknown" chick corneal digests was calculated using a standard curve from each plate, and collagen content extrapolated by multiplying hydroxyproline content by 7. This process is described in more detail in section 2.7, and serial dilutions given in appendix 2.

4.4 Results

Experimental results have been compiled and presented in a logical order to reflect the stepwise manner of this study. Individual results are presented in their relevant section, and the work discussed as a whole in conclusion.

4.4.1 Collagen fibril spacing and organisation

Low-angle x-ray diffraction patterns obtained from 78 developing chick corneas were analysed to provide interfibrillar (Bragg) spacing at specific daily timepoints from 12 to 18 days of incubation (n=10 to 12 at each developmental day). Further analysis of the same corneas allowed quantification of highly sulphated and lesser sulphated keratan sulphate by ELISA, and finally hydroxyproline assays for fibrillar type I collagen quantification. Tabulated results are shown in Appendix 1, with statistical analysis for normality and significance.

X-ray scatter patterns generated by day 12 corneas gave rise to poorly defined, diffuse diffraction patterns, representative of a crudely organised stroma, akin to that seen in figure 4.1A. However, by day 18 a broad first equatorial reflection is apparent, generated by regularly spaced collagen fibrils, as shown in figure 4.1B.

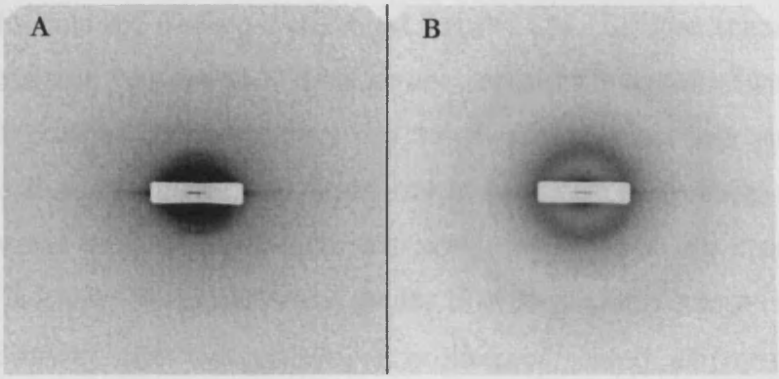

Figures 4.1A and B. Small angle x-ray scattering patterns from chick corneas taken at days 12 (A) and 18 (B) of development.

Interfibrillar reflections created by more mature corneas were much sharper than those recorded earlier in development. Intensity scans generated through the centre of each cornea gave rise to a one dimensional radial intensity profile (as shown in chapter 2) which shows the interfibrillar reflection as a smooth peak. These profiles were further analysed to reveal collagen fibril spacing, and local order.

From developmental days 12 to 18 collagen spacing decreases as the cornea thins and becomes more transparent. This is in line with the previous findings of Quantock *et al.* (1998) and Siegler and Quantock (2002). In the current study, mean collagen interfibrillar spacing (± SE) for each developmental day was found to be: 60.94nm ±0.56 (day 12), 62.55nm ±0.98 (day 13), 63.74nm ±0.92 (day 14), 62.89nm ±1.22 (day 15), 60.78nm ±1.61 (day 16), 57.04nm ±0.87 (day 17) and 52.70nm ±1.32 (day 18); a graph of mean centre-to-centre collagen spacing is shown in figure 3.2. Statistical significance was ascertained using robust statistical tests for large data groups; oneway ANOVA with Post-Hoc Tukey HSD, after initial tests for skewness and kurtosis, shown in Appendix 2. All data proved to be normally distributed.

X-ray diffraction patterns taken at specific daily timepoints show a non-significant ($P>0.005$) transient increase in mean interfibrillar spacing between days 12 and 13 of incubation (figure 4.2), after which time the rate of fibrillar condensation increases. A two-stage mode of compaction previously observed by Siegler and Quantock (2002), in which the main coming together of

homogenously packed collagen occurred between days 16 and 17 was not found to be so pronounced in this data set. Rather, it was found that P=0.984. Collagen spacing as measured here begins to decrease from day 14 of development, continuing in an almost linear fashion from day 16 onwards, collagen compaction from day 14 onwards coincides with tissue dehydration (Siegler and Quantock, 2002). A closer observation of the Siegler study reveals a high standard deviation, which may mean that the results are more similar than initially apparent, given the natural variation in a noisy biological system. By day 18 of development collagen spacing (52.7nm ±1.32) was significantly lower than at every other timepoint studied, all probabilities P=0.000, except at day 17 where P=0.028. Collagen fibril diameter remains constant during development, it is assumed that fibrils are formed at their mature diameter.

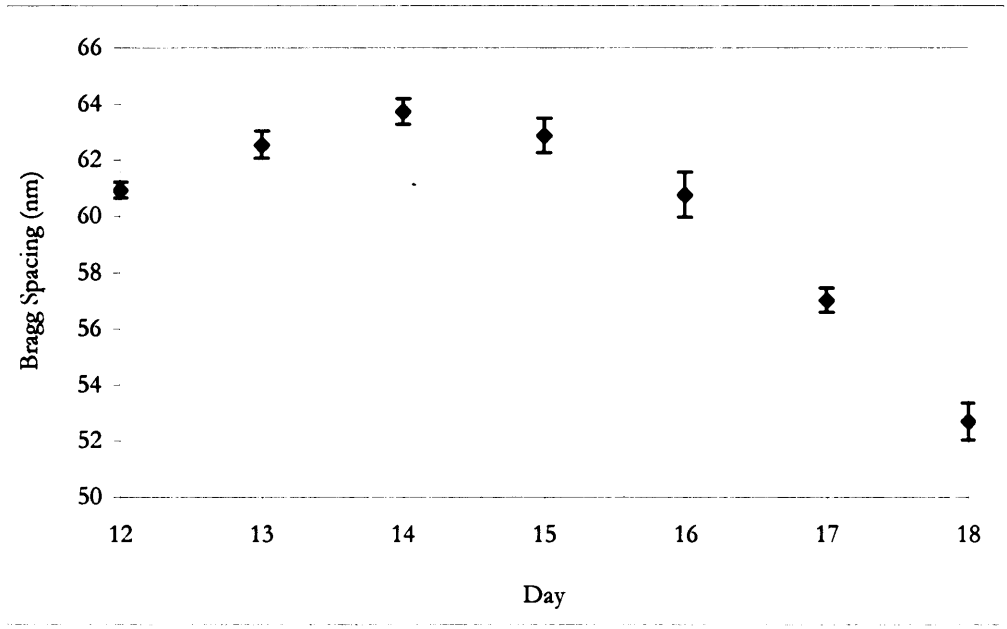

Figure 4.2. Mean interfibrillar Bragg spacing from days 12-18 of incubation. Standard error bars shown.

Further processing of the x-ray scatter patterns was also used to attempt to quantify local order. The height-to-width (at half height) ratio, is detailed in chapter 2, and is used as a measure of the spread of lattice spacing. The mean peak height-to-width at half height ratio (arbitrary units ± SE) for each developmental day was found to be: 17.00 ±2.05 (day 12), 33.59 ±3.51 (day 13), 34.16

±3.18 (day 14), 41.34 ±2.27 (day 15), 38.23 ±5.54 (day 16), 31.89 ±2.07 (day 17) and 30.96 ±3.16 (day 18). Results, shown in figure 4.3, were unsurprising, in that the ratio took a minimal value at day 12 of development; created by a smaller peak height (lesser scatter intensity) and larger peak width (less organised array). A wider interfibrillar peak reflects a relatively large range of sampled spacings - the interfibrillar spacing being taken as the highest point of the interfibrillar peak or most often sampled. This means that at the earlier stages of development, different regular lattice spacings in the Bragg value exist, which may explain the sharp rise in order at day 13 – these ordered lattices (of different sizes) may condense, creating a larger mean value of Bragg spacing and greater local order.

A second increase in local order occurs between days 14 and 15 when interfibrillar spacing only slightly decreases. This seems counterintuitive, as fibrils continue to condense after this point, and yet local order seems greatest at day 15. Perhaps the confusion can be untangled by considering the fundamental constraints of x-ray diffraction. If peak height is increased, and width at half height decreases, the ratio between these two figures will increase. Therefore, if scattering intensity increases due to collagen deposition and a concomitant increase in regularly spaced collagen to increase peak height, and the range of collagen spacing decreases – that is newly deposited fibrils are laid down in a similar lattice to those already in place, and perhaps condensation of existing fibrils, interfibrillar peak width will decrease.

After day 13, the height-to-width at half height ratio then fluctuates until day 18 of development, whilst at the same time Bragg spacing is decreasing. Increased sharpness of the interfibrillar peaks point to an increase in local order, and mean compaction of collagen fibrils more widely throughout the cornea.

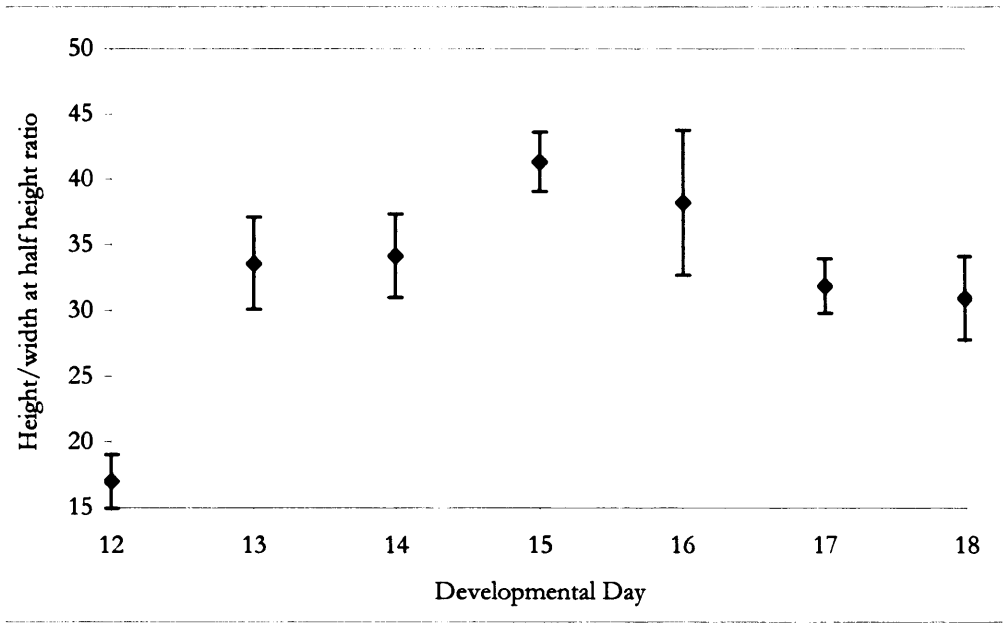

Figure 4.3. Mean height/width at half height ratio from days 12-18 of incubation. Standard error bars shown.

4.4.2 Keratan sulphate quantification

Quantification of linear pentasulphated hexasaccharides and tetrasulphated hexasaccharides on KS chains by ELISA show an inverse relationship with collagen spacing (figures 4.4 and 4.5) in both cases. The monoclonal antibody 1B4 used to quantify tetrasulphated hexasaccharides (± SE) on KS undergoes little change in the earlier stages of development; between days 12 and 15 levels rise from 0.291μg/mg cornea (±0.118) to 0.521μg/mg (±0.109). After this point, levels of lesser sulphated KS increase more rapidly; doubling from 0.732μg/mg cornea (±0.126) on day 16 to 1.501μg/mg cornea (±0.327μg/mg) on day 18. Results tables can be found included in appendix 2.

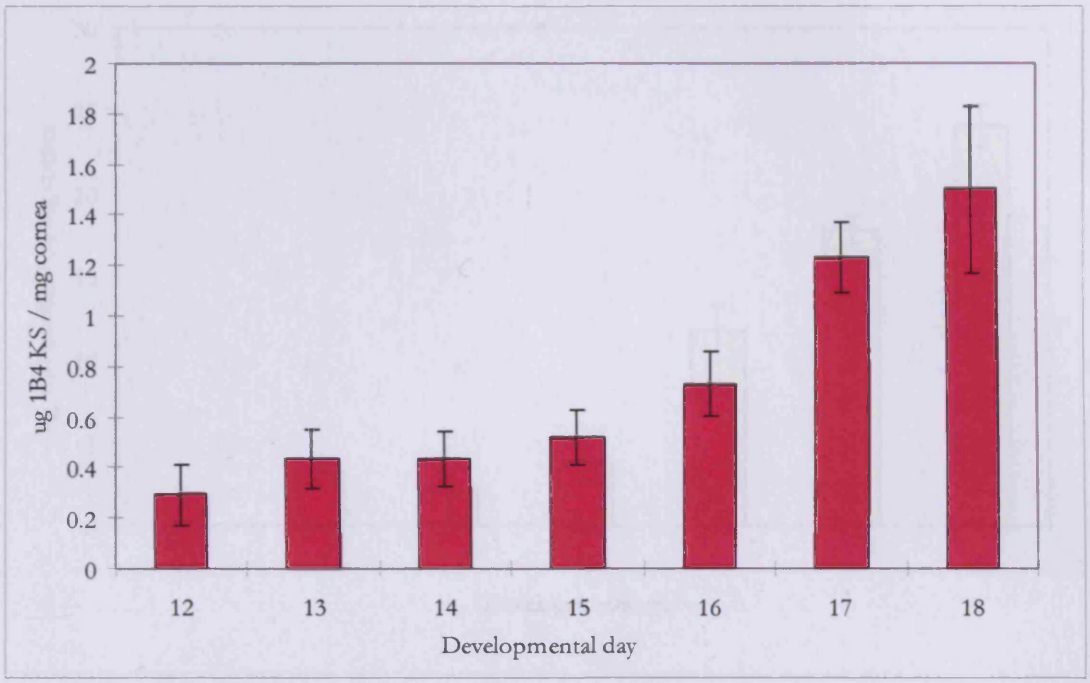

Figure 4.4. Mean 1B4 labelled KS labelling per mg cornea, quantification of low sulphated keratan sulphate during development shows an inverse relationship to collagen interfibrillar spacing between days 15 and 18.

The increasing presence of lesser sulphated KS at the time of stromal condensation supports suspicion of a link between these two events. Interestingly, a similar relationship is seen in more highly sulphated (pentasulphated) hexasaccharides on keratan sulphate chains. 5D4 measured KS (± SE) was quantified per mg of cornea as follows: 1.796 ±0.540μg/mg (day 12), 3.230μg/mg ±0.237 (day 13), 2.020μg/mg ±0.111 (day 14), 3.773μg/mg ±0.477 (day 15), 11.644μg/mg ±1.323 (day 16), 17.822μg/mg ±2.541 (day 17) and 24.099μg/mg ±2.497 (day 18).

Between days 12 and 15 there is little change in the measured quantities of highly sulphated KS, after which time there is a near three-fold increase in antigenic 5D4 between days 15 and 16. From day 16 onwards there is a near 50% increase in 5D4 measured KS in each 24 hour period, reaching a mean of 24.099μg/mg (±2.497) cornea by day 18. A graph of 5D4 measured KS against collagen spacing is shown below.

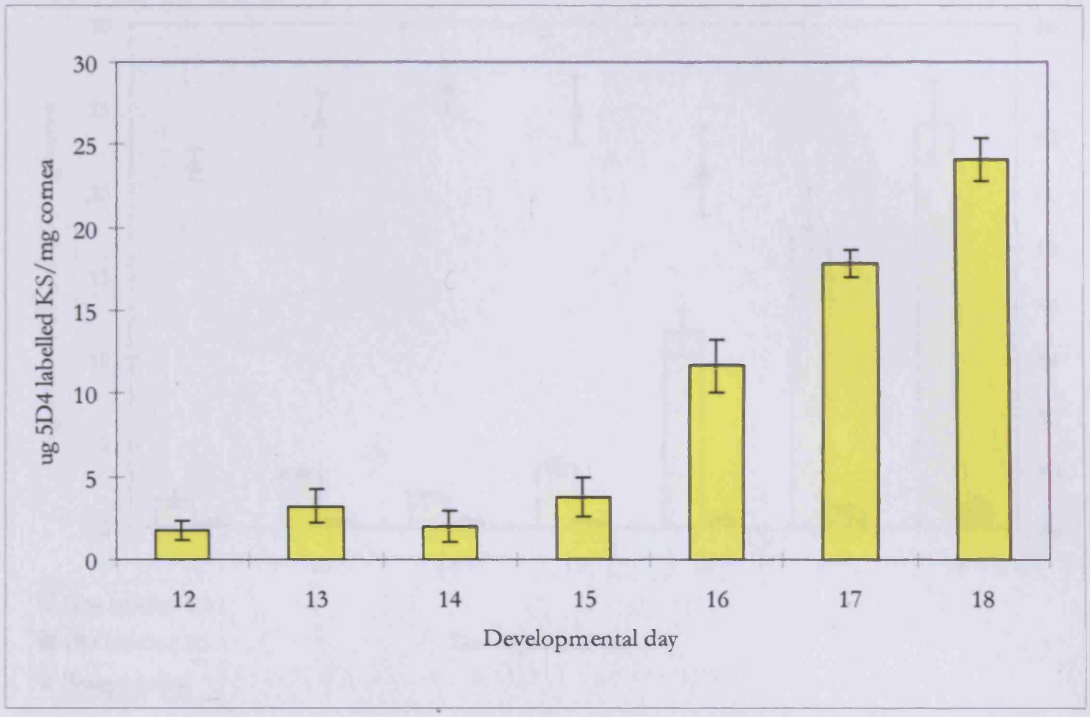

Figure 4.5. Mean 5D4 labelled KS per mg cornea, and the relationship with Bragg spacing from days 12-18 of incubation. Standard error bars shown. Quantification of highly sulphated keratan sulphate during development shows an inverse relationship to collagen interfibrillar spacing.

Previous studies point to keratan sulphate appearing in an unsulphated form before day 15 of development, (Cornuet, 1994) and begins to accumulate between days 15 and 18 of incubation (Dunlevy, 2000). These findings concur with the almost linear increase in highly sulphated KS after day 15 of development.

By directly comparing the relationship of highly sulphated and lesser sulphated keratan sulphate against collagen interfibrillar spacing, using 5D4 and 1B4 respectively (figure 4.6), it becomes clear that the more heavily sulphated form is a greater presence and may be of importance. Both forms of antibody labelled KS show a similar expression pattern (shown in indiviual graphs, figures 4.4 and 4.5), however the end point reached at day 18 is around sixteen times greater for 5D4 labelled KS. Indeed, highly sulphated KS expression undergoes significant increases every day between days 16 and 18 of development.

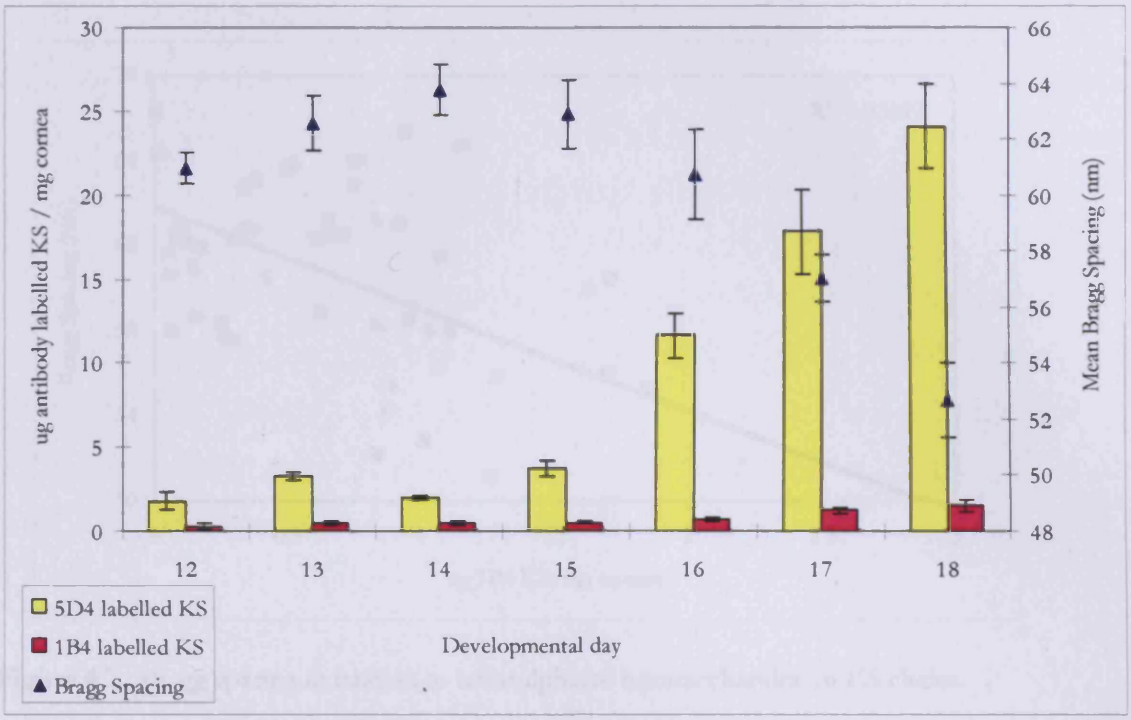

Figure 4.6. Comparing mean Bragg spacing (blue), 1B4 (purple) and 5D4 (yellow) labelled KS labelling (per mg corneal wet weight) from days 12-18 of incubation. Standard error bars shown. Quantification of highly and lesser sulphated keratan sulphate during development shows an inverse relationship to collagen interfibrillar spacing.

To examine this relationship more closely, the link between Bragg spacing and keratan sulphate may be further elucidated without the constraint of developmental day. Tetrasulphated hexasaccharides (figure 4.7) display a loose correlation with mean interfibrillar spacing; R^2=0.3897, whilst pentasulphated hexasaccharides (figure 4.8) have a more definite connection, R^2=0.5007. The R^2 value is a descriptive measure between 0 and 1 - generally, a high value of R^2 means that one term can be well predicted from another. R^2 is most often used in linear regression to obtain the formula of the line used to track a set of data points, the R^2 value is also used to ascertain how well the resulting line matches the original data points.

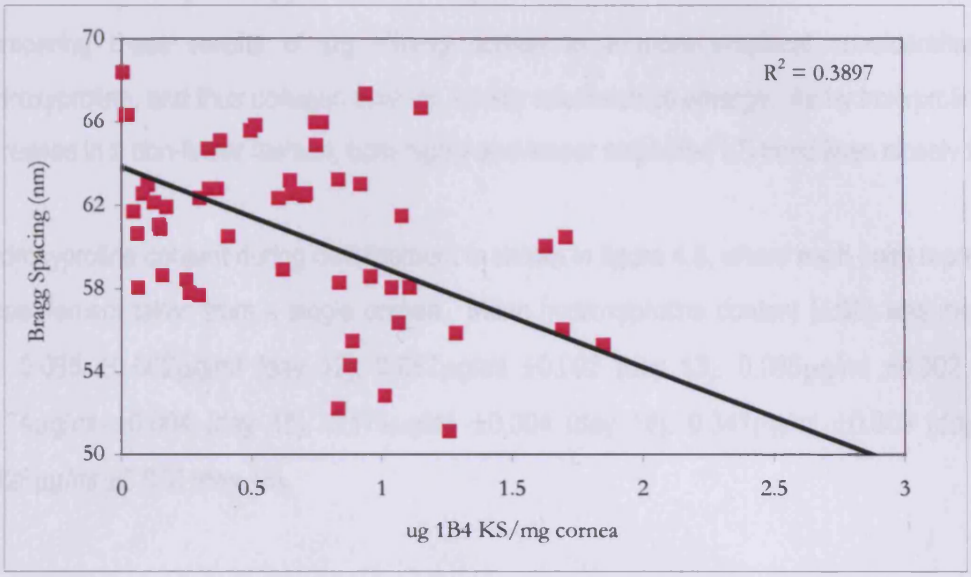

Figure 4.7. Bragg spacing in relation to tetrasulphated hexasaccharides on KS chains.

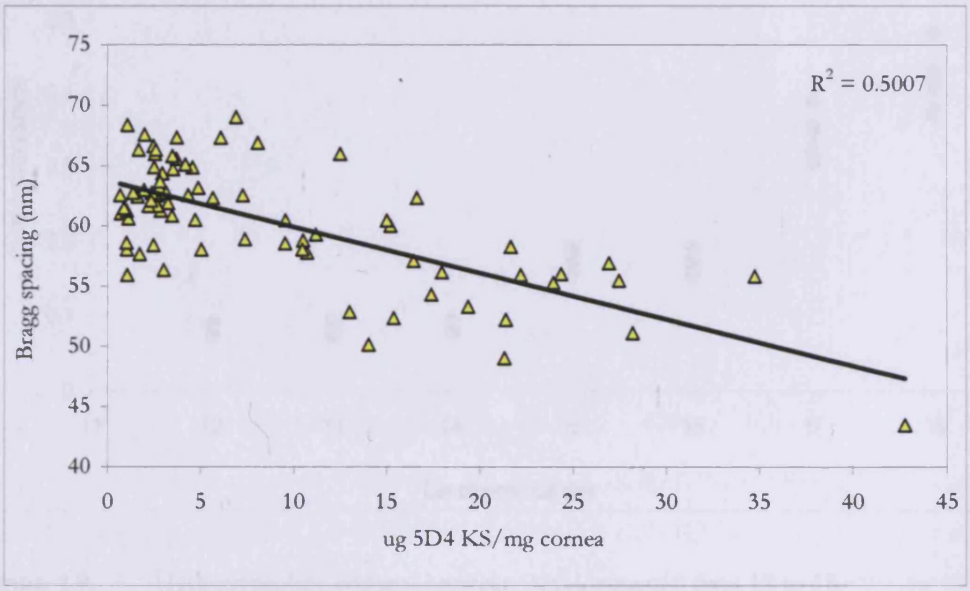

Figure 4.8. Bragg spacing in relation to pentasulphated hexasaccharides on KS chains.

4.4.3 Hydroxyproline assay

Comparing these results of μg KS/mg cornea to a more empirical consideration against hydroxyproline, and thus collagen content, similar relationships emerge. As hydroxyproline content increases in a non-linear fashion, both highly and lesser sulphated KS trend lines closely follow.

Hydroxyproline content during development is shown in figure 4.9, where each point represents the measurement taken from a single cornea. Mean hydroxyproline content (±SE) was measured to be: 0.085 ±0.002μg/ml (day 12), 0.087μg/ml ±0.002 (day 13), 0.085μg/ml ±0.002 (day 14), 0.174μg/ml ±0.004 (day 15), 0.174μg/ml ±0.004 (day 16), 0.341μg/ml ±0.009 (day 17) and 0.426μg/ml ±0.010 (day 18).

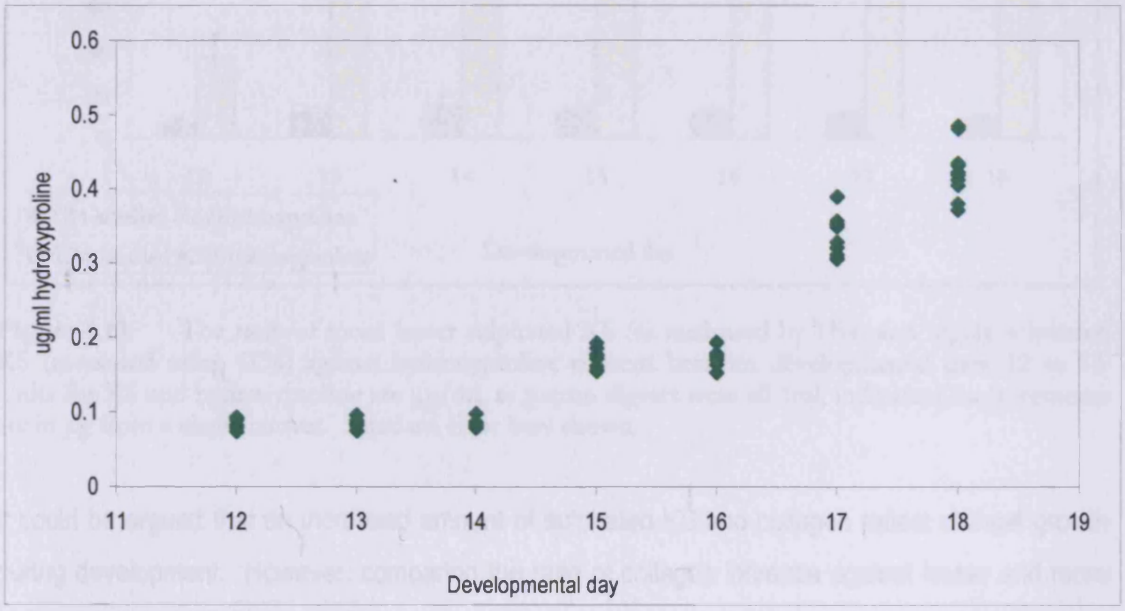

Figure 4.9. Hydroxyproline content between developmental days 12 to 18.

Highly significant changes ($P<0.001$) in hydroxyproline (indicative of collagen type I) content occur between days 16 and 18 of development. This result indicates that notable collagen deposition takes place in the latter stages of embryonic development, after KS levels are reported to rise

(Dunlevy *et al.*, 2000) and the sulphated form of KS begins to accumulate (Cornuet, 1994). The relationship between hydroxyproline and sulphated KS is shown below in figure 4.10.

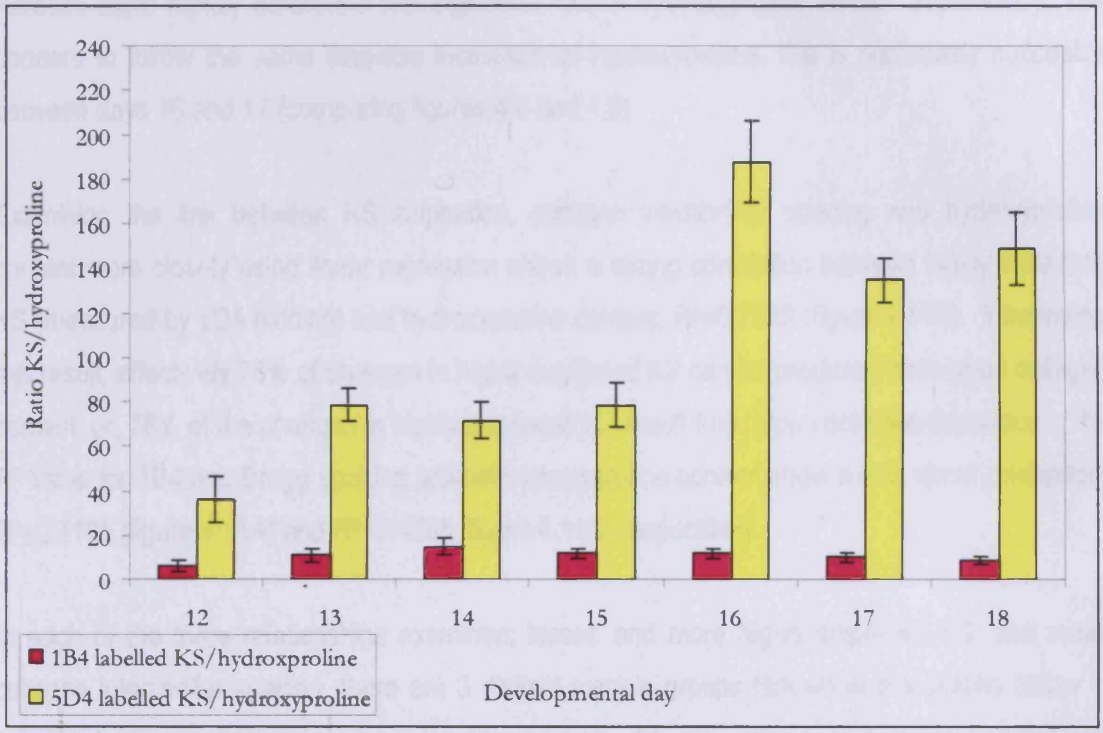

Figure 4.10. The ratio of mean lesser sulphated KS (as measured by 1B4) and highly sulphated KS (measured using 5D4) against hydroxyproline content between developmental days 12 to 18. Units for KS and hydroxyproline are μg/ml, as papain digests were all 1ml, individual measurements are in μg from a single cornea. Standard error bars shown.

It could be argued that an increased amount of sulphated KS and collagen reflect corneal growth during development. However, comparing the ratio of collagen increase against lesser and more highly sulphated KS (figure 4.10) shows that the relative increase of more highly sulphated KS (as labelled by 5D4) to hydroxyproline content is greater, i.e. there is proportionally more highly sulphated KS.

Both 1B4- and 5D4- labelled KS show remarkably similar relationships to and with hydroxyproline content. Both highly, and lesser sulphated KS rapidly increase at the time of significant increases in hydroxyproline content between days 16 and 17, although highly sulphated KS begins to increase more rapidly before the first significant rise in hydroxyproline levels. Superficially, 1B4 appears to follow the same stepwise increases as hydroxyproline, this is particularly noticeable between days 16 and 17 (comparing figures 4.6 and 4.9).

Examining the link between KS sulphation, collagen interfibrillar spacing and hydroxyproline content more closely using linear regression shows a strong correlation between highly sulphated KS (measured by 5D4 binding) and hydroxyproline content, R^2=0.7839 (figure 4.11B). Interpreting this result, effectively 78% of changes in highly sulphated KS can be predicted from type I collagen content; or, 78% of the changes in highly sulphated KS result from type I collagen deposition. The R^2 value for 1B4 and Bragg spacing against hydroxyproline content show a less direct correlation, R^2=0.4165 (figure 4.11A) and R^2=0.4268 (figure 4.11C) respectively.

In each of the three relationships examined; lesser, and more highly sulphated KS, and mean collagen interfibrillar spacing, there are 3 distinct sample groups (shown in the graphs below in figure 4.11, each point represents a single cornea). Clusters appear to form around 0.08μg, 0.18μg and between 0.31-0.49μg hydroxyproline, which would indicate three stages of collagen deposition related to a more widely spread highly sulphated KS content within the final week of incubation before hatch, relative to developmental day.

A

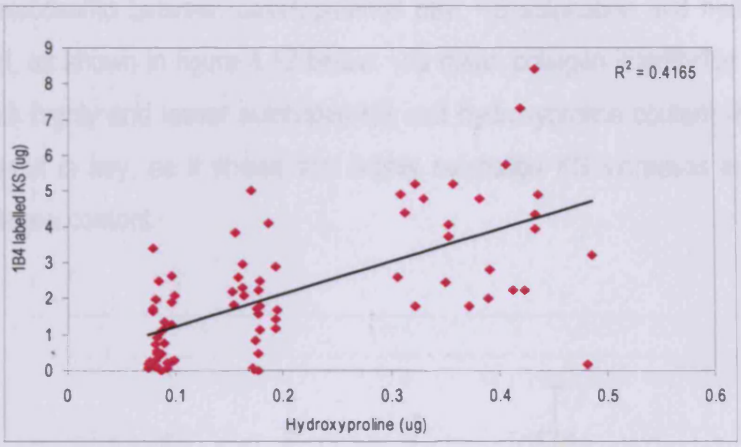

B

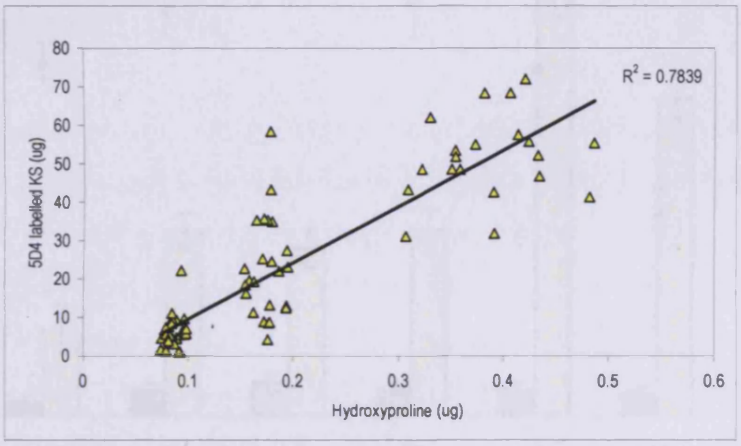

C

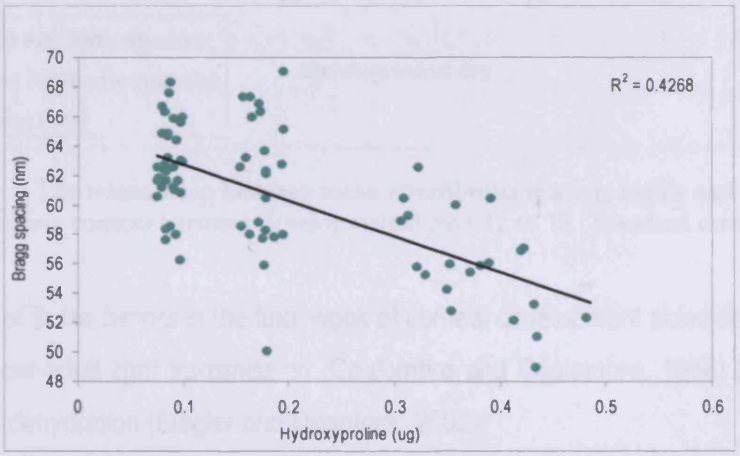

Figures 4.11A, B and C. The relationship between hydroxyproline and (A) lesser-, (B) highly-sulphated KS, and (C) Bragg interfibrillar spacing. R^2 values shown in the top right hand corner.

Finally, the relationship between developmental day, KS sulphation and hydroxyproline content was examined, as shown in figure 4.12 below. As mean collagen interfibrillar spacing decreases over time, both highly and lesser sulphated KS and hydroxyproline content rise at an increasing rate. This result is key, as it shows that highly sulphated KS increases in a disproportionate fashion to collagen content.

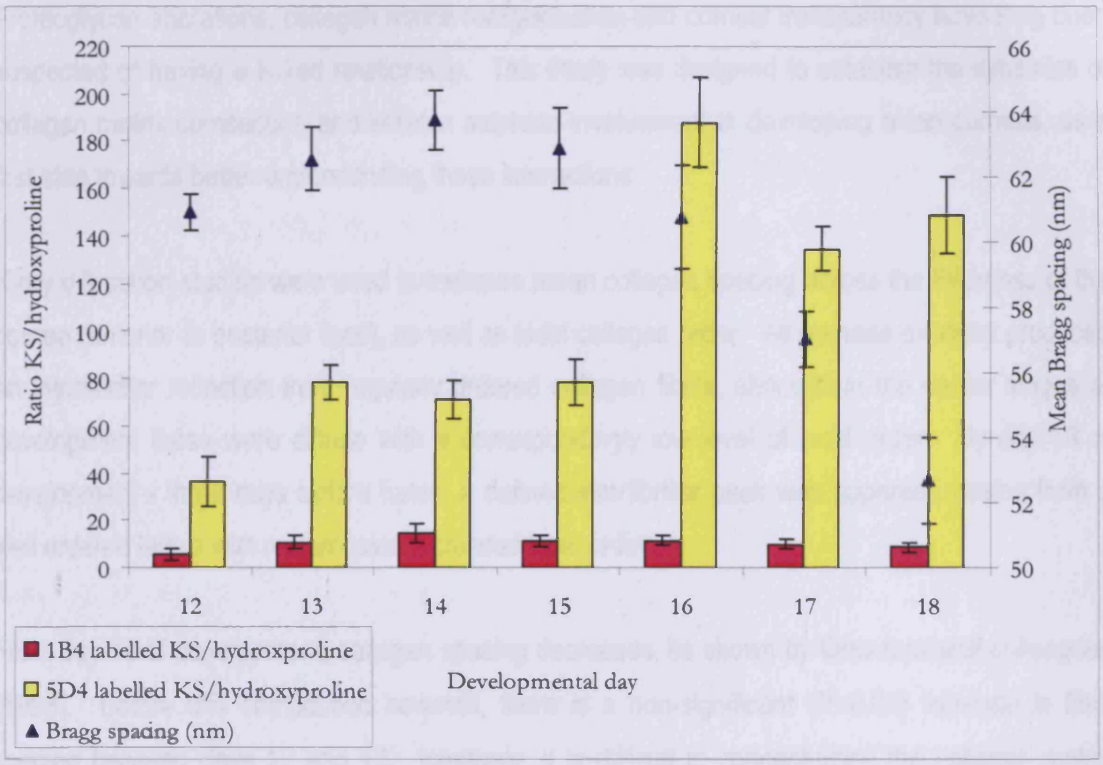

Figure 4.12. The relationship between mean interfibrillar spacing, highly and lesser sulphated KS, and hydroxyproline content between developmental days 12 to 18. Standard error bars shown.

The interplay of these factors in the final week of corneal development coincides with transparency changes to near-adult light transmission (Coulombre and Coulombre, 1958) by day 18, and two stage stromal dehydration (Siegler and Quantock, 2002).

4.5 Discussion

Between developmental day 9 and hatch at day 21, the chick secondary cornea undergoes significant structural, compositional and transparency changes. During the latter stages of morphogenesis adult levels of transparency are achieved (Coulombre and Coulombre, 1958), and the cornea becomes decidedly thinner (Hay and Revel, 1969) and experiences a switch in the type of keratan sulphate produced (Dunlevy *et al.*, 2000; Cai *et al.*, 1996; Cornuet *et al.*, 1994). Proteoglycan alterations, collagen matrix reorganisation and corneal transparency have long been suspected of having a linked relationship. This study was designed to establish the dynamics of collagen matrix compaction and keratan sulphate involvement in developing avian corneas, as a first step towards better understanding these interactions.

X-ray diffraction studies were used to measure mean collagen spacing across the thickness of the cornea (anterior to posterior face), as well as local collagen order. All corneas exposed produced an interfibrillar reflection from regularly ordered collagen fibrils, although in the earlier stages of development these were diffuse with a correspondingly low level of local order. By day 18 of development - three days before hatch, a defined interfibrillar peak was apparent, arising from a well ordered lattice with reciprocated increased local order.

From day 13 of development, collagen spacing decreases, as shown by Quantock and colleagues (1998). Before this compaction however, there is a non-significant ($P>0.05$) increase in fibril spacing between days 12 and 13. Intuitively, it is difficult to conceptualise the collagen matrix expanding, just before the major series of compaction is observed. This result cannot, however, be totally excluded. Siegler and Quantock (2002) report an increase in hydration at the same timepoint, which would explain an increase in the interfibrillar space if the cornea is turgid and fibrils are forced further apart. Coincidentally, there is a lactosaminoglycan to glycosaminoglycan switch in KS production between days 12 and 15 (Cornuet *et al.*, 1994), accumulation of hydrophilic sulphated KS could also be responsible for initially increasing mean interfibrillar spacing, by retaining water between collagen fibrils before activation of the endothelial pump.

After day 13, collagen compaction results in stromal condensation, as both highly and lesser sulphated forms of KS begin to accumulate. KS content of the corneas examined by x-ray diffraction was measured using ELISA, and finally hydroxyproline – a specific marker for collagen, was assayed to determine collagen content. Significant increases in highly sulphated KS were found between developmental days 16 and 18, at which time there is also a significant increase in hydroxyproline content and a decrease in collagen interfibrillar spacing. Linear regression reveals an R^2 value of 0.7839 for hydroxyproline content against highly sulphated KS, implying that changes in highly sulphated KS are linked to hydroxyproline content. Highly sulphated KS also shows a strong correlation with collagen interfibrillar spacing, with an R^2 value of 0.5007. The relationship between lesser sulphated KS, collagen spacing and collagen content appear less signficant in this study, with lower recorded R^2 values. These increases are likely to be linked to the natural growth of the cornea during development.

Dunlevy *et al.* (2000) reported that KS content increases between developmental days 15 and 18, Cornuet *et al.* (1994) also found that lumican is found in a sulphated form from developmental day 15 onwards. Superficially considered, it seems counterintuitive that a hydrophilic molecule accumulates as the cornea dehydrates. The water retentive properties of KS however, would be expected to swell the corneal matrix, rather than aid its compaction. Sulphated KS is highly hydrophilic and is considered critical for collagen organisation, also KSPGs are scarce in opaque, overly hydrated corneal scars with large interfibrillar spaces, and a return to normal spacing, tissue transparency and hydration compliments a rise in KSPG concentration (Hassell *et al.*, 1983). It is possible that during development the endothelial pump acts to dehydrate the corneal stroma, and KSPGs serve to fine tune the fibrillar array, although the timing of endothelial pump activation remains unknown.

Prior to day 14 of development, only 40% of incident light is transmitted through the cornea (Coulombre and Coulombre, 1958), which rises from day 15 onwards. Loose networks of apparently unordered collagen fibrils are well documented through quick-freeze, deep-etch electron microscopy between developmental days 8 to 13 (Hirsch *et al.*, 1999), along with roughly parallel

collagen fibrils arranged into perpendicular bundles. By day 15, these ordered regions predominate.

The reorganisation of collagen during morphogenesis is significant, because all theories of corneal transparency dictate that the spatial arrangement of collagen fibrils is a vital structural parameter that helps to govern tissue transparency (Farrell, 1994; Freund *et al.*, 1986; Benedeck, 1971; Hart and Farrell, 1969; Maurice, 1957). Collagen fibril diameter remains constant throughout development as centre to centre fibril separation decreases, reaching a value similar to average surface-surface fibril separation for birds (~35 nm) found by Meek and Leonard (1993) (Siegler and Quantock, 2002).

This present study shows that the major, homogeneous compaction of chick corneal collagen fibrils occurs between developmental days 16 and 18, accompanied by a significant increase in highly sulphated KS and hydroxyproline (representative of type I collagen) content. KSPGs are increasingly thought to have a role in cross-linking collagen fibrils, and their presence at a time of corneal dehydration could further serve their function as mediators of the collagen array. The avian cornea is an excellent model for developmental studies, and further research is warranted to elucidate the precise role of the KSPGs and associated molecules during development.

4.6 Further work

The results from this investigation imply that a more detailed investigation of collagen structure and KS emergence is warranted, to elucidate, for example, which PG core proteins bear the emerging KS GAGs. A major point of interest is the action of the endothelial pump. The embryonic environment is essentially aqueous, and the developing stroma would be expected to naturally swell due to osmosis. Possible immunofluorescence studies could be used to label the emergence and effective "switching on" of this mechanism.

Preliminary studies using the monoclonal antibodies Ker^{-1} and Lum^{-1} directed towards the core proteins of keratocan and lumican proteoglycans respectively, have been completed and would benefit from further investigation. Also, further electron microscopy studies would help to localise the emergence and sulphation patterns of KSPGs during the latter stages of embryonic development. Extending the subject of this research to CS/DS should also be a point of interest. CS/DS sulphation increases until day 14 of development, from which point expression falls, however corneal dehydration is initiated before this time, which implies that the first major dehydration occurs at a time when hydrophilic PGs are still increasing. A more full analysis could also potentially pinpoint the changes in the refractive index of the fibrils and material between, which is another important factor for transparency, as the chick cornea develops.

The results discussed in these two chapters suggest that from developmental day 18 chick corneal organisation shares similarities with the hatched chick cornea. In fact, at developmental day 18, the chick cornea transmits 80% of incidence light (Coulombre and Coulombre, 1961). Further analysis of developing chick corneas from developmental day 19 until after hatch would allow a more comprehensive understanding of corneal "fine tuning" before hatch.

4.7 Summary

- Collagen fibril spacing significantly decreases during development, this change is accompanied by a statistically significant increase in both highly and lesser sulphated KS, as measured using 5D4 and 1B4 respectively.
- Relating highly and lesser sulphated KS to hydroxyproline content, a measure of type I collagen, there is a disproportionate increase in the more highly sulphated epitope over time. This implies that highly sulphated KS expression is exceeding the natural corneal growth rate.

CHAPTER FIVE:
Collagen Spacing and the Influence of Keratan Sulphate

5.1 Introduction to Chapter

This chapter is an extension of the previous developing chick cornea X-ray/ELISA study. In the preceding chapter, an inverse correlation appeared between mean collagen interfibrillar spacing and both lesser- and more highly-sulphated KS. This discovery lead to a natural curiosity about the sulphation of KS - if the amount of highly sulphated KS is increasing during the final week of corneal development, is the total KS content similarly growing, or perhaps only the more highly sulphated epitope? The specificity of antibody-antigen interactions means that only the precise 1B4/5D4 sulphated epitopes have been measured in chapter 4, and for this study, another mode of operation is necessary. The monoclonal antibody 5D4, recognises all sulphated structures within one KS chain, whereas BKS-1 recognises a single neoepitope on KS after keratanase digestion. In this way, BKS-1 may be able to identify a more clearly defined pattern for KS in the cornea.

The BKS-1 antibody is a novel core protein label that specifically recognises a keratanase-generated neoepitope [N-acetyl-glucosamine-6-sulphate (GlcNAc-6-S)] for precise quantitative determination of the number of KS chains. Again, corneas from each daily interval during the final week of development will be studied to ascertain the involvement of keratanase sensitive KS (regardless of sulphation) in collagen organisation and spacing. A key aim of this study is to further biochemical analysis on single corneas with known structural parameters such as collagen order; ideally, the same data set from chapter 4 would have been be used, but preliminary studies confirmed that the use of papain had destroyed the BKS-1 epitope, necessitating another x-ray study cohort.

Firstly, the aims and objectives of this study will be identified, and an introduction to relevant current literature presented. Then, the progressive analysis of this series of corneas will be detailed, including X-ray technique, epitope unmasking, and ELISA. A more in depth examination of this method is shown in section 2.5. Results will be presented in a stepwise fashion to examine the cross-disciplinary evaluation of each cornea, and any findings discussed. Finally, possible further work will be outlined.

5.2 Introduction

The initial identification of KS in cornea in 1939 (Suzuki) reported an equal presence of glucose and galactose, as well as acetyl and sulphate groups. The term keratosulphate was coined by Meyer *et al.* after characterisation (1953), which has since evolved to the familiar term of KS.

The KSPGs are thought to interact with collagen fibrils via the protein core, to maintain a uniform diameter and spacing. A murine knockout for lumican, the principal corneal KSPG presented skin laxity and fragility and bilateral corneal opacity (Chakravarti *et al.*, 1998). Furthermore, previous studies of chick development suggest that glycosylation, the addition of saccharides to the PG protein core, is very important to the corneal transparency process. KS chains are of variable length and sulphation (Oeben *et al.*, 1987; Block *et al.*, 1992), bearing sulphation sites on both GlcNAc and Gal sugars in a disulphated disaccharide (Choi and Meyer, 1975), but only on GlcNAc in monosulphated disaccharides (Nazakawa *et al.*, 1998). The sequential sulphation of these sugars becomes apparent in the absence of the sulphotransferase enzyme, when neither GlcNAc nor Gal residues are sulphated (Akama *et al.*, 2001). The scope of KS chain length and sulphation are dictated by tissue specific factors, such as the presence of processing enzymes, galactose-transferase activity increases with KS biosynthesis during chick development, and is maintained at an unusually high level in adult cells (Cai *et al.*, 1996).

The importance of KS in corneal development is well studied, murine lumican knockout models show corneal haze after 3-6months of life (Chakravarti *et al.*, 1989), as KS would normally be expected to accumulate. In the chick cornea, lumican with non-sulphated keratan sulphate side chains is detectable early in development, at day 7, followed by the appearance of sulphated GAG side chains at day 15, when transparency starts to increase (Cornuet *et al.*, 1994). Chick KS accumulation has been also investigated by Funderburgh *et al.* (1986) who used a battery of three different antibodies to detect a sustained, exponential increase of KSPG in the 5 days prior to hatch, and continued accumulation after hatching. The authors suggest that KSPG primary structure may be modulated late in development and after hatch. In chick corneal explants, increased KS synthesis and decreased CS/DS synthesis are associated with the onset of tissue transparency, again suggesting a correlation between proteoglycan composition and corneal transparency (Nakazawa *et al.*, 1995).

The aim of this study was to measure total keratanase sensitive KS content of developing corneas to investigate the relationship between KSPG presence and collagen organisation.

5.3 Materials and Methods

Because this study is comprised of two main stages; X-ray diffraction and biochemical techniques, methods will be presented in a stepwise fashion outlining the overall process in separate sections.

5.3.1 Specimens

Fertilised hen eggs were obtained as described in chapter 4. A total of 81 embryonic corneas were obtained daily from developmental day 12 to day 18 (n=11 to 12 at each timepoint), as described in section 4.3.1, and stored at -80°C prior to X-ray analysis. All procedures were carried out in accordance with the ARVO statement for the use of animals in Ophthalmic and Vision Research.

5.3.2 Data collection and processing

Small angle X-ray scatter patterns were obtained as described in sections 4.3.2, and the resulting information used to deduce interfibrillar Bragg spacing as shown in section 4.3.3. Local collagen order was assessed using the peak width at half height ratio, as detailed in section 4.3.4.

5.3.3 Generation of the KS "stub" neoepitope

After X-ray analysis, corneas were refrozen and transported back to Cardiff at -20°C and stored at -80°C before further assay. The wet weight of each single cornea was recorded prior to quantification of the keratanase I (Sigma) generated 6-sulphated N-acetyl glucosamine stub at the non-reducing terminal on KS chains using sensitive, optimised competitive ELISAs. Background optimisation is shown in Appendix 1. Each cornea was individually incubated under 300µl 10ng/ml cyanogen bromide digest in 70% formic acid (AnalR) made up in acetyl

nitride (as described in section 2.5.1), and reconstituted under 500µl 20mU keratanase and 10mU chondroitinase digest (0.1M TrisAc, pH 6.8). A more detailed description of this process is given in section 2.5.1.

5.3.4 Competitive ELISA analysis

Optimised competitive ELISAs were carried out to selectively quantify the keratanase generated KS stub neoepitope selectively recognised by the novel monoclonal BKS-1 antibody (produced by Dr. Briedgeen Kerr). 96 well E.I.A. microtitre plates (MP Biomedical) were coated by passive adsorption using a 500ng/ml bovine corneal KSPG extract antigen in 20mM sodium carbonate coating buffer, pH 9.6, for 14 hours at 37°C. The plates were washed and blocked as described in section 4.3.6. Keratanase digests from individual corneas were serially diluted (as shown in appendix 1) and allowed to bind with an equal volume of BKS-1 antibody (1:3000 dilution in 1% BSA/TSA) for 1 hour at 37°C, and subsequently used to compete against the bovine corneal KSPG for 1 hour at 37°C using serial dilutions of the bovine KSPG/BKS-1 as a standard. Plates were washed, processed and analysed as described in section 4.3.6.

5.4 Results

For brevity, experimental results have been summarised below in a stepwise fashion. Mean results are presented in their relevant section (individual results and statistics are shown in appendix 2), and the work discussed as a whole in conclusion. As the initial portion of this study (small angle X-ray scattering) follows the same methodology and trend in results as chapter 4, the main points of interest will be highlighted to avoid unnecessary repetition. The two small angle (low angle) X-ray studies shown here chapter and in chapter 4 have not been combined, as the hatchery breeding line had altered in the intervening time, and it is possible that growth rates could be affected. This also allows further examination of the new X-ray data for patterns akin to those found by Siegler and Quantock (2002), not seen in the results from chapter 4.

5.4.1 Collagen spacing

Low-angle X-ray diffraction patterns obtained from 81 developing chick corneas were analysed to provide interfibrillar (Bragg) spacing and local order appreciation at specific daily timepoints from days 12 to 18 of incubation (n=11 to 12 at each developmental day). Further analysis of the same corneas allowed quantification of a KS neoepitope by ELISA.

X-ray scatter patterns generated by the collagen fibril lattice were used to calculate mean centre to centre fibril spacing. An increase in fibril order and decrease in Bragg spacing was seen during the developmental progression from days 12 to 18, apparent in the equatorial reflection of low angle scatter patterns. An example of this is shown in chapter 4, figure 4.1. Mean collagen interfibrillar spacing (± SE) for each developmental day was found to be: 64.85nm ±0.55 (day 12), 64.07nm ±0.55 (day 13), 65.98nm ±0.43 (day 14), 64.4317nm ±1.19 (day 15), 64.45nm ±0.82 (day 16), 58.71nm ±1.56 (day 17) and 57.44nm ±0.49 (day 18); a graph of mean centre to centre collagen spacing is shown below in figure 5.1. Statistical significance was tested using robust statistical tests for large data groups; Oneway ANOVA with Post-Hoc Tukey HSD, after initial tests for normality, shown in Appendix 2.

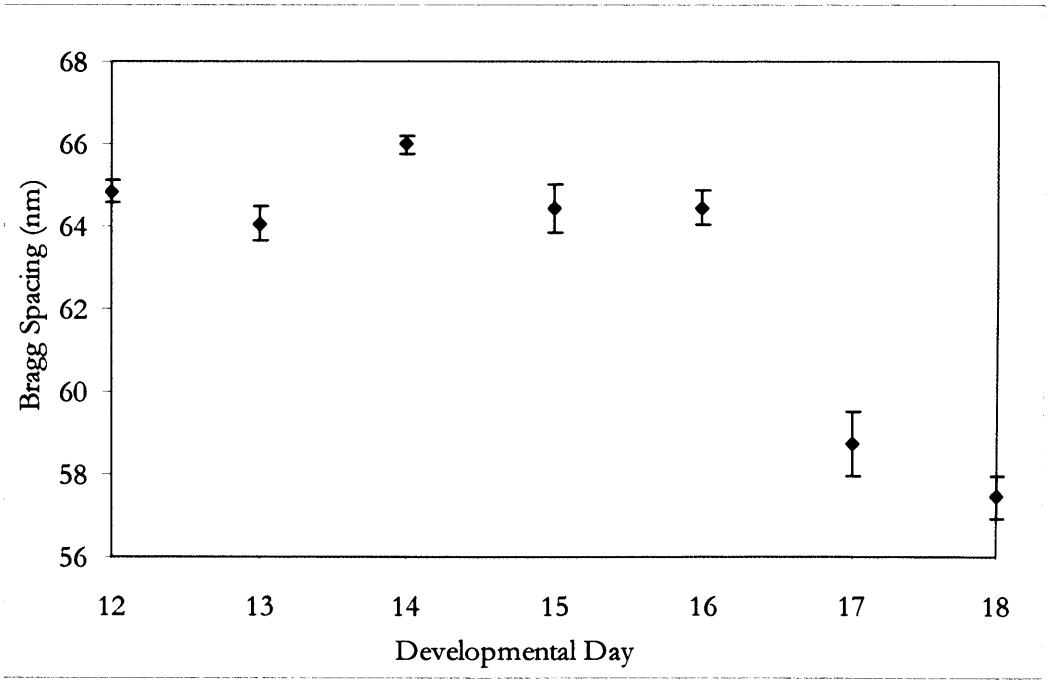

Figure 5.1. Mean collagen interfibrillar spacing (nm) in the week leading to hatch. SE shown.

The only recorded significant drop in Bragg spacing falls between developmental days 16 and 17 (P=0.002), and collagen interfibrillar spacing at days 17 and 18 of incubation are significantly different from every other timepoint, apart from each other. Interestingly, this fibril condensation echoes the previous two-stage mode of fibrillar compaction reported by Siegler and Quantock (2002), who discovered a similar compaction of collagen fibrils with a single, highly significant decrease between days 16 and 17. This earlier study was not found to be normally distributed however, and significance was measured using a Mann-Whitney U test, considered to be less powerful than the t-test used in this work.

Further analysis of the X-ray data was used to appreciate local collagen order. The peak height to width-at-half-height ratio is a measure of how well collagen fibril order conforms to the recorded Bragg spacing value. A graph of these results is shown below in figure 5.3

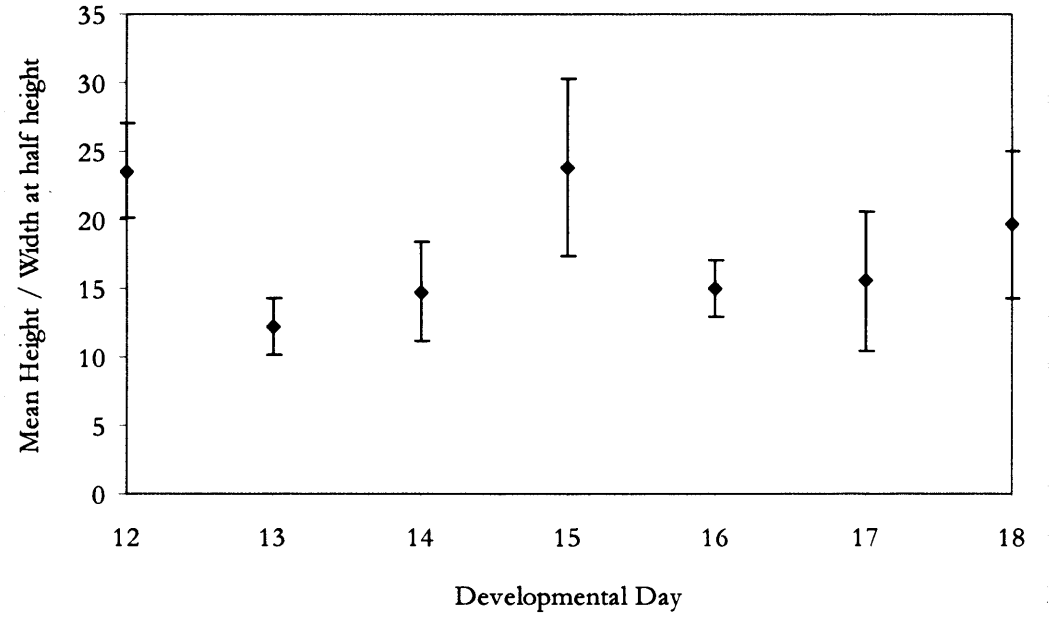

Figure 5.2. Mean height to width at half height ratio from days 12 to 18. SE shown.

These results point to a pattern similar to that seen in chapter 4. Local order fluctuates between days 12 and 18, but due to the large standard error, it is unlikely that any value can be taken from statistical testing. This result is interesting, because it implies that collagen fibrils are laid down in an ordered fashion, in agreement with the earlier study in this thesis.

5.4.2 Quantification of the KS neopeitope

Quantification of keratanase sensitive KS content by BKS-1 ELISA also yielded some interesting results, as shown in figure 5.3 below. KS expression (per cornea) also seems to fluctuate only slightly between days 12 and 18, measured as (mean ± SE) 1.27µg/ml ±0.19 (day 12), 1.20µg/ml ±0.20 (day 15), 1.31µg/ml ±0.36 (day 18), using the BKS-1 antibody. Statistical testing (see appendix 2) revealed no significant changes in BKS-1 labelled KS content. This result implies that despite the massive upregulation in highly sulphated KS measured in chapter 4, the total amount of keratanase sensitive KS (in any form of sulphation) is not significantly affected.

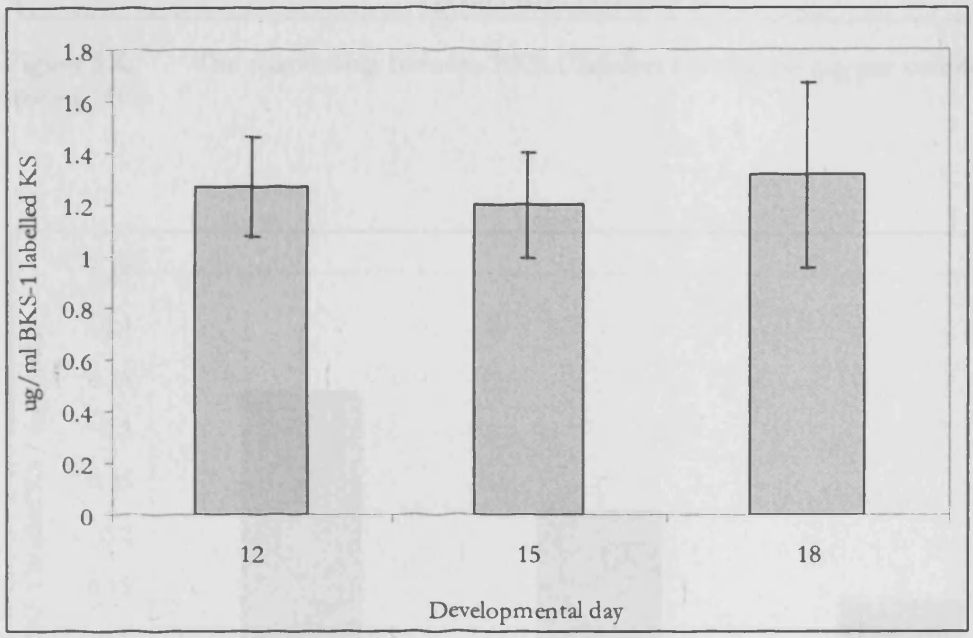

Figure 5.3. KS content measured using BKS-1 from days 12 to 18. SE shown.

Comparing this result to collagen fibril spacing in the same corneas shows little relationship to Bragg spacing, linear regression shows a correlation of $R^2 = 0.0048$, shown in figure 5.4. Surprisingly, the amount of keratanase sensitive KS per cornea seems to be of little importance to collagen interfibrillar spacing. Perhaps this is because further consideration of the data is needed; expressing these results in terms of wet weight (from each individual cornea), gives a more significant result, as shown in figure 5.5.

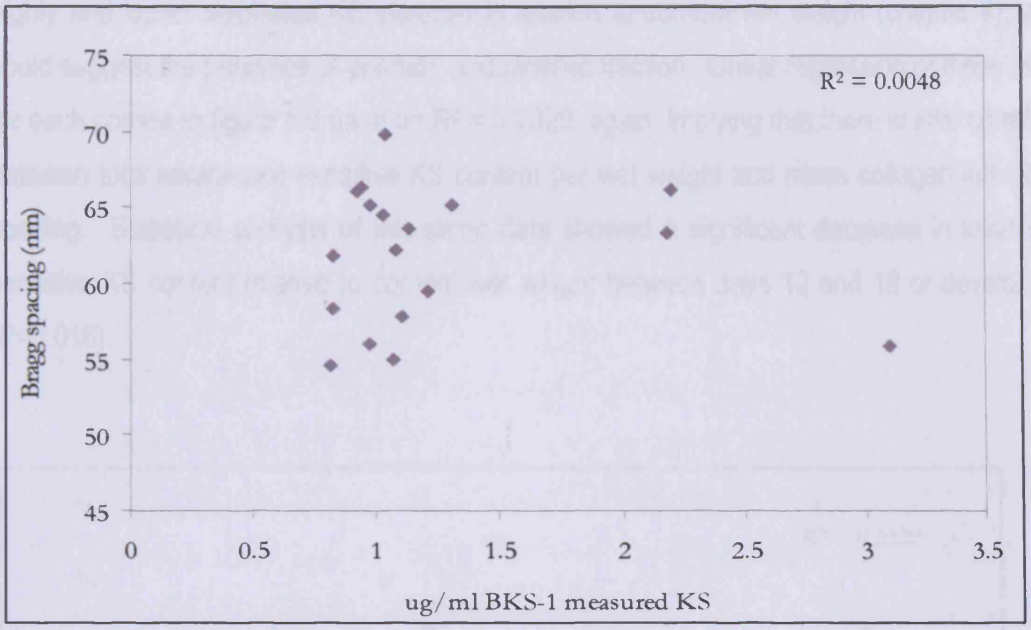

Figure 5.4. The relationship between BKS-1 labelled KS content (μg per cornea) and Bragg spacing (nm).

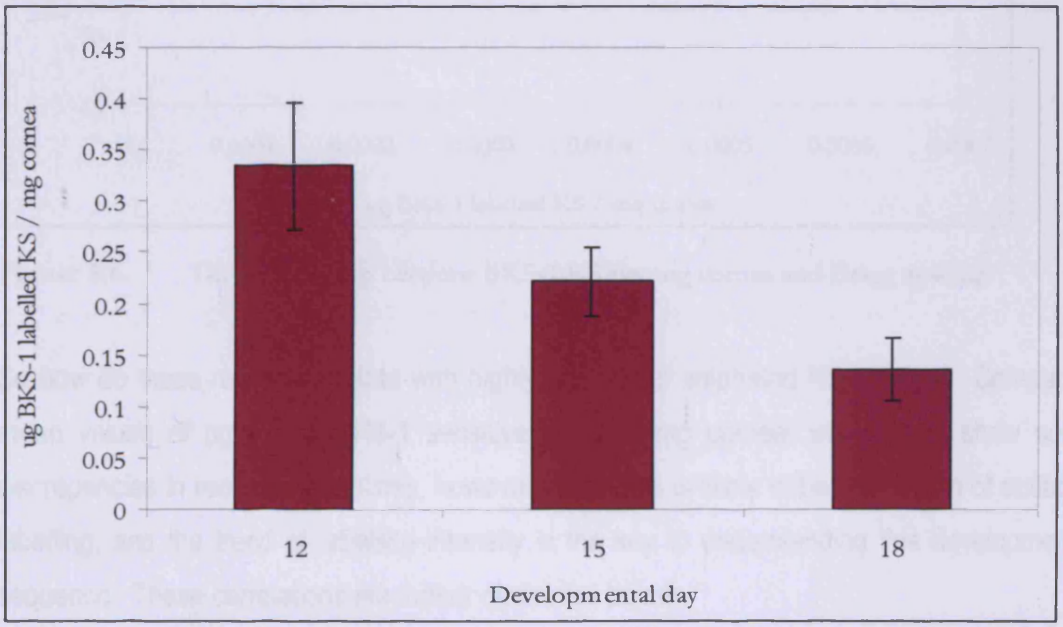

Figure 5.5. Keratanase sensitive KS content (in μg) per mg of cornea. SE shown.

Quantifying the BKS-1 epitope in terms of corneal wet weight (figure 5.5) shows a relative decrease during development, measured as (mean ± SE) 0.33μg/mg ±0.06 (day 12), 0.22μg/mg ±0.033 (day 15), 0.14μg/mg ±0.03 (day 18), by BKS-1. This is intriguing, as both

highly and lesser sulphated KS increase in relation to corneal wet weight (chapter 4), which could suggest the presence of another, unquantified fraction. Linear regression of these results for each cornea in figure 5.6 gave an $R^2 = 0.2329$, again, implying that there is little correlation between total keratanase sensitive KS content per wet weight and mean collagen interfibrillar spacing. Statistical analysis of this same data showed a significant decrease in keratanase sensitive KS content relative to corneal wet weight between days 12 and 18 of development (P=0.016).

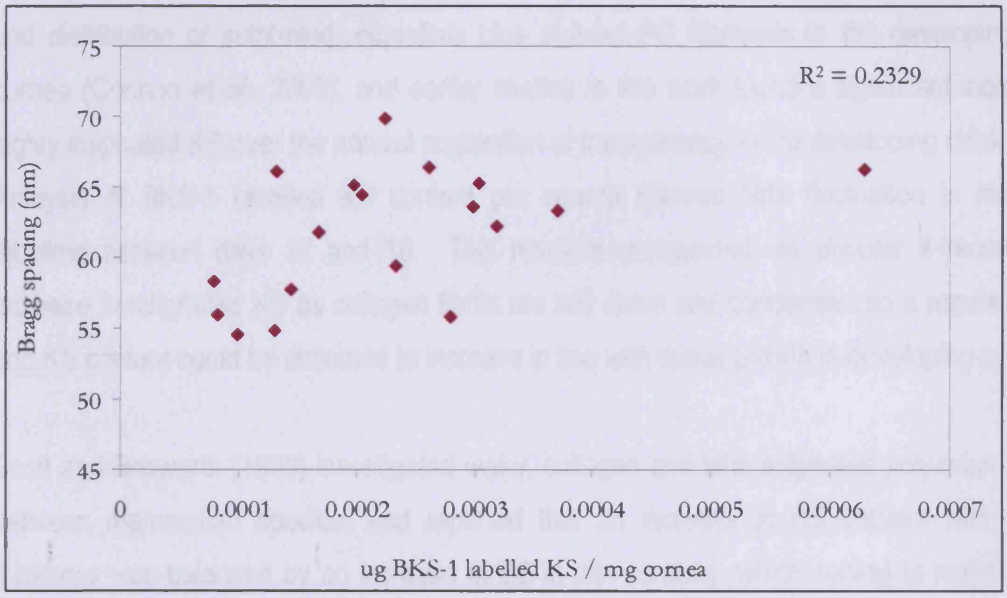

Figure 5.6. The relationship between BKS-1 KS per mg cornea and Bragg spacing.

So how do these results correlate with highly and lesser sulphated KS content? Comparing mean values of µg KS to BKS-1 sensitive KS with mg corneal wet weight, show some discrepancies in recorded quantities, however I think this is likely to be a limitation of antibody labelling, and the trend of labelling intensity is the key to understanding this developmental sequence. These correlations are further discussed below.

5.5 Discussion

This study has produced a number of unexpected results. The long history of KS and collagen structure would suggest that collagen fibrils condense (Siegler and Quantock, 2002; Quantock

et al., 1998; Hay and Revel, 1969) as sulphated KS expression increases (Cai *et al.*, 1996). KS has been identified in a wide range of tissues, although only a limited number of proteins are known to carry KS as a posttranslational modification, and the K SPG core protein is considered to be an important factor in KS biosynthesis (Funderburgh, 2000). Understanding the KSPG expression pattern is an important aspect of understanding of KS biosynthesis (Funderburgh, 2000).

The novel monoclonal antibody BKS-1 was used to monitor KS neoepitope expression in the developing chick cornea. Previous investigators have reported alterations in the size, number and distribution of sulphated, cuprolinic blue stained PG filaments in the developing avian cornea (Connon *et al.*, 2003), and earlier studies in this work found a significant increase in highly sulphated KS over the natural acquisition of transparency in the developing chick cornea. Analysis of BKS-1 labelled KS content per cornea showed little fluctuation in measured labelling between days 12 and 18. This result is unexpected, as chapter 4 recorded an increase in sulphated KS as collagen fibrils are laid down and condense into a regular lattice, and KS content could be assumed to increase in line with tissue growth in developing systems.

Scott and Bosworth (1990) investigated water, collagen and total sulphated polyanion content between mammalian species, and reported that an increase in KS content with corneal thickness was balanced by an increase of DS in thin corneas, which served to maintain total sulphated GAG levels at a constant "average" in the mammals investigated. Their result hints that it is the sulphation of GAG chains which is a critical determinant to structure, and functionally significant. The lack of KS growth could therefore be a reflection of another, different KS sulphation motif presence that is downregulated during development as the more highly sulphated forms being to accumulate, to effectively maintain a consistent KSPG core protein level.

Interestingly, KSPG content relative to corneal wet weight was found to significantly decrease over the timepoints studied. This finding certainly appears counterintuitive and rationalising a physiological cause for an overall KS decrease as sulphated KS labelling peaks is tricky. Considering the limitations of antibody based detection, especially those reliant on the generation of a neoepitope, I would suggest that the trend of these results points to a decrease

in the amount of keratanase sensitive KS and subsequent BKS-1 recognised epitopes, which may not totally reflect the amount of chick corneal KSPG.

KS sulphation is a key factor in susceptibility to keratanase digestion; keratanase cleaves at unsulphated galactose residues flanked by sulphated N-acetylglucosamines. The decrease in KS sensitivity could therefore be related to the increasing sulphation of KS with development. An explanation for this pattern also could involve another fraction of under- or lesser-sulphated KS (not explored in this thesis) that is suppressed or removed as the more highly sulphated epitope increases. Nazakawa *et al.* (1996) reported increased PG synthesis as a whole in cultured two day (hatched) chick corneal stromal cells, but a preferential increase in CS/DS synthesis to consequently decrease the proportion of KS synthesis to total synthesis, a possible future avenue to continue this study.

5.6 Further work

Microscopy studies using the BKS-1 antibody would provide an interesting insight into the accumulation of KSPGs during the chick corneal developmental sequence, previous studies by Young *et al.* (2006) in have showed KSPG labelling by the BKS-1 antibody in normal corneas that is much reduced in macular dystrophy counterparts. Further ELISAs over the time sequence examined here would also further our understanding of KSPG expression during chick development, originally ELISAs were planned for days 12 to 18 inclusive, but technical difficulties mean that complete data sets have not yet been achieved. The novel antibodies to the lumican and keratocan core proteins (Lum^{-1} and Ker^{-1} respectively) would be a suitable follow up to this work after further enzymatic digestion to create an antibody battery approach for measuring collagen order and spacing, KSPG content, lumican and keratocan content. Preliminary studies show that lumican undergoes a near ten-fold increase in labelling during the week before hatch. The anti-I antibody to unsulphated KS would be another possible candidate, although ELISAs would be difficult as this antibody is in limited supply.

5.7 Summary

- BKS-1 measured KS content shows no significant difference between days 12 and 18.

- Critically, BKS-1 measured KS content decreases in relation to wet weight between days 12 to 18, as dehydration is occurring.
- Could raise the possibilities of another, unmeasured sulphated KS fraction that is removed at this time, or a change in the sulphation motif, rendering KS keratanase insensitive.

CHAPTER SIX: Concluding Discussion

6.1 Introduction to Chapter

The aim of this thesis was to enhance current knowledge of proteoglycan involvement in collagen reorganisation during the natural progression towards embryonic chick corneal transparency. This quest has guided me through a variety of analytical techniques, including microscopy, X-ray diffraction, collagen assays, and the development of new ELISAs to quantify variously sulphated KS in individual chick corneas. In this final chapter, I shall try to link findings from previous investigators to my own work, and offer ideas as to their physiological relevance.

The chick cornea is an established model for structural and transparency studies. Formation of the corneal stroma in lower vertebrates such as the chicken, is a result of precisely controlled events. By capturing these stages of morphogenesis, we may be able to further our understanding of the molecular mechanisms at play and apply this knowledge to help advance clinical practice. Previous studies have established the importance of KS in collagen architecture, and I hope this work can continue a well beaten path.

6.2 Concluding remarks

Corneal structure is a major determinant of visual function and corneal mechanical properties. Formation of the avian corneal stroma is the result of a precisely controlled developmental sequence initiated on the third day of incubation. During the final week of embryonic development, the chick cornea undergoes a series of major structural transformations that govern tissue form and function. The most influential of these include matrix compaction (Hay and Revel, 1969; Quantock *et al.*, 1998; Siegler and Quantock, 2002), proteoglycan alterations (Dunlevy *et al.*, 2000; Cai *et al.*, 1996; Cornuet *et al.*, 1994) and changes in collagenous and noncollagenous extracellular matrix components (Birk *et al.*, 1986, 1990; Linsenmayer *et al.*, 1983, 1984, 1990). Adjustments in the lateral packing of collagen fibrils within the matrix seem functionally significant; current theories of corneal transparency require some sort of order in the fibrillar array for light transmission (Maurice, 1957). Early spectrophotometry experiments indicate that 40% of incident white light is transmitted through the embryonic chick cornea before and at day 14 of development, reaching 95% transmission by day 19 (Coulombre and Coulombre, 1958). Thus, the critical rearrangement of fibrillar collagens in this limited time frame is probably a driving force in the acquisition of corneal transparency.

Microscopy studies in chapter 3 served to identify KS emergence. Previous light level microscopy studies have produced conflicting data with respect to highly sulphated KS, with Funderburgh *et al.* (1986) reporting labelling with the I22 antibody in a posterior to anterior fashion, contested by Takahashi *et al.* (1999) who infer that 5D4 labelling appears homogenous throughout in the timepoints they examined. As we have seen, it is difficult to comprehensively identify the pattern of KS deposition because of vaguries in the immuno-fluoresence technique. Perhaps a more sophisticated approach would help to resolve this matter, but results delivered from this experiment conform to neither the Funderburgh nor Takahashi conclusions, and are more suggestive that KS appears in the anterior cornea first. Perhaps it should be remembered, however, that antibody selection and the small sample area considered by microscopy could have a bearing on the result. At day 12 of development, KS labelling under electron microscopy appeared greater in the superficial stroma, becoming uniform by day 18. Working backwards from this timepoint, successful highly sulphated KS labelling was noted as early as day 10 of development, two days before Cornuet *et al.* (1994) report the principle KSPG, lumican, accumulates. Labelling increases as the fibrils become more aligned, which would further suggest a more active role in collagen fibril mediation; highly sulphated KSPGs are expressed early in development and peak as collagen deposition increases, associating with collagen at cell surfaces, perhaps to facilitate the correct "laying down" of lamellae in a near mature formation. An interesting extension of this investigation would be to use confocal microscopy to establish both CS/DS- and KS-PG interaction with collagen in a location specific manner, i.e. posterior stroma versus anterior.

In chapters 4 and 5, I examined the relationship between collagen spacing and the influence of KS. For the first time, individual corneas have been assessed in terms of collagen structure, content and sulphated KS presence. As overall tissue dehydration and fibrillar compaction between days 12 and 14 precede the run up to corneal transparency, it would seem that the crude condensation of corneal matrix on its own is insufficient for a visually transparent lattice. Therefore, the presence of other, separate factors must be of importance. The interplay of collagen reorganisation and proteglycan expression would seem to suggest an intricate balance, indeed statistical analysis of these factors would proffer that the increased presence of highly sulphated keratan sulphate is indicative of increasing order; both lateral spacing and short range lattice order. An increase in local order is also apparent experimentally, as from day 15 of development, the cornea must be dissected away from the sclera in total, rather than

easily tearing at the limbus. This increase in tensile strength would imply that collagen fibrils become interlaced and more tightly packed.

The study shown in chapter 4 showed a key relationship between highly sulphated KS and collagen content. The avian cornea would be expected to naturally increase in size during the time frame under study, therefore a concurrent increase in collagen content and KS would not seem remarkable. ELISA results combined with hydroxyproline assay information show that proportionally more highly sulphated KS is laid down during days 12 to 18, above the level of natural collagen deposition and corneal growth.

GAG synthesis in the embryonic chick cornea before day 9 of development is principally hyaluronate. This is telling, as corneal swelling coincides with heavy hyaluronate expression which is associated with tissue hydration due to a high negative charge (Ogston, 1970), and the removal of hyaluronate by endogenous hyaluronidase coincides with the initiation of corneal compaction (Toole and Trelstad, 1971). The increase of highly sulphated KS described in chapter 4 follows the switch in GAG production documented by Dunlevy *et al.* (2000) at developmental day 14, and an increase in GAG sulphation has also been reported at this time in early chemical experiments (Anseth, 1961).

The sulphation of CS/DS- and KS- proteoglycans in the cornea is thought to affect corneal hydration state, and therefore collagen spacing, and certainly sets them apart from the systemic glycoprotein counterparts. The CS/DS PGs have been attributed to a water retentive tendency, whereas sulphated KSPGs are thought to form an open network with swelling capacity but little retentive power (Bettelheim and Plessy, 1976). In the normal stroma, DS is fully hydrated whereas KS is only partially hydrated, suggesting that KS provides a dynamic buffer for corneal hydration (Funderburgh, 2000). The importance of KS is supported by distortion of the GAG balance in diseases such as macular corneal dystrophy (Hassell *et al.*, 1980), and corneal scar tissue (Cintron *et al.*, 1990).

Corruption of dermatan sulphate synthesis leads to improper organisation in the developing avian cornea (Hahn and Birk, 1992), however decorin null mice show no apparent corneal abnormalities in the published mutant study (Danielson *et al.*, 1997). The cited paper by Danielson and associates reported whole animal morphology, and the focus given to corneal studies was limited. The "take home" message from their work suggested that the cornea was

not "obviously" affected, however some investigators have suggested that the decorin mutation does confer structural changes in the stroma. This phenomenon has recently been examined in closer detail by Birk *et al.* (2006), who concludes that decorin knock out abnormalities are masked by biglycan upregulation. In fact, double KO (decorin and biglycan) mice show severe fibril disruption in both collagen structure and organisation. Perhaps this warrants further investigation into CS/DS-PG involvement in the developing chick cornea and the interplay with KSPGs.

Previously, lumican, the major corneal KSPG, has been reported to appear between days 12 and 15 of development (Cornuet *et al.*, 1994), but the continued accumulation of highly sulphated KS expression in my study would suggest that another, significant increase in sulphated KSPGs is likely to occur later in development. Indeed, a subsequent study by Dunlevy *et al.* (2000) report increasing KS between days 15 and 18, in line with the laying down and compaction of collagen fibrils in this study. Perhaps the decreasing presence of sulphated, water retentive CS/DS PGs in the stroma coupled with endothelial pump activation allow dehydration and matrix compaction prior to the fine tuning of the collagen fibrillar array by KSPGs.

The sulphation of KS has long been offered as a determinant of corneal structure, lumican knock out mice have cloudy corneas with abnormally thick collagen fibrils (Chakravarti *et al.*, 2000), and keratocan mutants have altered fibril organisation too (Liu *et al.*, 2003; Meek *et al.*, 2003), however KS chains on mimecan appear to have limited functional importance (Tasheva *et al.*, 2002; Beecher *et al.*, 2005). Collagen structure in the posterior stroma was also found to be altered more in the lumican deficient mice with both increased fibril diameter and abnormal lateral growth. Superficially, it would appear counterintuitive that a hydrophilic structure such as KSPGs could participate in stromal dehydration and matrix compaction – KS would be expected to hamper water loss and create larger interfibrillar spaces through stromal swelling. It is more likely, I feel, that KS serves to mediate collagen organisation by helping to fine tune the collagen fibril array.

A point of interest this study has raised is the matter of sulphation. The antibody used throughout this project to localise highly sulphated KS, 5D4 recognises pentasulphated hexasaccharides as the smallest linear determinant. Therefore, only linear epitopes containing the correct number of sulphates will be acknowledged. When rationalising KS levels and

sulphation patterns we should appreciate the limitations of an antibody directed approach. For example, is it possible that two KS GAGs could have the same gross sulphation (i.e. total number of sulphate groups), and possibly perform an equal role in the mediation of collagen fibril ultrastructure, but one may have five linear sulphated hexasaccharides sparsely distributed whilst the other contains numerous sulphated hexasaccharides, without the requisite adjacent five for 5D4 labelling. BKS-1 experiments would certainly suggest that keratanase sensitive KS levels remain relatively constant throughout development, perhaps another antibody directed study towards different lesser sulphated KS epitopes could help to further define its importance.

Connon *et al.* (2004) used TEM and quantitative image analysis to analyse chick corneal collagen fibril density, and deduced that fibrils become more closely spaced; compacting first in the anterior stroma, and in the secondary stroma after day 16 of incubation. This is not to say that collagen fibril spacing becomes homogenous throughout the cornea, an earlier study by Connon *et al.* (2002) reported larger interfibrillar spacing in the posterior stroma. Microscopy studies in chapter 3 suggesting KS accumulation in the anterior cornea, correlate with the more recent study, as highly sulphated KS was shown to have a strong correlation with both collagen deposition and interfibrillar spacing in chapter 4 of this work. Similar anterior to posterior KSPG accumulation has also been reported in the young rabbit prior to eye opening (Cintron *et al.*, 1983), thought to be related to low oxygen tension in the anterior stroma.

Collagen organisation remains a critical factor in the progression from corneal opacity to transparency. It is worth remembering that results generated about collagen packing by x-ray diffraction originate from a naturally tensile tissue, and excision releases the strain on collagen fibrils; *in vivo* the triple helix tightens under tension, to resist stretching to make collagen inextensible. Ruberti *et al.* (2004) suggested that resistance to tension has a protective effect on collagen structures; so that collagen under tension is more resistant to damage and degradation. A worthwhile future venture would be to recreate physiological tension and reinvestigate collagen fibril spacing and orientation.

From microscopy, collagen fibril diameter appears to remain constant throughout development (Hirsch *et al.*, 1999; Birk *et al.*, 1986). The interaction of collagens type I and V is thought to be a controlling factor of fibrillogenesis, David Birk's *in vitro* studies (1990) have shown that increasing the proportion of type V collagen in a type I/V mix results in smaller diameter fibrils,

also mirrored by the *in vitro* assembly of type I/V collagen isolated from human placenta (Adachi and Hayashi, 1986; Adachi *et al.*, 1997). Proteoglycans may also perform some role in collagen fibril diameter regulation, both decorin and lumican core proteins have been linked to fibrillogenesis (Rada *et al.*, 1993).

Transparency models suggest that critical factors for light transmission are tissue thickness, collagen fibril diameter, refractive index of corneal components, and local matrix order (Farrell *et al.*, 1994). A recent study by Meek *et al.* (2003) proposed that tissue thickness has a degree of tolerance whereby light transmission is not affected. Meek's group established that tissue thickness can theoretically almost double with a negligible impact on light transmission, the key to transparency lying in the fibril density. If structural parameters are altered due to an increase in tissue thickness by oedema however, the interfibrillar spacing and refractive index are upset, and swelling leads to the formation of unnatural collagen free lakes. This in turn exerts a negative effect on light transmission as predicted by Benedek *et al.* (1971); if the spacing between fibrils approaches the wavelength of light, diffraction effects occur, in much the same way that x-rays are diffracted by normal unswollen collagen fibrils.

During the final week of embryonic development, the chick cornea undergoes compaction to half the initial thickness between developmental days 9 and 14 (Hay and Revel, 1969; Trelstad and Coulombre, 1971). Biochemical assays in chapter 4 determined that collagen is continuously deposited in the stroma, in line with previous findings (Hay and Revel, 1969); indeed from day 14 to hatch, Hay and Revel (1969) describe increased collagen deposition. Drying fresh bovine cornea results in a linear decrease in interfibrillar spacing squared as a function of hydration, meaning that dehydration causes collagen fibril compaction (Goodfellow *et al.*, 1978); as echoed in the chick cornea, during matrix compaction from 150μm at developmental day 14 to 160μm at hatch, and collagen fibril condensation as corneal water content falls. The relationship between collagen spacing and hydration has been examined previously by Siegler (2003), who found a non-linear relationship which implied the presence of another, unquantified factor for collagen fibril rearrangement.

Another key structural parameter in corneal development is the orientation of fibrillar collagen. Collagen fibrils that make up the bulk of the stromal matrix in the mature cornea lie in sheets in the plane of the cornea. Within each lamella, fibrils lie approximately parallel to each other, but

fibrils in adjacent lamellae tend to run at fairly large angles (Komai and Ushiki, 1991). The fibrils themselves are composed of long thin collagen molecules, laterally spaced by approximately 1.6 nm and axially staggered by defined distances. These collagen molecules (types I and V) tend to run within several degrees of the fibril's axis and approximate to fibrillar orientation. A study awaiting publication by Boote *et al.* shows the clear distinction of a thick preferentially aligned annulus around a central 3mm corneal button. In the embryonic chick cornea, the orientation of collagen may influence biomechanical stability, and in turn shape of the cornea. Collagen continues to be laid down even after hatch (Hay and Revel, 1969), and it could be possible that this later addition is a response to chick pecking behaviour – collagen is laid down in an orientated fashion to increase mechanical resilience when the ossicles contract. A wide angle x-ray study of the developing chick cornea would be an interesting extension to this work, pilot data obtained during the course of this thesis preclude proper conclusions, but further beamtime and sampled timepoints would provide information to the orientation of collagen deposition.

Although the current study could not provide a conclusive link between collagen fibril reorganisation and keratan sulphate, we have seen tangible evidence to support a causative relationship; and progress, in some part, in the methods used to track these changes.

APPENDIX ONE

A1.1 Introduction to chapter

In this chapter, recipes for experimental work detailed in chapters 3, 4, 5 and Appendix 2 will be listed. Ethanol, hydrochloric acid, sodium hydroxide and methanol were all obtained from Fisher Scientific.

A1.2 Biochemistry recipes

GUANIDINE EXTRACTION BUFFER:	4M Guanidine HCl
(10 corneas)	0.05M Benzamidine HCl
	0.05M Sodium Acetate
	0.01M Na_2EDTA
	0.1M 6-amino hexanoic acid
	0.5mM PMSF (in 0.5ml methanol)
PAPAIN DIGEST:	0.00936g Cysteine
(10 corneas)	0.02232g Na_2EDTA
	53.52µl Papain
	12ml PBS
DMMB REAGENT:	0.0032g 1,9-DMMB from SERVA (cat # 20335)
(2L)	20ml ETOH
	59ml 1M NaOH
	7ml 98% Formic Acid
	make up to 2L with MilliQ water
TRIS/SODIUM/AZIDE BUFFER:	50mM TRIZMA
	200mM NaCl
	0.02% NaN_3
	0.05% Tween
	pH 7.4 with conc. HCl
DEA BUFFER:	400ml MilliQ water
	12.8mg $MgCl_2$

48ml Diethanolamine
adjust to pH9.8 with 5M HCl
make up to 500ml with MilliQ water

COATING BUFFER: 1.06g Na_2CO_3
500ml MilliQ water
adjust to pH 9.6 with 5M HCl

SUBSTRATE: 4 x p-nitrophenylphosphate (disodium) tablets (Sigma 104-105, 5mg/tablet) per 20ml DEA buffer

5% BSA: 1g BSA in 20ml PBS (centrifuged to remove particles)

1% BSA: 5% BSA diluted 1 in 4 with milli-Q water

HYDROXYPROLINE ASSAY:

Conc. HCl, Stock buffer, and diluent can be prepared in advance and stored at RTP. Oxidant and Colour reagent must be prepared before use and can only be stored overnight at 4°C. Hydroxyproline stock and standards must be frozen.

Conc. HCl 11.7N

STOCK BUFFER: 28.5g Sodium acetate trihydrate
500ml 18.75g Tri sodium citrate dehydrate
2.75g Citric acid
200ml Propan-2-ol

Dissolve solids in 250ml distilled water, add propan-2-ol and make up volume to 500ml with distilled water.

DILUENT: 100ml Propan-2-ol
150ml 50ml distilled water

OXIDANT: 0.7g Chloramine T
10ml distilled water

50ml stock buffer

COLOUR REAGENT:

7.5g dimethylamino benzaldehyde
9.64ml Perchloric acid 70%
1.61ml distilled water (+ acid makes 60% acid)
62.5ml propan-2-ol

HYDROXYPROLINE STOCK SOLUTION:

Reconstitute 10mg purified hydroxyproline (Sigma) in 10ml distilled water
= 1µg/µl stock solution

CYANOGEN BROMIDE DIGEST:

(300µl digest per cornea, so 26.4ml digest needed)

For 50ml 70% Formic acid –
35ml 98/100% Formic acid (Anal R) + 15ml Deionised water

264µl CnBr + 26.4ml 70% Formic acid
CnBr is 1g/ml made up in acetyl nitride, make up at 10ng/ml in formic acid

KERATANASE DIGEST:

CnBr digests reconstituted in 470µl 1X Tris Acetate K'ase buffer (stock)
K'ase added at 20mU per mg cornea, C'ase at 10mU per mg cornea
(from stock 0.001U/µl pH7.5 20mM Tris HCl)

A1.3 Microscopy recipes

SORENSON PHOSPHATE BUFFER 0.2M:

1.56g $NaH_2PO_4 . 2H_2O$
50ml

1% GLUTARALDEHYDE:
(50ml in 0.1M Sorenson buffer)

2ml stock Glutaraldehyde
25ml 0.2M Sorenson buffer
23ml deionised water

"205":	2% Paraformaldehyde
	0.05% Glutaraldehyde
	in 0.1M Sorenson buffer
	10ml 10% Paraformaldehyde
	25ml Sorenson buffer
	100µl 25% Glutaraldehyde (stock)
	14.9ml deionised water
PBS:	60ml 0.5M PB solution
(0.01M)	25.5g NaCl
	into 3l deionised water

A1.4 Serial dilutions

HIGHLY SULPHATED KS (5D4) ELISA

Final dilutions were found through a series of optimisation experiments shown in section A1.5, the quantities listed below serve a single plate:

Coating solution; coat plate at 125ng/ml Bovine Articular Cartilage abc core:
12.5µl 0.1mg/ml BAC + 10ml 20mM Na_2Co_3 pH9.6

Standard curve for competitive ELISAs:

Start tube:	9000ng antigen/ml	
	30µl BAC abc core + 303.33µl 1% BSA	
#1	200µl start	9000ng antigen/ml
#2	100µl start + 200µl 1% BSA	3000ng antigen/ml
#3	100µl #2 + 200µl 1% BSA	1000ng antigen/ml
#4	100µl #3 + 200µl 1% BSA	333.3'ng antigen/ml
#5	100µl #4 + 200µl 1% BSA	111.1'ng antigen/ml

#6	100µl #5 + 200µl 1% BSA		37.04ng antigen/ml
#7	100µl #6 + 200µl 1% BSA	*discard 100µl	12.34ng antigen/ml
#8	No competing antigen, 200µl 1% BSA		0ng antigen/ml

Antibody dilutions; 5D4 working dilution is 1:8000, therefore make up to 1:4000 to allow for further dilution by antigen:

#1	10µl 5D4 technomouse media + 90µl 1% BSA	1:10
#2	10µl #1 + 990µl 1% BSA	1:1000
#3	950µl #2 + 950µl 1% BSA	1:2000
#4	1800µl #3 + 1800µl 1% BSA	1:4000

Chick (unknown) dilutions:

Day 12		
	100µl neat digest + 200µl 1% BSA	1:3
Day 13		
#1	40µl neat digest + 80µl 1% BSA	1:3
#2	110µl #1 + 110µl 1% BSA	1:6
Day 14		
#1	40µl neat digest + 80µl 1% BSA	1:3
#2	110µl #1 + 110µl 1% BSA	1:6
Day 15		
#1	30µl neat digest + 60µl 1% BSA	1:3
#2	80µl #1 + 160µl 1% BSA	1:9
Day 16		
#1	15µl neat digest + 120µl 1% BSA	1:9
#2	110µl #1 + 110µl 1% BSA	1:18
Day 17		
#1	15µl neat digest + 120µl 1% BSA	1:9

#2	100µl #1 + 200µl 1% BSA	1:27

Day 18

#1	15µl neat digest + 120µl 1% BSA	1:9
#2	110µl #1 + 110µl 1% BSA	1:18

200µl of each final dilution (both chick unknowns and standard curve) was transferred to a labelled tube, and 200µl final antibody dilution added.

LESSER SULPHATED KS (1B4) ELISA

Final dilutions were found through the series of optimisation experiments shown in section A1.5, these quantities are listed for a single plate:

Coating solution; coat plate at 125ng/ml Bovine Articular Cartilage abc core:
12.5µl 0.1mg/ml BAC + 10ml 20mM Na_2Co_3 pH9.6

Standard curve for competitive ELISAs:
Start tube: 9000ng antigen/ml
30µl BAC abc core + 303.33µl 1% BSA

#1	200µl start		9000ng antigen/ml
#2	100µl start + 200µl 1% BSA		3000ng antigen/ml
#3	100µl #2 + 200µl 1% BSA		1000ng antigen/ml
#4	100µl #3 + 200µl 1% BSA		333.3'ng antigen/ml
#5	100µl #4 + 200µl 1% BSA		111.1'ng antigen/ml
#6	100µl #5 + 200µl 1% BSA		37.04ng antigen/ml
#7	100µl #6 + 200µl 1% BSA		12.34ng antigen/ml
#8	100µl #7 + 200µl 1% BSA	*discard 100µl	4.11ng antigen/ml
#9	No competing antigen, 200µl 1% BSA		0ng antigen/ml

Antibody dilutions; 1B4 working dilution is 1:4000, therefore make up to 1:2000 to allow for further dilution by antigen:

#1	3µl 1B4 Ascites + 27µl 1% BSA	1:10
#2	10µl #1 + 990µl 1% BSA	1:100
#3	180µl #2 + 1620µl 1% BSA	1:1000
#4	1700µl #3 + 1700µl 1% BSA	1:2000

Chick (unknown) dilutions:

Day 12	Use neat digest
Day 13	Use neat digest
Day 14	Use neat digest
Day 15	Use neat digest
Day 16	Use neat digest
Day 17	Use neat digest

Day 18

#1	70µl neat digest + 140µl 1% BSA	1:3

200µl of each final dilution (both chick unknowns and standard curve) was transferred to a labelled tube, and 200µl final antibody dilution added.

KERATANASE SENSITIVE KS (BKS-1) ELISA

Final dilutions were found through optimisation experiments shown in section A1.5. These quantities are correct for a single 96 well plate.

Coating solution; coat plate at 0.5µg/ml Bovine Corneal KSPG:

2.5µl 2mg/ml Bovine Corneal KSPG + 10ml 20mM Na_2CO_3 pH9.6

(where 500ng/ml = 0.5µg/ml, and 2mg/ml = 2µg/µl)

Standard curve for competitive ELISAs:

Start tube: 27,000ng antigen/ml = 9µg KSPG in 333.33µl 1% BSA

4.5µl Bovine Corneal KSPG 2mg/ml stock + 328.83µl 1% BSA

#1	200µl start	27,000ng antigen/ml
#2	100µl start + 200µl 1% BSA	9000ng antigen/ml
#3	100µl #2 + 200µl 1% BSA	3000ng antigen/ml
#4	100µl #3 + 200µl 1% BSA	1000ng antigen/ml
#5	100µl #4 + 200µl 1% BSA	333.3'ng antigen/ml
#6	100µl #5 + 200µl 1% BSA	111.1'ng antigen/ml
#7	100µl #6 + 200µl 1% BSA	37.04ng antigen/ml
#8	100µl #7 + 200µl 1% BSA	12.34ng antigen/ml
#9	100µl #8 + 200µl 1% BSA	4.11ng antigen/ml
#10	100µl #9 + 200µl 1% BSA	1.34ng antigen/ml
#11	No competing antigen, 200µl 1% BSA	0ng antigen/ml

Antibody dilutions; BKS-1 working dilution is 1:3000, therefore make up to 1:1500 to allow for further dilution by antigen:

#1	2.5µl 5D4 BKS-1 + 247.5µl 1% BSA	1:10
#2	200µl #1 + 800µl 1% BSA	1:500
#3	800µl #2 + 1600µl 1% BSA	1:1500

Chick (unknown) dilutions:
(Corneas were reconstituted in 500ml Tris Acetate Buffer)

Day 12 use neat

Day 15 use neat

Day 18 use neat

200µl of each final dilution (both chick unknowns and standard curve) was transferred to a labelled tube, and 200µl final antibody dilution added.

Secondary antibody dilution:

4µl Antimouse (H+L) Alkaline Phosphatase Conjugate 1mg/ml (S372B, Promega, USA) in 10ml 1% BSA

Substrate dilution:

2 Phosphatase (*p*-nitrophenylphosphate) substrate tablets (A3469, Sigma, UK) in 10ml DEA buffer

A1.5 Optimisation

A brief outline to optimisation experiments will be given, with results and inferences.

A1.5.1 Proteoglycan/GAG extraction method analysis

To determine the most suitable extraction method for individual corneal ELISAs, the established method of Hassell *et al.* (1983) was used as a template. This preliminary study used only day 18 corneas, as these are likely to contain the most GAG and yield a positive result.

Methods

The wet weight of each D18 cornea was taken before transfer into 1ml Guanidine (Gdn) extraction buffer, agitated at 4°C to loosen PGs. After 24hrs corneas were transferred into fresh buffer and a 24hr, 4°C incubation repeated. The primary tube containing PGs and extraction buffer was frozen at -35°C. Each cornea was removed and placed into 1ml papain digest to break down remaining proteoglycans, and the secondary Gdn extraction tube frozen. Papain digest tubes were incubated at 60°C for 12h, and then denatured at 100°C for 15 mins.

Respective sample pairs of Gdn extraction buffer (primary and secondary extraction) were combined in cellulose membrane visking tubing and dialysed against 3 changes of milliQ™ water over 24hrs. Samples were spun down and reconstituted in 400µl milliQ for quantitative assay. A select number of corneas were also placed directly into papain digest, without prior Gdn extraction, to ascertain the efficiency of this mulit-stage method.

Dimethylmethylene Blue, DMMB binds negatively charged sulphate and carboxyl groups on GAG chains forming a complex which causes a metachromatic shift in the absorbance maxima (Farndale *et al.*, 1986), and can therefore be used to detect sulphated GAGs. 4M Guanidine extracts PGs with GAG still attached into solution. Papain digest of the cornea extracts GAG that has not moved out into solution to quantify total GAG. Assay protocol (Chandrasekhar *et al* 1987, Farndek *et al* 1987) was followed as shown below.

DMMB dye was made by dissolving 32mg DMMB in 20ml ethanol, and leaving on a rotator at room temperature overnight. 1.5L milliQ water, 59ml 1M NaOH and 7ml Formic acid were added to a 2L measuring cylinder. The dissolved DMMB was added to the cylinder and made up to the 2L mark with milliQ, and stirred for two hours. MiiliQ water was used as a blank to check DMMB absorbance at 525nm and 592nm, which gave rise to readings of ~0.3 and 1.3 respectively at the correct solution saturation.

Five standard curve solutions were prepared using Chondroitinase Sulphate C (Sodium salt from shark cartilage, SIGMA c-4384), made up with milliQ water – final concentrations 0μg/ml, 10μg/ml, 20μg/ml, 30μg/ml, 40μg/ml. 40μl of each GAG standard solution was pipetted in triplicate into 96 well flat bottomed EIA microtitre plate (Elkay, UK), and 40μl PG extract added in duplicate into remaining wells after visual assessment of neat extract concentration (linear range of DMMB assay short, therefore sample concentration must be in the linear portion of the curve). A labsystems multiscan MS plate reader was prepared at 525nm, then 200μl DMMB reagent added to all wells and the plate read immediately. Total GAG can be calculated using dilution factor and total sample volume.

Results

KS proteoglycans from day 18 corneas were extracted and quantified by double guanidine extraction (Hassell *et al*, 1982) and papain digestion. These results indicate experimental problems with the extraction method – a white suspension was visible after dialysis, thought to be collagen, presumably a limiting factor preventing complete GAG extraction. This loss of GAG means an average extraction of 9.172μg, with standard deviation 4.042μg, compared to a mean total extraction of 21.676μg, standard deviation 1.920μg from immediate papain

digest, implying that effectively only 42.3% of GAG is obtained using the combined Gdn and papain method.

The ratio of GAG extract to corneal wet weight was calculated to ascertain whether the extraction method was consistent. The results in table 1.1 overleaf show that significant error occurs (not statistically tested) during the double extraction. Mean GAG irrespective of method was measured as 13.719µg with standard deviation 7.019µg.

A

Cornea - treatment	Wet weight (mg)	µg/ml GAG extracted	Extracted GAG (µg)	Total extract (µg) (1st extract. + 2nd extract)	Total GAG (µg)	Extract / Wet weight (µg GAG/mg cornea)
30R 1st extraction	4	4.715	1.886	4.972	15.53	388.23
30R 2nd extraction		7.715	3.086			
30R Papain		10.557	10.557	10.557		
30L 1st extraction	3.6	11.915	4.766	5.224	13.39	370.51
30L 2nd extraction		1.145	0.458			
30L Papain		8.1145	8.1145	8.1145		
31R 1st extraction	3.7	9.224	3.6896	6.1066	14.43	390.02
31R 2nd extraction		6.0425	2.417			
31R Papain		8.324	8.324	8.324		
31L 1st extraction	4.4	3.9545	1.5818	3.7908	11.78	267.76
31L 2nd extraction		5.225	2.209			
31L Papain		7.9905	7.9905	7.9905		

B

Cornea - treatment	Wet weight (mg)	µg/ml GAG extracted	Extracted GAG (µg)	Total extract (µg) (1st extract. + 2nd extract)	Total GAG (µg)	Extract / Wet weight (µg GAG/mg cornea)
34R Double extraction	3.3	4.161	3.3288	3.3288	6.5608	198.81
34R Papain		4.04	4.04	3.232		
34L Double extraction	5.1	2.209	1.7672	1.7672	3.3352	65.40
34L Papain		1.96	1.96	1.568		
35R Double extraction	3.2	1.664	1.3312	1.3312	1.9632	61.35
35R Papain		0.79	0.79	0.632		
35L Double extraction	3.6	5.0085	4.0068	4.0068	9.7636	271.21
35L Papain		7.196	7.196	5.7568		
36R Double extraction	5.1	2.916	2.3328	2.3328	7.5592	148.22
36R Papain		6.533	6.533	5.2264		
36L Double extraction	4.6	9.1585	7.3268	7.3268	12.1908	265.02
36L Papain		6.08	6.08	4.864		
37R Double extraction	4.8	2.9015	2.3212	2.3212	6.9404	144.59
37R Papain		5.774	5.774	4.6192		
37L Double extraction	4.4	2.194	1.7552	1.7552	6.66	151.36
37L Papain		6.131	6.131	4.9048		
38R Double extraction	4.4	3.4245	2.7396	2.7396	7.7636	176.45
38R Papain		6.28	6.28	5.024		
38L Double extraction	4.4	5.008	4.0064	4.0064	10.5845	240.56
38L Papain		8.223	8.223	6.5784		

C

Cornea	Wet weight (mg)	µg/ml GAG extracted	Extracted GAG (µg)	Total extract (µg)	Total GAG (µg)	Extract / Wet weight (µg GAG/mg cornea)
28R Papain	3.2	20.78	20.78	20.78	20.78	649.22
28L Papain	3.7	26.02	26.02	26.02	26.02	709.24
29R Papain	4.2	21.48	21.48	21.48	21.48	511.43
29L Papain	4.1	20.32	20.32	20.32	20.32	495.49
32R Papain	3.8	19.73	19.73	19.73	19.73	519.08
32L Papain	5.2	22.23	22.23	22.23	22.23	427.50
33R Papain	4.7	21.42	21.42	21.42	21.42	455.64
33L Papain	3.7	21.45	21.45	21.45	21.45	579.73

Tables A1.1 A, B and C. Individual cornea GAG extraction results (A) double guanidine extraction, first and second extracts not pooled, (B) double guanidine extraction, extracts pooled, (C) direct papain digest. µg/ml GAG differs from extracted GAG in some cases due to variation in method – reconstitution in 800µl milliQ rather than 400µl. Total GAG is the combined value for Gdn and papain extractions. All corneas were taken at day 18 of incubation, confirmed using Hamilton-Hamburger staging.

Inference

Modification of the current method was used to try and improve extraction efficiency to no avail. Immediate papain digest was found to be the most reliable method for GAG extraction and subsequent analysis, although digests are unsuitable for originally planned further investigation such as Western blotting, as proteoglycans are cleaved.

A1.5.2 Storage study: Silicon oil

Silicon oil is a commonly used storage medium for biological specimens. Previous studies of collagen interfibrillar spacing have been performed using freeze-thawed corneas. Although little structural damage occurs (Fullwood and Meek, 1994) a different storage method such as silicon oil (Si), may prove more appropriate. Immersion in Si oil stores the cornea without ice formation within the tissue, and Silicon oil is commonly used in endothelial studies as it does not penetrate. Although little structural damage occurs at -80°C (Fullwood and Meek, 1994), extensive structural damage has been reported in 0°C studies (Yamasaki and Inoue, 2001); this alternative storage method may prove more appropriate for x-ray studies. The aim of this study was to investigate sample degradation over time and obtain corneal x-ray data in a near-physiological state.

Methods

Corneal pairs from developmental days 12-18 inclusive were excised at known time points over a 2 month period and stored at 4°C submerged in 2ml Si oil. 3 pairs were selected for low-angle analysis, as detailed previously in chapters 2 and 4. Alternative corneas were also frozen in dry ice and stored at –80°C until use, as described in more detail in chapter 2. Samples were processed as described in chapter two, corneas were dabbed dry and positioned into the mylar sample holder without orientation, although the epithelial face was aligned closest to the x-ray beam. Low angle diffraction patterns were collected using a computer operated translation stage, camera length of 8.25m, and 1mm x 1mm beam. Exposure time = 2mins.

Results

Table A1.2 below shows Bragg interfibrillar spacing measured from each Silicon oil stored cornea.

A

Developmental day	Minimum Bragg spacing (nm)	Maximum Bragg spacing (nm)	Range (nm)
12	66.90	199.63	132.73
13	59.72	73.01	13.29
14	64.90	182.49	117.59
15	71.56	210.34	138.77
16	62.31	81.70	19.39
17	45.54	65.63	20.08
18	50.43	62.42	12.00

B

Developmental day	Mean Bragg spacing (nm) 6 days storage	Mean Bragg spacing (nm) 2 months storage
12	122.04	184.49
13	63.69	71.914
14	66.014	126.12
15	76.36	72.18
16	73.50	80.31
17	61.98	55.58
18	58.4728	56.43

Tables A1.2 A and B. Silicon oil study results, (A) shows data spread, and (B) storage effects. N = 6 at each timepoint.

Inference

The results obtained from this experiment show that Si oil proves a variable method of storage for structural determination. X-ray diffraction patterns showed polar inconsistency – individual results were either excellent or exceedingly poor. Storage time did not affect the quality of the x-ray data; little degradation occurred over a two-month interval. Diffraction patterns from samples excised one week prior to x-ray analysis were indistinguishable to those taken 8 weeks earlier.

Extreme variation in sample quality was apparent at the time of data collection, a number of corneas were discoloured and structural analysis indicates damage to collagen organisation. In fact, mean Bragg spacing was found to *increase* between developmental days 13-15, as shown in table A1.2. Collagen compaction during embryonic development is a well documented morphological process, not supported by these findings.

Statistical testing showed that Bragg spacing was significantly altered from developmental D12 to every consecutive day of incubation. These results indicate that Si oil is an unsuitable storage method, as diffraction patterns show massive inter- and intra-group variation, illustrated in table A1.2, and are not repeatable.

A1.6 ELISA coating and primary antibody dilutions

ELISA plates must be coated with a suitable antigen to allow antibody binding and competition against the chick KS antigen. It is well known that bovine articular and nasal cartilage digests are suitable competitors as both 5D4 and 1B4 show an affinity. Bovine corneal KSPG extract is a suitable competitor for the BKS-1 antibody, as proven in previous GAG studies (Kerr, thesis, 2005). An absorbance value of around 1 is optimal.

Methods

A more detailed account of ELISA protocol can be found in chapters 2 and 4. For 1B4 and 5D4 EIA microtitration plates (96 well, capacity 0.35ml) were coated (as shown in figure A1.1) with 125ng and 250ng/ml bovine articular cartilage, BAC abc core antigen in 20mM Na_2CO_3 pH 9.6 (to prevent non-specific H-bonding to polystyrene plate and provide antigen competition). For BKS-1, 0.5µg/ml Bovine corneal extract were tested, after advice from Dr. Briedgeen Kerr. Plates were covered with parafilm and incubated at 37°C overnight. Wells were washed twice with 300µl TSA, then blocked with 200µl blocking buffer at 37°C for 1hr to prevent non-specific bonding.

The primary MAb recognises a specific KS epitope on the respective coating antigen, and is used at the lowest dilution at which antigen interaction is apparent. After washing twice with

TSA (300µl/well), a shot gun titre of primary Ab dilution in BSA was added 100µl/well, as also shown in figure A1.1, in this case for 5D4.

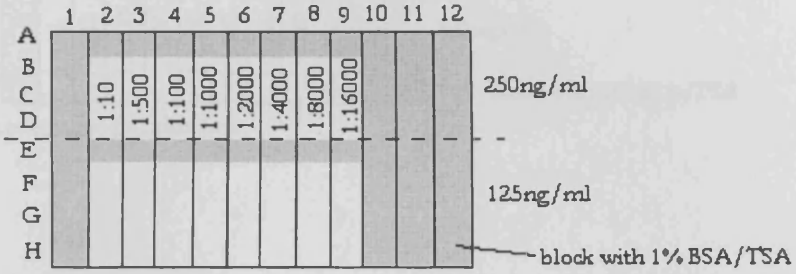

Figure A1.1 Triplicate primary antibody dilutions.

Antibody dilutions (in 1% BSA) tested were as follows:

5D4- 1:500, 1:1000, 1:1500, 1:2000, 1:2500, 1:3000, 1:3500, 1:4000, 1:4500, 1:5000

1B4- 1:25, 1:50, 1:100, 1:200, 1:400, 1:800, 1:1600, 1:3200, 1:6400, 1:12,800, 1:25,600, 1:51,200

BKS1- 1:50, 1:100, 1:250, 1:500, 1:750, 1:1000, 1:1250, 1:1500, 1:1750, 1:2000, 1:2500, 1:3000

Plates were incubated at 37 °C for 1hr then washed six times with TSA 300µl/well. Secondary antimouse alkaline phosphatase conjugated H+L chain (Promega) antibody was added at 1:5000 dilution in 1% BSA, 100µl/well, and incubated at 37°C for 1hr. The plate was washed four times with 300µl/well TSA and phosphatase substrate added (2 tablets in 10ml DEA buffer), 100µl/well to all wells. After 1hr incubation at 37°C the absorbance was read at 405nm.

Fine tuning of antibody dilutions was achieved by repeating this method if (necessary) with less crude dilutions, as shown in figure A1.2 for 5D4.

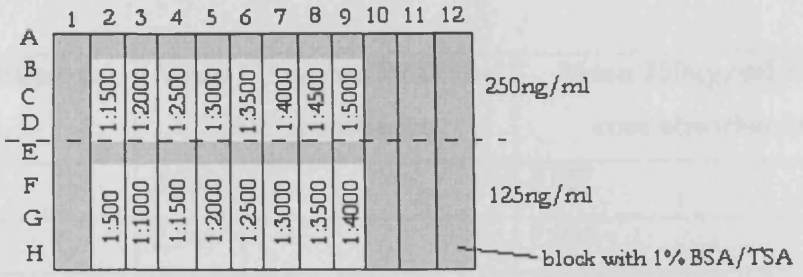

Figure A1.2 Secondary antibody dilutions

Results

Mean absorbance readings for coating dilutions are shown below in tables A1.3 A, B and C.

(A)

5D4 Antibody dilution	Mean 125ng/ml BAC abc core absorbance	Mean 250ng/ml BAC core absorbance
1:10	0.173	3.079
1:100	3.043	3.008
1:500	2.964	2.894
1:1000	2.821	2.832
1:2000	2.251	1.991
1:4000	1.992	0.885
1:8000	1.213	0.343

(B)

1B4 Antibody dilution	Mean 125ng/ml BAC abc core absorbance	Mean 250ng/ml BAC core absorbance
1:10	2.098	3.057
1:50	2.241	2.991
1:100	2.374	3.345
1:200	2.561	3.069
1:400	2.782	2.982
1:600	2.089	3.046
1:1600	2.010	2.716
1:3200	1.963	3.044
1:4000	1.532	2.587
1:8000	0.735	1.831
1:16000	0.411	1.143

(C)

BKS-1 Antibody dilution	Mean 500ng/ml Bovine corneal extract optical absorbance
1:50	3.540
1:100	2.834
1:250	3.215
1:500	3.242
1:750	2.938
1:1000	2.668
1:1250	2.317
1:1500	2.154
1:1750	2.006
1:2000	1.911
1:2500	1.697
1:3000	1.213

Tables A1.3: A, B and C. Results of coating ELISAs, and primary antibody dilutions.

Inference

An optical absorbance of around 1 is optimal for maximum sensitivity on the plate reader, the results of these coating experiments suggest that reactivity is best using BAC abc core antigen at 125ng/ml with both 5D4 and 1B4 antibodies, at a dilution of 1:8000 and 1:4000 respectively. BKS-1 coated well at 500ng/ml Bovine corneal KSPG extract in previous experiments, and a working antibody concentration of 1:3000.

A1.7 Inhibition optimisation for ELISA

Competing antigen is added to the standard ELISA in excess to ensure 100% antibody binding, to generate a standard curve and allow quantification of future "unknown" KSPG extractions. Preliminary ELISA results were used to generate a standard curve which indicated that the sensitivity range of competing antigen to be 60-500ng/ml (linear portion of the curve). Because ELISAs centre around minute quantities of reagent, error is easily incurred. Repetition and refinement of this method was used to produce more reliable data and allow future unknown GAG concentrations to be calculated for chick corneal extracts.

Methods

EIA Microtitration plates (96 well, capacity 0.35ml) were coated with 125ng/ml bovine articular cartilage, BAC abc core antigen (5D4, 1B4) or 500ng/ml Bovine corneal KSPG extract (BKS-1) in 20mM Na_2CO_3, pH 9.6 and incubated at 37°C overnight. Wells were washed twice with 300µl TSA, then blocked with 200µl blocking buffer at 37°C for 1hr to prevent non-specific bonding.

200µl of competing antigen dilutions were prepared as shown in figure A1.3 using serial dilution of 1:3 and 1:2 antigen solutions in BSA. 200µl of half working dilution antibody was added to each tube, and the resulting Ab/competing Ag mixture incubated at 37°C for 30mins.

Blocked plates were washed twice with 300µl/well TSA, then 100µl of the relevant Ab/competing Ag mixture added as shown below, and incubated at 37°C for 1hr.

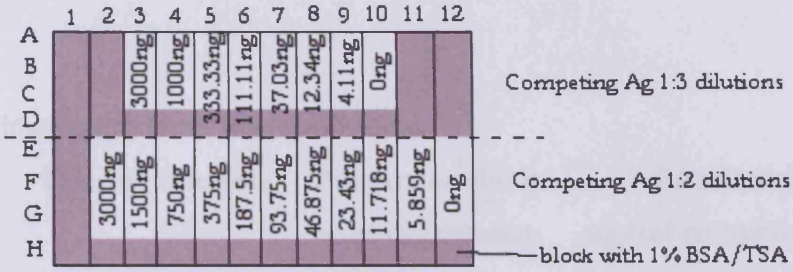

Figure A1.3. Competing antibody concentrations.

Plates were incubated at 37 °C for 1hr then washed six times with TSA 300µl/well. Secondary antimouse alkaline phosphatase conjugated H+L chain (Promega) antibody was added at 1:5000 dilution in 1% BSA, 100µl/well, and incubated at 37°C for 1hr. Plates were washed four times with 300µl/well TSA and phosphatase substrate added (2 tablets in 10ml DEA buffer), 100µl/well to all wells. After 1hr incubation at 37°C the absorbance was read at 405nm.

Results

Mean optical absorbance values were calculated as a percentage of 0ng/ml competing antigen, and plotted onto a semi-logarithmic graph, an example of which is shown in figure 2.12. In all cases, multiple dilutions by a factor of three gave a smoother curve with a greater linear portion.

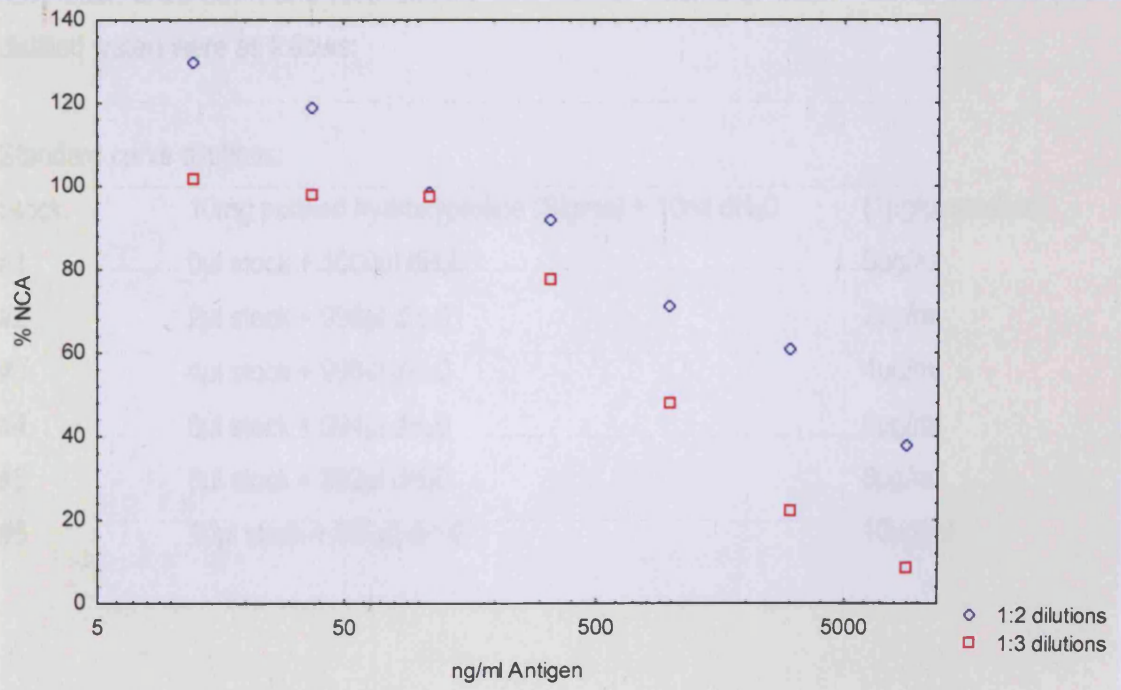

Figure A1.4. Standard curve dilutions.

Inference

Optimal experimental conditions are shown below:

Antibody	Coating dilution	Primary antibody working dilution	Standard Curve ng/ml competing antigen
5D4	125ng/ml BAC abc core	1: 8000	9000, 3000, 1000, 333.33, 111.1, 37.04, 12.34, 0
1B4	125ng/ml BAC abc core	1: 4000	9000, 3000, 1000, 333.33, 111.1, 37.04, 12.34, 4.11, 0
BKS-1	500ng/ml Bovine Corneal KSPG	1: 3000	3000, 1000, 333.3, 111.1, 37.04, 12.34, 4.11, 1.34, 0

Table A1.4. Optimisation results.

A1.8 Hydroxyproline assay

Chick "unkown" samples were found to need dilution after preliminary single-well assays to optimise the sensitivity of the plate reader (also used for ELISAs). Previously, a 300µl aliquot of the papain digest had been hydrolysed overnight and freeze dried. These dried down samples were reconstituted in 300µl distilled water; had samples been too dilute, they would have been dried down and reconstituted in a smaller volume of water. Serial dilutions (with distilled water) were as follows:

Standard curve dilutions:

Stock:	10mg purified hydroxyproline (Sigma) + 10ml dH_20	(1µg/µl solution)
#1	0µl stock + 1000µl dH_20	0µg/ml
#2	2µl stock + 998µl dH_20	2µg/ml
#3	4µl stock + 996µl dH_20	4µg/ml
#4	6µl stock + 994µl dH_20	6µg/ml
#5	8µl stock + 992µl dH_20	8µg/ml
#6	10µl stock + 990µl dH_20	10µg/ml

Chick dilutions:

Day 12	Use neat digest	
Day 13	Use neat digest	
Day 14	Use neat digest	
Day 15		
#1	50μl neat digest + 50μl distilled water	1:2
Day 16		
#1	50μl neat digest + 50μl distilled water	1:2
Day 17		
#1	35μl neat digest + 35μl distilled water	1:2
#2	50μl #1 + 50μl distilled water	1:4
Day 18		
#1	25μl neat digest + 37.5μl distilled water	1:2½
#2	50μl #1 + 50μl distilled water	1:5

A1.9 Standard curve calculations

This project has used many forms of assay to calculate the amount of antibody labelling or collagen constituents. Although individual methods may differ, the manner of retrieving information from a standard curve is the same in each case. The term "standard curve" can be misleading, ELISA standards form a logarithmic curve, however, in hydroxyproline assays, this "curve" is actually a straight line. An example of an ELISA standard curve is shown in figure 2.12, and, for completeness, standard curve generation and accompanying calculations for hydroxyproline assay are shown below.

Mean optical absorbance was measured for each of the "known" standard dilutions, as shown in table A1.6 (for the standard curve). A standard curve was generated using Statistica for each assay plate, and in this case the hydroxyproline content was deduced using Excel '97 (from the standard curve shown in figure A1.5). If the equation of a straight line is y=m*x + c, and we know m (gradient of the standard curve), x (mean optical absorbance of chick sample)

and c (intercept calculated by Statistica), then y (µg/ml hydroxyproline in chick sample) can be calculated.

µg/ml Hydroxyproline standard	Mean Absorbance
0	0.07633'
2	0.12166'
4	0.22866'
6	0.29866'
8	0.35233'
10	0.43366'

Table A1.5. Example of standards from hydroxyproline assay.

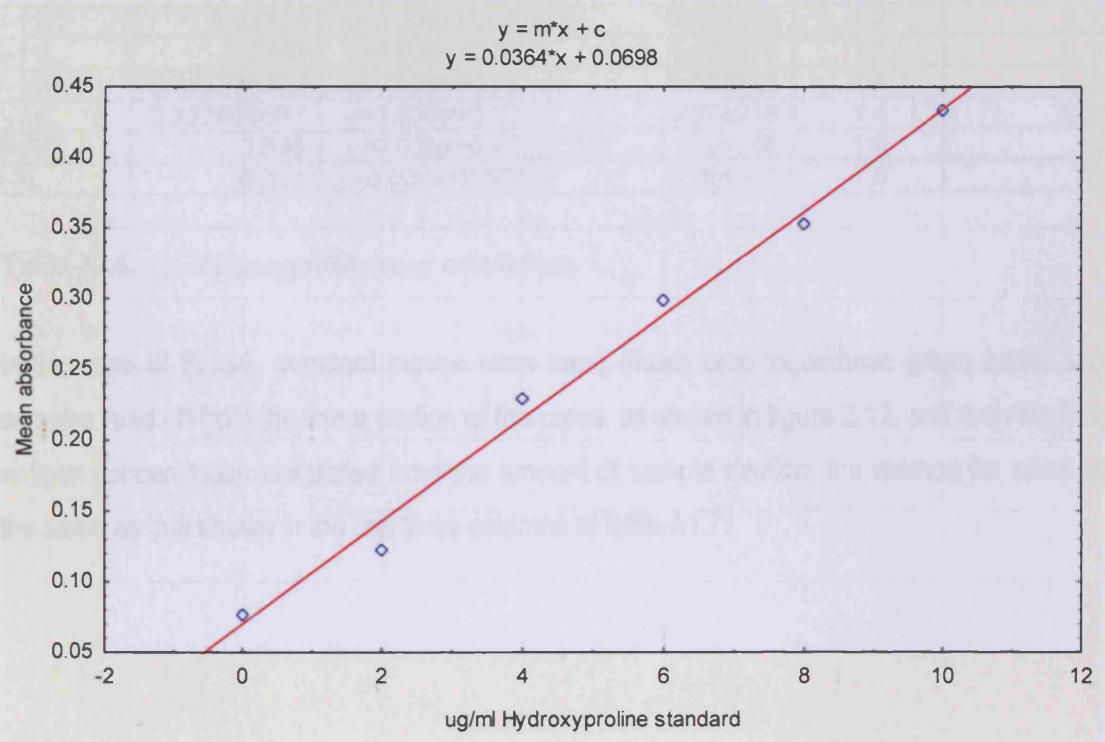

Figure A1.5. Standard curve generated from table A1.5. Statistica automatically generates the equation of the line given by the standard solutions.

So, for example, in the plate shown above (table A1.6), cornea D12-12R (taken at day 12, number 12 sample, right eye) has a mean absorbance of 0.2345.

Equation A1.1 $y = m^*x + c$

from the graph we know that y = 0.0364*x + 0.0698

and x is the mean optical absorbance, 0.2345

therefore,in equation A1.1, y (µg/ml hydroxyproline in chick sample) = (0.036 * 0.2345) + 0.07 = 0.078442

Cornea	Mean abs. (x)	y=mx+c for Standard curve	µg/ml Hydroxyproline assayed	Dilution	µg/ml Hydroxyproline content
D12-12R	0.2345	y=0.036x+0.07	0.078442	neat	0.078442
D12-12L	0.246333333	y=0.036x+0.07	0.078868	neat	0.078868
D13-14R	0.33225	y=0.036x+0.07	0.081961	neat	0.081961
D13-14L	0.3225	y=0.036x+0.07	0.08161	neat	0.08161
D14-17R	0.302	y=0.036x+0.07	0.080872	neat	0.080872
D14-17L	0.3125	y=0.036x+0.07	0.08125	neat	0.08125
D15-11R	0.31	y=0.036x+0.07	0.08116	1:2	0.16232
D15-11L	0.307	y=0.036x+0.07	0.081052	1:2	0.162104
D16-11R	0.42175	y=0.036x+0.07	0.085183	1:2	0.170366
D16-11L	0.3355	y=0.036x+0.07	0.082078	1:2	0.164156
D17-14R	0.292333333	y=0.036x+0.07	0.080524	1:4	0.322096
D17-14L	0.222666667	y=0.036x+0.07	0.078016	1:4	0.312064
D18-13R	0.385	y=0.036x+0.07	0.08386	1:5	0.4193
D18-7L	0.322	y=0.036x+0.075	0.086592	1:5	0.43296

Table A1.6. Hydroxyproline assay calculations.

In the case of ELISA, standard curves were hand drawn onto logarithmic graph paper and samples read off from the linear portion of the curve, as shown in figure 2.12, and then the true antigen concentration calculated from the amount of sample dilution, the method for which is the same as that shown in the last three columns of table A1.7.

APPENDIX TWO

A2.1 Introduction to chapter

In this chapter, a brief overview of statistical testing methods is given, and results tables from individual chapters shown. Results from statistical tests are summarised alongside experimental results.

A2.2 Statistics

Descriptive statistics are used to summarise data sets graphically and numerically. The most common numerical measure for quantitative data is the arithmetic mean (or average) of a variable, defined as the sum of all the observations divided by the number of observations, and gives an idea of the central tendency of the variable.

The simplest measure of variability is the range between the largest value and smallest value, however this basic calculation will only take into account two extreme values – perhaps not the most appropriate way to measure the relevance of results. The spread or variability of data within a sample population can also be measured using the standard deviation, σ. This is defined as the positive square root of variance (a weighted measure of squared deviations from the mean), which measure of the average (or standard) difference (i.e. deviation) of a result from the mean in a set of scores. The SD is measured in the same units as the variable it represents, which makes it a preferable measure.

$$\sigma = \sqrt{\frac{1}{N}\sum_{i=1}^{N}(x_i - \overline{x})^2}$$

Figure A2.1. Standard deviation, where xi is the individual value, x bar is the mean value and N is the number of measurements. *Taken from:* http://en.wikipedia.org/wiki/Standard_deviation

The standard error of the mean (SE) is a good estimate of the standard deviation of many sample means often used to construct confidence intervals. SE is defined in figure A2.2 overleaf.

$$\frac{\sigma}{\sqrt{n}}$$

Figure A2.2. Standard error, σ is the population standard deviation, and n is the sample size. *Taken from:* http://en.wikipedia.org/wiki/Standard_ error_(statistics)

The confidence interval represents the range within which the 'true' mean of the population would be expected to fall, within a defined probability. Confidence intervals of 95% are typically given, representing a range of values from mean -1.96SE to mean +1.96SE, and will not include the true population mean value 5% of times. Confidence intervals are based on the Normal distribution and equal variance assumptions.

A2.2 The P-value

The statistical significance of a result, the P-value or alpha level, is calculated to ascertain the probability of an outcome due to chance. The P-value is used to accept or reject a null hypothesis, which states that there is no difference between the two (or more) mean values of the populations under comparison. In standard scientific practice, values of $p \leq 0.05$ are considered statistically significant and $p \leq 0.001$ statistically highly significant. In effect, this means that if $p = 0.001$, there is a 0.1% probability that the difference between the two mean values considered arose by pure chance if the null-hypothesis is true. Nevertheless, it is important to not to misinterpret the *p*-value; a low *p*-value does not necessarily mean that the null-hypothesis is not true, but simply that the null-hypothesis is implausible. Equally, a *p*-value of >0.05 means that *either* there is no difference between the populations *or* that there were too few subjects to demonstrate that such a difference exists. The *p*-value is two-sided (or nondirectional) as any difference between the two values compared can occur in both directions.

A2.3 The Normal distribution

In order to determine which type of statistical test to use, it is necessary to assess whether or not a variable is Normally distributed. Most parametric methods (based on assumptions about distributions) are based on a Normal distribution, which is symmetric about the mean value and bell-shaped. This empirical pattern of distribution is observed in many biological phenomena, and most tests are robust enough to work well despite only an approximate Normal distribution.

There are two methods implemented for determining the distribution of a sample, discussed below.

A2.4 Testing for Normality

It is possible to visually assess the shape of a variable frequency distribution by plotting a histogram and fitting a Normal 'bell-shaped' probability density function for comparison. However, if the sample population is small then the degree of Normality is difficult to assess. Therefore, it is often more appropriate to assess Normality using calculated Normality tests.

The Kolmogorov-Smirnov test and Shapiro-Wilk's W test are available in SPSS11 statistics package and are commonly used to measure the degree of data Normality. However, in situations where n (population size) is less than 50, the Shapiro-Wilks' W test is more appropriate, as it is suitable for testing both small and large populations.

$$W = \frac{\left(\sum_{i=1}^{n} a_i x_{(i)}\right)^2}{\sum_{i=1}^{n}\left(x_i - \bar{x}\right)^2}$$

Figure A2.3. The Shapiro-Wilk's test, where the $x_{(i)}$ are the ordered sample values ($x_{(1)}$ is the smallest), and the a_i are constants generated from the means, variances and covariances of the order statistics of sample size n from a normal distribution. *Taken from:* http://www.itl.nist.gov/div898/handbook/prc/section2/prc213.htm

From this, the W statistic value is calculated, with significantly different values (≤0.05) as an indicator that the data set does not follow a Normal Gaussian distribution.

A2.5 Data screening

The aim of screening data is to check that the conditions for statistical analysis are fulfilled. There are basic criteria for parametric testing, as shown below:

- Data for two (Independent samples t-test) or more (oneway ANOVA) comparable groups an approximately Normal distribution. If a group of corneas show interfibrillar

spacing or KS content are similar to normal, it is reasonable to assume that the distribution of these variables within the greater population is Normal.

- The data variance in each group under comparison should be similar.

A greater population size is beneficial, as central limit theorem determines that the higher the n value, the more Normal the distribution tends to be. If these criteria are not met, then non-parametric statistical tests (Kruskal-Wallis H test and Mann-Whitney U test) must be used. These distribution-free methods do not require any specific population distribution or equality of variance from the group, and rely on ranks rather than raw values for the statistics.

The following statistical tests were implemented for collagen spacing, ELISA results and hydroxyproline results after suitability was established using SPSS11.

A2.6 The t-test

The t-test is one of the most popular statistical methods used to determine whether the means of two group scores differ to a statistically significant degree. T tests are robust and used for almost all parametric methods. There are two types of t-test; the independent samples test for comparing two sets of data from different subjects, such as collagen fibril spacing data from different time points), and the non-independent samples test, for the comparing two groups of data collected from the same subject, such as corneal wet and dry weights. The independent samples t-test is most appropriate in this study.

A2.7 Oneway analysis of variance (ANOVA)

The one-way ANOVA is used to test for statistical significance of the differences among the means of three or more groups of data and has few constraints; the fixed-effects model assumes that data comes from a Normal population with different means. P values of less than 0.05 imply a statistical difference between some of the groups tested, and further Post Hoc testing can be applied, such as Tukeys Honestly Significant Difference, to determine exactly where these differences lie. Levene's test is also calculated as part of the Independent

samples T-test and oneway ANOVA, which explores the homogeneity of group variances under comparison. A Levene's statistical significance of ≤0.05 indicates that group variances are not equal, and that parametric testing would not be appropriate.

A2.8 Chapter 4:

Collagen Spacing and the Sulphation of Keratan Sulphate

This study examined the collagen spacing of a large cohort of chick corneas at specific timepoints using x-ray diffraction, which were then subject to immunoquantification of highly- and lesser- sulphated KS by ELISA. Finally, type I collagen content was approximated using hydroxyproline as a measure.

A2.8.1 Results

Mean results from each experimental stage are shown below in tables A2.1A, B, C and D. For ease of reading, individual results (from single corneas) are shown over a full page in table A2.2.

A Bragg Spacing

Day	Bragg spacing (nm)	σ	Standard error
12	60.94042222	1.678018625	0.559339542
13	62.55282222	2.924251398	0.974750466
14	63.73886667	3.172953136	0.915952674
15	62.88619	3.87100674	1.224119814
16	60.77587273	5.325677248	1.605752108
17	57.03646	2.743149068	0.867459902
18	52.69617	4.185020121	1.323419563

B Height to width at half height ratio

Day	µg/ml 5D4 KS	σ	Standard error
12	17.00641	6.141661	2.047222
13	33.59179	10.53303	3.511011
14	34.16388	11.04349	3.18798
15	41.34247	7.189188	2.273421
16	38.23291	18.38447	5.543125
17	31.88685	6.556614	2.073383
18	30.96271	10.05919	3.164432

C 5D4 measured KS ELISA

Day	µg/ml 5D4 KS	σ	Standard error
12	4.92	1.620333875	0.540111292
13	6.534545455	0.709833741	0.236611247
14	6.06	0.384315436	0.11094231
15	13.065	1.509938678	0.477484535
16	31.98	4.38656864	1.322600209
17	46.197	8.034283743	2.5406636
18	57.312	7.8951803	2.496675229

D 1B4 measured KS ELISA

Day	µg/ml 1B4 KS	σ	Standard error
12	0.5575	0.353863716	0.117954572
13	0.975	0.353255308	0.117751769
14	1.230333333	0.384315436	0.11094231
15	1.977	0.343991508	0.108779666
16	2.06225	0.419189211	0.126390303
17	3.660833333	0.450457779	0.142447257
18	4.1	1.035299987	0.327390602

E Hydroxyproline assay

Day	µg/ml Hydroxyproline	σ	Standard error
12	0.084741931	0.007291813	0.002104965
13	0.087166194	0.007949794	0.002294908
14	0.085127978	0.0065826	0.001900233
15	0.174175597	0.012915241	0.003728309
16	0.174050111	0.012844588	0.003707913
17	0.3409196	0.029446042	0.00850034
18	0.425913264	0.033661028	0.009717102

Tables A2.1: A, B, C, D and E. Mean results for (A) small angle x-ray scattering to determine Bragg interfibrillar spacing, (B) height to width at half height ratio, (C) highly sulphated KS ELISA assay using 5D4, (D) lesser sulphated KS ELISA assay using 2D3, and (E) collagen content measured by hydroxyproline assay.

In chapter 4, the quantification of sulphated KS was also linked to corneal wet weight. Results of this comparison are shown overleaf in table A.2.2 It is important to note that these values differ from those above because KS is shown as µg per mg cornea, not as µg per ml digest.

Day	n (for analysis)	Mean Bragg spacing (nm)	Bragg spacing σ (nm)	Bragg spacing SE (nm)	Mean 1B4 labelled KS (μg/mg cornea)	1B4 labelled KS σ (μg/mg cornea)	1B4 labelled KS SE (μg/mg cornea)	Mean 5D4 labelled KS (μg/mg cornea)	5D4 labelled KS σ (μg/mg cornea)	5D4 labelled KS SE (μg/mg cornea)
12	9	60.9404222	1.678019	0.55934	0.29139	0.353864	0.117955	1.796355	1.620334	0.540111
13	9	62.5528222	2.924251	0.97475	0.433263	0.353255	0.117752	3.230358	0.709834	0.236611
14	12	63.7388666	3.172953	0.915953	0.434638	0.384315	0.110942	2.020463	0.384315	0.110942
15	10	62.88619	3.871007	1.22412	0.521846	0.343992	0.10878	3.772618	1.509939	0.477485
16	11	60.7758727	5.325677	1.605752	0.731886	0.419189	0.12639	11.64437	4.386569	1.3226
17	10	57.03646	2.743149	0.86746	1.233501	0.450458	0.142447	17.82247	8.034284	2.540664
18	10	52.69617	4.18502	1.32342	1.501436	1.0353	0.327391	24.09929	7.89518	2.496675

Table A2.2. Results for KS quantification in terms of corneal wet weight. Graphs shown in section 4.4.2.

Sample	Wet weight (g)	Bragg Spacing (nm)	µg/ml 5D4 KS	µg/ml 1B4 KS	µg/ml Hydroxyproline
D12-7R	0.001	58.0497	1.02	0.064	0.092205333
D12-7L	0.0016	61.06	1.11	0.23	0.091344
D12-8R	0.00178	62.5784	4.74	1.16	0.08886
D12-8L	0.00156	61.2747	4.44	-	0.088936
D12-9R	0.00218	58.4341	5.34	0.54	0.082308
D12-9L	0.00154	62.3573	8.7	0.46	0.082758
D12-10R	0.00185	64.4055	5.46	-	0.092616
D12-10L	0.00214	61.7032	22.2	-	0.092910667
D12-11R	0.0024	62.5784	1.62	0.196	0.073756667
D12-11L	0.0015	60.643	1.68	0.09	0.0738985
D12-12R	0.0013	61.2747	1.32		0.078442
D12-12L	0.0016	61.4882	1.41	1.72	0.078868
D13-9R	0.00248	56.3445	7.44	2.64	0.096387333
D13-9L	0.00259	65.6026	9.6	1.28	0.096115333
D13-10R	0.00265	65.8474	9.24	1.36	0.089088
D13-10L	0.00281	-	8760	0.78	0.089004
D13-11R	0.0021	64.8791	9.6	0.44	0.084576
D13-11L	0.00226	67.6134	4.5	-	0.085272
D13-12R	0.0016	60.8521	5.52	0.24	0.096373
D13-12L	0.0021	63.0254	6.36	1.92	0.095664667
D13-13R	0.0014	61.92	4.56	0.24	0.0753785
D13-13L	0.0017	61.7032	4.56	-	0.0745645
D13-14R	0.0024	61.7032	5.28	0.11	0.081961
D13-14L	0.0022	62.8011	5.22	0.74	0.08161
D14-12R	0.0032	68.3996	3.42	0.016	0.08622
D14-12L	0.0031	58.6283	3.12	0.484	0.0868399
D14-13R	0.0031	57.6703	5.28	0.92	0.082574
D14-13L	0.0045	66.3425	7.56	0.11	0.081584
D14-14R	0.00301	63.2513	8.4	2.5	0.084264
D14-14L	0.00313	64.7363	11.04	1.04	0.08445
D14-15R	0.00294	63.003	5.76	0.294	0.097999333
D14-15L	0.00273	65.9952	6.96	2.1	0.098158
D14-16R	0.00296	66.6683	7.32	3.4	0.0785975
D14-16L	0.0022	64.9029	5.52	1.64	0.078727
D14-17R	0.0028	62.4676	4.5	1.96	0.080872
D14-17L	0.0028	62.8011	3.84	0.3	0.08125
D15-6R	0.0028	60.5182	13.14	1.14	0.17775
D15-6L	0.0222	57.8214	21.96	4.08	0.18597
D15-7R	0.004	55.9515	4.14	1.71	0.175912
D15-7L	0.0034	66.3425	8.82	0.045	0.172312
D15-8R	0.003	63.708	8.46	-	0.176712
D15-8L	0.0037	62.1377	8.64	0.462	0.177648
D15-9R	0.00309	65.1185	12.96	1.17	0.193392
D15-9L	0.00393	62.8011	12.42	1.44	0.193256
D15-10R	0.00435	67.3811	16.2	3.84	0.1549565
D15-10L	0.00403	63.206	19.62	2.6	0.157774667
D15-11R	0.00316	67.3553	19.26	2.96	0.16232
D15-11L	0.00222	58.05	11.16	2.3	0.162104

Sample	Wet weight (g)	Bragg Spacing (nm)	µg/ml 5D4 KS	µg/ml 1B4 KS	µg/ml Hydroxyproline
D16-6R	0.0025	50.1338	34.92	1.8	0.17892
D16-6L	0.0027	58.2797	58.32	2.25	0.17728
D16-7R	0.0033	57.7836	35.28	0.858	0.174814
D16-7L	0.0034	58.8237	35.64	0.069	0.171268
D16-8R	0.0022	-	24.48	2.49	0.179016
D16-8L	0.0026	62.3573	43.2	1.56	0.17754
D16-9R	0.00262	58.05	27.36	2.9	0.19346
D16-9L	0.00333	69.0419	23.04	1.68	0.194446
D16-10R	0.00193	58.5699	18.36	1.84	0.154124
D16-10L	0.00312	62.5784	22.68	2.2	0.153211333
D16-11R	0.00312	66.9211	25.2	5	0.170366
D16-11L	0.00282	65.9952	35.28	2.1	0.164156
D17-8R	0.0022	56.0226	53.46	3.72	0.35284
D17-8L	0.004	52.8356	51.84	4.05	0.3532
D17-9R	0.0026	55.2854	62.1	4.8	0.329072
D17-9L	0.0014	55.8453	48.6	1.8	0.321008
D17-10R	0.0028	54.2988	48.6	2.46	0.349632
D17-10L	0.0032	60.0242	48.6	5.2	0.3573552
D17-12R	0.00334	60.4974	31.86	2.8	0.390592
D17-12L	0.00238	56.1567	42.66	2	0.38964
D17-13R	0.00422	58.9219	31.05	2.6	0.305954
D17-13L	0.00288	60.4767	43.2	4.9	0.307582
D17-14R	0.00398	62.6006	-	5.2	0.322096
D17-14L	0.00319	59.2981	-	4.4	0.312064
D18-1R	-	-	-	8.4	0.43215
D18-12R	0.0039	51.1214	109.8	4.92	0.43525
D18-6R	0.0027	52.2104	57.6	2.25	0.4126
D18-6L	0.0034	57.1104	55.8	2.25	0.42286
D18-7R	0.0027	53.3145	52.2	4.356	0.43179
D18-7L	0.0022	49.0197	46.8	3.96	0.43296
D18-8R	0.0022	-	55.44	3.204	0.4853925
D18-8L	0.0027	52.3653	41.4	0.2	0.48127
D18-11R	0.00309	55.9515	68.4	4.8	0.380561667
D18-11L	0.00201	55.4766	55.08	1.78	0.371805
D18-13R	0.00268	56.9261	72	7.32	0.4193
D18-13L	0.0016	-	68.4	5.76	0.40502

Table A2.3. Combined individual results showing collagen spacing, highly and lesser sulphated KS and hydroxyproline content.

A2.9 Statistics:

(1) Normality testing before analysis of variance. Shapiro-Wilk test used as $n<50$. $p<0.05$ implies that the W statistic is significant, and the hypothesis that the respective distribution is normal should be rejected.

(2) Descriptive statistics. A significance level less than p=0.01 implies that there is a significant difference between groups.

(3) ANOVA to show where significant differences lie. X = not significant.

A2.9.1 Bragg Spacing

A Normality testing

Developmental day	Shapiro-Wilk test
12	0.106
13	0.283
14	0.455
15	0.477
16	0.640
17	0.258
18	0.564

Inference: Normal distribution

B Descriptives:

	Sum of squares	df	Mean square	F	Significance
Between groups	943.849	6	157.308	11.907	0.000
Within groups	845.496	64	13.211		
Total	1789.346	70			

Inference: Significant difference

C Tukey HSD

	D12	D13	D14	D15	D16	D17	D18
D12	-	x	x	x	x	x	p=0.000
D13	x	-	x	x	x	p=0.025	p=0.001
D14	x	x	-	x	x	p=0.001	p=0.000
D15	x	x	x	-	x	p=0.011	p=0.002
D16	x	x	x	x	-	x	p=0.000
D17	p=0.05	p=0.025	p=0.001	p=0.011	x	-	x
D18	p=0.000	p=0.000	p=0.000	p=0.000	p=0.000	x	-

Tables A2.4A, B and C. Bragg statistics calculations, height to width ratio was unsuitable for statistical analysis as standard deviation is large.

A2.9.2 1B4 labelled KS

A Normality testing

Developmental day	Shapiro-Wilk test
12	0.052
13	0.244
14	0.265
15	0.801
16	0.459
17	0.155
18	0.863

Inference: Normal distribution

B Descriptives:

	Sum of squares	df	Mean square	F	Significance
Between groups	12.485	6	2.081	7.431	0.000
Within groups	17.920	64	.280		
Total	30.405	70			

Inference: Significant difference

C Tukey HSD

	D12	D13	D14	D15	D16	D17	D18
D12	-	x	x	x	x	p=0.005	p=0.000
D13	x	-	x	x	x	p=0.026	p=0.001
D14	x	x	-	x	x	p=0.013	p=0.000
D15	x	x	x	-	x	x	p=0.002
D16	x	x	x	x	-	x	p=0.023
D17	p=0.05	p=0.026	p=0.013	x	x	-	x
D18	p=0.000	p=0.001	p=0.000	p=0.002	p=0.023	x	-

Tables A2.5A, B and C. 1B4 lesser sulphated KS ELISA statistics calculations.

A2.9.3 5D4 labelled KS

A Normality testing

Developmental day	Shapiro-Wilk test
12	0.025
13	0.283
14	0.620
15	0.873
16	0.285
17	0.475
18	0.035

Inference: Normal distribution

B Descriptives:

	Sum of squares	df	Mean square	F	Significance
Between groups	12.485	6	2.081	7.431	0.000
Within groups	17.920	64	.280		
Total	30.405	70			

Inference: Significant difference

C Tukey HSD

	D12	D13	D14	D15	D16	D17	D18
D12	-	x	x	x	x	p=0.005	p=0.000
D13	x	-	x	x	x	p=0.026	p=0.001
D14	x	x	-	x	x	p=0.013	p=0.000
D15	x	x	x	-	x	x	p=0.002
D16	x	x	x	x	-	x	p=0.023
D17	p=0.05	p=0.026	p=0.013	x	x	-	x
D18	p=0.000	p=0.001	p=0.000	p=0.002	p=0.023	x	-

Tables A2.6A, B and C. 5D4 highly sulphated KS ELISA statistics calculations.

A2.9.4 Hydroxyproline content

A Normality testing

Developmental day	Shapiro-Wilk test
12	0.349
13	0.104
14	0.120
15	0.427
16	0.554
17	0.355
18	0.466

Inference: Normal distribution

B Descriptives:

	Sum of squares	df	Mean square	F	Significance
Between groups	12.485	6	2.081	7.431	0.000
Within groups	17.920	64	.280		
Total	30.405	70			

Inference: Significant difference

C Tukey HSD

	D12	D13	D14	D15	D16	D17	D18
D12	-	x	x	x	x	p=0.005	p=0.000
D13	x	-	x	x	x	p=0.026	p=0.001
D14	x	x	-	x	x	p=0.013	p=0.000
D15	x	x	x	-	x	x	p=0.002
D16	x	x	x	x	-	x	p=0.023
D17	p=0.05	p=0.026	p=0.013	x	x	-	x
D18	p=0.000	p=0.001	p=0.000	p=0.002	p=0.023	x	-

Tables A2.7A, B and C. Hydroxyproline assay statistics calculations.

A2.10 Chapter 5:

Collagen Spacing and the Influence of Keratan Sulphate

This study was a follow up to chapter 4, in which the relationship between KS (regardless of sulphation) and collagen spacing was investigated. Again, a large number of corneas were analysed for both collagen interfibrillar spacing and KS content. Results are shown in tables A2.8 (means) and A2.9 (individually).

A2.10.1 Results

A Bragg Spacing

Day	Bragg spacing (nm)	σ	Standard error
12	64.8515	1.815913231	0.54752
13	64.0682	2.95530	0.85312
14	65.97756667	1.50970	0.43581
15	64.4317	4.13429	1.19347
16	64.4580	2.83076	.81718
17	58.7134	5.15941	1.55562
18	57.4447	3.63770	0.49404

B Height to width at half height ratio

Day	Ratio	σ	Standard error
12	23.5585534	11.38233	3.431903
13	12.1955992	7.133519	2.05927
14	14.7708395	12.36789	3.570302
15	23.8019165	22.40826	6.468709
16	14.9560047	7.167694	2.069135
17	15.5154428	16.94334	5.108609
18	19.6490762	18.41505	5.315968

C BKS-1 measured KS ELISA

Day	µg/ml BKS-1 KS	σ	Standard error
12	1.270	0.4733709	0.1932529
15	1.196	0.4989055	0.2036773
18	1.311	0.8844754	0.3610856

D Wet weight for ELISA corneas

Day	g	σ	Standard error
12	0.003917	0.000578	0.000236
15	0.005433	0.000882	0.00036
18	0.009583	0.001772	0.000724

E Bragg spacing for ELISA corneas

Day	Mean Bragg spacing (nm)	σ	Standard error
12	64.8124	1.617351	0.660281
15	64.16057	3.583273	1.462865
18	56.24005	1.500864	0.612725

F Height to width at half height ratio for ELISA corneas

Day	Mean Ratio	σ	Standard error
12	28.98605	6.42444	1.07074
15	18.86498	14.16015	2.360025
18	25.24226	22.34825	3.724709

Tables A2.8: A, B, C, D, E and F. Mean results for (A) small angle x-ray scattering to determine Bragg interfibrillar spacing, (B) local order ratio, (C) KS ELISA assay using BKS-1, (D) wet weight for ELISA corneas and (E) local order for ELISA corneas.

(A)

Sample number	Bragg Spacing (nm)	Peak height	Peak width at half height (R)	Height to width ratio (R)	Peak width at half height (scatang)	Height to width ratio (scatang)
D12-4L	66.54262453	66335	25	2653.4	0.0668	993038.9222
D12-3L	66.36744659	695	23.6	29.44915254	0.0627	11084.52951
D12-1R	61.91966537	719	20	35.95	0.0776	9265.463918
D12-2R	62.18148202	982	25.4	38.66141732	0.094	10446.80851
D12-1L	63.66199274	487	20	24.35	0.0626	7779.552716
D12-3R	65.21472352	720	26.6	27.06766917	0.0692	10404.62428
D12-4R	65.18098656	911	27.7	32.88808664	0.0743	12261.10363
D12-5L	66.09402279	474	24	19.75	0.0632	7500
D12-2L	63.11553813	312	26.2	11.90839695	0.0686	4548.104956
D12-6R	66.81978035	240	27.7	8.664259928	0.0709	3385.049365
D12-6L	66.2677584	180	26.1	6.896551724	0.0679	2650.95729
D13-5R	60.78920016	187	30.4	6.151315789	0.0793	2358.13367
D13-7R	62.84581378	259	25.5	10.15686275	0.0674	3842.72997
D13-4L	58.492228	545	29.4	18.53741497	0.0763	7142.857143
D13-7L	67.87347647	754	23.7	31.81434599	0.062	12161.29032
D13-1R	63.2512704	293	24.4	12.00819672	0.0668	4386.227545
D13-3L	63.38758773	235	25.2	9.325396825	0.065	3615.384615
D13-5L	65.04645856	368	26.8	13.73134328	0.0757	4861.294584
D13-6R	63.52449391	353	27.7	12.74368231	0.0728	4848.901099
D13-2L	62.84581378	213	25	8.52	0.0662	3217.522659
D13-3R	67.43154071	265	25.2	10.51587302	0.0637	4160.125589
D13-4R	68.85331163	159	25	6.36	0.0667	2383.808096
D13-1L	64.47763316	188	29	6.482758621	0.0745	2523.489933
D14-6L	65.35964506	293	28.6	10.24475524	0.09	3255.555556
D14-3L	63.93878389	155	25	6.2	0.065	2384.615385
D14-4L	63.52449391	236	26.7	8.838951311	0.0704	3352.272727
D14-6R	68.66577352	182	25	7.28	0.0638	2852.664577
D14-2L	66.06927775	425	26.5	16.03773585	0.691	615.0506512
D14-5R	64.64140755	618	25.1	24.62151394	0.0668	9251.497006
D14-1R	65.79830024	219	25.8	8.488372093	0.068	3220.588235

Sample number	Bragg Spacing (nm)	Peak height	Peak width at half height (R)	Height to width ratio (R)	Peak width at half height (scatang)	Height to width ratio (scatang)
D14-2R	67.12478086	1331	26.8	49.6641791	0.0745	17865.77181
D14-5L	66.99735756	275	23.2	11.85344828	0.0608	4523.026316
D14-1L	65.50521213	458	23.7	19.32489451	0.2301	1990.43894
D14-4R	66.51754251	164	26.1	6.283524904	0.0685	2394.160584
D14-3R	67.58752932	212	25.2	8.412698413	0.0667	3178.410795
D15-6L	70.30718571	176	26.5	6.641509434	0.0698	2521.489971
D15-3L	63.38758773	127	26.6	4.77443609	0.0698	1819.484241
D15-2L	61.76795473	174	28.4	6.126760563	0.0757	2298.546896
D15-4L	69.80105873	1103	28.8	38.29861111	0.0757	14570.67371
D15-3R	59.43787479	764	31.1	24.5659164	0.0823	9283.110571
D15-5R	64.49965014	239	26.6	8.984962406	0.071	3366.197183
D15-1R	66.06927775	901	29.6	30.43918919	0.0787	11448.53875
D15-6R	61.81122473	280	28.8	9.722222222	0.0769	3641.092328
D15-1L	70.56019031	1664	24	69.33333333	0.0701	23737.51783
D15-2R	64.05482518	1849	29.6	62.46621622	0.0713	25932.67882
D15-4R	63.6620389	265	35	7.571428571	0.078	3397.435897
D15-5L	57.82148181	526	31.5	16.6984127	0.093	5655.913978
D16-6R	59.8004374	282	24.4	11.55737705	0.0841	3353.151011
D16-1L	64.78384072	300	27.2	11.02941176	0.0644	4658.385093
D16-3L	68.21457648	203	25.3	8.023715415	0.0655	3099.236641
D16-2L	63.25131472	407	26.3	15.47528517	0.0704	5781.25
D16-4L	63.52453945	248	26.7	9.288389513	0.0716	3463.687151
D16-5R	66.21804657	321	28	11.46428571	0.0757	4240.422721
D16-3R	60.9782656	924	31.2	29.61538462	0.0828	11159.42029
D16-2R	64.07813205	340	26.6	12.78195489	0.0704	4829.545455
D16-4R	63.11558184	781	30	26.03333333	0.0804	9713.930348
D16-6L	63.25131472	393	27.5	14.29090909	0.0716	5488.826816
D17-3R	56.07597785	341	27.1	12.58302583	0.0775	4400
D17-5R	63.11558184	184	25.3	7.272727273	0.0674	2729.970326
D17-5L	66.66834059	286	28.3	10.10600707	0.0739	3870.094723

(A)

Sample number	Bragg Spacing (nm)	Peak height	Peak width at half height (R)	Height to width ratio (R)	Peak width at half height (scatang)	Height to width ratio (scatang)
D17-6L	56.1830956	373	30.1	12.39202658	0.0793	4703.656999
D17-2R	47.92807552	320	34.4	9.302325581	0.0276	11594.2029
D17-4L	57.37033745	378	25.3	14.94071146	0.0668	5658.682635
D17-2L	58.76494404	1832	29	63.17241379	0.0767	23885.26728
D17-6R	57.70803183	132	21.6	6.111111111	0.0578	2283.737024
D17-3L	56.48884419	262	25.9	10.11583012	0.0692	3786.127168
D17-4R	65.33546367	272	29.7	9.158249158	0.0835	3257.48503
D18-3L	58.27977775	317	25.8	12.28682171	0.068	4661.764706
D18-2R	55.84529837	238	15.6	15.25641026	0.0632	3765.822785
D18-1R	67.58755441	275	30.8	8.928571429	0.0811	3390.875462
D18-4R	55.75706141	1074	27.2	39.48529412	0.0721	14895.97781
D18-6L	54.61810243	1484	23	64.52173913	0.0619	23974.15186
D18-1L	60.76830073	168	34.9	4.813753582	0.0924	1818.181818
D18-3R	57.82148181	193	27.2	7.095588235	0.068	2838.235294
D18-5L	54.92408707	333	26	12.80769231	0.0685	4861.313869
D18-5R	56.38055852	229	14.8	15.47297297	0.0602	3803.986711
D18-4L	56.59754661	231	14.6	15.82191781	0.059	3915.254237

(Table A2.9A, description overleaf)

(B)

Sample	Bragg spacing (nm)	BKS-1 labelled KS (ng/ml)	Wet Wt (g)	Height To Width at half height ratio
D12-6L	66.26776	2200	0.0035	26.1
D12-3L	66.36745	940	0.0036	29.44915
D12-2R	62.18148	1080	0.0034	38.66142
D12-1L	63.66199	1130	0.0038	27.06767
D12-3R	65.21472	1300	0.0043	32.88809
D12-4R	65.18099	970	0.0049	19.75
D15-3L	63.38759	2180	0.0059	4.774436
D15-2L	61.76795	820	0.0049	6.126761
D15-4L	69.80106	1030	0.0046	38.29861
D15-3R	59.43787	1210	0.0052	24.56592
D15-5R	64.49965	1020	0.005	8.984962
D15-1R	66.06928	920	0.007	30.43919
D18-3L	58.27978	820	0.0104	12.28682
D18-2R	55.8453	3100	0.0111	15.25641
D18-6L	54.6181	810	0.0082	39.48529
D18-2L	55.95154	970	0.0119	64.52174
D18-3R	57.82148	1100	0.0077	7.095588
D18-5L	54.92409	1070	0.0082	12.80769

Tables A2.9A and B. Individual results for (A) Bragg spacing of 81 corneas, (B) BKS-1 ELISA corneas.

A2.11 Statistics

Statistical analysis follows the same pattern as 2.9:

(1) Normality testing before analysis of variance. Shapiro-Wilk test used as n<50. $p<0.05$ implies that the *W* statistic is significant, and the hypothesis that the respective distribution is normal should be rejected.

(2) Descriptive statistics. A significance level less than $p=0.05$ implies that there is a significant difference between groups, $p=0.01$ or less implies a highly significant difference.

(3) ANOVA to show where significant differences lie. X = not significant.

A2.11.1 Bragg spacing

(A) Normality testing

Developmental day	Shapiro-Wilk test
12	0.082
13	0.688
14	0.998
15	0.444
16	0.878
17	0.445
18	0.097

Inference: Normal distribution

(B) Descriptives:

	Sum of squares	df	Mean square	F	Significance
Between groups	779.085	6	129.847	11.565	0.000
Within groups	842.037	75	11.227		
Total	1621.121	81			

Inference: Significant difference

(C) Tukey HSD

	D12	D13	D14	D15	D16	D17	D18
D12	-	x	x	x	x	p=0.001	p=0.000
D13	x	-	x	x	x	p=0.005	p=0.000
D14	x	x	-	x	x	p=0.000	p=0.000
D15	x	x	x	-	x	p=0.002	p=0.000
D16	x	x	x	x	-	p=0.002	p=0.000
D17	p=0.001	p=0.005	p=0.000	p=0.002	p=0.002	-	x
D18	p=0.000	p=0.000	p=0.000	p=0.000	p=0.000	x	-

Tables A2.10A, B and C. Statistical tables for Bragg spacing

A2.11.2 Height to Width ratio

Developmental day	Mean peak height to width ratio	σ	Standard error
12	23.5585534	11.38233	3.431903
15	23.8019165	22.40826	6.468709
18	19.6490762	18.41505	5.315968

Tables A2.11. Mean peak height to width at half height ratio.

Because standard deviations are so large, it would be difficult to attribute any value to statistical significance.

A2.11.3 BKS-1 labelled KS

(A) Normality testing ng/ml

Developmental day	Shapiro-Wilk test
12	0.735
15	0.735
18	0.622

Inference: Normal distribution

(B) Descriptives ng/ml:

	Sum of squares	df	Mean square	F	Significance
Between groups	40677.8	2	20338.889	0.49	0.953
Within groups	6276417	15	418427.778		
Total	6317094	17			

Inference: No significant difference

(C) Normality testing µg/mg cornea

Developmental day	Shapiro-Wilk test
12	0.759
15	0.898
18	0.785

Inference: Normal distribution

(D) Descriptives µg/mg cornea:

	Sum of squares	df	Mean square	F	Significance
Between groups	0.000	2	0.000	5.120	0.020
Within groups	0.000	15	0.000		
Total	0.000	17			

Inference: Significant difference

(E) Tukey HSD µg/mg cornea:

	D12	**D15**	**D18**
D12	-	x	p=0.016
D15	x	-	x
D18	p=0.016	x	-

Tables A2.12A, B, C, D and E. Statistical tables for BKS-1 KS ELISA.

Abbruzzese, C., Kuhn, U., Molina, F. *et al.* 2004. Novel mutations in the CHST6 gene causing macular corneal dystrophy. *Clinical Genetics* 65, 120-125.

Akama, T.O., Nishida, K., Nakayama, J. *et al.* 2000. Macular corneal dystrophy type I and type II are caused by distinct mutations in a new sulphotransferase gene. *Nature Genetics* 26, 237-241.

Akama, T.O., Nakayama, J., Nishida, K. *et al.* 2001. Human corneal GlcNAc 6-O-sulfotransferase and mouse intestinal GlcNac 6-O-sulfotransferase both produce keratan sulfate. *Journal of Biological Chemistry* 276, 16271-16278.

Akama, T.O., Misra, A.K., Hindsgaul, O. *et al.* 2002. Enzymatic synthesis in vitro of the disulfated disaccharide unit of corneal keratan sulfate. *Journal of Biological Chemistry* 277, 42505-42513.

Akhtar, S., Kerr, B., et al. 2005 Localisation of a novel keratan sulphate stub neoepitope monoclonal antibody BKS-1 in normal human cornea, sclera and limbus. *Acta Ophthalmologica*-e249

Akimoto, Y., Yamakawa, N., Furukawa, K. *et al.* 2002. Changes in distribution of the long form of type XII collagen during chicken corneal development. *Journal of Histochemistry and Cytochemistry* 50, 851-862.

Aldave, A.J., Yellore, V.S., Thonar, E.J. *et al.* 2004. Novel mutations in the carbohydrate sulfotransferase gene (CHST6) in American patients with macular corneal dystrophy. *American Journal of Ophthalmology* 137, 465-473.

Anseth, A. 1961a. Glycosaminoglycans in corneal regeneration. *Experimental Eye Research 1*, 122-127.

Anseth, A. 1961b. Glycosaminoglycans in the developing corneal stroma. *Experimental Eye Research 1*, 116-121.

Anseth, A. 1969. Studies on corneal polysaccharides. V. Changes in corneal glycosaminoglycans in transient stromal edema. *Experimental Eye Research 8*, 297-301.

Axelsson, I. and Heinegard, D., 1978. Characterization of the keratan sulphate proteoglycans from bovine corneal stroma. *Biochemical Journal* 169, 517-530.

Bella, J., Eaton, M., Brodsky, B. *et al.*, 1994. Crystal and molecular structure of a collagen-like peptide at 1.9 A resolution. *Science* 226, 75-81.

Benedek, G.B. 1971. Theory of transparency of the eye. *Applied Optics* 10, 459-473.

Bengtsson, E., Neame, P.J.*et al.* 1995 The primary structure of a basic leucine-rich repeat protein, PRELP, found in connective tissues. *Journal of Biological Chemistry* 270, 25639-44.

Bettelheim, F.A. and Plessy, B. 1975. The hydration of proteoglycans of bovine cornea. *Biochimica et Biophysica Acta*, 381; 203-214.

Birk, D.E. and Lande, M.A. 1981. Corneal and scleral collagen fiber formation in vitro. *Biochimica et Biophysica Acta* 670, 362-369.

Birk D.E. and Trelstad R.L.1984. Extracellular compartments in matrix morphogenesis: collagen fibril, bundle, and lamella formation by corneal fibrilblasts. *Journal of Cell Biology* 99, 2024-33.

Birk, D.E., Fitch, J.M. and Linsenmayer, T.F. 1986 Organisation of collagen types I and V in the embryonic chicken cornea. *Invest. Ophthalmol. Vis. Sci.* 27, 1470–1477

Birk, D. E., Fitch, J. M., Babiarz, J.P. *et al.* 1988. Collagen type I and type V are present in the same fibril in the avian corneal stroma. *Journal of Cell Biology 106*, 999-1008.

Birk, D. E., Fitch, J. M., Babiarz, J. P. *et al.* 1990. Collagen fibrillogenesis in vitro: interaction of types I and V collagen regulates fibril diameter. *Journal of Cell Science* 95, 649-657.

Birk, D.E. 2001 Type V collagen: heterotypic type I/V collagen interactions in the regulation of fibril assembly. *Micron* 32, 223-37

Birk, D.E., Zhang, D. and Simpson, H.E. 2006 Dysfunctional Regulation of Fibril Assembly and Stromal Organization in the Compound Decorin/Biglycan–Deficient Cornea *Invest. Ophthalmol. Vis. Sci.* 47: E-Abstract 2999.

Blochberger, T.C., Vergnes, J.P., Hempel, J. *et al.* 1992. cDNA to chick lumican (corneal keratan sulfate proteoglycan) reveals homology to the small interstitial proteoglycan gene family and expression in muscle and intestine. *Journal of Biological Chemistry* 267, 347-352.

Block, J.A., Inerot, S.E. and Kimura, J.H. 1992 Heterogeneity of keratan sulfate substituted on human chondrocytic large proteoglycans. *Journal of Biological Chemistry* 267, 7245-7252

Boot-Handford, R. P., Tuckwell, D. S., Plumb, D. A. *et al.* 2003. A novel and highly conserved collagen (pro(alpha)1(XXVII)) with a unique expression pattern and unusual molecular characteristics establishes a new clade within the vertebrate fibrillar collagen family. *Journal of Biological Chemistry* 278, 31067-31077.

Bonaldo, P., Mucignat, M.T., Colombatti, A. 1990. Efficient expression of chicken alpha 1 (VI) collagen chain in transiently transfected mammalian cells. *Matrix* 10, 139-147.

Borcherding, M.S., Blacik, L.J., Sittig, R.A. *et al.* 1975. Proteoglycans and collagen fibre organization in human corneoscleral tissue. *Experimental Eye Research* 21, 59-70.

Bozzola, J.J. and Russell, L.D. ed./eds. 1992. Electron microscopy: principles and techniques for biologists. Boston: Jones and Bartlett Publishers.

Branden, C., and Tooze, J. 1998 *Introduction to Protein Structure.* Garland Publishing Inc., NY.

Bruns R.R. 1984. Beaded filaments and long-spacing fibrils. Relation to type VI collagen. *Journal of Ultrastruct.Res.* 89,136-45.

Brown *et al.* 1999 *Exp. Eye Res.* 11, 7111-19.

Brown,G.M., Huckerby,T.N., Abram,B.L. and Nieduszynski,I.A. 1996 Characterization of a non-reducing terminal fragment from bovine articular cartilage keratan sulphates containing α(2–3)-linked sialic acid and α(1–3)-linked fucose. A sulphated variant of the VIM-2 epitope. *Biochemical Journal*, 319, 137–141.

Buttice, G., Kaytes, P., D'Armiento, J., Vogeli, G., Kurkinen, M. 1990 Evolution of collagen IV genes from a 54-base pair exon: a role for introns in gene evolution. *Journal of Molecular Evolution* 30, 479–488

Burgeson, R.E., Lunstrum, G.P., *et al.* 1990 The structure and function of type VII collagen. *Annals of the N.Y. of Sciences* 580, 32-43.

Cai, D., Shen, Y., De Bellard, M., Tang, S. and Filbin, M.T., 1999. Prior exposure to neurotrophins blocks inhibition of axonal regeneration by MAG and myelin via a cAMP-dependent mechanism. *Neuron* 22, 89–101

Cai, C.X., Fitch, J.M., *et al.* 1994. Cellular invasion and collagen type IX in the primary corneal stroma *in vitro. Developmental dynamics* 201, 206-15

Cai, C.X., Gibney, E., Gordon, M.K., Marchant, J.K., Birk, D.E., Linsenmayer, T.F. 1996 Characterization and developmental regulation of avian corneal ß-1, 4-galactosyltransferase mRNA *Exp Eye Res* 63,193-200

Canty, E.G. and Kadler, K.E. 2005 Procollagen trafficking, processing and fibrillogenesis *Journal of Cell Science* 118, 1341-1353.

Canty, E.G., Lu, Y., Meadows, R.S., Shaw, M.K., Holmes, D.F. and Kadler, K.E. 2004 Coalignment of plasma membrane channels and protrusions (fibripositors) specifies the parallelism of tendon *The Journal of Cell Biology* 165, 553-563.

Carlemalm, E., Garavito, R.M. and Villiger, W., 1982 Resin development for electron microscopy and an analysis of embedding at low temperature. , *Journal of Microscopy* 126, 123-143

Carlson, E.C., Liu, C-Y., Chikama, T.I. *et al.* 2005. Keratocan, a cornea-specific keratan sulfate proteoglycan, is regulated by lumican. *Journal of Biological Chemistry* 280, 25541-25547.

Carlson, E.C., Mamiya, K., Liu, C-Y. *et al.* 2003. Role of Cys41 in the N-terminal domain of lumican in ex vivo collagen fibrillogenesis by cultured corneal stromal cells. *Biochemical Journal 369*, 461-468.

Caspersson, T., and Engstrom, A., 1949 Corneal. Transparency *Nord. Med.* 30, 1279.

Castoro, J.A., Bettelheim, A.A., Bettelheim, F.A. 1988. Water gradients across bovine cornea. *Investigative Ophthalmology and Visual Science* 29, 963-968.

Caterson B, Baker JR, Christner JE, Lee Y, Lentz M. 1985 Monoclonal antibodies as probes for determining the microheterogeneity of the link proteins of cartilage proteoglycan. *Journal of Biological Chemistry* 260,11348-56.

Caterson B, Brooks K, Sattsangi S, Ratcliffe A, Hardingham T, Muir H (1989) Factors affecting the determination of keratan sulfate using monoclonal antibodies in immunoassay procedures. In Grieling H, Scott JE, eds. Keratan Sulfate. London, Biochemical Society TJ Press, 199-204

Chakravarti, S. 2001. The cornea through the eyes of knockout mice. *Experimental Eye Research* 73, 411-419.

Chakravarti, S., Magnuson, T., Lass, J.H. *et al.* 1998. Lumican regulates collagen fibril assembly: skin fragility and corneal opacity in the absence of lumican. *Journal of Cell Biology* 141, 1277-1286.

Chakravarti, S., Petroll, W.M., Hassell, J.R. *et al.* 2000. Corneal opacity in lumican-null mice: defects in collagen fibril structure and packing in the posterior stroma. *Investigative Ophthalmology and Visual Science* 41, 3365-3373.

Chatterjee, S. 1997 *The* Rise of Birds: 225 Million Years of Evolution, Baltimore, The Johns Hopkins University Press

Cheah, K. S. E., Lau, E. T., Au, P. K. C., and Tam, P. P. L. 1991 Expression of the mouse α 1(II) collagen gene is not restricted to cartilage during development. *Development* 111, 945-953.

Chiquet, M., Mumenthaler, U., *et al.* 1998 The chick and human collagen alphal(XII) gene promoter-activity of highly conserved regions around the first exon and the first intron. *European Journal of Biochemistry* 257, 362-71.

Choi, H.U. and Meyer, K. 1975 The structure of keratan sulphates from various sources. *Biochemical Journal* 151, 543-53.

Cintron, C., Covington, H.I., Kublin, C.L. 1983. Morphogenesis of rabbit corneal stroma. *Investigative Ophthalmology and Visual Science* 24, 543-546.

Cintron, C., Covington, H.I., Kublin, C.L. 1990. Morphologic analyses of proteoglycans in rabbit corneal scars. *Investigative Ophthalmology and Visual Science* 31, 1789-1798.

Clarke, N.D. and J.A. Bee 1996. Innervation if the chick cornea analysed in vitro. *Invest.Ophtlamol.Vis.Sci.* 37, 1761-1771

Comper, W.D. 1996 Extracellular Matrix, Amsterdam: Harwood Academic.

Connon, C.J., Siegler, V. *et al.* Proteoglycans alterations and collagen reorganisation in the secondary avian cornea during development. *Opthalmic Research* 35, 177-184.

Connon, C.J., Meek, K.M., Kinoshita, S. *et al.* 2004. Spatial and temporal alterations in the collagen fibrillar array during the onset of transparency in the avian cornea. *Experimental Eye Research* 78, 909-1015.

Conrad, G.W. 1970 Collagen and mucopolysaccharide biosynthesis in the developing chick cornea. *Developmental Biology* 21, 292-317

Conrad, A.H. and G.W. Conrad. 2003. The keratocan gene is expressed in both ocular and non-ocular tissues during early chick development. *Matrix Biology* 22, 323-337.

Cornuet, P.K., Blochberger, T.C., Hassell, J.R. 1994. Molecular polymorphism of lumican during corneal development. *Investigative Ophthalmology and Visual Science* 35, 870-877.

Corpuz, L.M., Funderburgh, J.L., Funderburgh, M.L. *et al.* 1996. Molecular cloning and tissue distribution of keratocan. Bovine corneal keratan sulfate proteoglycan 37A. *Journal of Biological Chemistry* 271, 9759-9763.

Coulombre, A.J. and Coulombre, J.L. 1958. Corneal development. I. Corneal transparency. *Journal of Cell Physiology* 51, 1-11.

Coulombre, AJ, Coulombre, JL 1961 The development of the structural and optical properties of the cornea Smelser, GK eds. The Structure of the Eye,405-420 Academic Press New York

Coulombre, A. J. 1965. Organogenesis. New York: Academic Press.

Coulombre, A.J. and Coulombre, J.L. 1975 Mechanisms of ocular development. *International Ophthalmology Clinics* 15, 7-18.

Creighton, Proteins, Structures and Molecular Properties. W.H.Freeman, 1984, p.7

Danielson, K.G., Baribault, H., Holmes, D.F. *et al.* 1997. Targeted disruption of decorin leads to abnormal collagen fibril morphology and skin fragility. *Journal of Cell Biology* 136, 729-743.

Davies, Y., Lewis, D., *et al.* 1999 Proteoglycans on normal and migrating human corneal endothelium. *Experimental Eye Research* 68, 303-11.

Davson, H. 1984. The Eye, Volume IB, 3rd edition, New York, Academic Press.

Davson, H. 1990. Physiology of the Eye, 1st Edition, London, Macmillan.

Darwin, C. 1859 The Origin of Species by Means of Natural Selection, 1st Edition, John Murray, London

Degroote, S., Lo-Guidice, J.M., Strecker, G. *et al.* 1997. Characterization of an N-acetylglucosamine-6-O-sulfotransferase from human respiratory mucosa active on mucin carbohydrate chains. *Journal of Biological Chemistry* 272, 29493-29501.

Doane K.J., Yang G. and Birk D.E.(1992) Corneal cell matrix interactions : type VI collagen promotes adhesion and spreading of corneal fibroblasts. *Experimental Cell Res.* 200, 490-9.

Doane K.J.and Birk D.E.(1994). Differences in integrin expression during avian corneal stromal development. *Invest.Ophthalmol.Vis.Sci* . 35, 2834-42.

Doane K.J.,Ting W-H., McLaughlin J.S., and Birk D.E. (1996).Spatial and Temporal variations in extracellular matrix of periocular and corneal regions during corneal stromal development *Experimental Eye Research.* 62, 271-83.

Dolhnikoff, M., Morin, J., Roughley, P.J. and Ludwig, M.S. 1998 Expression of Lumican in Human Lungs. *Am. J. Respir. Cell Mol. Biol.* 19, 582-587.

Dunlevy, J.R., Beales, M.P., Berryhill, B.L. *et al.* 2000. Expression of the keratan sulfate proteoglycans lumican, keratocan and osteoglycin/mimecan during chick corneal development. *Experimental Eye Research* 70, 349-362.

Dunlevy, J.R., Beales, M.P., Berryhill, B.L., Cornuet, P.K. and Hassell, J.R. 2000 Expression of the Keratocan and Osteoglycin/Mimecan during chick corneal development. *Experimental Eye Research* 70, 349-362.

Dunlevy, J.R., Chakravarti, S., Gyalzen, P. *et al.* 1998. Cloning and chromosomal localization of mouse keratocan, a corneal keratan sulfate proteoglycan. *Mammalian Genome* 9, 316-319.

Elliott, G. F., J. M. Goodfellow, and A. E. Woolgar. 1980. Swelling studies of bovine corneal stroma without bounding membranes. *J. Physiol. (Lond.).* 298, 453-470.

Elliott, G., and Hodson, S. 1998 Cornea, and the swelling of polyelectrolyte gels of biological interest, *Rep. Prog. Physics* 61, 1325-1365.

Ezura, Y., Chakravarti, S., Oldberg, A. *et al.* 2000. Differential expression of lumican and fibromodulin regulate collagen fibrillogenesis in developing mouse tendons. *Journal of Cell Biology* 151, 779-788.

Farrell R.A. 1994. Corneal Transparency. In: Albert, D.M. and Jacobiec, S.A. ed./eds. Principles and Practice of Ophthalmology. Philadelphia: Saunders.

Fisher, L.W., Termine, J.D., *et al.* 1989 Deduced protein sequence of bone small proteoglycan I (biglycan) shows homology with proteoglycan (decorin) and several nonconnective tissue proteins in a variety of species. *Journal of Biological Chemistry* 264, 4571-6.

Fitch, J. M., Mentzer, A., Mayne, R. *et al.* 1988. Acquisition of type IX collagen by the developing avian primary corneal stroma and vitreous. *Developmental Biology* 128, 396-405.

Fitch JM, Gross J, Mayne R, Johnson Wint B, Linsenmayer TF. 1984 Organization of collagen types I and V in the embryonic chicken cornea: monoclonal antibody studies; *Proceedings of the National Academy of Sciences* USA. 81, 2791-2795

Fitch, J.M., Birk, D.E., Linsenmayer, C., and Linsenmayer T.F. 1990. The spatial organization of Descemet's membrane-associated type IV collagen in the avian cornea. *Journal of Cell Biology* 110, 1457-68.

Fitch, J.M., Birk, D.E., Linsemayer, C., and Linsenmayer, T.F. 1991. Stromal assemblies containing types IV and VI and fibronectin in the developing avian cornea. *Developmental Biology* 144, 379-91.

Fitch, J.M., Birk, D.E., Linsemayer, C., and Linsenmayer, T.F 1994 Collagen Fibril Assembly in the Developing Avian Primary Corneal Stroma. *Invest.Ophthalmol.Vis.Sci* 35, 862-869.

Fitch, J.M., Gordon, M.K., *et al.* 1995 Analysis of transcriptional isoforms of collagen types IX, II and I in the developing avian cornea by polymerase chain reaction. *Developmental Dynamics* 202, 42-53.

Fitch, J., Fini, M.E. *et al.* 1998 Collagen type IX and developmentally regulated swelling of the avian corneal primary stroma. *Developmental Dynamics* 212, 27-37.

Fitzgerald J. and Bateman J.F. 2001 A new FACIT of the collagen family: COL21A1. *FEBS Letters* 505, 275-80.

Fleischmajer, R., Fisher, L.W., *et al.* 1991 Decorin interacts with fibrillar collagen of embryonic and adult human skin. *Journal of Structural Biology* 106, 82-90.

Fukuta, M., Inazawa, J., Torii, T. *et al.* 1997. Molecular cloning and characterization of human keratan sulfate Gal-6-sulfotransferase. *Journal of Biological Chemistry* 272, 32321-32328.

Fratzl, P., and Daxer, A. 1993. Structural transformation of collagen fibrils in corneal stroma during drying. An x-ray scattering study. *Biophys. J.* 64, 1210-1214.

Freund, D.E., McCally, R.L., *et al.* 1995 Ultrastructure in anterior and posterior stroma of perfused human and rabbit corneas. Relation to transparency. *Invest.Ophthalmol.Vis.Sci* 36, 1508-23.

Friedman, J.S., Ducharme R. *et al.* 2000 Isolation of a novel iris-specific and leucine-rich repeat protein (oculoglycan) using differential selection. *Invest.Ophthalmol.Vis.Sci* 41, 2059-66.

Fullwood, N.J. and Meek, K.M. 1994. An ultrastructural, time-resolved study of freezing in the corneal stroma. *Journal of Molecular Biology* 236, 749-758.

Fullwood, N.J., Davies, Y., *et al.* 1996 Cell surface associated keratin sulphate on normal and migrating corneal endothelium. *Invest.Ophthalmol.Vis.Sci* 37, 1256-70.

Funderburgh,J.L., Funderburgh,M.L., Mann,M.M. and Conrad,G.W. 1991 Unique glycosylation of three keratan sulfate proteoglycan isoforms. *J. Biol. Chem.*, 266, 14226–14231

Funderburgh,J.L., Funderburgh,M.L., Mann,M.M. and Conrad,G.W. 1991 Physical and biological properties of keratan sulphate proteoglycan. *Biochem. Soc. Trans.*, 19, 871–876.

Funderburgh,J.L., Caterson,B. and Conrad,G.W. 1987 Distribution of proteoglycans antigenically related to corneal keratan sulfate proteoglycan. *Journal of Biological Chemistry*, 262, 11634–11640.

Funderburgh, J.L., Cintron, C., Covington, H.I. *et al.* 1988. Immunoanalysis of keratan sulphate proteoglycan from corneal scars. *Investigative Ophthalmology and Visual Science* 29, 1116-1124.

Funderburgh, J.L., Corpuz, L.M., Roth, M.R. *et al.* 1997. Mimecan, the 25-kDa corneal keratan sulfate proteoglycan, is a product of the gene producing osteoglycin. *Journal of Biological Chemistry* 272, 28089-28095.

Funderburgh, J.L. 2000. Keratan sulfate: structure, biosynthesis, and function. *Glycobiology* 10, 951-958.

Funderburgh, J.L. 2002 Keratan sulfate biosynthesis. *International Union of Biochemistry and Molecular Biology: Life* 54, 187-194

Glasser, A.D., and Howland, H.C. 1996. A history of studies of visual accommodation in birds. *Q. Rev. Biol* 71, 475-509.

Goodfellow, J.M., Elliott, G.F., Woolgar, A.E. 1978. X-ray diffraction studies of the corneal stroma. *Journal of Molecular Biology* 119, 237-252.

Gordon, M.K., Gerecke, D.R., *et al.* 1987 Type XII collagen: distinct extracellular matrix component discovered by cDNA cloning. *Proceedings of the National Academy of Sciences* USA 84, 6040-4.

Gordon, M.K., Fitch, J.M., *et al.* 1997 Type XVII collagen (BP180) in the developing avian cornea. *Investigative Ophthalmology and Visual Science* 38, 153-66.

Gordon, M. K., Gerecke, D. R., Dublet, B. *et al.* 1989. Type XII collagen. A large multidomain molecule with partial homology to type IX collagen. *Journal of Biological Chemistry* 264, 19772-19778.

Gottleib M.D., Fugate-Wentzekm L.A., *et al.* 1987 Different visual deprivations produce different ametropias and different eye shapes. *Investigative Ophthalmology and Visual Science* 288, 1225-35.

Gross, E. and Witkop, B. 1962 Nonenzymatic Cleavage of Peptide Bonds: The Methionine Residues in Bovine Pancreatic Ribonuclease *J. Biol. Chem.* 237, 1856-1860.

Grover, J., Liu, C.Y., Kao, W.W., and Roughley, P.J. 2000 Analysis of the human lumican gene promoter. *J Biol Chem* 275, 40967-73.

Habuchi, O., Hirahara, Y., *et al.* 1996 Enzymatic sulfation of galactose residue of keratin sulphate by chondroitin 6-sulfotransferase. *Glycobiology* 6, 51-57.

Hahn, R.A. and D.E.Birk 1992 . β-D xyloside alters dermatan sulfate proteoglycan synthesis and the organization of the developing avian corneal stroma. *Development.*115, 383-393.

Hamburger, V., 1992 The stage series of the chick embryo. *Developmental Dynamics* 195, 273–275

Hamburger, V. and Hamilton, H. 1951 A series of normal stages in the development of the chick embryo. *Journal of Morphology* 88, 49–92

Hart, R.W. and Farrell, R.A. 1969. Light scattering in the cornea. *Journal of the Optical Society of America* 59, 766-774

Hart, G.W. 1976 Biosynthesis of glycosaminoglycans during cornealdevelopment. *Journal of Biological Chemistry* 251, 6513-21

Hassell, J.R., Cintron, C., Kublin, C. *et al.* 1983. Proteoglycan changes during restoration of transparency in corneal scars. *Archives of Biochemistry and Biophysics* 222, 362-369.

Hassell, J.R., Newsome, D.A., Krachmer, J.H. *et al.* 1980. Macular corneal dystrophy: failure to synthesize a mature keratan sulfate proteoglycan. *Proceedings of the National Academy of Sciences USA* 77, 3705-3709.

Hay, E.D. 1991. Cell biology of extracellular matrix (2nd edition) New York: Plenum Press.

Hay, E.D., Revel, J.P. 1969 Fine structure of the developing avian cornea Wolsky, A Chen, PS eds. Monographs in Developmental Biology 1,1-144 S. Karger Basel, Switzerland

Hayashi, T., and Mizuno, K. 1999 Collagen In: Encyclopedia of Molecular Biology. Thomas Creighton ed., pp. 500-511, John Wiley & Sons

Hendrix, M.J., Hay, E.D., von der Mark, K. *et al.* 1982. Immunohistochemical localisation of collagen types I and II in the developing chick cornea and tibia by electron microscopy. *Investigative Ophthalmology and Visual Science* 22, 359-375.

Henry, S.P., Takanosu, M., *et al.* 2001 Expression pattern and gene characterisation of asporin, a newly discovered member of the leucine-rich repeat protein family. *Journal of Biological Chemistry* 276, 12212-21.

Hirsch, M., Noske, W., Prenant, G. and Renard, G. 1999 Structure of the Developing Avian Corneal Stroma as Revealed by Quick-freeze, Deep-etch Electron Microscopy. *Experimental Eye Research* 69, 267-277.

Hodge, A.J. and Petruska, J.A. 1963. Recent studies with the electron microscope on ordered aggregates of the tropocollagen molecule. In: Ramachandran, G.N. ed. Aspects of protein chemistry. London: Academic Press.

Hodson, S., D. Kaila, S. Hammond, G. Rebello, and Y. Al-Omari. 1992. Transient chloride binding as a contributory factor to corneal stromal swelling in the ox. *J. Physiol. (Lond.).* 450, 89-103

Holmes, D.F, Graham, H.K. *et al.* 1998 Collagen fibrils forming in developing tendon show an early and abrupt limitation in diameter at growing tips. *Journal of Molecular Biology* 283, 1049-58.

Holmes, D.F., Gilpin, C.J., Baldock, C. *et al.* 2001. Corneal collagen fibril structure in three dimensions: Structural insights into fibril assembly, mechanical properties, and tissue organization. *Proceedings of the National Academy of Sciences USA* 98, 7307-7312.

Hounsell, E.F., Feeney, J. *et al.* 1986 1H-NMR studies at 500Mhz of a neutral disaccharide and sulphated di-, tetra-, hexa-, and larger oligosaccharides obtained by endo-beta-galactosidase treatment of keratan sulphate. *European Journal of Biochemistry* 157, 375-84.

Hulmes, D.J. and Miller, A. 1979 Quasi-hexagonal molecular packing in collagen fibrils. *Nature* 282, 878-80.

Hunziker, E.B. 1993 Application of cryotechniques in cartilage tissue preservation and immunoelectron microscopy: potentials and problems. *Microsc Res Tech* 24, 457-464

Inatani, M. and Tanihara, H. 2002 Proteoglycans in retina. *Prog. Retin. Eye Res.* 21, 429-47.

Iozzo, R.V. 1999. The biology of the small leucine-rich proteoglycans. Functional network of interactive proteins. *Journal of Biological Chemistry* 274, 18843-18846.

Jakus, M.A. 1956 studies on the cornea. The fine structure of descemet's membrane The *Journal of Cell Biology*, 2, 243-252

Kadler, K.E., Holmes, D.F., Trotter, J.A. and Chapman, J.A. 1996 Collagen fibril formation *Biochemical Journal* 316, 1–11.

Kadler, K.E., Hojima, Y. and Prockop, D.J. 1987. Assembly of collagen fibrils de novo by cleavage of the type I pC- collagen with procollagen C-proteinase. Assay of critical concentration demonstrates that collagen self-assembly is a classical example of an entropy-driven process *Journal of Biological Chemistry*, 262, 15696-15701

Kadler, K.E. 1995 Extracellular Matrix 1: fibril-forming collagens. *Protein Profile* 2, 491-619

Kao, W.W. and Liu, C.Y. 2002. Roles of lumican and keratocan on corneal transparency. *Glycoconjugate Journal* 19, 275-285.

Kato, T., Nakayasu, A., Kanai, A., Nishiyama, T., Imamura, Y., Hayashi, T. 2000 Distribution and Isoform Characterization of Type XII Collagen in Bovine Cornea *Ophthalmic Research* 32, 215-221.

Kavanagh, E., Osborne, A.C., Ashhurst, D.E. and Pitsillides, A.A. 2002 Keratan Sulfate Epitopes Exhibit a Conserved Distribution During Joint Development That Remains Undisclosed on the Basis of Glycosaminoglycan Charge Density *Journal of Histochemistry and Cytochemistry,* 50, 1039-1047

Klintworth, G.K. 1976 Tissue culture in the inherited corneal dystrophies: possible applications and problems. *Birth Defects Orig. Artic. Ser.* 12, 115-32.

Klyce, S.D. and Beuerman, R.W. 1988. Structure and function of the cornea. In: Kaufmann, H.E. ed. The cornea. New York: Churchill Livingston.

Knudson, C.B. and Knudson, W. 2001 Cartilage proteoglycans. *Seminars in Cell and Developmental Biology* 12, 69-78.

Koch, M., Foley, J. *et al.* 2001 Alpha 1(Xx) collagen, a new member of the collagen subfamily, fibril associated collagens with interrupted triple helices. *Journal of Biological Chemistry* 276, 23120-6.

Koch, M., Veit, G., *et al.* 2006 Expression of Type XXIII Collagen mRNA and Protein. *J. Biol. Chem.*, 281, 21546-21557

Komai, Y. and Ushiki, T. 1991. The three-dimensional organization of collagen fibrils in the human cornea and sclera. *Investigative Ophthalmology and Visual Science* 32, 2244-2258.

Kreis, T. and Vale, R. 1993 Guidebook to the Extracellular Matrix and Adhesion Proteins, Oxford University Press

Krusius, T. and Ruoslahti, E. 1986 Primary structure of an extracellular matrix proteoglycan core protein deduced from cloned cDNA. *Proc Natl Acad Sci USA* 83, 7683-7.

Lanza, R.P and Langer, R. 2000 Principles of tissue engineering, Academic Press, San Diego, CA.

Leonard, D.W. and Meek, K.M. 1997 Refractive indices of the collagen fibrils and extrafibrillar material of the corneal stroma. *Biophys Journal* 72, 1382–1387.

Li, W., Vergnes, J.P., Cornuet, P.K. *et al.* 1992. cDNA clone to chick corneal chondroitin/dermatan sulfate proteoglycan reveals identity to decorin. *Archives of Biochemistry and Biophysics* 296, 190-197.

Lindahl, B., Eriksson, L., Spillmann, D., Caterson, B., and Lindahl, U. 1996 Selective Loss of Cerebral Keratan Sulfate in Alzheimer's Disease. *Journal of Biological Chemistry* 271, 16991-16994

Linsenmayer, T.F., Fitch, J.M., Schmid, T.M., Zak, N.B., Gibney, E., Sanderson, R.D. and Mayne, R. 1983 Monoclonal antibodies against chicken type V collagen: production, specificity, and use for immunocytochemical localization in embryonic cornea and other organs *The Journal of Cell Biology*, 96, 124-132.

Linsenmayer, T. F., Fitch, J. M., Mayne, R. 1984. Extracellular matrices in the developing avian eye: type V collagen in corneal and noncorneal tissues. *Investigative Ophthalmology and Visual Science* 25, 41-47.

Linsenmayer, T. F., Bruns, R. R., Mentzer, A. *et al.* 1986. Type VI collagen: immunohistochemical identification as a filamentous component of the extracellular matrix of the developing avian corneal stroma. *Developmental Biology* 118, 425-431.

Linsenmayer, T. F., Fitch, J. M., Birk, D. E. 1990. Heterotypic collagen fibrils and stabilizing collagens. Controlling elements in corneal morphogenesis? *Annals New York Academy of Sciences* 580, 143-160.

Linsenmayer, T.F. *et al.* 1993 Type V collagen: molecular structure and fibrillar organization of the chicken α1(V) NH2-terminal domain, a putative regulator of corneal fibrillogenesis. *Journal of Cell Biology* 121, 1181–1189.

Linsenmayer, T.F., Fitch, J.M., *et al.* 1998 Development and roles of collagenous matrices in the embryonic avian cornea. *Prog. Retin. Eye Res.* 17, 231-65.

Liu, C-Y., Birk, D.E., Hassell, J.R. *et al.* 2003. Keratocan-deficient mice display alterations in corneal structure. *Journal of Biological Chemistry* 278, 21672-21677.

Lorenzo, P., Aspberg, A., *et al.* 2001 Identification and characterisation of asporin, a novel member of the leucine-rich repeat family closely related to decorin and biglycan. *Journal of Biological Chemistry* 276, 12201-11.

Madisen, L., Neubauer, M., *et al.* 1990 Molecular cloning of a novel bone-forming compound: osteoinductive factor. *DNA Cell Biol.* 9, 303-9.

Marchant, J.K., Linsenmayer, T.F., *et al.* 1991 cDNA analysis predicts a cornea-specific collagen. *Proc Natl Acad Sci USA* 88, 1560-4.

Marchini, M., Morocutti, M., Ruggeri, A. *et al.* 1986. Differences in the fibril structure of corneal and tendon collagen. An electron microscopy and X-ray diffraction investigation. *Connective Tissue Research* 15, 269-281.

Marshall, G.E., Konstas, A.G., Lee, W.R. 1993. Collagens in ocular tissues. *British Journal of Ophthalmology* 77, 515-524.

Mathews, C.K. and van Holde, K.E. 1995. In: Biochemistry (2nd edition). The Benjamin/Cummings Publishing Company, Inc.

Maurice, D.M. 1957. The structure and transparency of the cornea. *Journal of Physiology* 136, 263-286.

Maurice, D.M. 1969. The cornea and sclera. In: Davson, H. ed. The eye. New York: Academic Press. pp. 489-599.

Maurice, D.M. 1970. The transparency of the corneal stroma. *Vision Research* 10, 107-108.

Maurice, D.M. 1984. The cornea and sclera. In: Davson, H. ed. The eye. New York: Academic Press. pp. 1-158.

Maurice, D.M. and Monroe, F. 1990. Cohesive strength of corneal lamellae. *Experimental Eye Research* 50, 59-63.

Meek, K.M., Chapman, D.A., and Hardcastle, R.A. 1979 The staining pattern of collagen fibrils. Improved correlation with sequence data. *Journal of Biological Chemistry* 254, 21, 10710-10714,

Meek, K.M., Elliott, G.F., Nave, C. 1986. A synchrotron X-ray diffraction study of bovine cornea stained with cupromeronic blue. *Collagen Related Research* 6, 203-218.

Meek, K.M. and Leonard, D.W. 1993. Ultrastructure of the corneal stroma: a comparative study. *Biophysical Journal* 64, 273-280.

Meek, K.M., Leonard, D.W., Connon, C.J. *et al.* 2003a. Transparency, swelling and scarring in the corneal stroma. *Eye* 17, 927-936.

Meek, K.M. and Quantock, A.J. 2001. The use of x-ray scattering techniques to determine corneal ultrastructure. *Progress in Retinal and Eye Research* 20, 95-137.

Meek, K.M., Quantock, A.J., Boote, C. *et al.* 2003b. An X-ray scattering investigation of corneal structure in keratocan-deficient mice. *Matrix Biology* 22, 467-475.

Mehmet, H., Scudder, P., *et al.* 1986 The antigenic determinants recognised by three monoclonal antibodies to keratan sulphate involved sulphated hepta- or larger oligosaccharides of the poly(N-acetyllactosamine) series. *European Journal of Biochemistry* 157, 385-91.

Midura, R.J., Toledo, R.M., *et al.* 1989 Analysis of the proteoglycans synthesised by corneal explants from embryonic chicken. I. Characterisation of the culture system with emphasis on stromal proteoglycan biosynthesis. *Journal of Biological Chemistry* 264, 1414-22.

Midura, R.J., Hascall, V.C. 1989 Analysis of the proteoglycans synthesised by corneal explants from embryonic chicken. II. Structural characterisation of the keratan sulphate and dermatan sulphate proteoglycans from corneal stroma. *Journal of Biological Chemistry* 264, 1423-30

Miller, A., and Parry, D.A. 1973 Structure and packing of microfibrils in collagen. *Journal of Molecular Biology* 75, 441-7.

Miller, E.J. and Matukas, V.J. 1969 Chick cartilage collagen: a new type of alpha I chain not present in bone or skin of the species. *Proc. Natl. Acad. Sci.USA.* 64, 1264-8.

Nakayasu, K. Tanaka, M., Konomi, H. *et al.* 1986. Distribution of types I, II, III, IV and V collagen in normal and keratoconus corneas. *Ophthalmic Research* 18, 1-10.

Nakazawa K, Suzuki S., Wada K., Nakazawa K. 1995. Proteoglycan synthesis by corneal explants from developing chick corneas *Journal of Biochemistry* 117, 707-18

Nakazawa,K., Takahashi,I. and Yamamoto,Y. 1998 Glycosyltransferase and sulfotransferase activities in chick corneal stromal cells before and after *in vitro* culture. *Arch. Biochem. Biophys.*, 359, 269–282.

Neame, P.J., Choi, U., *et al.* 1989 The primary structure of the core protein of the small, leucine-rich proteoglycan (PG I) from bovine articular cartilage. *Journal of Biological Chemistry* 264, 8653-61.

Newsome, D. A., Gross, J., Hassell, J. R. 1982. Human corneal stroma contains three distinct collagens. *Investigative Ophthalmology and Visual Science* 22, 376-381.

Nilsson, B., Nakazawa, K., Hassell, J.R. *et al.* 1983. Structure of oligosaccharides and the linkage region between keratan sulfate and the core protein on proteoglycans from monkey cornea. *Journal of Biological Chemistry* 258, 6056-6063.

Nimni, M.E., and Harkness, R.D. 1987. Collagen, volume 1: Biochemistry. C.R.C. Press Inc., Boca Raton, Florida.

Oeben, M., Keller, R., Stuhlsatz, H.W. *et al.* 1987. Constant and variable domains of different disaccharide structure in corneal keratan sulphate chains. *Biochemical Journal* 248, 85-93.

Oldberg, A., Antonsson, P., Lindblom, K. *et al.* 1989. A collagen-binding 59-kd protein (fibromodulin) is structurally related to the small interstitial proteoglycans PG-S1 and PG-S2 (decorin). *EMBO Journal* 8, 2601-2604.

Orgel, J.P.R.O, Irving, T.E., Miller, A. and Wess, T.J. 2006 Microfibrillar structure of type I collagen *in situ Proc Natl Acad Sci* 103, 9001-9005.

Orgel, J. P., Miller, A., Irving, T. C. *et al.* 2001. The in situ supermolecular structure of type I collagen. *Structure* (Cambridge) 9, 1061-1069.

Ottani, V., Raspanti, M. *et al.* 2001 Collagen structure and functional implications. *Micron* 32, 251-60.

Ottani, V., Martini, D. *et al.* 2002 Hierachical structures in fibrillar collagens. *Micron* 33, 587-96.

Pace, J.M., Corrado, M., Missero, C. *et al.* 2003. Identification, characterization and expression analysis of a new fibrillar collagen gene, COL27A1. *Matrix Biology* 22, 3-14.

Pellegata, N.S., Dieguez-Lucena, J.L., *et al.* 2000 Mutations in KERA, encoding keratocan, cause cornea plana. *Nature Genetics* 25, 91-5.

Peters D.M.P. and Mosher D.F. 1994 Formation of fibronectin extracellular matrix. In Extracellular matrix assembly and structure pp 315-40. Academic Press: New York, U.S.A.

Pfister, R.R. 1973. The normal surface of the corneal epithelium: a scanning electron microscopic study. *Investigative Ophthalmology and Visual Science*. 12, 654-668.

Piszkiewicz D, Landon M, Smith EL. 1970 Anomalous cleavage of aspartyl-proline peptide bonds during amino acid sequence determinations. *Biochem Biophys Res Commun.* 40, 1173-8.

Piez, K. A. and Trus, B. L. 1978 Sequence regularities and packing of collagen molecules. *Journal of Molecular Biology* 122, 419-432.

Piez, K. A. and Trus, B. L. 1981 A new model for packing of type-I collagen molecules in the native fibril. *Bioscience Reports* 1, 801-810.

Plaas, A.H., West, L.A., Midura, R.J. 2001a. Keratan sulfate disaccharide composition determined by FACE analysis of keratanase II and endo-beta-galactosidase digestion products. *Glycobiology* 11, 779-790.

Plaas, A.H., West, L.A., Thonar, E.J. *et al.* 2001b. Altered fine structures of corneal and skeletal keratan sulfate and chondroitin/dermatan sulfate in macular corneal dystrophy. *Journal of Biological Chemistry* 276, 39788-39796.

Pringle, G.A., and Dodd, C.M. 1990 Immunoelectron microscopic localization of the core protein of decorin near the d and e bands of tendon collagen fibrils by use of monoclonal antibodies. *J Histochem Cytochem.* 38,1405-11

Prockop, D. J. and Kivirikko, K. I. 1995 Collagens: molecular biology, diseases, and potentials for therapy. *Annu. Rev. Biochem.* 64, 403–434.

Prockop, D. J.; Kivirikko, K. I. 1984 Heritable diseases of collagen. *New England Journal of Medicine* 311, 376-386.

Quantock, A. J., Kinoshita, S., Capel, M. S. *et al.* 1998. A synchrotron x-ray diffraction study of developing chick corneas. *Biophysical Journal* 74, 995-998.

Quantock, A.J., Meek, K.M., Chakravarti, S. 2001. An x-ray diffraction investigation of corneal structure in lumican-deficient mice. *Investigative Ophthalmology and Visual Science 42*, 1750-1756.

Quantock, A.J., Meek, K.M., Ridgway, A.E.A. *et al.* 1990. Macular corneal dystrophy: reduction in both corneal thickness and collagen interfibrillar spacing. *Current Eye Research* 9, 393-398.

Rada, J.A., Cornuet, P.K., Hassell, J.R. 1993. Regulation of corneal collagen fibrillogenesis in vitro by corneal proteoglycan (lumican and decorin) core proteins. *Experimental Eye Research* 56, 635-648.

Radner, W. and Mallinger, R. 2002. Interlacing of collagen lamellae in the midstroma of the human cornea. *Cornea* 21, 598-601.

Ramachandran, G.W. and Kartha, G. 1954 Structure of collagen. *Nature* 174, 269-270.

Ramachandran, G.W. and Kartha, G. 1954 Structure of collagen. *Nature* 176, 593-595.

Rand JH, Patel N.D. *et al.* 1990. 150-kD von Willerbrand factor binding protein extracted from human vascular subendothelium is type-VI collagen. *Journal of Clinical Investigation* 88, 253-9.

Reardon, A.J., Le Goff, M. *et al.* 2000 Identification in vitreous and molecular cloning of opticin, a novel member of the family of leucine-rich repeat proteins of the extracellular matrix. *Journal of Biological Chemistry* 275, 2123-9.

Regini, J.W., Elliott, G.F., Hodson, S.A. 2004 The ordering of corneal collagen fibrils with increasing ionic strength. *Journal of Molecular Biology* 6, 336, 179-86

Robert, L., Legeais, J.M., Robert, A.M. *et al.* 2001. Corneal collagens. *Pathologie Biologie* (Paris) 49, 353-363.

Rosenberg, L.C., Choi, U., *et al.* 1985 Isolation of dermatan sulphate proteoglycans from mature bovine articular cartilages. *Journal of Biological Chemistry* 260, 6304-13.

Roth, J. 1982 The PAG technique. Qualitative and quantitative approach for antigen localisation on thin section. In: Techniques in immunocytochemistry, Vol. 1, Academic Press, London, pp104-137.

Rowe, M.P. 2000. Inferring the Retinal Anatomy and Visual Capacities of Extinct Vertebrates. *Palaeontologia Electronica* 3, 1-43

Ruberti, J.W. and Hallab, N.J. 2004. Mechanical load protects fibrillar collagen against enzymatic degradation. *Ophthalmic Res.* 36, 290.

Ruggiero, F., Burillon, C., Garrone, R. 1996. Human corneal fibrillogenesis. Collagen V structural analysis and fibrillar assembly by stromal fibroblasts in culture. *Investigative Ophthalmology and Visual Science* 37, 1749-1760.

Ruter, E.R. and Kresse, H. 1984. Partial purification and characterization of 3'-phosphoadenylylsulfate: keratan sulfate sulfotransferases. *Journal of Biological Chemistry* 259, 11771-11776.

Saika, S., Shiraishi, A., Liu, C-Y. *et al.* 2000. Role of lumican in the corneal epithelium during wound healing. *Journal of Biological Chemistry* 275, 2607-2612.

Saamanen, A.M.K., Salminen, A.H., *et al.* 2001 Murine fibromodulin: cDNA and genomic structure, and age-related expression and distribution in the knee joint. *Biochem. J.* 355, 577–585.

Sampaio, L de O., Bayliss, M.T., Hardingham, T.E. and Muir, H. 1988 Dermatan sulphate proteoglycan from human articular cartilage. Variation in its content with age and its structural comparison with a small chondroitin sulphate proteoglycan from pig laryngeal cartilage. *Biochemical Journal* 254, 757–764.

Sasaki, K., Kurata-Miura, K. *et al.* 1997 Expression cloning of cDNA encoding a human beta-1,3-N-acetylglucosaminyltransferase that is essential for poly-N-acetyllactosamine synthesis. *Proc. Natl. Acad. Sci. USA* 94, 14294-299.

Sawaguchi, S., Yue, B.Y., *et al.* 1991 Proteoglycan molecules in keratoconus corneas. *Investigative Ophthalmology & Visual Science*, 32, 1846-1853.

Sayers, Z., M. H. J. Koch, S. B. Whitburn, K. M. Meek, G. F. Elliott, and A. Harmsen. 1982. Synchrotron x-ray diffraction study of corneal stroma. *J. Mol. Biol.* 160, 593-607.

Schaefer L, Grone HJ, Raslik I, Robenek H, Ugorcakova J, Budny S, Schaefer RM, Kresse H. 2000 Small proteoglycans of normal adult human kidney: distinct expression patterns of decorin, biglycan, fibromodulin, and lumican. *Kidney International* 58, 1557-68

Schmut, O. 1977. The identification of type III collagen in calf and bovine cornea and sclera. *Experimental Eye Research* 25, 505-509.

Scott, J.E. 1980 Collagen--proteoglycan interactions. Localization of proteoglycans in tendon by electron microscopy. *Biochemical Journal* 187, 887-8911

Scott, J.E. and Orford, C.R. 1981 Dermatan sulphate-rich proteoglycan associates with rat tail-tendon collagen at the d band in the gap region. *Biochemical Journal* 197, 213–216.

Scott, J.E. and Haigh, M. 1985. Small-proteoglycan:collagen interactions: keratan sulphate proteoglycan associates with rabbit corneal collagen fibrils at the 'a' and 'c' bands. *Bioscience Reports* 5, 765-774.

Scott, J.E. and Haigh, M. 1988 Identification of specific binding sites for keratan sulphate proteoglycans and chondroitin-dermatan sulphate proteoglycans on collagen fibrils in cornea by the use of cupromeronic blue in 'critical-electrolyte-concentration' techniques. Biochemical Journal, 253, 607–610.

Scott, P.G., Winterbottom, N., Dodd, C.M. *et al.* 1986. A role for disulphide bridges in the protein core in the interaction of proteodermatan sulphate and collagen. *Biochemical and Biophysical Research Communications* 138, 1348-1354.

Scott, J.E. 1988. Proteoglycan-fibrillar collagen interactions. *Biochemical Journal* 252, 313-323.

Scott, J.E. 1990. Proteoglycan-collagen interactions and sub-fibrillar structure in collagen fibrils: implications in the development and remodelling of connective tissues. *Biochemical Society Transcripts* 18, 489-490.

Scott, J.E. and Bosworth, J.R. 1990 A comparative biochemical and ultrastructural study of proteoglycan-collagen interactions in corneal stroma. Functional and metabolic implications. *Biochemical Journal* 270, 491–497.

Scott J.E. 1991. Proteoglycan collagen interactions and corneal ultrastructure. *Biochemical Society Transcripts*.19, 877-81

Scott, J.E. 1992. Supramolecular organization of extracellular matrix glycosaminoglycans, in vitro and in the tissues. *FASEB Journal* 6, 2639-2645.

Scott J.E. 1996. Proteodermatan and proteokeratan sulphate(decorin, lumican/fibromodulim) proteins are horesehoe shaped. Implication for their interactions with collagen. *Biochemistry* 35, 8795-9.

Shinomura, T. and Kimata, K. 1992 Proteoglycan-Lb, a small dermatan sulphate proteoglycan expressed in developing chick epiphysal cartilage is structurally related to osteoinductive factor. *Journal of Biological Chemistry* 267, 1265-70.

Siegler, V., and Quantock, A.J. 2002 Two stage compaction of the secondary avian cornea during development *Experimental Eye Research* 74, 427-431

Siegler, V. 2003 Thesis: The Development of Avian Corneal Transparency. UCW, Cardiff.

Smith, J.W. 1968. Molecular pattern in native collagen. *Nature* 219, 157-158.

Smith, J.W. 1969. The transparency of the corneal stroma. *Vision Research* 9, 393-396.

Sorrell, J.M. and Caterson, B. 1989 Detection of Age-Related Changes in the Distributions of Keratan Sulfates and Chondroitin Sulfates in Developing Chick Limbs: An Immunocytochemical Study. *Development* 106, 657-663.

Stiemke M.M., Roman R.J., Palmer M.L., and Edelhauser H.F. 1992. Sodium activity in the aqueous humor and corneal stroma of the rabbit. *Experimental Eye Research.* 55, 425-433
Suzuki, M. 1939.

Suzuki, M. 1939. Prosthetic group of cornea mucoid. *Journal of Biochemistry* 30, 185-191.

Svensson, L., Aszodi, A., Reinholt, F.P. *et al.* 1999. Fibromodulin-null mice have abnormal collagen fibrils, tissue organisation, and altered lumican deposition in tendon. *Journal of Biological Chemistry* 274, 9636-9647.

Svensson, L., Heinegard, D., Oldberg, A. 1995. Decorin-binding sites for collagen type I are mainly located in leucine-rich repeats 4-5. *Journal of Biological Chemistry* 270, 20712-20716.

Svensson, L., Narlid, I., Oldberg, A. 2000. Fibromodulin and lumican bind to the same region on collagen type I fibril. *FEBS Letters* 470, 178-182.

Svoboda K.K., Nishimura I., Sugrue S.P. *et al.* 1988. Embryonic chicken cornea and cartilage synthesize type IX collagen molecules with different amino-terminal domains. *Proc Natl Acad Sci* USA. 85, 7496-7500.

Tai, G.H., Huckerby, T.N., Nieduszynski, I.A. 1996. Multiple non-reducing chain termini isolated from bovine corneal keratan sulfates. *Journal of Biological Chemistry* 271, 23535-23546.

Tai, G.H., Nieduszynski, I.A., Fullwood, N.J. *et al.* 1997. Human corneal keratan sulfates. *Journal of Biological Chemistry* 272, 28227-28231.

Takahashi, T., Cho, I. *et al.* 1993 Keratan sulphate and dermatan sulphate proteoglycans associate with type VI collagen in fetal rabbit cornea. *J. Histochem. Cytochem.* 41, 1447-57.

Takahashi, I., Nakamura, Y. *et al.* 1999 Immunohistochemical analysis of proteoglycan biosynthesis during early development of the chicken cornea. *Journal of Biochemistry (Tokyo)* 126, 801-14.

Tang, P.W., Scudder, P. *et al.* 1986 Sulphate groups are involved in the anitgenicity of keratan sulphate and mask I antigen expression on their poly-N-acetyllactosamine backbones. An immunochemical and chromatographic study of keratan sulphate oligosaccharides after desulphation or nitrosation. *European Journal of Biochemistry* 160, 537-45.

Tasheva, E.S., Corpuz, L.M., Funderburgh, J.L. *et al.* 1997. Differential splicing and alternative polyadenylation generate multiple mimecan mRNA transcripts. *Journal of Biological Chemistry* 272, 32551-32556.

Tasheva, E.S., Funderburgh, M.L., McReynolds, J. *et al.* 1999. The bovine mimecan gene. Molecular cloning and characterization of two major RNA transcripts generated by alternative use of two splice acceptor sites in the third exon. *Journal of Biological Chemistry* 274, 18693-18701.

Tasheva, E.S., Koester, A., Paulsen, A.Q. *et al.* 2002. Mimecan/osteoglycin-deficient mice have collagen fibril abnormalities. *Molecular Vision* 8, 407-415.

Toole B.P., and Trelstad R.L. 1971 Hyaluronate production and removal during corneal development in the chick. *Developmental Biology* 26, 28-35

Trelstad RL, Coulombre AJ. 1971 Morphogenesis of the collagenous stroma in the chick cornea *J Cell Biol.* 50, 840-858.

Troilo, D. and Wallman, J. 1987 Changes in corneal curvature during accommodation in chicks. *Vision Research* 27, 241-247.

Uchimura, K., Muramatsu, H. *et al.* 1998 Molecular cloning and characterisation of an N-acetylglucosamine-6-O-sulfotransferase. *Journal of Biological Chemistry* 273, 22577-83.

van der Rest, M., Dublet, B., Champliaud, M.F. 1990. Fibril-associated collagens. *Biomaterials* 11, 28-31.

Vogel, K.G., Paulsson, M., Heinegard, D. 1984. Specific inhibition of type I and type II collagen fibrillogenesis by the small proteoglycan of tendon. *Biochemical Journal* 223, 589-597.

Weber, I.T., Harrison, R.W., Iozzo, R.V. 1996. Model structure of decorin and implications for collagen fibrillogenesis. *Journal of Biological Chemistry* 271, 31767-31770.

Wei, Z.G., Sun, T.T., and Lavker, R.M. 1996. Rabbit conjunctival and corneal epithelial cells belong to two separate lineages. *Investigative Ophthalmology and Visual Science* 37, 523-33

Weibull, C. Carlemalm E., Villiger, W., Kellenberger, E., Fakan, J., Gautier, A., and Larsson, C. 1980 Low-temperature embedding procedures applied to chloroplasts. *J. Ultrastruct. Res.* 73, 233.

Wendel, M., Sommarin, Y. *et al.* 1998 Bone matrix proteins: isolation and characterization of a novel cell-binding keratin sulfate proteoglycan (osteoadherin) from bovine bone. *Journal of Cell Biology* 141, 839-47.

Wenstrup, R. J., Langland, G. T., Willing, M. C., D'Souza, V. N., Cole, W. G., 1996. A splice-junction mutation in the region of COL5A1 that codes for the carboxyl propeptide of pro-alpha-1(V) chains results in the gravis form of the Ehlers-Danlos syndrome (type I). *Human Molecular Genetics* 5, 1733-1736.

Wess, T.J. and Cairns, D.E. 2005 Nanoarchitectures of the animal extracellular matrix: opportunities for synchrotron radiation studies on collagen and fibrillin. *Journal of Synchrotron Radiation* 12, 751-757.

Wess, T. J., Hammersley, A. P., Wess, L. *et al.* 1998. A consensus model for molecular packing of type I collagen. *Journal of Structural Biology* 122, 92-100.

Wessel, H., Anderson, S., Fite, D. *et al.* 1997. Type XII collagen contributes to diversities in human corneal and limbal extracellular matrices. *Investigative Ophthalmology and Visual Science* 38, 2408-2422.

Worthington, C.R. and Inouye, H. 1985. X-ray diffraction study of the cornea. *International Journal of Biological Macromolecules* 7, 2-8.

Yamaguchi, N., Mayne, R., *et al.* 1991 The alpha 1 (VII) collagen gene is homologous to the alpha 1(X) collagen gene and contains a large exon encoding the entire triple helical and carboxyl-terminal non-triple helical domains of the alpha (VIII) polypeptide. *Journal of Biological Chemistry* 266, 4508-13.

Ying, S., Shiraishi, A., Kao, C.W. *et al.* 1997. Characterization and expression of the mouse lumican gene. *Journal of Biological Chemistry* 272, 30306-30313.

Young, R.D. *et al.* 2000. Immunolocalization of Collagen Types II and III in Single Fibrils of Human Articular Cartilage. *Journal of Histochemistry and Cytochemistry*, 48, 423-432

Young, B.B., Zhang, G., *et al.* 2002 The roles of types XII and XIV collagen in fibrillogenesis and matrix assembly in the developing cornea. *J.Cell.Biochem.* 87, 208-20.

Young, R.D., Tudor, D., Hayes, A.J. *et al.* 2005. Atypical composition and ultrastructure of proteoglycans in the mouse corneal stroma. *Investigative Ophthalmology and Visual Science* 46, 1973-1978.

Young, R.D., Quantock, A.J., Sotozono, C., Koizumi, N. and Kinoshita, S. 2006 Sulphation patterns of keratan sulphate proteoglycan in sclerocornea resemble cornea rather than sclera. *British Journal of Ophthalmology* 90, 391-393.

Yurchenko, P.D. and Ruben, G.C. (1987). Basement membrane structure in situ: Evidence for lateral associations in the type IV collagen network. *J.Cell.Biol.,* 105, 2559-68.

Yurchenko and Furthmayr, H. (1984). Self-assembly of basement membrane collagen. *Biochemistry* 23, 1839-50.

Zanetti, M., Ratcliffe, A., *et al.* 1985 Two subpopulations of differentiated chondrocytes identified with a monoclonal antibody to keratan sulphate. *Journal of Cell Biology* 101, 53-59.

Zhou,D., Dinter,A., Gallego,R.G., *et al.* 1999 A ß-1,3-N-acetylglucosaminyltransferase with poly-N- acetyllactosamine synthase activity is structurally related to ß-1,3- galactosyltransferases. *Proc. Natl. Acad. Sci. USA*, 96, 406–411.

Zieske, J.D. 2004. Corneal development associated with eyelid opening. International *Journal of Developmental Biology* 48, 903-911.

CARDIFF UNIVERSITY
PRIFYSGOL CAERDYDD